THE COLLAPSE BEHAVIOUR OF TAPERED STEEL BEAMS

BY

SATYA NARAYAN MANDAL B.Sc.Eng.(Civil)

A THESIS SUBMITTED TO THE UNIVERSITY OF
NOTTINGHAM FOR THE DEGREE OF
DOCTOR OF PHILOSOPHY

May 1978

TO MY ELDER BROTHER AND SISTER-IN-LAW

ABSTRACT

In this thesis, the collapse mode of failure of tapered steel beams is examined for three different loading cases. Firstly, for the case when the beam is loaded inside the tip; secondly, when the beam is loaded outside the tip, and thirdly, when the beam is loaded at the tip. The theoretical collapse mode of failure presented here provides an identical collapse load whether obtained from lower or upper bound solutions. Fourteen tests on tapered steel beam specimen were carried out to examine the collapse modes of failure and their ultimate strengths for steel tapered beams loaded inside, outside and at the tip. The experimental collapse loads and their collapse modes of failure are compared with theoretically predicted collapse loads and the proposed collapse mechanisms respectively.

The first elastic yield load of the tapered web panels is assessed on the basis of 'circular Arc Theory' simplified by Davies et al.[6] and is compared with the predicted theoretical collapse loads.

Conclusions are drawn relating to the plastic collapse modes of failure and ultimate strengths of tapered steel beams.

ACKNOWLEDGEMENTS

The author is most grateful for the guidance and encouragement offered to him by Dr. G. Davies under whose supervision the work presented in this thesis was carried out.

The author wishes to express his sincere gratitude to Professor R. C. Coates for the provision of the excellent facilities in the department.

Sincere gratitude is also expressed to Mr. C. Snell for his help, concern and encouragement so generously given to the author and his family.

Messrs. J. Leonardi, J. Barlow, N. Hardy and M. Bettison provided considerable assistance in the instrumentation and testing of the beam specimens and the author is grateful for their help. Tapered beam specimens were fabricated in the Faculty Workshop, and thanks are due to Messrs. R. Steel, G. Andrews and D. Oakland for their help.

The author wishes to thank the Government of India for awarding the scholarship.

The author extends his thanks to all his friends and research colleagues for their pleasant company. Thankful appreciation goes to Mr. H. A. Khan and Mr. J. W. Pappin for their help and suggestions in the preparation of this thesis.

The author would like to thank Miss Ginny Howard for her skillful typing of this thesis.

Finally, the author wishes to thank his wife, Padmini, for her deepest understanding, tolerance and great care during the preparation and writing of this thesis.

LISTS OF CONTENTS

LIST OF FIGURES

Page No.

Page No.

Page No.

LIST OF TABLES

LISTS OF PHOTOGRAPHS

NOTATIONS

b = Width of the panel between central line of stiffeners

d_1 = Smaller depth of the tapered panel

d_2 = Greater depth of the tapered panel

d = Average depth of the panel

z = Distance of the tip from centre of the central stiffner

t = thickness of web plate

E = Modulus of Elasticity

ν = Poission's ratio

σ_{yw} = tensile yield stress of web material

σ_t^y = Tensile membrane yield stress of web material

τ_{cr} = Critical shear stress

V_{cr} = Critical shear force (Buckling load)

F_s = Resultant tensile membrane force

C_t = Distance between the plastic hinges in tension flange

C_c = Distance between the plastic hinges in compression flange

θ = Inclination of the tensile membrane stress field

γ = Inclination of the inclined compression flange

W_{ult} = Theoretical ultimate load

W_{exp} = Experimental collapse load

θ_m = value of θ required to provide maximum value of W_{ult}

A_{cf} = Cross-sectional area of compression flange

A_{tf} = Cross-sectional area of tension flange

F_c = Axial force in compression flange

F_t = Axial force in tension flange

σ_{cf} = Average axial stress in compression flange

σ_{tf} = Average axial stress in tension flange

M_{pc} = Full plastic moment capacity of compression flange

M_{pt} = Full plastic moment capacity of tension flange

M'_{pc} = Reduced plastic moment capacity of compression flange

M'_{pt} = Reduced plastic moment capacity of tension flange

CHAPTER ONE

INTRODUCTION

Owing to their economy, aesthetic appeal, suitability for fabrication and reduced self weight, tapered beams are becoming more and more popular in various types of structural construction. The cause of economy is best served when the beams have adequate lateral support, and their design capacities can easily be determined.

Although, tapered steel members have been used in a large variety of structural applications for some time, and some analysis procedures were available prior to 1955, a joint task committee of the Column Research Council (C.R.C.) and the Welding Research Council (W.R.C.) was formed, in 1966, in the United States of America, to study and formulate design information and recommendations relating to tapered members. Since then numerous results including the studies of elastic behaviour of tapered members and its stability aspects by Lee and Morrell[1, 2, 3], Chong et. al.[4], Kitiponarchai and Trahair[5], Davies et. al.[6] and Butler et. al.[7, 8] have been published. Along with the analytical studies, two test programmes were carried out in the United States of America. The first experimental program was conducted at Columbia University under the direction of Butler. In the Columbia test program, I-shaped beams and channel sections, tapered in both web and flanges, were tested as a cantilever beam-columns. The primary interest was the elastic stability of these beams and their bracing requirements.

The second experimental program under the technical guidance of C.R.C. - W.R.C. joint task committee was begun in 1966 by

Lee et. al.[1] at the state university of New York at Buffalo. The results of this series of tests are reported by Prawel et. al.[9]. The primary interest in the second set of tests was inelastic stability of tapered I-shaped beam-columns.

However, still very limited information is available to facilitate the plastic design of tapered beams.

On the other hand there has been a progressive development in the field of parallel flange plate girders to establish the plastic collapse mode of failure and to predict its ultimate strength. A review of the existing method of analysis of the collapse behaviour of parallel flange plate girder is presented in Chapter Three of this thesis. However, the principles of buckling and post buckling behaviour and the design criteria of plate girders are briefly discussed in the present chapter.

Until the early 1960's, web buckling was accepted as a basis for the design of plate girders. Principally, this was due to the fact that formulas for predicting buckling are relatively simple and have been known for many years, while suitable analyses of post buckling strength were relatively new. However, the post buckling strength was acknowledged in most specifications by using a smaller factor of safety for web buckling than for yielding or failure of other elements. But all this work gave poor correlation with ultimate strength test results.

The sources of the post buckling strength of stiffened plate girder webs in shear was explained by Wilson[10] in 1886. He discovered by means of a paper model with very thin flexible web, that when stiffeners were properly introduced the web no longer resisted by compression, but by tension, the stiffeners taking up the duty of compressive resistance, like the post of a

Pratt truss, and dividing the girder into panels equivalent to those of an open truss, the web in each panel acting as an inclined tie as shown in Figure 1.1.1. However he did not explain his analysis.

Wagner[11] in the 1930's developed a diagonal tension theory of web shear. Extensive studies, both analytical and experimental, were made in the late 1950's by Basler and Thurlimann[12, 13, 14] on the post buckling behaviour of web panels in bending, shear and also under the action of combined bending and shear. Practical procedures were developed and have been adopted in some specifications in the U.S.A. Widespread interest in the post buckling strength of plate girders resulted in a number of modifications to the Basler-Thurlimann's approach to achieve better correlation between theoretical predictions and experimental results. Among those modifications, the most considerable work was presented by Gaylord[15], Fujii[16], Rockey and Skaloud[17, 18, 19, 20, 21, 22], Ostapenko and Chern[23], Komatsu[24] and Calladine[25], whose analyses and results are described and discussed in Chapter Three. However, it seems that the collapse mode of failure presented by Porter, Rockey and Evans[26] is the true collapse model for plate girders loaded in shear, which contains all the best features of the already existing ones. It provides identical lower and upper bound solutions, and is also capable of predicting the collapse load which has good agreement with the experimental results. In addition to their previous work[26] Rockey et. al.[27], very recently, presented a design method which is applicable to both symmetrical and unsymmetrical plate girders, reinforced by both transverse and longitudinal stiffeners and subjected to the combined action of bending moment and shear force.

In this thesis, the post buckling behaviour of steel beams

having tapered web and inclined compression flange have been studied both analytically and experimentally. The tapered beams were reinforced by transverse stiffeners and were loaded inside the tip, outside the tip and at the tip. Where the tip of a tapered beam is defined as the point of intersection of the top flange and the projection of the sloping flange. For the analyses, the load acting at any point on a tapered beam can be replaced by an equivalent 'tip-load' and a 'tip-moment'. However, the magnitude and direction of 'tip-moment' will depend upon the way of loading as shown in Figures I.1.2(a), I.1.2(b) and I.1.2(c). Clearly the direction of tip-moments for the two cases viz. when loads are inside and outside the tip, will be opposite to each other and its magnitude will be zero when the load is at the tip.

In the next chapter, for all the three different cases mentioned above, the first elastic yield load of the tapered panels is assessed by using the 'circular arc theory' simplified by Davies et. al.[6]. The comparison shows that these loads are significantly lower than either the predicted or the experimental collapse load of the panel.

Although, the specified depth/thickness ratios (B.S. 153, Part 3B and 4) for transversely stiffened webs of plate girders are limited to 180 or 270 . It was decided to use higher values of an average depth/thickness ratio of tapered webs. The ratios of an average depth/thickness of tapered webs considered in this thesis vary from 235 to 309 which is in similar range to the d/t ratio (between 255-316) used by Basler et. al.[28] and Rockey and Skaloud[21] in their tests on transversely stiffened plate girders. The aspect ratio (width/depth ratio) specified to limit the web-buckling (B.S. 153, Part 3B and 4) for transversely stiffened web

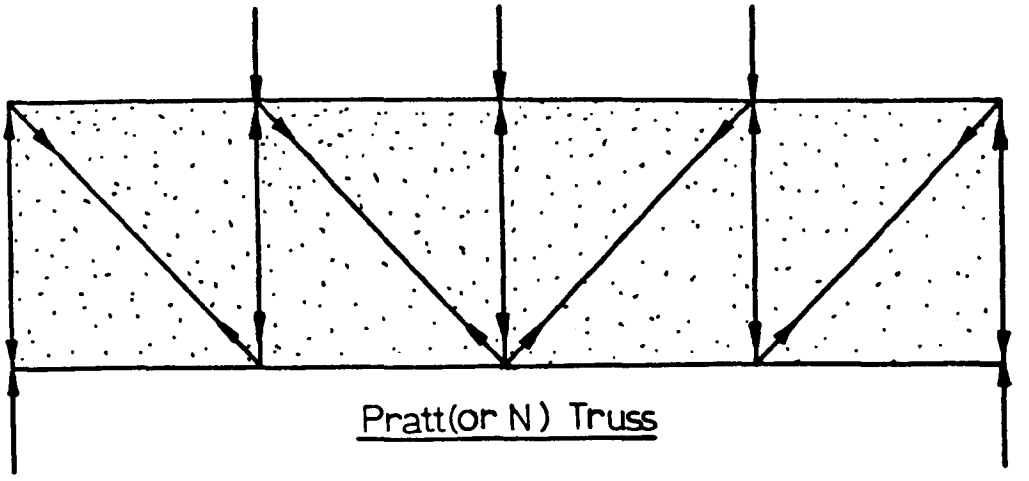

Figure 1.1.1

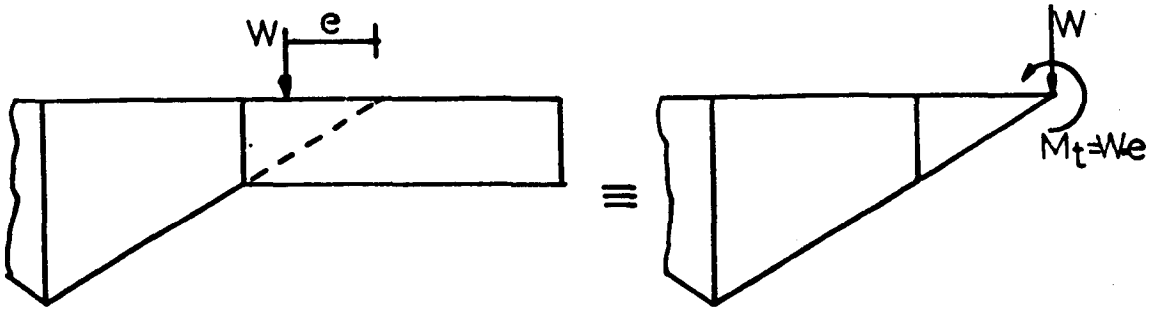

Beam loaded inside the tip

Equivalent tip force and moment

Figure 1.1.2(a)

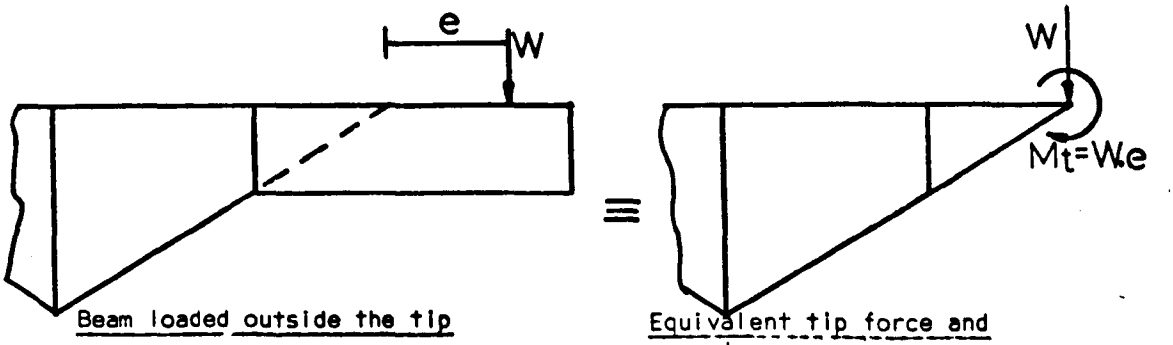

Beam loaded outside the tip

Equivalent tip force and moment

Figure 1.1.2(b)

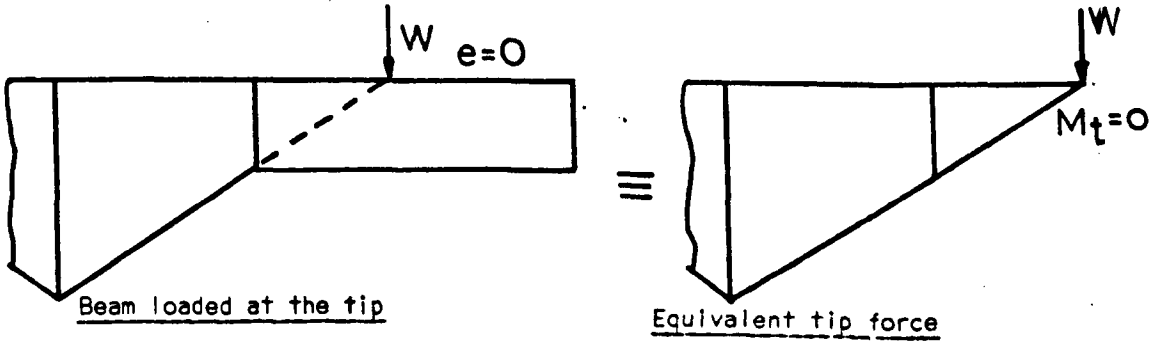

Beam loaded at the tip

Equivalent tip force

Figure 1.1.2(c)

of thickness less than d/85 (Grade 43 Steel) is 1.5, whereas the ratios of width/average depth of tapered web panel considered in this thesis vary from 1.55 to 1.57.

The analytical and experimental studies show that the post buckling strength of a tapered web panel makes a significant contirbution to its ultimate strength. After the web plate buckles, the tensile membrane stress field develops along the tension diagonal of the tapered panel. However, it is interesting to note that the tension and compression diagonals of a tapered panel interchange with the change in the direction of the tip moment as shown in Figures 1.1.3(a) and 1.1.3(b). This reversal in the direction of the tension diagonal can also be demonstrated by a pin jointed statically determinate cantilever shown in Figures 1.1.4(a) and 1.1.4(b), where the web members occurring are either solid or dotted line members. As mentioned previously the effect of a load 'W' at an eccentricity 'e' from the tip can be estimated from the combined effect of 'W' applied at the tip and an equivalent tip moment (M_t = W.e). Using the method of sections, it is quickly seen that the force in the internal member is easily obtained, e.g.

$$F_{cd} = \frac{M_t}{p_{cd}} = \frac{W.e}{p_{cd}} \qquad (1.1)$$

where p_{cd} is the perpendicular distance of the member cd under consideration from the tip. Clearly as the eccentricity changes the sign, i.e. depending on whether the load 'W' is inside or outside the tip, the sign of F_{cd} will also change and web members which were tensile in Figure 1.1.4(a) become compressive in Figure 1.1.4(b). On the other hand, when the tip moment is zero

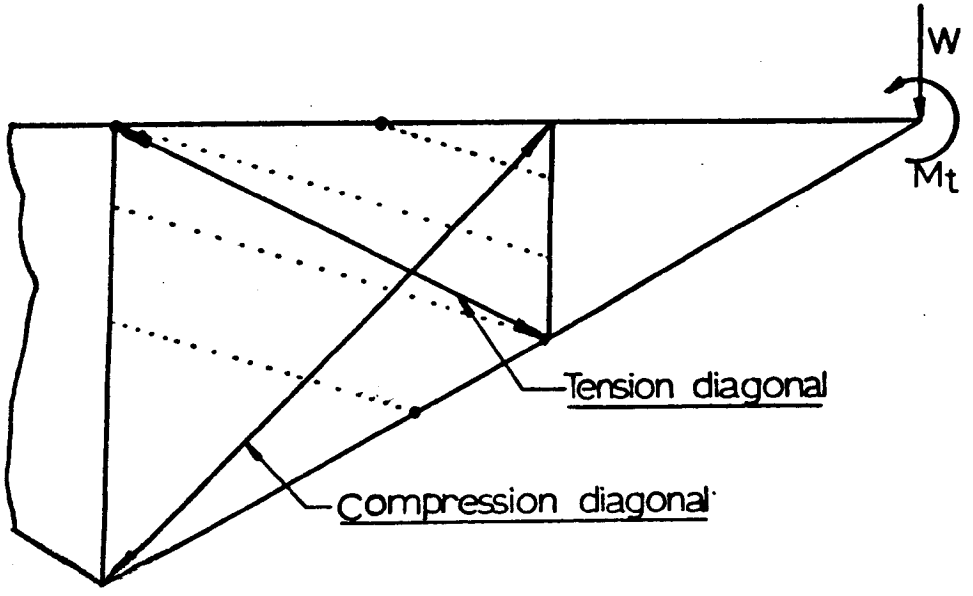

Beam loaded inside the tip
(tip moment anticlockwise)

Figure 1.1.3(a)

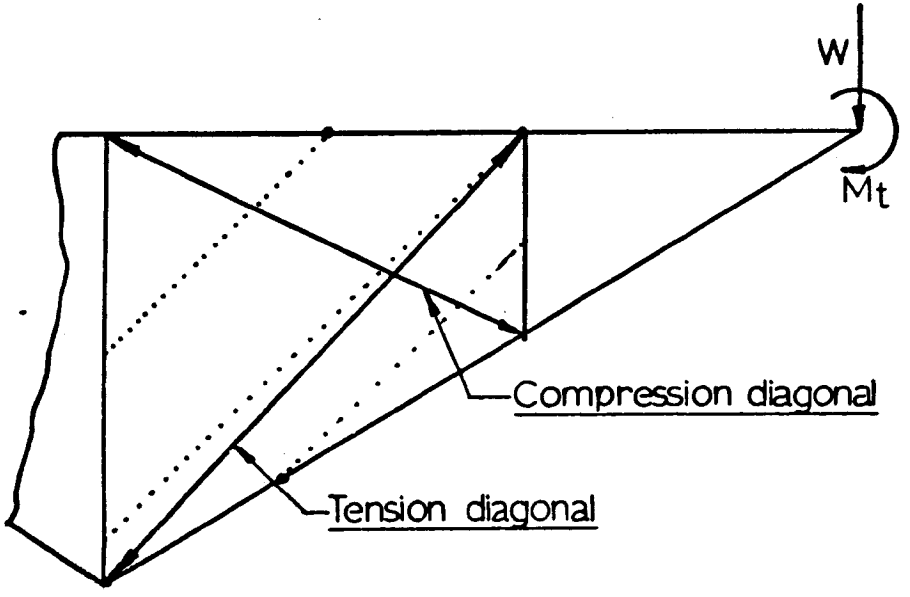

Beam loaded outside the tip
(tip moment clockwise)

Figure 1.1.3(b)

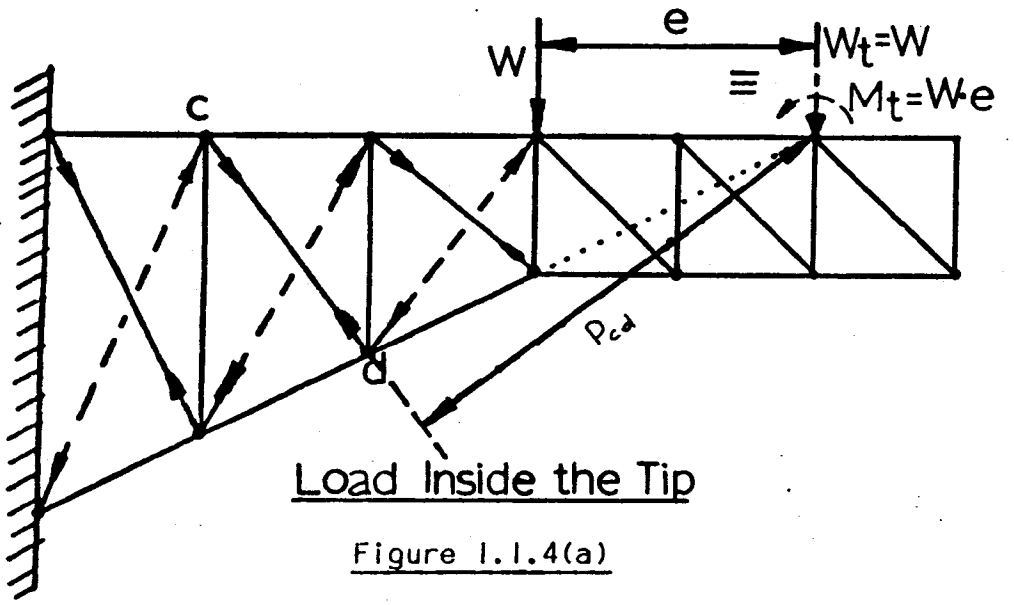

Load Inside the Tip

Figure 1.1.4(a)

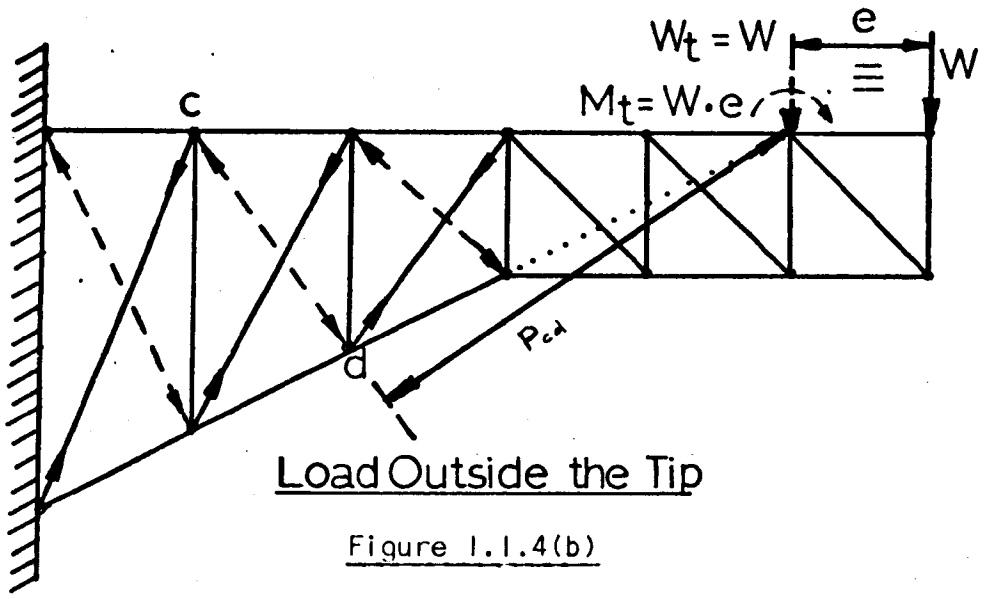

Load Outside the Tip

Figure 1.1.4(b)

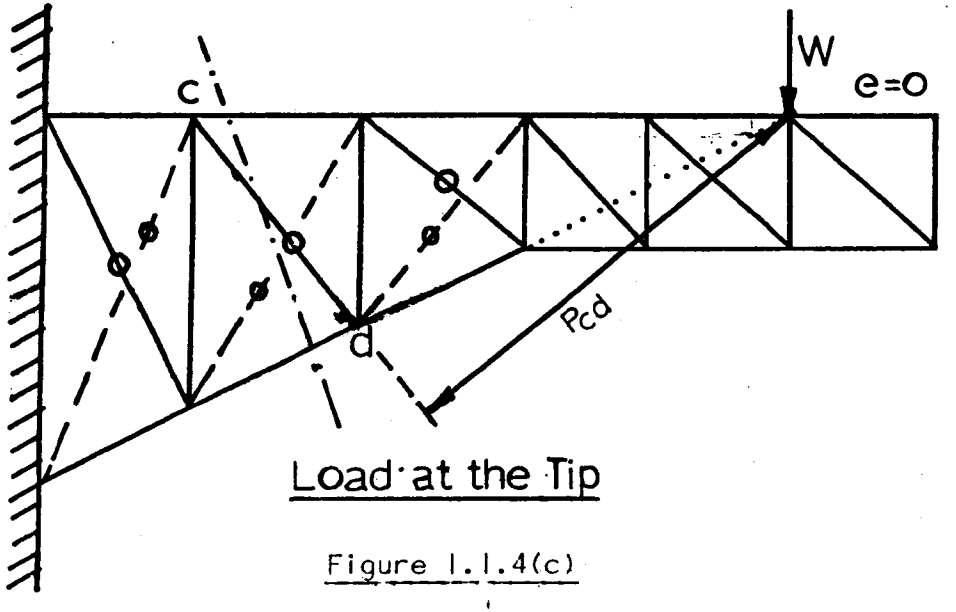

Load at the Tip

Figure 1.1.4(c)

(beam loaded at the tip) the shear stress in the web becomes zero and hence in this particular case the tensile membrane stress field does not form in the web, this causes the girder to fail due to yielding of the inclined compression flange. However, it can be seen that when the load 'W' is at the tip of a pin jointed statically determinate cantilever, shown in Figure 1.1.4(c), there is no force in the internal member. This verifies the fact that there will be no tension field action in the web of a tapered beam loaded at the tip.

Because the axial forces in the inclined compression flange is very high, the lateral instability of tapered beams becomes more critical. In particular, tapered beams loaded at or near the tip (where the beams fail due to yielding of the compression flange), would fail due to lateral instability unless sufficient lateral supports were provided. It is evident from the theoretical predictions that as the eccentricity of load about the tip decreases, axial forces in the tension and compression flanges increase, this increase in axial forces cause more lateral instability problems. Although, in this thesis the author's sole aim is to study the collapse behaviour and ultimate strengths of tapered beams (beams failing in the plane of the girder), it was found during the experimental studies that lateral supports of adequate strength were necessary in order to develop a proper collapse mechanism.

The collapse modes of failure of tapered beams loaded inside, outside and at the tip are presented in this thesis. One of the interesting features of the collapse mechanism proposed for the two cases (beam loaded inside and outside the tip), is that it provides an identical collapse load whether obtained from an upper or lower bound solution. It is shown that the stress con-

dition assumed in the presented collapse mechanism does not violate the plasticity yield condition. The collapse loads, with full plastic moment capacity and reduced plastic moment capacity (due to the presence of axial forces) of the flanges, are predicted. However, it must be recognised that the actual predicted collapse loads are those which take into consideration a reduced plastic moment capacity of the flanges. The experimental studies which examine the collapse behaviour and ultimate strengths of fourteen tapered steel girders are presented. Experimental results are described and discussed. The predicted collapse loads are in good agreement with the experimental collapse loads. On the basis of analytical studies and comparison with the experimental results, conclusions are drawn about the collapse modes of failure and ultimate strengths of tapered steel beams.

CHAPTER TWO

THE ELASTIC ANALYSIS OF TAPERED STEEL BEAMS

2.1 Introductory Remarks

In order to proceed to the collapse load behaviour of tapered beams, it is necessary, as a first stage, to assess the first elastic yield. It is then possible to examine and verify whether the calculated theoretical collapse load is significantly higher than the first elastic yield load or not. Therefore, in this chapter, the existing methods of elastic analysis of tapered beams are reviewed and the first elastic yield load (for beams loaded inside, outside and at the tip) is calculated and finally conclusions are drawn.

2.2 Existing Methods of Elastic Analysis of Tapered Beams

The various approaches may be split into two distinct groups:

1. Those which examine the equilibrium of an element bounded by two vertical faces (vertical cut theory).
2. Those which evaluate component stresses at points on circular arc drawn about the beam tip (circular arc theory).

1. Vertical cut theory

The simplest and crudest approach is to ignore the effect of the taper and merely to apply 'conventional' prismatic beam theory to the vertical section. Thus (from Figure 2.2.1);

$$\sigma_x = \frac{M_s . y_p}{I_{xx}} + \frac{N_s}{A_x} \qquad (2.1)$$

and $$\tau_{xy} = \frac{V_s \int y dA_x}{b_p . I_{xx}} \qquad (2.2)$$

where the integration extends from the top of the beam down to the point considered, and σ_x and τ_{xy} are the normal and shear stresses at a point y_p on a vertical section due to the forces V_s, M_s and N_s as shown in Figure 2.2.1.

I_{xx} = Second moment of area of vertical section

A_x = Area of vertical section

b_p = Breadth of section at the point 'p'.

Guyon[35] suggested that the equation of a 'conventional' analysis should be retained, except that in calculating the shear stress 'τ_{xy}', the external force 'V_s' should be replaced by 'V_g', a modified 'shear force' which takes into account the inclination to the horizontal of the stresses on the 'elementary fibres'. It is assumed that the value of the flexural stress 'σ_f' in the 'elementary fibre' at the point p (Figure 2.2.1) on the vertical section, is inclined along PO, where O is the point of intersection of the extreme tangents to the vertical section under consideration. He assumes that the horizontal component of force, due to a stress σ_f along the elementary fibre is $\sigma_x.dA_x$, so that vertical component (d_q) is given by

$$-dq = \sigma_x.\tan\gamma.dA_x \qquad (2.3)$$

where γ = angle of inclination of the line PO.

$$\text{i.e.} \quad \tan\gamma = \frac{(y_t - y_p)}{X_g} \qquad (2.4)$$

$$\text{and} \quad \alpha = \frac{y_p}{X_g} \qquad (2.5)$$

assuming γ is small, $\gamma = \tan\gamma$

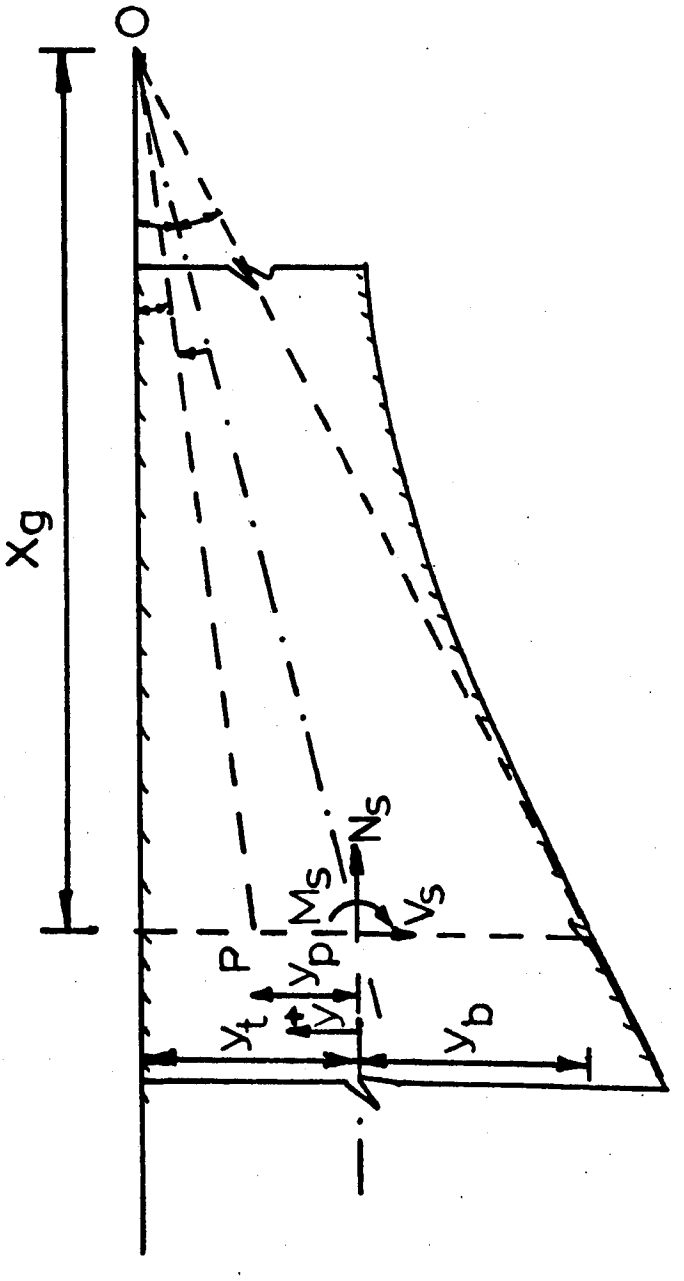

Figure 2.2.1 Notations and sign convention for Guyon's Analysis

$$\therefore -dq = \left(\frac{M_s \cdot y_p}{I_{xx}} + \frac{N_s}{A_x}\right) \frac{(y_t - y_p)}{X_g} \cdot dA_x \qquad (2.6)$$

Integrating over the complete cross section the upward force (q) is given by

$$-q = \frac{y_t}{X_g} \int \left(\frac{M_s \cdot y}{I_{xx}} + \frac{N_s}{A_x}\right) dA_x - \frac{I}{X_g} \int \left(\frac{M_s \cdot y^2}{I_{xx}} + \frac{N_s y}{A_x}\right) dA_x \qquad (2.7)$$

Equation (2.7) reduced to:

$$q = \frac{M_s}{X_g} - \frac{N_s Y_t}{X_g} \qquad (2.8)$$

and if β_o is small, one can write;

$$V_g = V_s - \frac{M_s}{X_g} + N_s \cdot \beta_o \qquad (2.9)$$

$(\because V_g = V_s - q)$

Guyon then evaluates principal stresses using the values of σ_x and τ_{xy} thus obtained. Clearly the internal arrangement of stresses cannot alter the shear force V_s which is carried on the vertical section and which is governed by basic equilibrium, but the reduction may be regarded as that portion of the shear force which is carried by the inclined flexural stresses.

Although, the net vertical shear can be calculated using the vertical cut theory (as explained above), this does not explain the presence of radial and tangential stresses in the panel. It was, therefore, decided not to use this method to analyse the first elastic yield of the panel.

2. Circular arc theory

The Boussinesq[36] solution for a plane elastic wedge relates radial and tangential stresses to forces applied at the

tip of a wedge shown in Figure 2.2.2. It would seem that such a solution could be applied to a plane wedge with loads acting at points other than the tip, provided equivalent tip forces are calculated and used.

Using the notation and sign convention illustrated in Figure 2.2.2, the Boussinesq solution, at any point P(R,α) for a plate of thickness t; gives radial stresses at point P(R,α):

$$\sigma_r = \frac{N_t}{R.t} \cdot \frac{\cos\alpha}{(\beta + \frac{1}{2}\sin 2\beta)} + \frac{V_t}{R.t} \cdot \frac{\sin\alpha}{(\beta - \frac{1}{2}\sin 2\beta)} + \frac{2M_t}{R^2.t} \cdot \frac{2.\sin 2\alpha}{(\sin 2\beta - 2\beta.\cos 2\beta)} \qquad (2.10)$$

Tangential stress at point P(R,α)

$$\sigma_\alpha = 0 \qquad (2.11)$$

$$\tau_{r\alpha} = \frac{M_t}{R^2.t} \cdot \frac{(\cos 2\alpha - \cos 2\beta)}{(\sin 2\beta - 2\beta.\cos 2\beta)} \qquad (2.12)$$

For these solutions, σ_α is identically zero, and hence there can be no bearing pressure on the faces of the wedge. It should be noted that for the case of shear force V_t only, the shearing stresses along the arc are zero. It can be recognised as arising from pairs of symmetric equally stressed 'fibres' giving a contribution to V_t only, and extending or contracting so as to require no shear stress between adjacent fibres. However, since the radial fibres pass through the tip, a moment M_t applied at that point can only be resisted by shear stresses along the arc.

Since σ_α is always zero then when $M_t = 0$, $\tau_{r\alpha}$ is also zero and σ_r may be found from equation (2.10). The simple form that this equation takes leads to the result that for a more general cross section made up from a web and flanges, each of constant

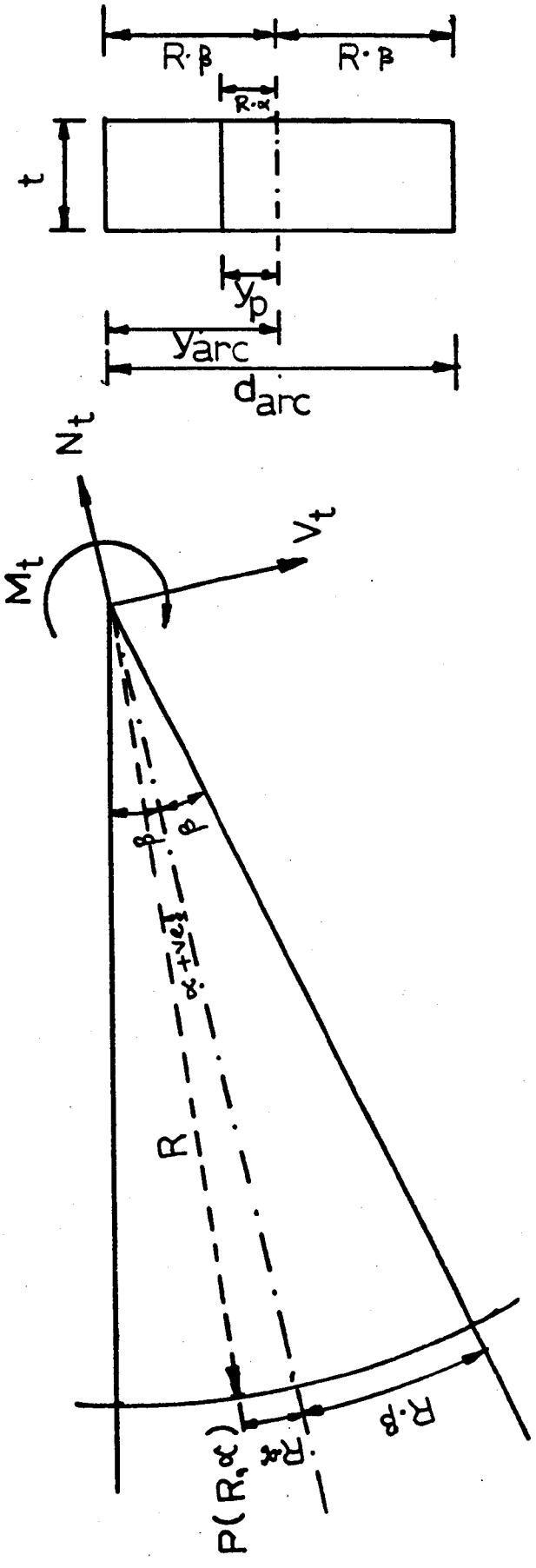

Figure 2.2.2 Notation and sign conventions for Boussinesq solution

thickness as shown in Figure 2.2.3, the modified radial stresses is given by:

$$\sigma_r = \frac{N_t \cos\alpha}{R[b_1(\beta + \tfrac{1}{2}\sin 2\beta) - (b_1 - b_2)(\gamma + \tfrac{1}{2}\sin 2\gamma)]} +$$

$$\frac{V_t \sin\alpha}{R[b_1(\beta - \tfrac{1}{2}\sin 2\beta) - (b_1 - b_2)(\gamma + \tfrac{1}{2}\sin 2\gamma)]} \qquad (2.13)$$

$$\sigma_\alpha = 0 \qquad (2.14)$$

$$\tau_{\gamma\alpha} = 0 \qquad (2.15)$$

For cases where the angles α,β and γ are small, which is generally true for bridge structures, an approximate form of the basic equations were obtained by Davies et al[6]. By expanding the trigonometrical functions, and only retaining first order quantities they (Ref. 6) approximated the equations (2.10) and (2.12) in the form:

$$\sigma_r = \frac{N_t}{A_{arc}} + \frac{(V_t.R + M_t)\, Y_{arc}}{I_{arc}} \qquad (2.16)$$

and $$\tau_{r\alpha} = \frac{M_t}{R.t.I_{arc}} \int Y_{arc}.dA_{arc} \qquad (2.17)$$

where suffix 'arc' refers to dimensions and properties measured around the arc, the integral is again for the part area above the point under consideration. It can be noted that $(V_t.R + M_t)$ and (M_t/R) are respectively the moment and shear at the centroid of arc-section.

The extension of equations (2.16) and (2.17) for the case when M_t does not equal to zero, and when the arc section is symmetrical, involves the same assumptions that are made in the

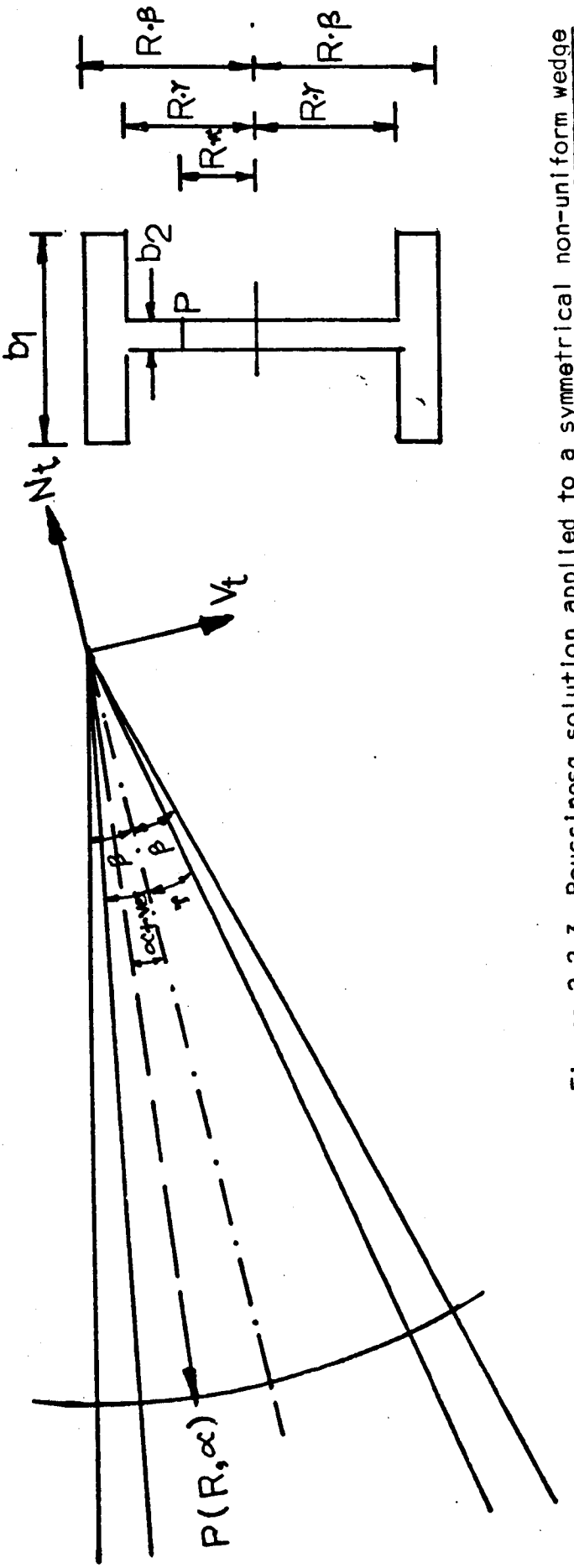

Figure 2.2.3 Boussinesq solution applied to a symmetrical non-uniform wedge

derivation of conventional beam theory at the web flange interface. Therefore these equations can be used to calculate the radial and shear stresses of the tapered steel beams and hence the first elastic yield load can be assessed by considering any yield criterion.

The distributions of elastic shear and radial stress in a tapered panel are shown in Figure 2.2.4. It can be seen that shear stresses in this case vary along the length of the panel, which is not the case with the rectangular panel.

2.3 The first elastic yield load of tapered steel beams loaded inside the tip

For the case when a tapered beam is loaded inside the tip, the equivalent tip forces and moment are shown in Figure 2.3.1(a).

The magnitude of 'V_t', 'N_t' can be obtained by resolving the components of the load 'W';

$$V_t = W.\cos\beta \tag{2.18}$$

$$N_t = -W.\sin\beta \tag{2.19}$$

and $$M_t = -W.e \tag{2.20}$$

where 'e' is the eccentricity of the load about the tip.

For any point P(X,Y), one can obtain the following relations (Figure 2.3.1)

$$R = \sqrt{x^2 + y^2} \tag{2.21}$$

$$\phi = \beta - \tan^{-1}(Y/X) \tag{2.22}$$

$$Y_{arc} = R.\phi \tag{2.23}$$

$$Y_{arc(max.)} = R.\beta \tag{2.24}$$

where 'x' and 'y' are measured along the direction shown in

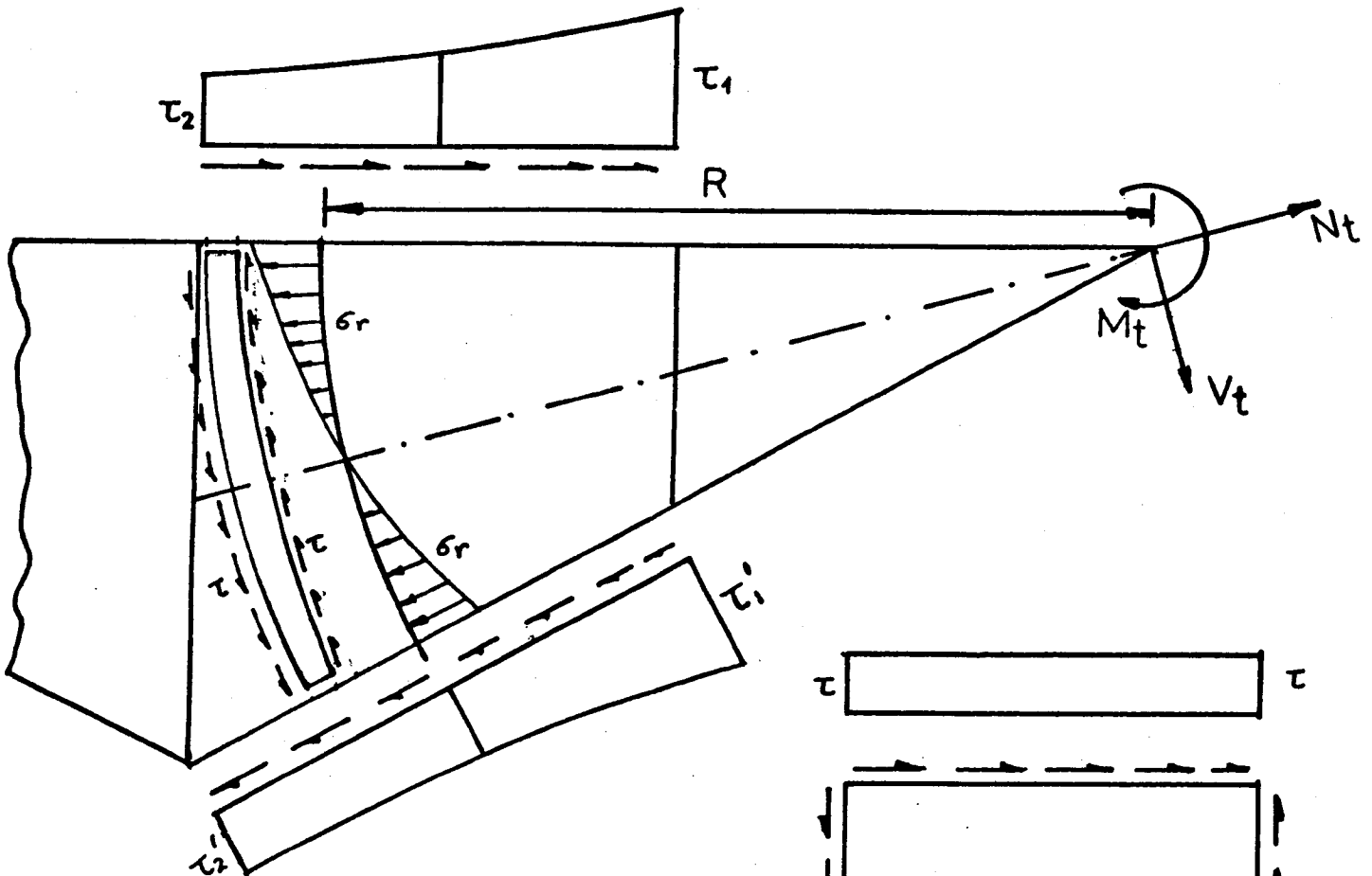

Figure 2.2.4

Shear and radial stress distributions in a tapered panel

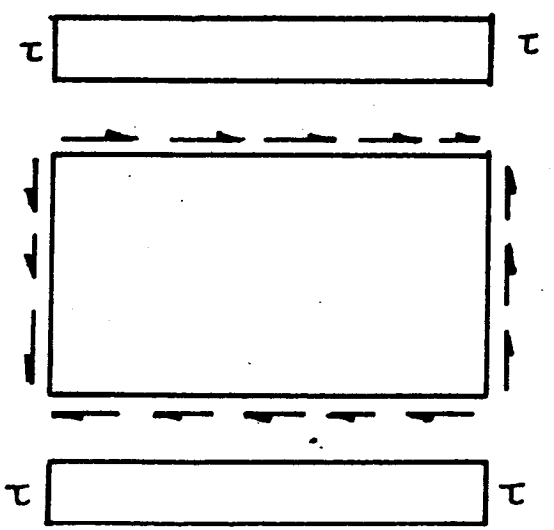

Shear stress distributions in a rectangular panel

Figure 2.3.1(b).

$$A_{arc} = 2(A_f + R.\beta.t) \tag{2.25}$$

$$I_{arc} = 2\left[I_f + A_f(R.\beta + \frac{T}{2})^2\right] + \frac{1}{12}.t(2R.\beta)^3 \tag{2.26}$$

$$\int Y_{arc}.dA_{arc} = A_f(R.\beta + \frac{T}{2}) + t(R.\beta - R.\phi).\frac{(R.\beta + R.\phi)}{2} \tag{2.27}$$

By substituting the values of N_t, V_t, M_t, R, Y_{arc}, A_{arc}, I_{arc}, t and $\int Y_{arc}.dA_{arc}$ in equations (2.16) and (2.17) one can calculate the values of radial and shear stresses at any point.

For the stress system shown in Figure 2.3.3(a) and 2.3.3(b), the first elastic yield load can be calculated by using the Huber von Mises plasticity condition. For uniaxial stress system this plasticity condition reduces to:

$$\sigma_{yw} = \sqrt{(\sigma_r)^2 + 3\tau^2} \tag{2.28}$$

where σ_{yw} is the yield stress of the web material. However, in the case where the flange has a lower yield stress than the web, the first elastic yield may occur in the flange and therefore in place of 'σ_{yw}', σ_{yf} should be used where 'σ_{yf}' is the yield stress of the flange material.

Table 2.3.1 presents the first elastic yield load of the web panels for the beams loaded inside the tip and compares them with the predicted plastic collapse loads (with full plastic moment capacity and reduced plastic moment capacity of flanges). It can be noted that the predicted collapse load of the beams is sufficiently large when compared to the first elastic yield of the webs. However, it is interesting to note that the first elastic yield occurs at the same point (X = 750, Y = 398 (Figure 2.3.1(a))) of the web panels irrespective of the eccentricity of

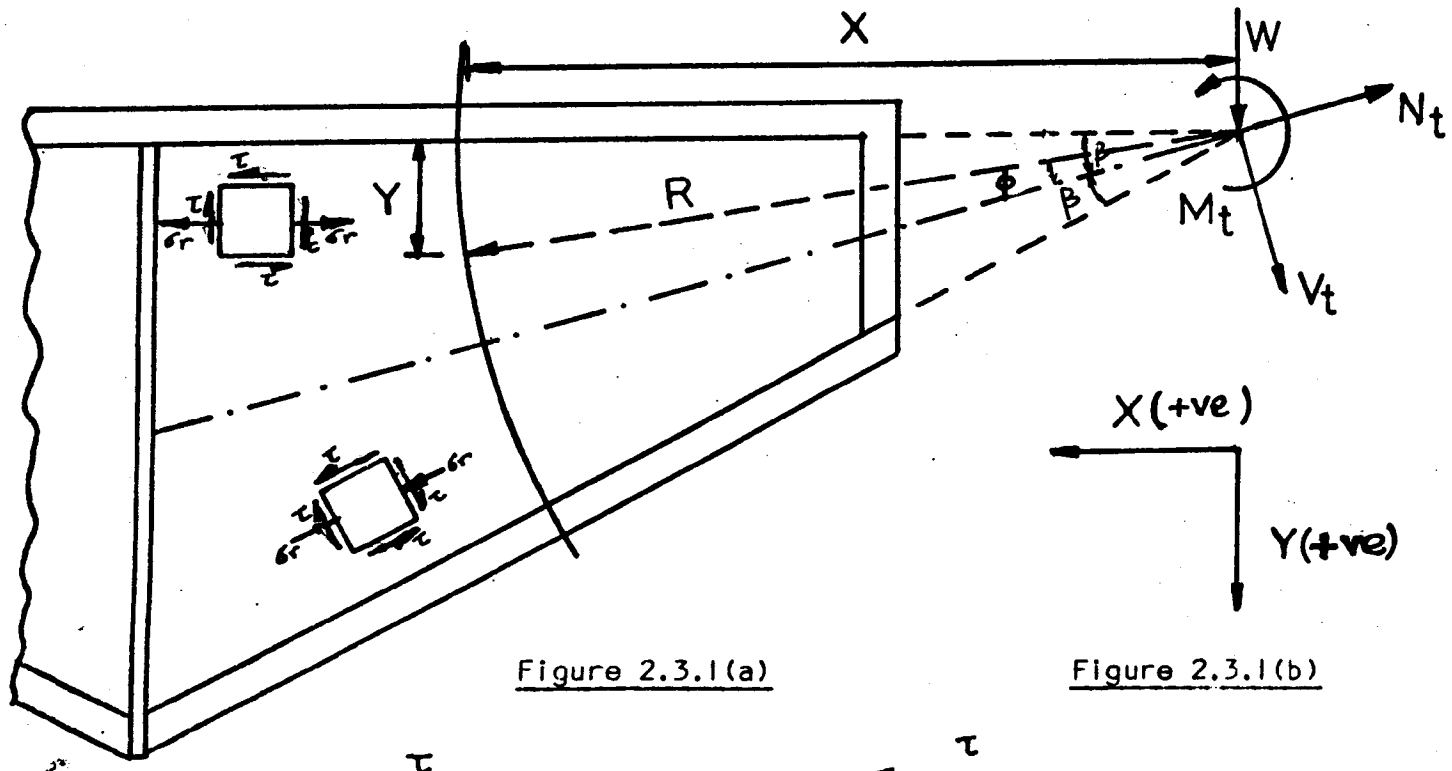

Figure 2.3.1(a)

Figure 2.3.1(b)

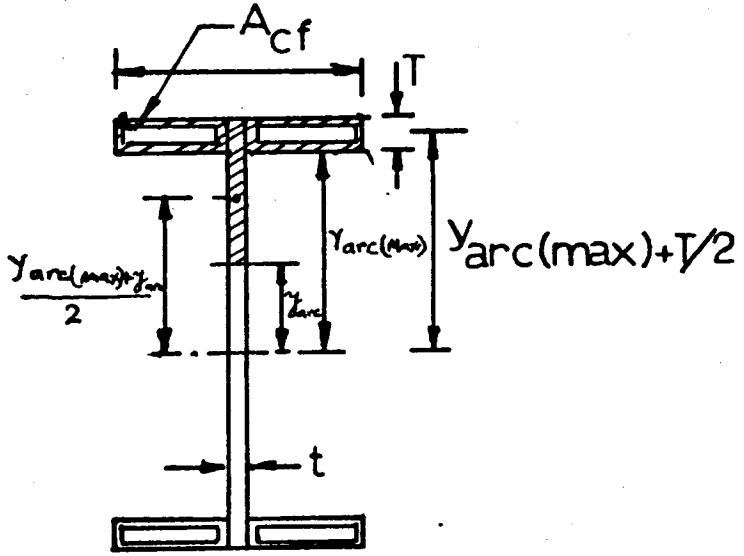

Figure 2.3.2

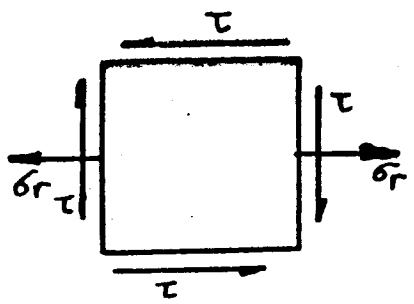

Stress system at top fibre

Figure 2.3.3(a)

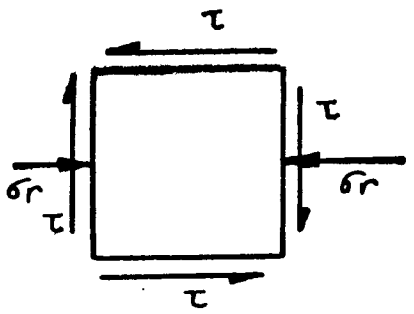

Stress system at bottom fibre

Figure 2.3.3(b)

Girder No.	'X' (Figure 2.3.1a) mm	'Y' (Figure 2.3.1a) mm	(W_{el}) First elastic yield load (KN)	(W_{cl}) Predicted collapse load with M_p (KN)	(W_{c2}) Predicted collapse load with reduced M_p (KN)	$\frac{W_{el}}{W_{cl}}$	$\frac{W_{el}}{W_{c2}}$	Eccentricity 'e' (mm)
10 (A)	750	398	95.5	135.5	127.5	0.70	0.75	545
10 (B)	750	398	145.6	262.2	177.10	0.56	0.82	245
20 (A)	750	398	130.4	178.10	154.0	0.73	0.85	395
20 (B)	750	398	162.0	516.80	181.60	0.31	0.89	95
60 (A)	750	398	109.20	185.5	175.0	0.59	0.62	572
70 (A)	750	398	152.40	270.0	233.0	0.56	0.65	422
70 (B)	750	398	176.30	378.80	257.8	0.47	0.68	272

Table 2.3.1

* calculations for the predicted collapse loads are shown in Chapter Four.

the loads about the tip.

2.4 The first elastic yield load of tapered steel beams loaded outside the tip

The equivalent tip forces and moment for a tapered beam loaded outside the tip are shown in Figure 2.4.1(a). It can be noticed that apart from the reverse direction of the tip moment 'M_t', all the relations obtained in the previous section (2.3) can be used to assess the first elastic yield load. For this case 'M_t' is given by:

$$M_t = +W.e \qquad (2.29)$$

The first elastic yield load of the web panels for the beams loaded outside the tip is presented and is compared with the predicted plastic collapse loads (with full plastic moment and reduced plastic moment capacity of flanges) in Table 2.4.1. It can be noticed that the ratios of the first elastic yield load and the predicted collapse load are much lower when compared to the previous case when the beam was loaded inside the tip. However, it is interesting to note that the first yield occurs at the same point on the web panel, irrespective of the eccentricity of the loads about the tip and the direction of the 'tip-moment'.

2.5 The first elastic yield load of tapered steel beams loaded at the tip

As explained previously the shear stress 'τ_{cr}' becomes zero when the tip moment 'M_t' is zero. In other words, there will be no shear stresses in the webs when the tapered beams are loaded at the tip. The equivalent tip forces and the stresses in the web panel are shown in Figure 2.5.1. The radial stresses are given by:

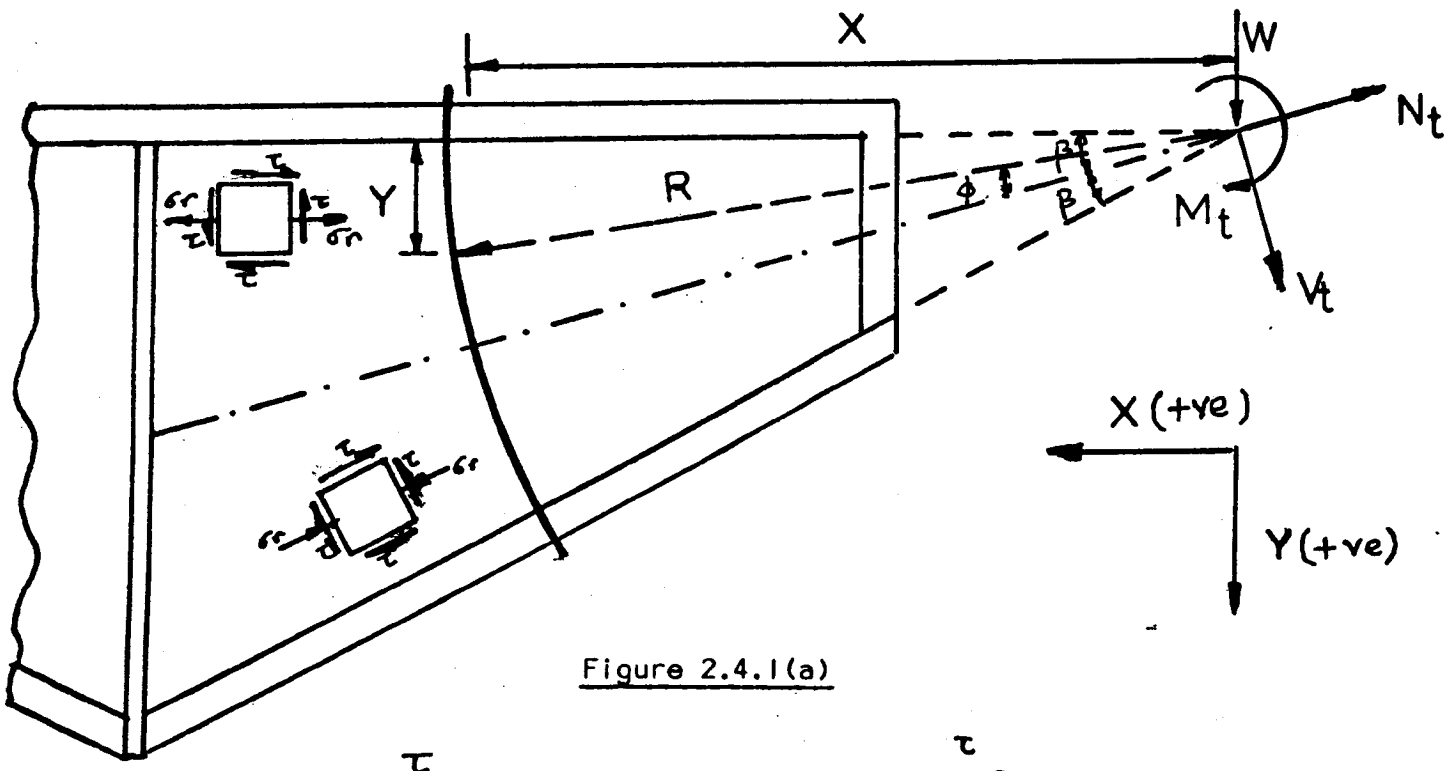

Figure 2.4.1(a)

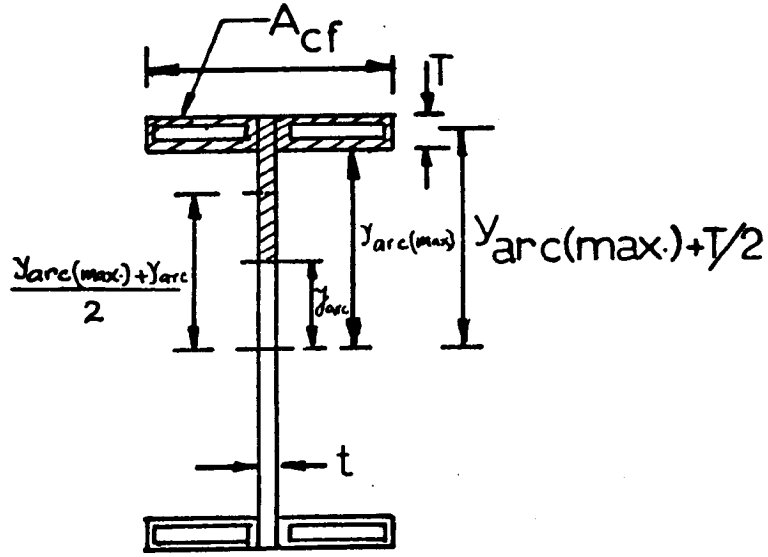

Figure 2.4.2

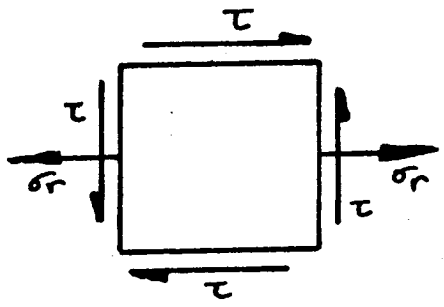

Stress system
at top fibre

Figure 2.4.3(a)

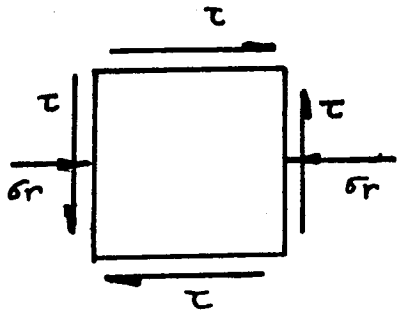

Stress system
at bottom fibre

Figure 2.4.3(b)

Girder No.	'X' (mm)	'Y' (mm)	First elastic yield load (W_{el}) (KN)	Collapse load with full MP (W_{c1}) (KN)	Collapse load with reduced MP (W_{c2}) (KN)	Eccentricity 'e' (mm)	$\frac{W_{el}}{W_{c1}}$	$\frac{W_{el}}{W_{c2}}$
30 (A)	750	398	64.9	162.8	97.5	522	0.40	0.67
30 (B)	750	398	96.6	440.8	133.50	222	0.22	0.72
40 (A)	750	398	75.10	241.0	124.90	372	0.31	0.60
60 (B)	750	398	73.80	201.0	125.00	522	0.37	0.59

Table 2.4.1

* calculations for the collapse loads are shown in Chapter Five.

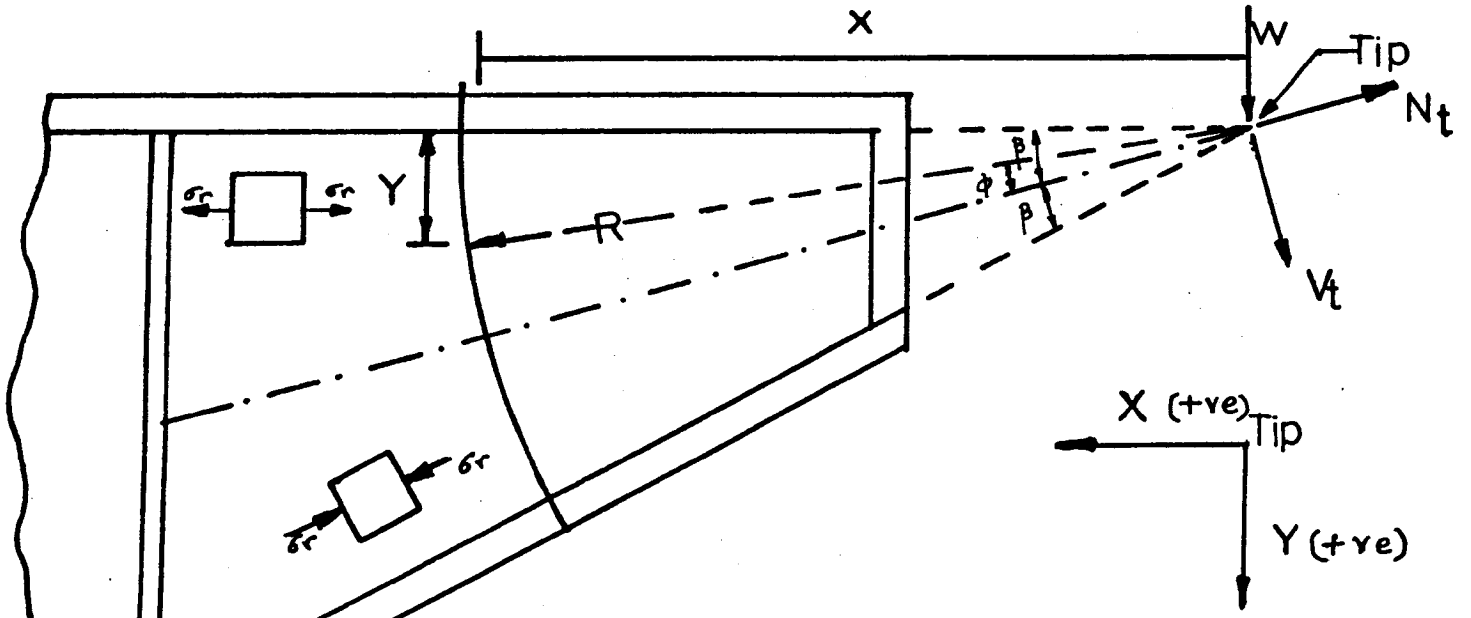

Figure 2.5.1

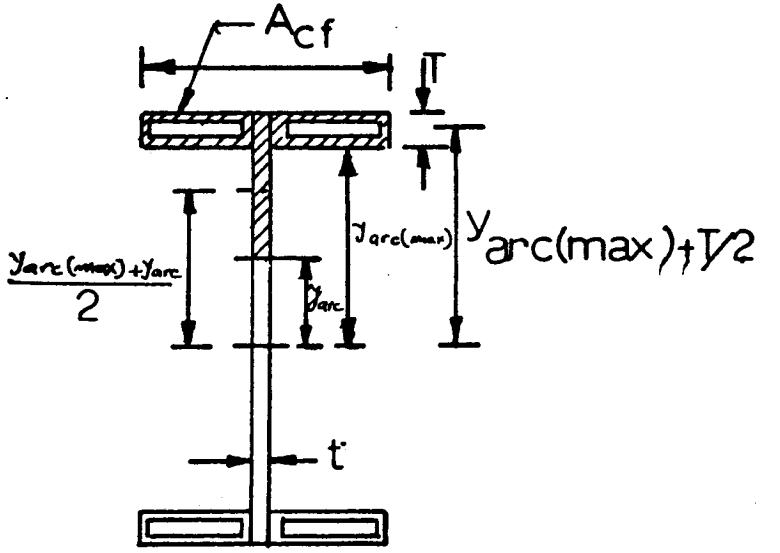

Figure 2.5.2

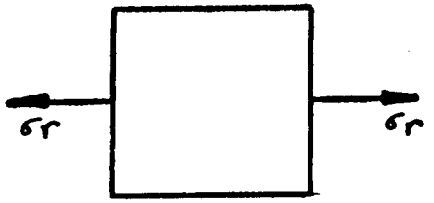

Stress system
at top fibre

Figure 2.5.3(a)

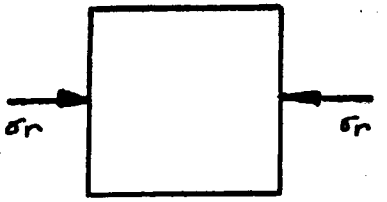

Stress system
at bottom fibre

Figure 2.5.3(b)

Girder No.	'X' (mm)	'Y' (mm)	First elastic yield load (W_{el}) (KN)	Collapse load (W_c) (KN)	$\frac{W_{el}}{W_c}$
40 (B)	750	398	127.10	165.0	0.77
50 (A)	750	398	123.40	162.0	0.76
50 (B)	750	398	123.40	162.0	0.76

Table 2.5.1

* calculations for the collapse loads are shown in Chapter Six.

$$\sigma_r = \frac{N_t}{A_{arc}} + \frac{V_t . R . y_{arc}}{I_{arc}} \qquad (2.30)$$

In the same way as for the previous cases (beams loaded inside and outside the tip), the first elastic yield loads presented in Table 2.5.1 are calculated by using 'Huber von Mises yield criterion'. The comparison between the estimated first elastic yield load of the web panel and the plastic collapse load (based on the plastic yield of the inclined compression flange) is also shown in Table 2.5.1.

However, it is clear that for similar dimensions of the panels, the first elastic yield occurs at a particular point irrespective of the eccentricity of the load about the tip and the magnitude and direction of the 'tip moment'.

2.6 General Conclusions

On the basis of the analyses of the theoretical results, the following conclusions can be drawn:

(i) The equations modified by Davies et al[6] to calculate the radial and shear stresses of tapered beams provide simple solutions to assess the first elastic yield load of tapered web panels.

(ii) With the change in direction of the 'tip moment' the direction of the shear stresses changes.

(iii) The shear stresses in the web panel of beams loaded at the tip are zero.

(iv) The first elastic yield load of the web panels loaded inside, outside and at the tip are 62% to 89%, 59% to 72% and 76% to 77% of the predicted collapse loads respectively.

(v) For a tapered web panel, the first elastic yield occurs at the same point irrespective of the eccentricity of the load

about the tip and the magnitude and direction of the 'tip moment'.

CHAPTER THREE

THE COLLAPSE LOAD BEHAVIOUR OF PLATE GIRDERS - HISTORICAL DEVELOPMENT

3.1 Introductory Remarks

In this chapter a review of the existing methods for the analysis of the collapse behaviour of parallel flange plate girders is presented. Also, significant developments in the design method of predicting the collapse load of plate girders are described and discussed.

3.2 Development in Design Methods and Collapse Load Behaviour of Plate Girders

The shearing stresses in webs of plate girders may be analysed according to the classical beam theory established by Navier and St. Venant. According to this theory the shear force is resisted by the shearing stresses as shown in Figure 3.2.1(a). The principal stresses at the neutral axis are of the same magnitude as the shear stress and act at 45^{o} with the longitudinal axis (Figure 3.2.1(b)). Such a shear carrying action may be called "beam action". To satisfy the condition of small deformations, on which this beam theory is based, transverse stiffeners must be spaced close enough so that instability due to shear is excluded.

Ever since plate girders were introduced, it has been recognised that beam action alone is not the only way that shear can be carried. Extensive discussion of the problem of web stiffening took place near the end of the last century (Ref. 37, 38, 39, 40, 41). Intuition led to the opinion that the action of a plate girder was similar to that of a Pratt-Truss[37].

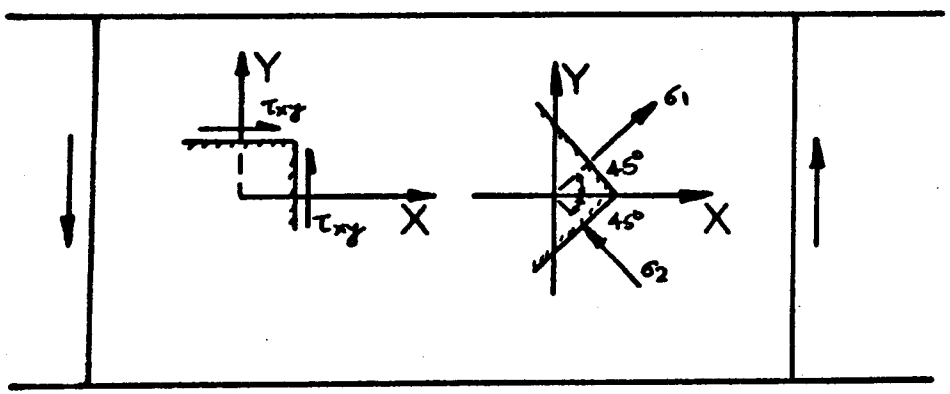

Figure 3.2.1(a)

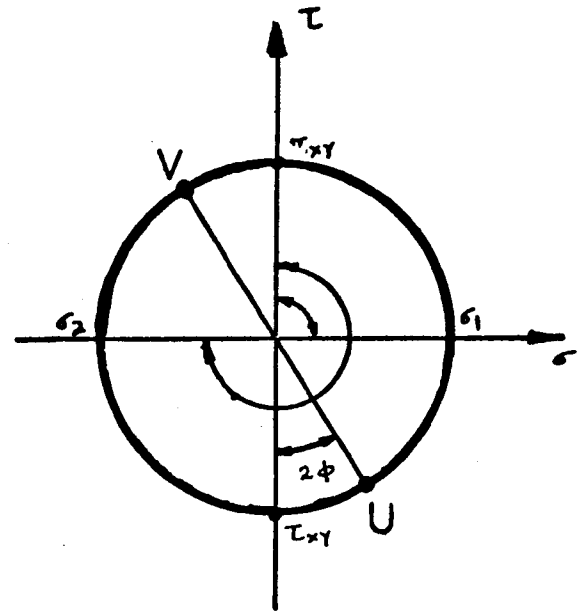

Figure 3.2.1(b)

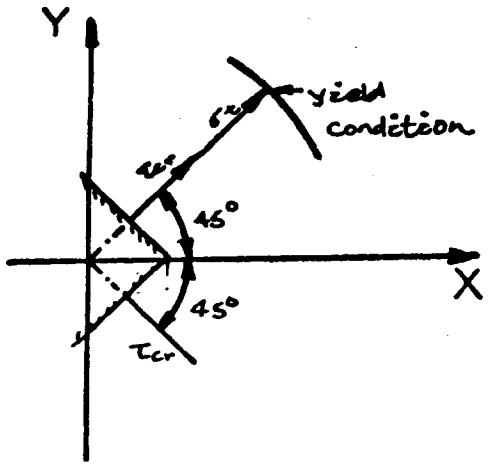

Figure 3.2.1(c)

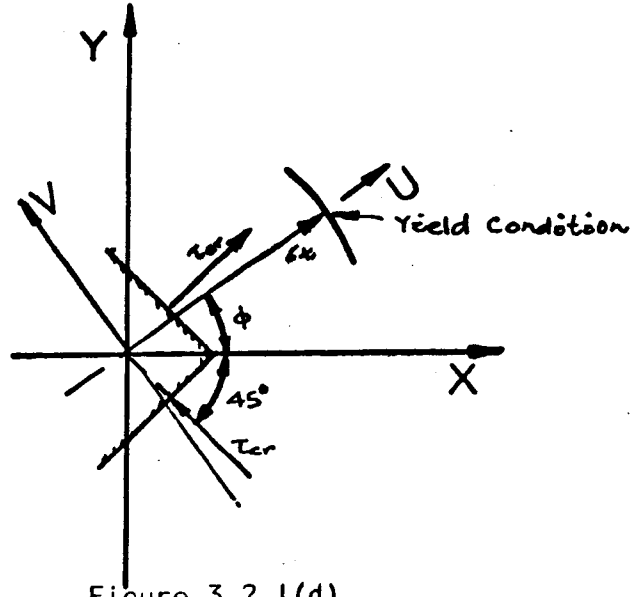

Figure 3.2.1(d)

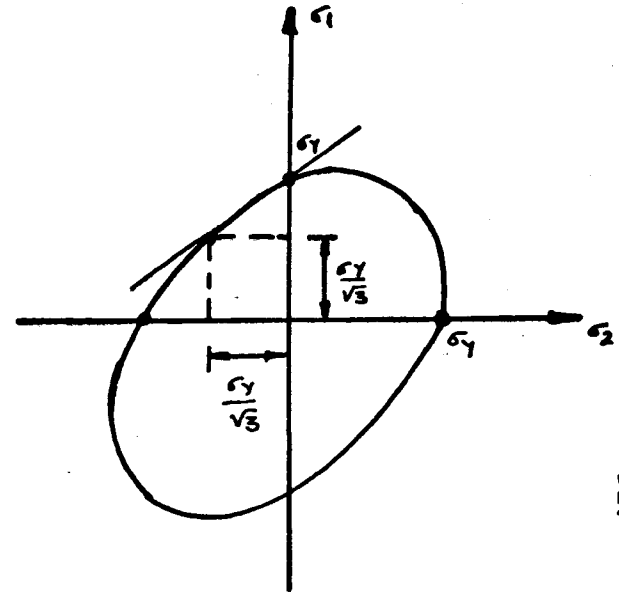

Figure 3.2.1(d)

Turneaure[39] concluded from a girder test "that there is as much reason to suppose that the web stresses follow down the web and up the stiffeners, as in a Howe-Truss, as to suppose that they follow the line of a Pratt-Truss". However, model studies (Ref. 38 and 41) and a girder test (Ref. 40) clearly indicated the importance of the web as a tension element and the stiffeners as compression elements. The goal, at that time, was to assess the nature of the stress-flow in the web rather than to estimate the load carrying capacity. Thus, more qualitative than quantitative results emerged. At the beginning of this century, this led to a rather liberal design of girder webs, with web depths greater than 170 times the web thickness. Meanwhile, a web-buckling theory was developed to determine safe limits for the design of plate girders. A possible truss action was advanced merely to justify a somewhat lower factor of safety against web buckling than that required against other stability cases such as column failure.

It appears that Rode[42] may have been the first to formulate mathematically the effect of a 'tension field' or 'truss action' which develops after the web loses its rigidity due to buckling. He proposed to evaluate its influence by considering a 'tension diagonal' of a width equal to 80 times the web thickness.

With the development of aeronautical science the shear-carrying capacity of membrane-like structures received new attention. The paramount requirement of aircraft design (to minimise the weight of the structure) led to extremely thin webs. Since such structures were built of aluminium alloys, the modulus of elasticity and hence the web buckling stress were

correspondingly lower than for steel girders. By neglecting the beam action completely in such structures and considering the web as a membrane resistant only to tension, Wagner formulated the "Theory of Pure Diagonal Tension".

Although Wagner formulated the theory of pure diagonal tension for thin webs, he did not explain any methods to predict its load carrying capacity. Later Rockey[43, 44, 45] explained the buckling phenomena and its effect on the load carrying capacity of plate girders and showed that the buckling of a plate subjected to shear does not result in immediate failure of the panel, but merely produces a change in the manner in which any additional shear load is carried by the plate. After the plate has buckled, the rigidity of the plate normal to the direction of the principal compressive stresses are equal, but is carried in part by a pure shear action, and in part by truss action as illustrated in Figure 3.2.2. Thus, after buckling has occurred, the principal compressive stresses increase slowly, whilst the principal tensile stresses increase rapidly. These principal tensile stresses, which act along the length of the waves, exert lateral and direct loads upon the flanges which obviously have to be stiff enough to take these loads.

However, later it was realised that the compressive stresses do not increase but remain constant and, once the plate has buckled, any additional load is carried by the tensile membrane stresses developed along the tension diagonal of web.

Although Rockey[45] showed the influence of the flexural rigidity of the flanges on the ultimate load of the plate girders and also demonstrated the 'truss action' forming along the tension diagonal, he did not propose any method for predict-

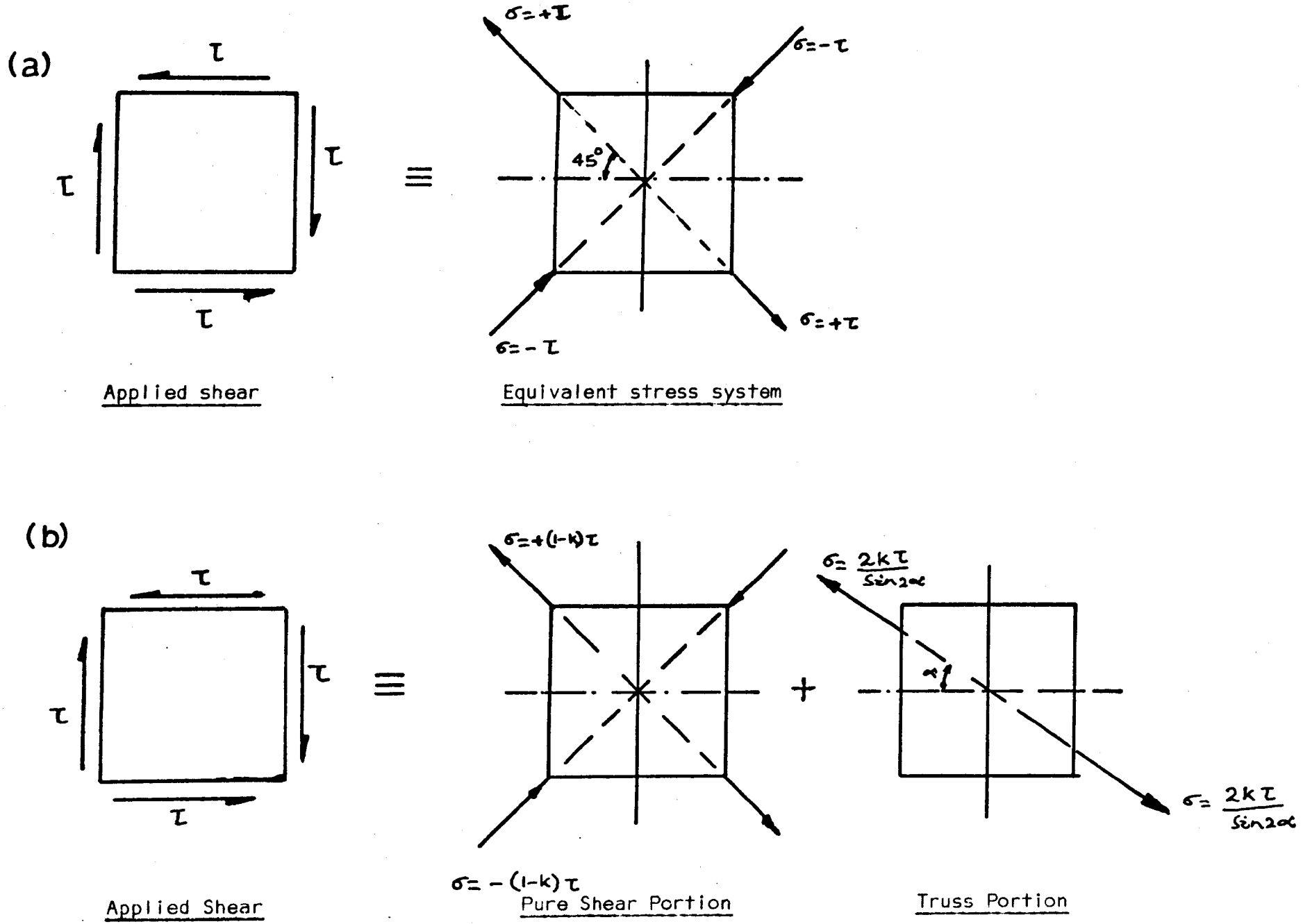

*N.B. - 'K' is a Factor which varies with $\frac{\tau}{\tau_{cr}}$ Ratio.

Figure 3·2·2

ing the failure load of plate girders.

In 1960, Basler and Thurlimann[12, 13, 14] were the first to propose the ultimate load method for predicting the failure load of plate girders. A web plate which is subjected to shear, prior to buckling, develops equal tensile (σ_1) and compressive (σ_2) direct stresses inclined at 45^o and 135^o to the flanges as shown in Figure 3.2.1(b). Once the web plate buckles, it loses the capacity to carry any additional compressive loading. Any additional shear load is carried by tensile membrane stresses 'σ_t' (Figure 3.2.3a). Basler and Thurlimann assumed that the flanges of a conventionally built welded plate girder have so little rigidity in the plane of the web that they cannot effectively resist vertical stresses at its junction with the web and therefore such flanges do not serve as anchors for a tensile stress field. They established that in such a case the girders fail when an 'off diagonal yield band' (EFIH) develops in the web as shown in Figure 3.2.3(a). They also assumed that the stresses in the triangular wedge 'DEF' and 'GHI' remain equal to the critical shear stress 'τ_{cr}' (which causes buckling of the web) and the girder fails with the yield of web material in the region of 'EFIH' caused by the tensile membrane stresses 'σ_t^y' which acts together with the critical shear stresses.

Since the increase in the width of the 'tension field' (s) is gained by virtue of a decrease in the 'inclination of the tensile stress' (ϕ), an optimum value of the tension field contribution 'ΔV_σ' to the shear force 'V_σ' is reached. It was postulated that, at ultimate shear load, the inclination of the tension field is the one that furnishes the greatest total shear

component 'ΔV_σ' of this tension field and can be obtained from the condition - (Figure 3.2.3(a))

$$\frac{d}{d\phi}(\Delta V_\sigma) = \frac{d}{d\phi}(\sigma_t^y . s . t . \sin\phi) = 0 \tag{3.1}$$

which gives:

$$\tan\phi = \sqrt{1 + \alpha^2} - \alpha \tag{3.2}$$

$$\sin\phi = \left[\frac{1}{2} - \frac{\alpha}{2\sqrt{1 + \alpha^2}}\right]^{\frac{1}{2}} \tag{3.3}$$

and

$$\cos\phi = \left[2\sqrt{1 + \alpha^2}\,(\sqrt{1 + \alpha^2} - b)\right]^{-\frac{1}{2}} \tag{3.4}$$

where $\alpha = \frac{b}{d}$ (Figure 3.2.3(a)).

A succession of equal web panels all subjected to the same shear force was assumed as shown in Figure 3.2.4(a). By cutting sections through A-A, B-B and C-C a free body diagram can be obtained as shown in Figure 3.2.4(b), where F_w, F_f and F_s are the forces in the webs, flanges and the stiffener respectively. The flange force changes by amount ΔF_f. By considering the horizontal and vertical equilibrium of forces and moment about O (Figure 3.2.4(b)), one obtains:

$$\Delta F_f = -\sigma_t^y . t . b . \sin\phi . \cos\phi = -\sigma_t^y . t . d . \frac{\alpha}{2\sqrt{1 + \alpha^2}} \tag{3.5}$$

$$V_\sigma = \frac{d}{b} \cdot \Delta F_f = \sigma_t^y . t . d \, \frac{1}{2\sqrt{1 + \alpha^2}} \tag{3.6}$$

As explained before, the ultimate shear load (V_{ult}) is the sum of shear action (τ) and tension field action. Therefore

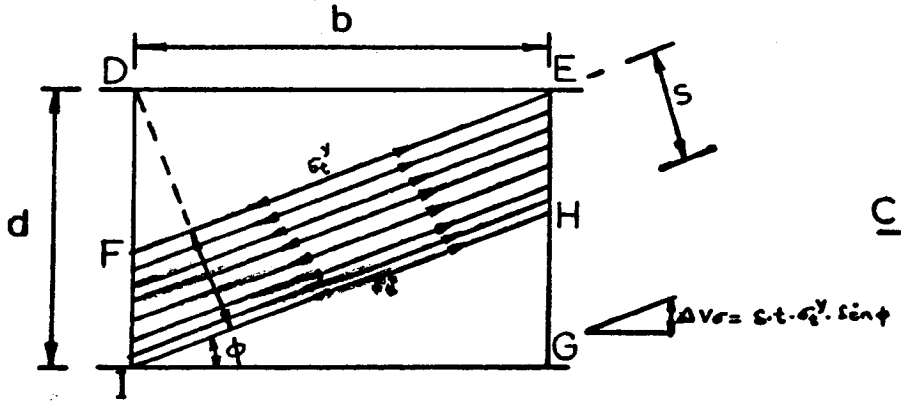

Figure 3.2.3(a)

Ultimate Load Mechanism developed by Basler and Thurlimann

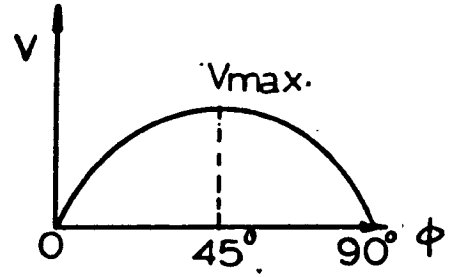

Figure 3.2.3(b)

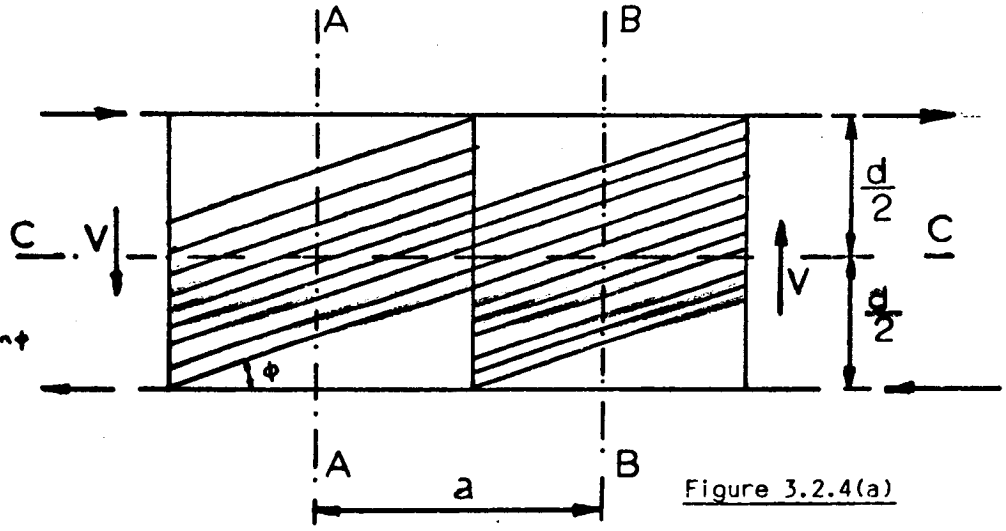

Figure 3.2.4(a)

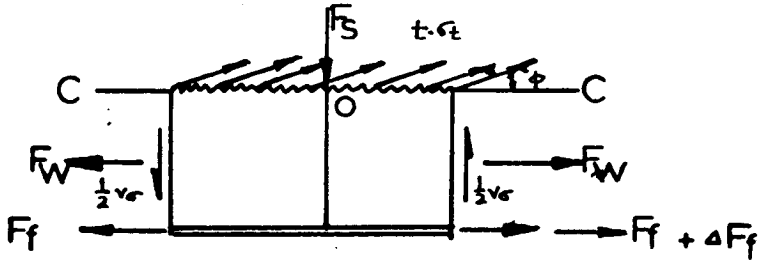

Figure 3.2.4(b)

the ultimate shear load is:

$$V_{ult} = V_{\tau} + V_{\sigma} \tag{3.7}$$

$$V_{ult} = \tau_{cr}.d.t + \frac{t.\sigma_t^{y}.d}{2\sqrt{1 + \alpha^2}} \tag{3.8}$$

where $$\sigma_t^{y} = \sigma_{yw}\left[1 - \frac{\tau_{cr}}{\tau_{yw}}\right] \tag{3.9}$$

$$\tau_{cr} = K.\frac{\pi^2 E}{12(1 - \nu^2)}.\left(\frac{t}{d}\right)^2 \tag{3.10}$$

The values of K are given by:

$$K = 5.35 + 4\left(\frac{d}{b}\right)^2 \text{ for } \frac{b}{d} \geq 1 \tag{3.11}$$

$$K = 5.35\left(\frac{d}{b}\right)^2 + 4.0 \text{ for } \frac{b}{d} \leq 1 \tag{3.12}$$

By making the assumption that σ_t^{y} could be represented by equation (3.9) which does not allow the effect of the inclination of the tensile field, Basler and Thurlimann were able to show that "off diagonal band" would develop at an inclination equal to half the inclination of the web diagonal.

It was pointed out first by Gaylord[15] and later by Fujii[16] that equation (3.8) does not actually represent the true resistance of the Basler model, which was correctly given by equation (3.13)

$$V_{ult} = \tau_{cr}.d.t + \frac{\sigma_{yw}.d.t}{(2\sqrt{1 + \alpha^2} + \alpha)}\left(1 - \frac{\tau_{cr}}{\tau_{yw}}\right) \tag{3.13}$$

Although, Basler's solution gave a new approach to predict the ultimate strength of plate girders, clearly the assumption that the flanges could not withstand any lateral loading imposed

by the inclined tension field was a conservative assumption.

Rockey and Skaloud[17, 18, 21] showed that for plate girders having proportions similar to those employed in civil engineering construction, the flexural stiffness of flanges have a significant effect upon the load carrying capacity of plate girders loaded in shear. They also showed that the girders fail with the formation of a collapse mechanism in which a diagonal strip of the web yields plastically with the development of plastic hinges in the flanges as shown in Figure 3.2.5. They noted that the positions of internal plastic hinges A and A', (Figure 3.2.5) varied with the flange stiffness, the value of 'C' (Figure 3.2.5) increasing from near zero in the case of flexible flanges to approximately half of the width of the panel (0.5b) when the flanges were very stiff.

Rockey and Skaloud[21] considered that the collapse of plate girders could be represented by a two-phase action as shown in Figure 3.2.6(a) and 3.2.6(b). They noted that if the diagonal tension loading is insufficient to develop the plastic hinges in the flanges, then after the web has yielded, any additional load has to be carried by the 'frame-mechanism' as a Vierendeel girder (Figure 3.2.6(b)). However, they restricted their analysis to the beam action shown in Figures 3.2.6(a) and 3.2.7 and assumed that the tensile membrane stress field developed in the direction of the tension diagonal. The value of 'σ_t^y' which causes the web to yield can be computed by using the Von Mises Hencky yield criterion. From the stress conditions shown in Figure 3.2.8(a), 3.2.8(b) and 3.2.8)c), one can obtain:

$$\sigma_\varepsilon = \tau_{cr}.\sin 2\theta_d + \sigma_t^y \qquad (3.14)$$

$$\sigma_\eta = -\tau_{cr}.\sin 2\theta_d \qquad (3.15)$$

$$\tau = \tau_{cr}.\cos 2\theta_d \qquad (3.16)$$

Using the Huber von Mises plasticity condition, the material yields when $\sigma_{mc} = \sigma_{yw}$, where:

$$\sigma_{mc} = \sqrt{\sigma_\varepsilon^2 + \sigma_\eta^2 - \sigma_\eta.\sigma_\varepsilon + 3\tau^2} \qquad (3.17)$$

Substituting the values of σ_ε, σ_η and τ in equation (3.17) and rearranging the terms, one can obtain:

$$\sigma_t^y = -\frac{3}{2}\tau_{cr}.\sin 2\theta_d + \sqrt{\sigma_{yw}^2 + (\tau_{cr})^2\left[(\tfrac{3}{2}\sin 2\theta_d)^2 - 3\right]} \qquad (3.18)$$

The vertical component v_σ of the diagonal stress σ_t^y is given by equation (3.19)

$$v_\sigma = 2.c.t.\sin^2\theta_d\left[-\frac{3}{2}\tau_{cr}.\sin 2\theta_d + \sqrt{\sigma_{yw}^2 + (\tau_{cr})^2\left[(\tfrac{3}{2}\sin 2\theta_d)^2 - 3\right]}\right]$$

... (3.19)

The total shear force (V_{ult}) is equal to the sum of v_σ and the shear force (v_{cr}) necessary to cause the plate to buckle.

$$V_{ult} = v_\sigma + v_{cr}$$

i.e. $$V_{ult} = \tau_{cr}.d.t + 2.c.t.\sin^2\theta_d\left[-\frac{3}{2}\cdot\tau_{cr}\sin 2\theta_d + \sqrt{\sigma_{yw}^2 + (\tau_{cr})^2\left((\tfrac{3}{2}\sin 2\theta_d)^2 - 3\right)}\right] \qquad (3.20)$$

The position of the internal plastic hinge may be obtained

from the beam mechanism shown in Figure 3.2.7, which gives the following relationship between $\frac{c}{b}$ and the plastic moment of resistance of the flanges (M_p):

$$(\frac{c}{b})^3 - (\frac{c}{b})^2 + \frac{4M_p}{b^2.t.\sin^2\theta_d.\sigma_{t_y}} = 0 \qquad (3.21)$$

Although this solution proposed by Rockey and Skaloud was first to demonstrate the influence of flange rigidity upon the width of the 'diagonal' yield band and provided better agreement between the experimental and the predicted collapse loads of plate girders than that provided by the Basler formula, clearly the assumption that the angle of inclination of the tensile band coincides with the inclination of the panel diagonal was a weakness.

Fujii et al[46], in 1969, presented a solution for the ultimate strength of plate girders in which they considered that the web panel fails with the development of a plastic hinge at the central, mid-panel, positions under the action of a uniformly distributed tensile field. Although, like Rockey and Skaloud, Fujii et al recognised the presence of an internal plastic hinge, their solution was limited to only the case of the mid-span hinge position.

Chern and Ostapenko[47], in the same year presented a modified version of the Basler collapse mechanism. The ultimate shear strength of a transversely stiffened plategirder was composed of three contributions: (i) the beam action shear V_τ, (ii) the tension field action shear V_σ, and (iii) the frame action shear V_f. i.e.

$$V_{ult} = V_\tau + V_\sigma + V_f \qquad (3.22)$$

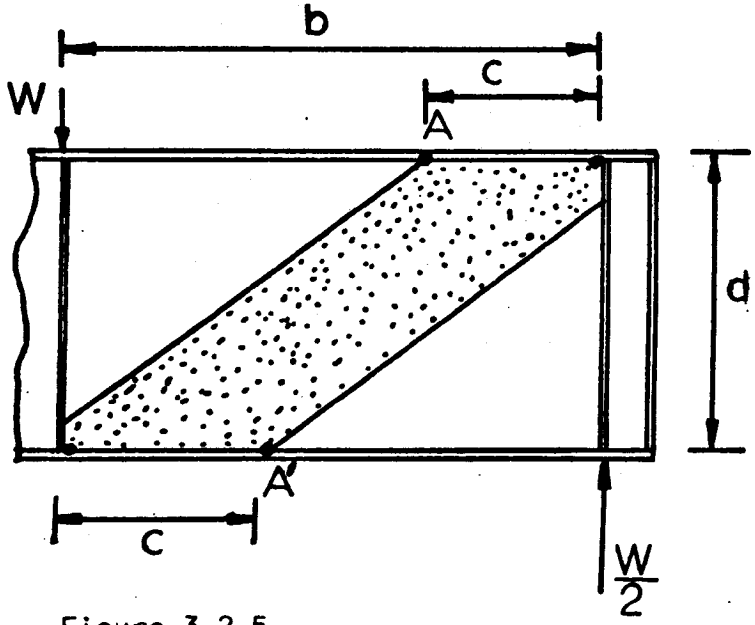

Figure 3.2.5

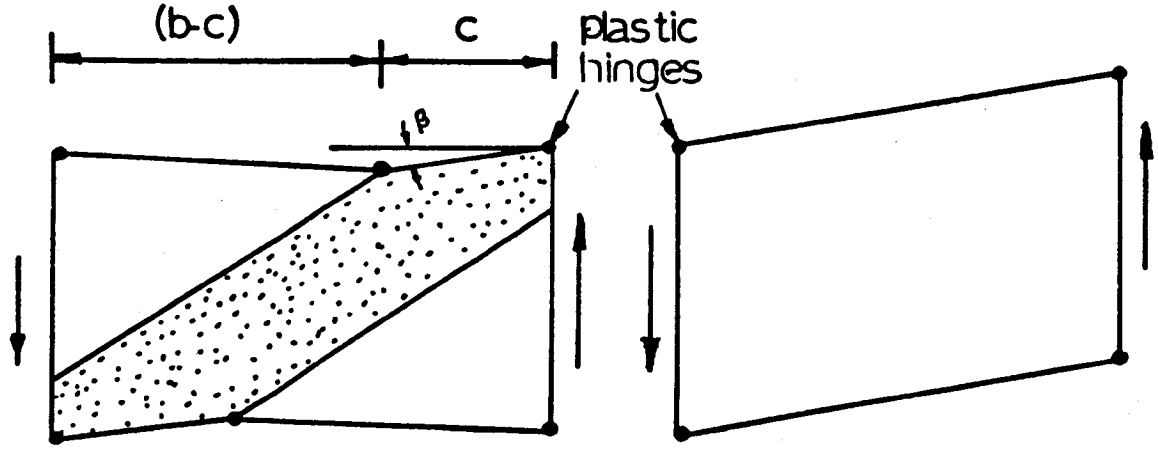

Beam Mechanism

Figure 3.2.6(a)

Vierendeel (Frame) Mechanism

Figure 3.2.6(b)

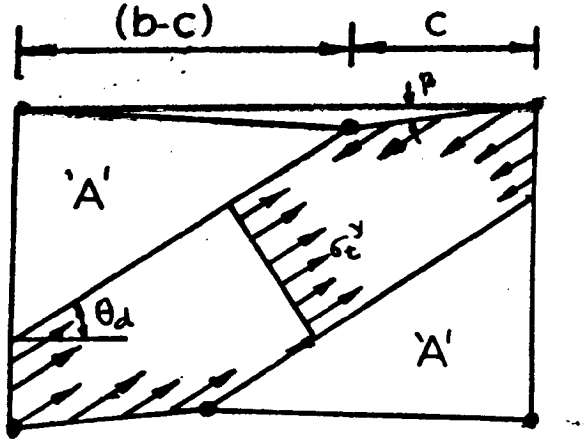

Collapse mechanism proposed by Rockey and Skaloud (ref 21).

Figure 3,2.7

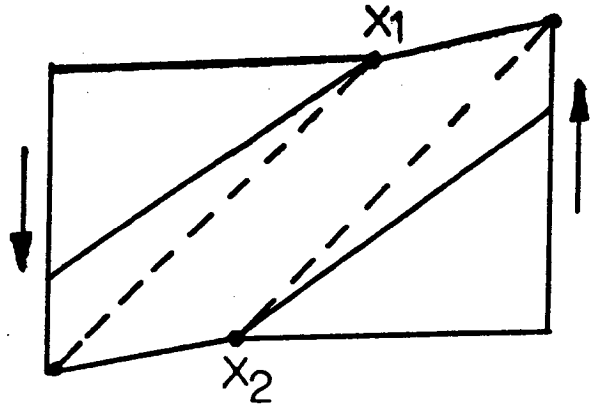

Combined Mechanism

Figure 3.2.6(c)

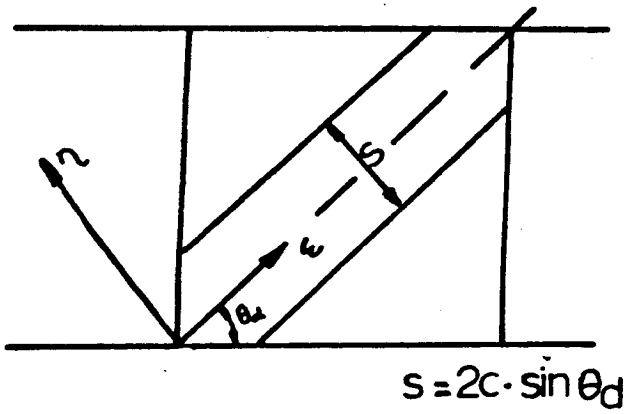

Figure 3.2.8(a)

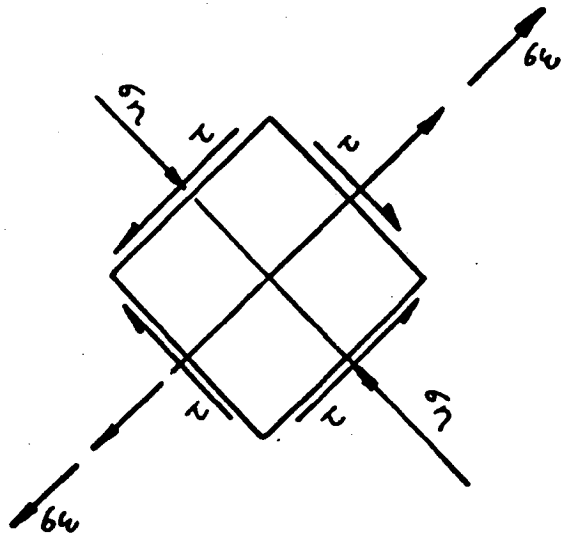

Figure 3.2.8(b)

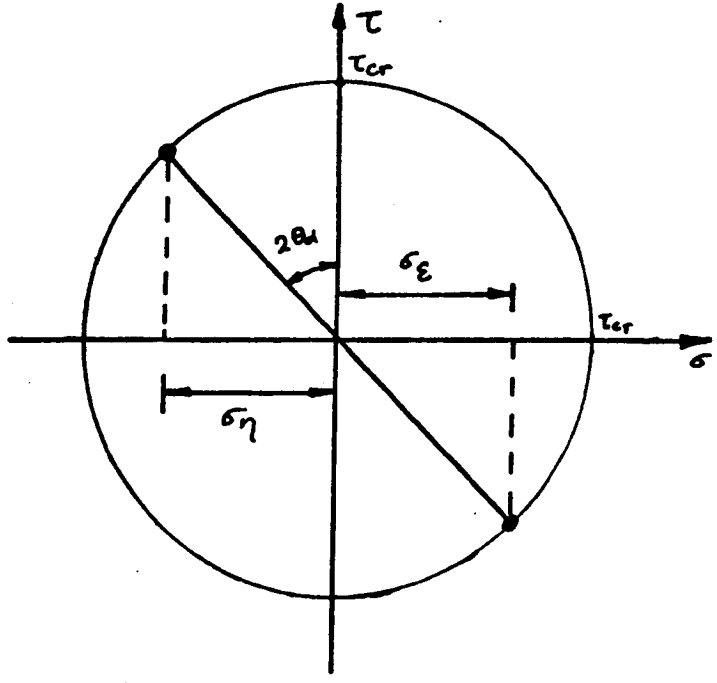

Figure 3.2.8(c)

However, the first two contributions of loads by beam action and tension field action are similar to Basler's[13] considerations.

$$V_\tau = \tau_{cr}.d.t \qquad (3.23)$$

where the values of critical shear stresses were calculated from equation (3.10).

Unlike Basler[13], Chern and Ostapenko assumed that the tensile membrane stresses in the web vary across the section as shown in Figure 3.2.9(a) and 3.2.9(b).

For ease of calculation, they replaced the unevenly distributed stresses in the triangular portions by a uniform stress$\rho.\sigma_t^y$, as shown in Figure 3.2.9(b), where ρ is the parameter depending on the rigidity of the flanges.

The tension field action shear is given by the vertical component of the tension field force (Figure 3.2.9(b)):

$$V_\sigma = \tfrac{1}{2}t.d.\sigma_t^y \left[\sin 2\phi - (1-\rho)\frac{b}{d} + (1-\rho)\frac{b}{d}.\cos 2\phi\right] \qquad (3.24)$$

However, they recognised that the value of 'σ_t^y' varies with the inclination of the yield band (ϕ) and hence they obtained and used the value of ϕ which provides the maximum value of V_σ. This value of ϕ may be defined as ϕ_m and hence:

$$V_\sigma = \tfrac{1}{2}t.d.\sigma_t^y \left[\sin 2\phi_m - (1-\rho)\frac{b}{d} + (1-\rho)\frac{b}{d}.\cos 2\phi_m\right] \qquad (3.25)$$

wherethe values of σ_t^y were calculated from equation (3.18).

The frame mechanism assumed by Chern and Ostapenko is shown in Figure 3.2.10. They considered that each flange behaves like a beam with both ends fixed. The maximum frame action contribution is given by:

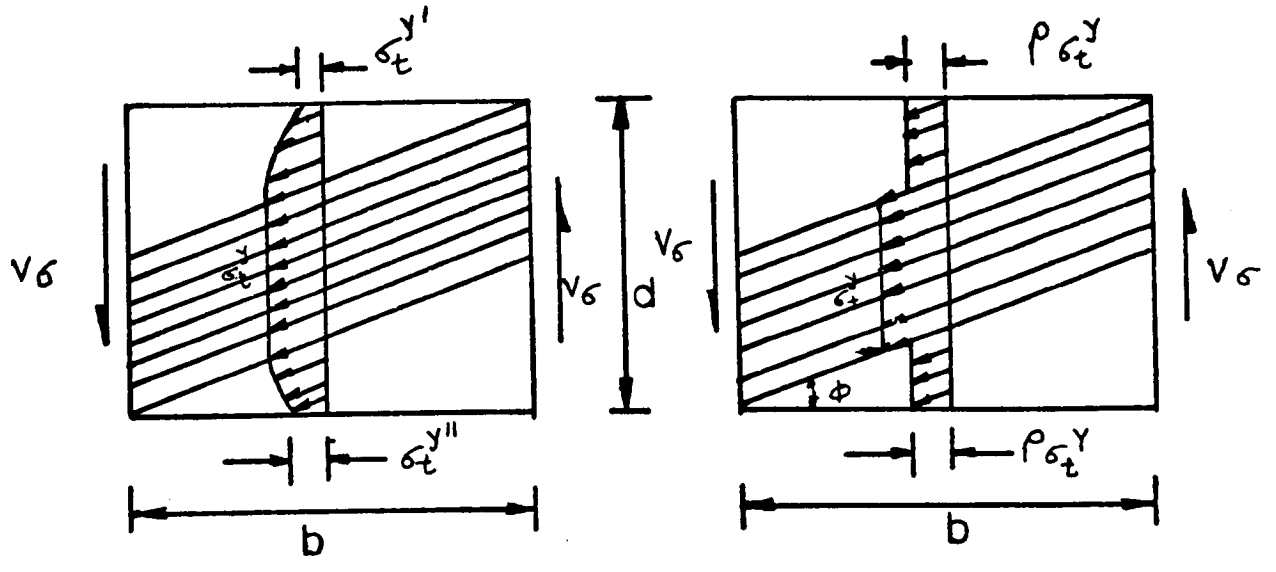

(a) Probable Tension Field
Figure 3.2.9(a)

(b) Equivalent Tension Field
Figure 3.2.9(b)

The Chern and Ostapenko Tension Field Model

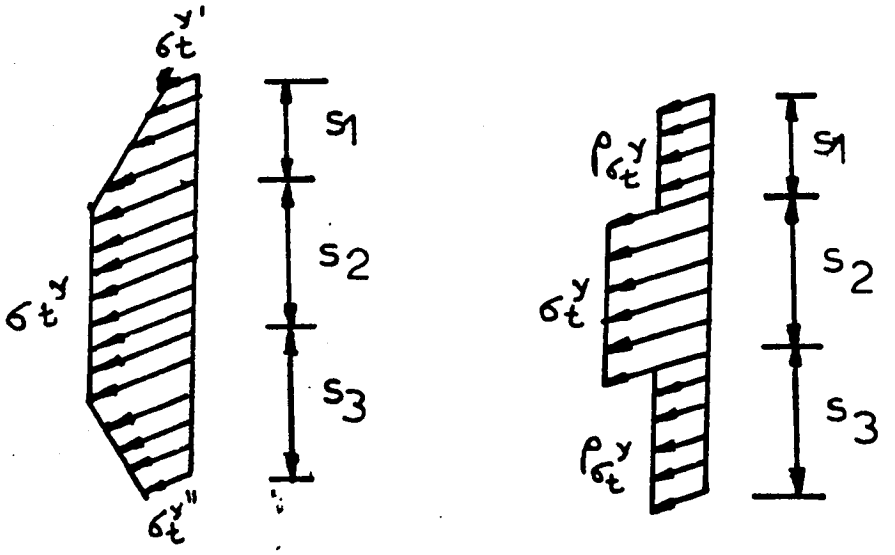

(c) Probable Tension Field
Stress Distribution
Figure 3.2.9(c)

(d) Equivalent Tension Field
Stress Distribution
Figure 3.2.9(d)

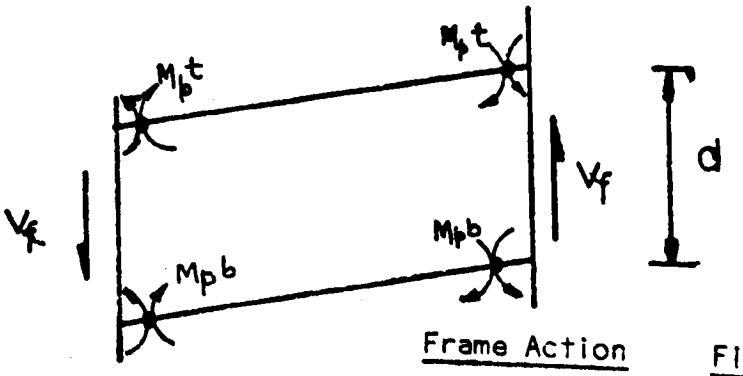

Frame Action

Figure 3.2.10.

$$V_f = \frac{2}{d}\,(M_p^{\,t} + M_p^{\,b}) \qquad (3.27)$$

The final form of the static ultimate shear strength formula can be obtained by adding equations (3.23), (3.25) and (3.27),

$$\text{i.e. } V_{ult} = \tau_{cr}.d.t + \tfrac{1}{2}d.t.\sigma_t^{\,y}\left[\sin 2\phi_m - (1-\rho)\frac{b}{d} + (1-\rho)\frac{b}{d}\cdot\cos 2\phi_m\right] + \frac{2}{d}\,(M_p^{\,t} + M_p^{\,b}) \qquad (3.28)$$

Although Chern and Ostapenko demonstrated quite clearly that the inclination of the yield band varies with the panel dimensions and the buckling stress (τ_{cr}) of webs, they ignored the formation of the internal plastic hinges in the flanges.

Komatsu[24] in 1971 studied the collapse behaviour of plate girders stiffened by transverse and longitudinal stiffeners, loaded in shear. The collapse mechanism proposed by him is shown in Figure 3.2.6(c). He concluded that a pure shear loading caused various failure modes which were chiefly dependent on the relation between the slenderness of web and the strength of smaller flange. Although his solution recognised the presence of internal plastic hinges and that the inclination of the tensile membrane field varied with the flange and panel properties, it was based on a study of elastic shear deformations.

In 1973, Calladine[25] presented a plastic theory for the collapse of plate girders under combined shearing force and bending mement. He considered a model of a typical panel of a plate girder restrained against lateral buckling and subjected to a shear load 'Q' and a couple 'M' as shown in Figure 3.2.11. As the value of 'Q' increases the thin web eventually buckled and the 'tension field' developed along the diagonal BD. He

assumed that the action of the web having negligible buckling resistance could be represented by a series of parallel tendons and proposed that the panel fails when the web yields between the two inclined lines 'DE' and 'BF' with the formation of plastic hinges in the flange at these points (Figure 3.2.12(b)). He assumed that the zone 'J' and 'K' (Figure 3.2.12(a)) may either be unbuckled or elastically buckled; but since they do not undergo changes in strain during rotation of the plastic hinges they can be idealised as 'rigid' in a plastic collapse. He showed that the position of the plastic hinges and the inclination of the tensile membrane stress field varied with flange stiffness. He also showed that for a thick web which yielded before it buckled, the failure would occur because the web yields and simultaneously with this plastic hinges develop at the corners of the panel.

As explained previously, Rockey and Skaloud[21] located the position of the internal plastic hinge 'E' by analysing the plastic collapse of the flange 'AB' as a beam and then found the shear load 'Q' by resolving the forces in the web across the section X-X (Figure 3.2.12(a)). Calladine pointed out that this assumption of a full plastic moment at A, corresponding to rotation of a plastic hinge, was geometrically incompatible with the fact that the region 'J' was not straining plastically. Therefore equation (3.21) presented by Rockey and Skaloud is not valid for the calculation of the position of plastic hinges.

However, Calladine did not extend his solution for the practical engineering cases where the webs may have significant load carrying capacity before it buckled.

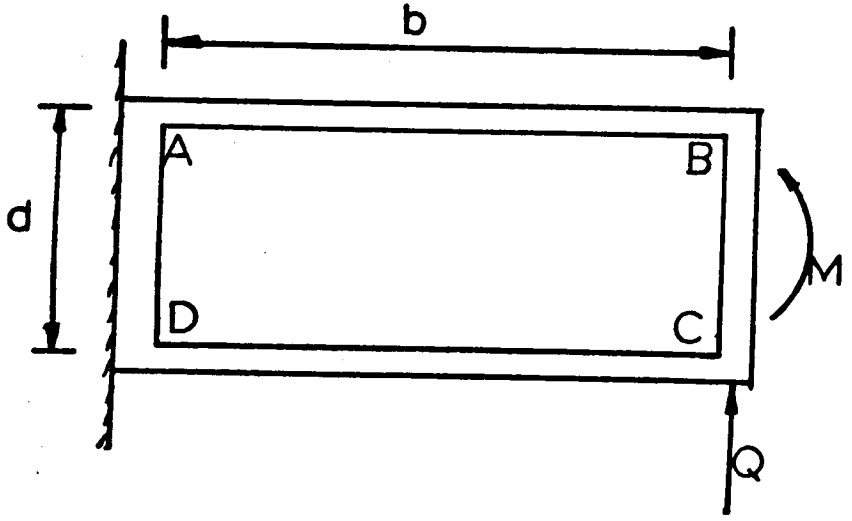

Figure 3.2.11

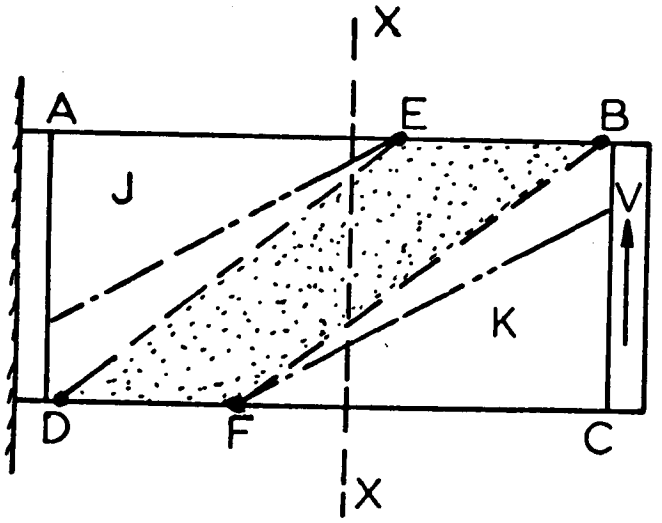

Figure 3.2.12(a)

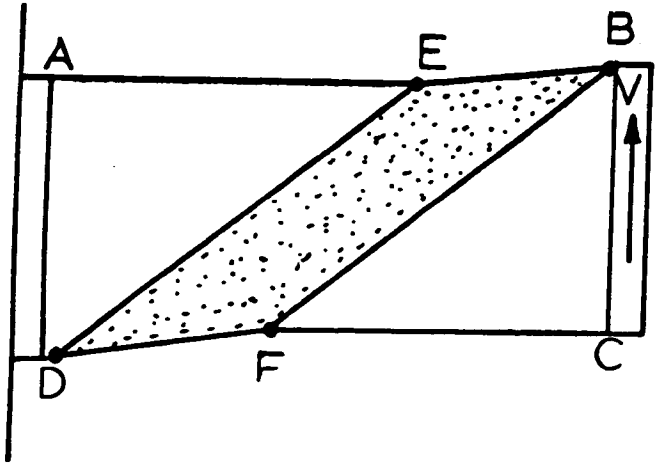

Figure 3.2.12(b)

Porter, Rockey and Evans[26], in 1975, presented an ultimate load method of design for predicting the collapse load of conventional plate girders having webs reinforced by both longitudinal and transverse stiffeners. Their proposed collapse mechanism which provides identical lower and upper bound solutions is shown in Figure 3.2.13(c).

They divided the loading of the panel into three phases (Figures 3.2.13(a), 3.2.13(b) and 3.2.13(c)), which are:

Phase : 1

As explained previously, prior to buckling, there will be a uniform shear stress in a perfectly flat web plate and the principal tensile and compressive stresses of equal magnitude 'τ' will act at 45^{o} and 135^{o} to the flange (Figure 3.2.1(b)). This stress system exists until the shear stress reaches the value of critical shear stress (τ_{cr}).

For a simply supported rectangular plate, the value of 'τ_{cr}' may be calculated from equations (3.10), (3.11) and (3.12).

Phase : 2 POST BUCKLED BEHAVIOUR

Once the shear stress (τ) reaches the value of critical shear stress (τ_{cr}), the panel cannot sustain any increase in the compressive stress and it buckles. After the panel has buckled any additional load is supported by the tensile membrane stress 'σ_{t}' (Figure 3.2.13(b)) which develops along the tension diagonal. This membrane stress 'σ_{t}' imposes a lateral thrust on the flanges and under this action, the flanges clearly bend inward (Figure 3.2.13(b)).

Phase : 3 ULTIMATE BEHAVIOUR

With a further increase of load, a stage is reached where the tensile membrane stress (σ_{t}^{y}) together with the critical shear

stress (τ_{cr}) cause yielding in the web. The panel fails when the plastic hinges in the flanges have formed which together with the yield zone 'WXYZ' make up a plastic mechanism (Figure 3.2.13(c)).

Because the inclined membrane stress field having uniform magnitude acts throughout the zone 'WXYZ' (Figure 3.2.14(a)), the region 'WXYZ' may be considered to be cut out from the web plate and its action upon the flanges and the adjacent web material can be replaced by the inclined membrane stresses as shown in Figure 3.2.14(a). The failure load can then be determined by considering the collapse mechanism developed in 'Phase 3'.

Upper bound (Mechanism) Solution

Porter et al considered a particular case of pure shear with identical flanges where 'ct' and 'cc' were equal. In that case, however, the rotations of the plastic hinges at W, X, Y and Z will also be equal. Clearly the displacement of the web section 'WZ' is zero and hence the stresses acting on section 'WZ' do no work. The virtual work done by σ_t^y acting on the tension and compression flanges will be equal and of opposite sign and hence will be cancelled. Other work done is:

(i) The internal virtual work done by 'σ_t^y' acting on the web section 'XY' will be

$$= t.\sigma_t^y(YP)\sin\theta.(c\phi)$$

where ϕ = rotation of the plastic hinges

$$(YP) = c.\sin\theta + (d - b\tan\theta).\cos\theta \qquad (3.29)$$

(ii) The internal virtual work done due to rotations at the plastic hinges will be equal to:

$$M_p(\phi + \phi + \phi + \phi) = 4M_p\phi$$

Therefore the total internal virtual work done will be equal to:

$$t.\sigma_t^y\ (YP).\sin\theta.(c\phi) + 4M_p\phi$$

and the external work done will be equal to:

$$V^m_{ult}.(c\phi)$$

By equating the external and internal work done and substituting the value of (YP) from equation (3.29) the following relationship can be obtained:

$$V^m_{ult} = \frac{4M_p}{c} + t.\sigma_t^y.c.\sin^2\theta + t.\sigma_t^y.d\left[\cot\theta - \frac{b}{d}\right]\sin^2\theta \quad (3.30)$$

The ultimate load will be equal to the load 'V^m_{ult}' carried by the membrane field and the flanges plus the shear load which causes buckling:

$$V_{ult} = V^m_{ult} + \tau_{cr}.d.t \quad (3.31)$$

$$\therefore V_{ult} = \frac{4M_p}{c} + t.\sigma_t^y.c.\sin^2\theta + t.\sigma_t^y.d(\cot\theta - \cot\theta_d)\sin^2\theta + \tau_{cr}.d.t \quad \ldots \quad (3.32)$$

where M_p is the full plastic moment capacity of the flanges.

θ is the inclination of the tensile membrane stress field 'σ_t^y'.

and θ_d is the inclination of the panel diagonal.

Since the internal plastic hinges occur at the point of maximum bending moment where the shear is zero, the positions of W and Y can be determined by considering the free body diagrams of the beam sections W-X and Z-Y, and taking moments about the position X and Z respectively;

$$c(t.\sigma_t^y)\ \sin^2\theta.\frac{c}{2} = 2M_p \qquad (3.33)$$

$$\text{i.e.}\quad c = \frac{2}{\sin\theta}\cdot\sqrt{\frac{M_p}{t.\sigma_t^y}} \qquad (3.34)$$

Equation (3.34) holds for all positive values of 'σ_t^y' and for all values of 'c' within the range of $0 < c < b$.

By substituting the value of M_p from equation (3.33) into equation (3.32) the following relationship can be obtained:

$$V_{ult} = 2.c.t.\sigma_t^y.\sin^2\theta + t.\sigma_t^y.d.\sin^2\theta\ (\cot\theta - \cot\theta_d) + \tau_{cr}.d.t \qquad \ldots\ (3.35)$$

Lower bound (Equilibrium) Solution

Consider a section 'W-Y' passing through the two internal plastic hinges as shown in Figure 3.2.14(b) which also shows the internal and external forces acting in the post-buckled range.

To satisfy the vertical equilibrium of forces, the following equation can be obtained:

$$F_s.\sin\theta = V_{ult}^m = V_{ult} - V_{cr}$$

where $F_s = t.\sigma_t^y.(WR)$

and $(WR) = 2.c.\sin\theta + (d - b\ \tan\theta).\cos\theta$

therefore by substituting the values of 'F_s' and 'V_{cr}' one can obtain:

$$V_{ult} = 2.c.t.\sigma_t^y.\sin^2\theta + t.\sigma_t^y.d.\sin^2\theta\ (\cot\theta - \cot\theta_d) + \tau_{cr}.d.t \qquad \ldots\ (3.36)$$

It can be seen that the equations (3.35) and (3.36) obtained for the ultimate load from an upper bound and a lower bound

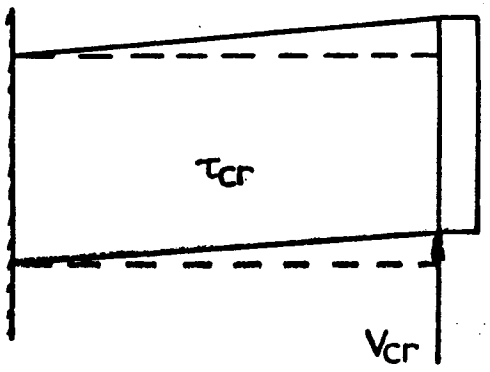

Phase : 1

Figure 3.2.13(a)

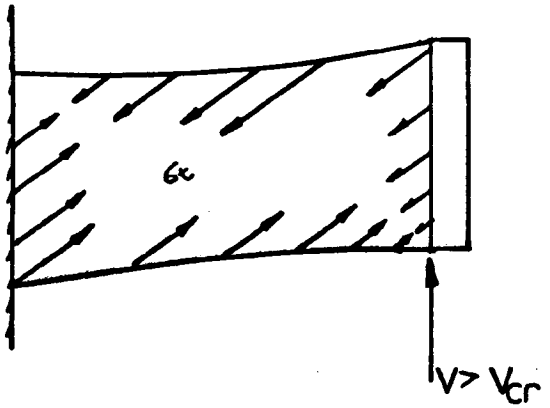

Phase : 2

Figure 3.2.13(b)

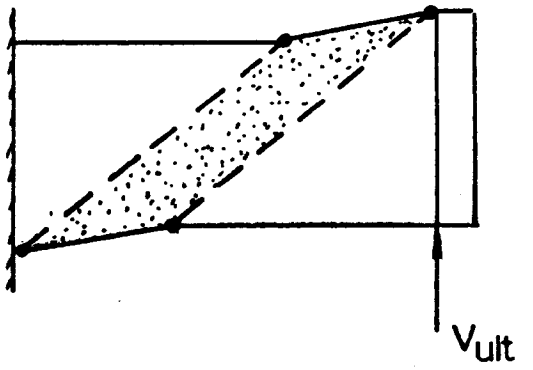

Phase : 3

Figure 3.2.13(c)

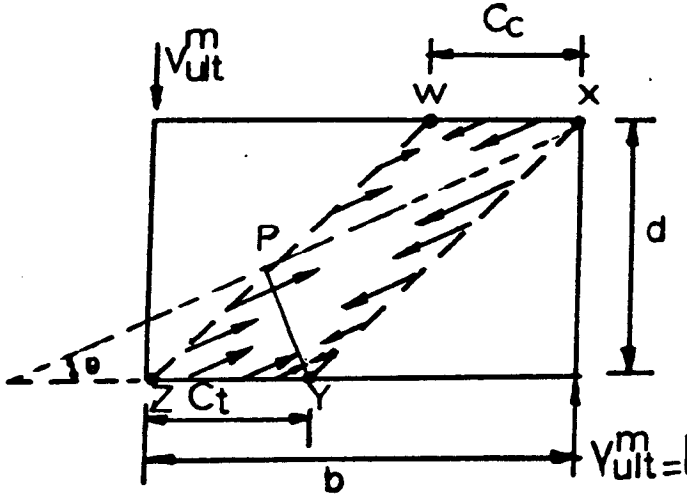

Figure 3.2.14(a)

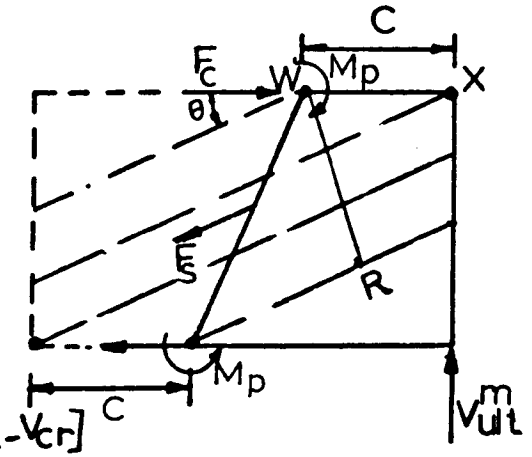

Figure 3.2.14(b)

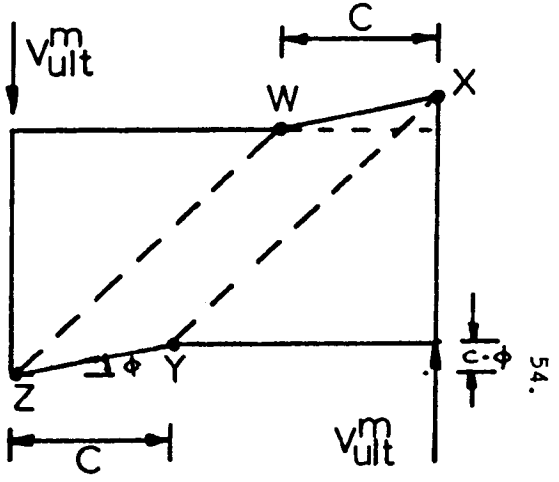

Figure 3.2.14(c)

solutions are identical.

Porter et al showed that the extent and inclination of the tensile membrane stress field is greatly influenced by the flange rigidity. They also showed that many of the existing solutions (for the ultimate load of plate girders) are contained as special cases of their solution. Their solution not only provided very good agreement between the predicted and experimental collapse loads, but also gave good agreement between predicted and experimental plastic hinge positions.

Although the work of Porter et al is confined to a study of the method of predicting the failure load of panels loaded mainly in shear, it established a new and unifying method of predicting the failure load of webs loaded in shear and also is capable of predicting accurately the overall collapse behaviour of transversely and longitudinally stiffened panels loaded in shear.

However, recently in March 1978, Rockey et al[27], in addition to their previous work[26], presented a design method which is applicable to both symmetrical and unsymmetrical plate girders, reinforced by both transverse and longitudinal stiffeners and subjected to the combined action of bending moment and shear force.

CHAPTER FOUR

THE COLLAPSE MODE OF FAILURE OF TAPERED BEAMS LOADED INSIDE THE TIP

4.1 Introductory Remarks

In this chapter a plastic collapse mode of failure for tapered steel beams loaded inside the tip is presented which gives an identical collapse load whether determined from an upper bound or a lower bound solution. The effect of the axial forces on the full plastic moment capacity of flanges is considered and the collapse loads are predicted using these reduced values of plastic moment. Finally, the theoretical results are described and discussed and conclusions are drawn.

4.2 Possible Modes of Failure

The possible collapse modes of failure of tapered beams loaded inside the tip are divided into three phases which are similar to the loading phases considered by Porter, Rockey and Evans[26] for parallel flange plate girders.

Phase : 1 PURE SHEAR BEHAVIOUR

Because the buckling load of the tapered panel is not significant in comparison with the collapse load of the beam, and as there is very limited information available to assess the buckling load of the tapered web panel, it was decided to consider the tapered panel as an equivalent rectangular panel (as shown in Figure 4.2.1(a)) in order to assess the buckling load. Although it is shown in Chapter Two that in comparison with a rectangular panel the shear stress distribution in a tapered panel is different, it is assumed that for an equivalent rectangular panel considered in this chapter, the shear stress

distribution is similar to a rectangular plate.

For a perfectly flat rectangular web plate, there will be a uniform shear stress throughout the panel prior to buckling. A principal tensile stress (σ_t) and a principal compressive stress (σ_c) of magnitude 'τ' will act at 45^o and 135^o respectively to the horizontal (Figure 4.2.2). This stress system which exists for the loading below the critical shear stress 'τ_{cr}' is known as the state of pure shear behaviour.

Although the torsional rigidity of the Rectangular Hollow Section used for the flanges is higher than the rectangular flange plates normally used, it is nevertheless assumed that the web is simply supported on all edges and the value of critical shear stress is calculated using equations (4.1), (4.2) and (4.3) for equivalent rectangular plates. The depth of the panel indicated in these equations is the average depth of the tapered panel.

$$\tau_{cr} = \frac{K.\pi^2.E}{12(1-\nu^2)\,(d/t)^2} \qquad (4.1)$$

where the value of 'K' for simply supported edge conditions is given by the following equations.

$$K = 5.35 + 4\,(\frac{d}{b})^2 \quad \text{if } \frac{b}{d} > 1.0 \qquad (4.2)$$

$$K = 5.35\,(\frac{d}{b})^2 + 4.0 \quad \text{if } \frac{b}{d} < 1.0 \qquad (4.3)$$

Clearly the values obtained for the critical shear stress from the above equations is conservative. However, the buckling load of the tapered panel can be assessed more accurately by using the corresponding value of 'K' analysed by Cook and

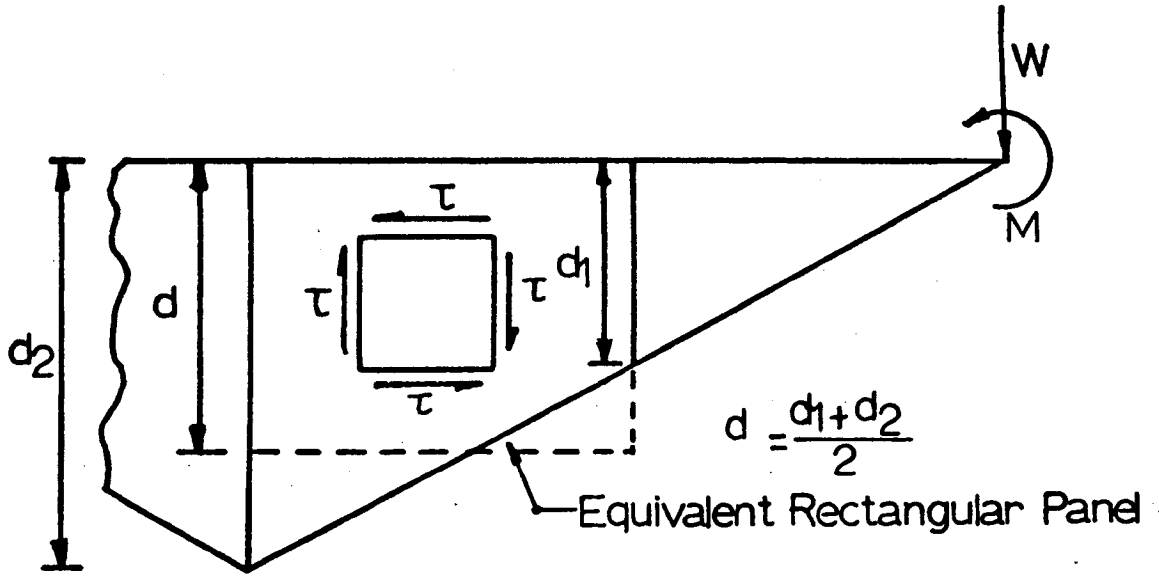

Phase : 1 $\tau < \tau_{cr}$ Figure 4.2.1(a)

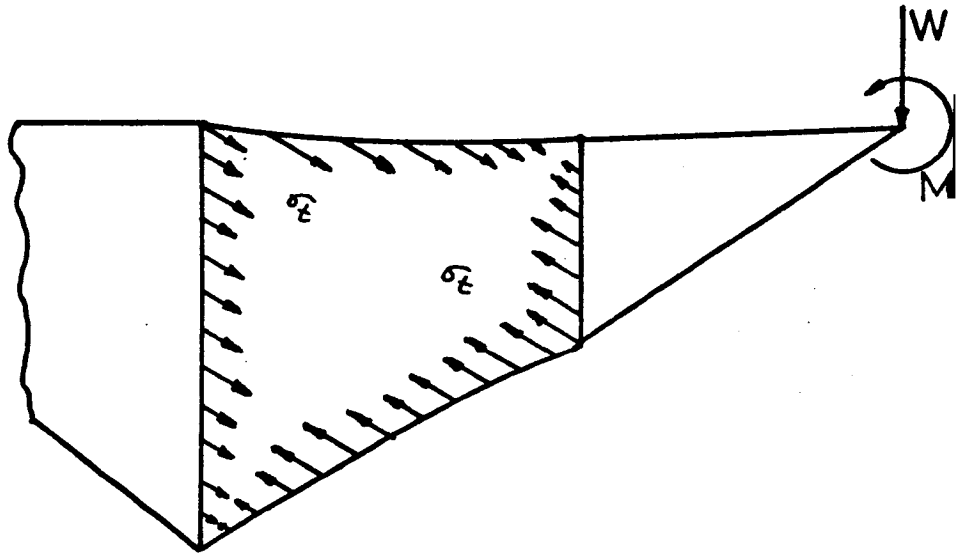

Phase : 2 $\tau \geq \tau_{cr}$ Figure 4.2.1(b)

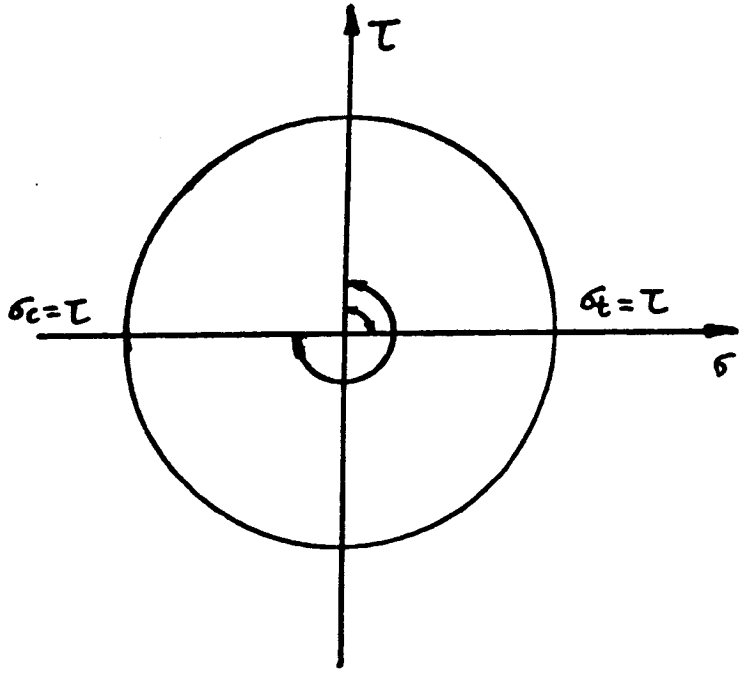

Figure 4.2.2

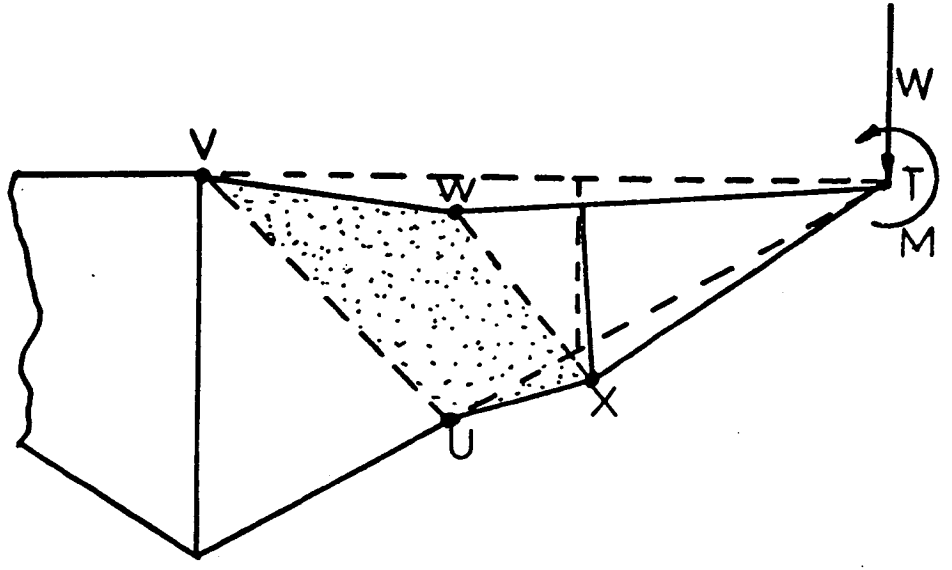

Phase : 3 Figure 4.2.1(c)

Rockey[48] or El-Gaaly[49].

Phase : 2 POST BUCKLED BEHAVIOUR

Once the value of critical shear stress is reached, the panel cannot sustain any increase in the compressive stress and it buckles. Subsequently any additional load has to be carried by the tensile membrane stress 'σ_t' (Figure 4.2.1(b)) which develops along the tension diagonal. The solution presented in this chapter does not attempt to deal with the very complicated stress field which occurs in the elastic post-buckled range; it is solely concerned with the final collapse mode. This membrane stress imposes a lateral pull on the flanges and, under this action, the flanges clearly bend inwards as shown in Figure 4.2.1(b).

Phase : 3 ULTIMATE BEHAVIOUR

On further loading the tensile membrane stress (σ_t) and the buckling stress (τ_{cr}) produces yielding in the web. The membrane stress at yield is defined as σ_t^y. The panel fails when the plastic hinges in the flanges have formed which, together with the yield zone 'UVWX' (Figure 4.2.1(c)),makes up a plastic collapse mechanism. Because the shear stress is considered uniform throughout the web plate, the membrane stress σ_t^y which causes yielding will be a constant value throughout the yielded region. It should be appreciated that the plastic yielding could extend beyond the boundaries 'UVWX', but the minimum requirement for a plastic mechanism to form is that the complete region 'UVWX' must yield.

4.3 Collapse Mechanism Proposed

The proposed collapse mechanism consists of two plastic hinges in the tension flange and two plastic hinges in the

compression flange as shown in Figure 4.4.1. At collapse it is assumed that the wedge 'WXT' (Figure 4.2.1(c)) rotates about the tip in the direction of the tip-moment, such that the vertical displacement of the tip is zero. Obviously, for the tapered beams loaded inside the tip, the direction of the tip-moment will be anticlockwise and hence the wedge 'WXT' will rotate about the tip in an anticlockwise direction as shown in Figure 4.2.1(c).

The failure load can be determined by considering the mechanism developed in 'phase 3' (Figure 4.2.1.(c)). It is important to recognise that the stresses shown in Figure 4.4.1 are the membrane stresses developed in the web after it buckles. Thus there is an inclined tensile membrane stress field of uniform magnitude acting throughout the region 'UVWX'. Therefore it is possible to consider the region 'UVWX' cut out from the web plate and its action upon the flanges and the adjacent web material replaced by the inclined membrane stresses as shown in Figure 4.4.1.

4.4 Lower Bound (Equilibrium) Solution

The ultimate load condition is considered to be comprised of a critical shear stress condition plus the post buckled action. As mentioned before in the critical stress condition there is no lateral pull on the flanges and the load is carried by the pure shear action of the web panel.

Consider a section 'WU', passing through the two internal plastic hinges where the internal and external forces acting in the post buckled range are shown in Figure 4.4.2.

To satisfy the equilibrium of vertical forces and moments at W, the following equations are obtained:

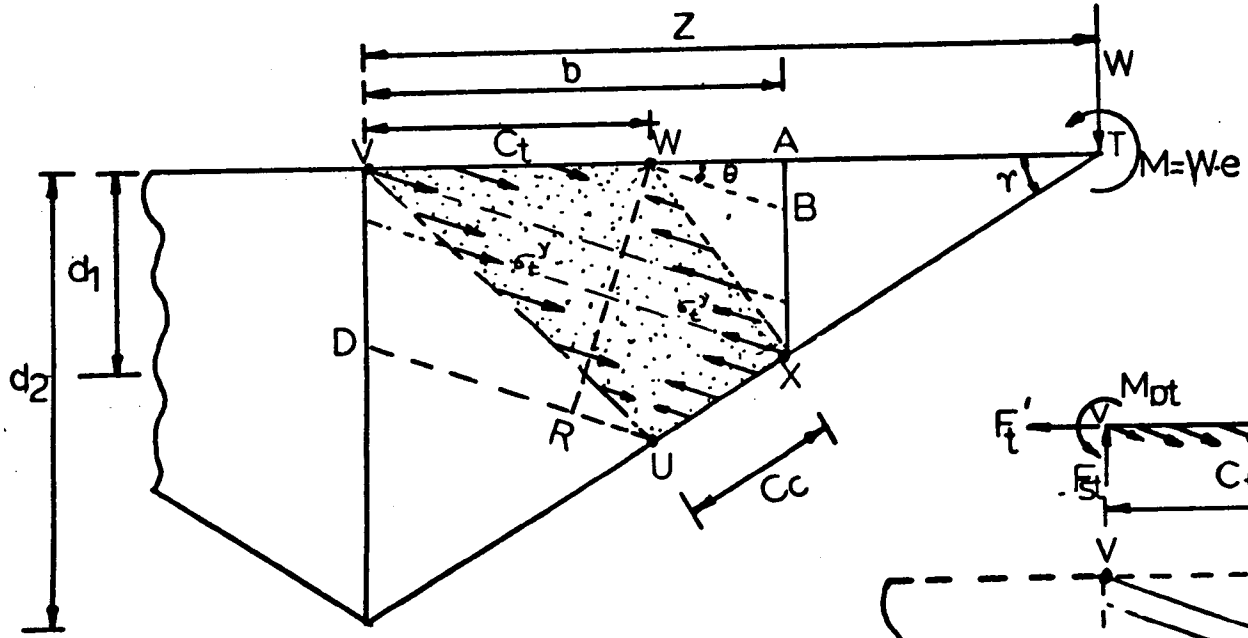

Figure 4.4.1

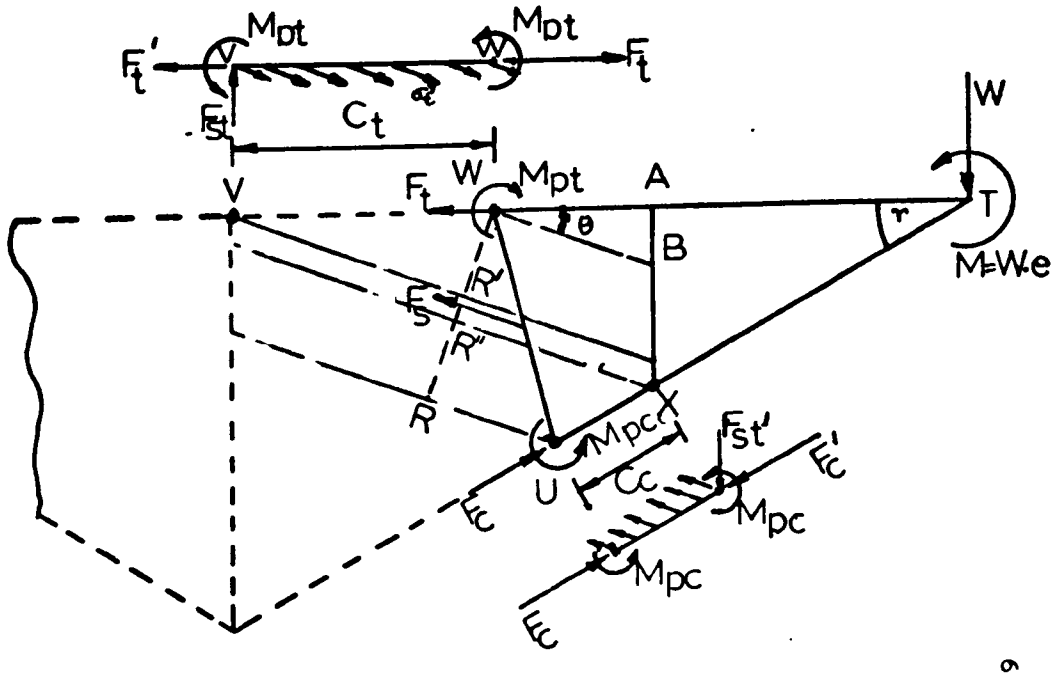

Figure 4.4.2

$$\Sigma V = 0$$

$$W = F_s.\sin\theta + F_c.\sin\gamma$$

$$\therefore F_c.\sin\gamma = W - F_s.\sin\theta \qquad (4.4)$$

$$F_c = [W - F_s.\sin\theta]/\sin\gamma \qquad (4.5)$$

ΣM at $W = 0$

$$W(z - C_t) + F_s\left(\frac{WR}{2}\right) - M + M_{pt} - M_{pc} - F_c.(z - C_t)\sin\gamma = 0$$

After substituting the value of $F_c.\sin\gamma$ from (4.4) and letting $M_{pt} = M_{pc}$ (for full plastic moments of the flanges) the above equation can be expressed as:

$$W(z - C_t) + F_s\left(\frac{WR}{2}\right) - W.e - (z - C_t)[W - F_s.\sin\theta] = 0$$

i.e. $$W.e = F_s\left[(z - C_t)\sin\theta + \frac{(WR)}{2}\right]$$

$$W = \frac{F_s}{e}\left[(z - C_t)\sin\theta + \frac{(WR)}{2}\right]$$

$$\therefore W_{ult} = \frac{F_s}{e}\left[(z - C_t)\sin\theta + \frac{(WR)}{2}\right] + V_{cr} \qquad (4.6)$$

Also the axial forces in the tension flange can be calculated from the horizontal equilibrium of forces $\Sigma H = 0$, i.e.

$$F_t = [F_c.\cos\gamma - F_s.\cos\theta]$$

i.e. $$F_t = [W.\cot\gamma - F_s(\cos\theta + \cot\gamma.\sin\theta)] \qquad (4.7)$$

Since the internal plastic hinge will occur at the point of maximum bending moment where the shear is zero. The positions

of the internal plastic hinges 'W' and 'U' can be obtained by considering the equilibriums of the beam section 'V-W' and 'U-X' respectively (Figure 4.4.2). By taking moments at V and X one can obtain the following equations respectively

$$C_t = \frac{2}{\sin\theta}\sqrt{\frac{M_{pt}}{t.\sigma_t^y}} \tag{4.8}$$

and $$C_c = \frac{2}{\sin(\theta + \gamma)}\sqrt{\frac{M_{pc}}{t.\sigma_t^y}} \tag{4.9}$$

Equations (4.8) and (4.9) hold for all positive values of σ_t^y and for all values of 'C_t' and 'C_c' within the range of $0 < C_t < b$ and $0 < C_c < b\sec\gamma$ respectively.

The value of σ_t^y is obtained by applying the von Mises Hencky yield criterion to the two stress fields which are acting on the web plate i.e. the shear buckling stress and the membrane stress σ_t^y which is acting at an angle of 'θ' to the horizontal flange (Figure 4.4.3(a)).

From the stress condition shown in Figure 4.4.3(b) and 4.4.3(c) one can obtain the values of σ_η, σ_Σ and τ:

$$\sigma_\Sigma = \tau_{cr}.\sin2\theta + \sigma_t^y \tag{4.10}$$

$$\sigma_\eta = \tau_{cr}.\sin2\theta \tag{4.11}$$

$$\tau = \tau_{\eta\Sigma} = \tau_{\Sigma\eta} = \tau_{cr}.\cos2\theta \tag{4.12}$$

Using the Huber von Mises plasticity condition for biaxial stress system which can be expressed as:

$$\sigma_{yw}^2 = \sigma_\eta^2 + \sigma_\Sigma^2 - \sigma_\eta.\sigma_\Sigma + 3\tau^2$$

and substituting the values of σ_Σ, σ_η and τ from equations (4.10),

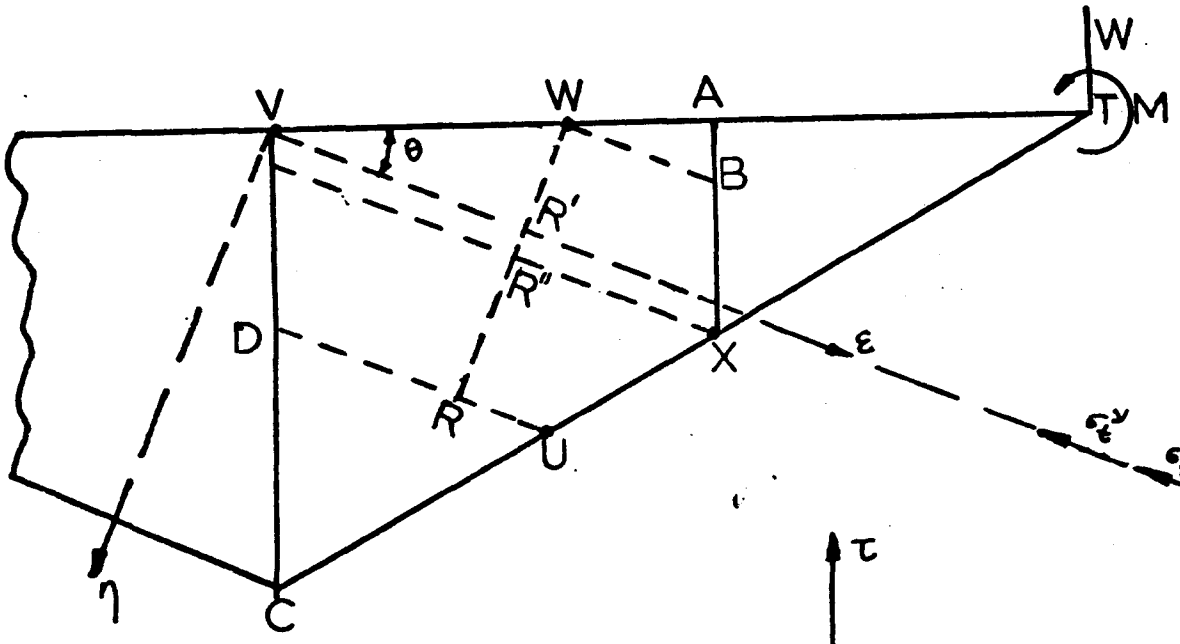

Figure 4.4.3(a)

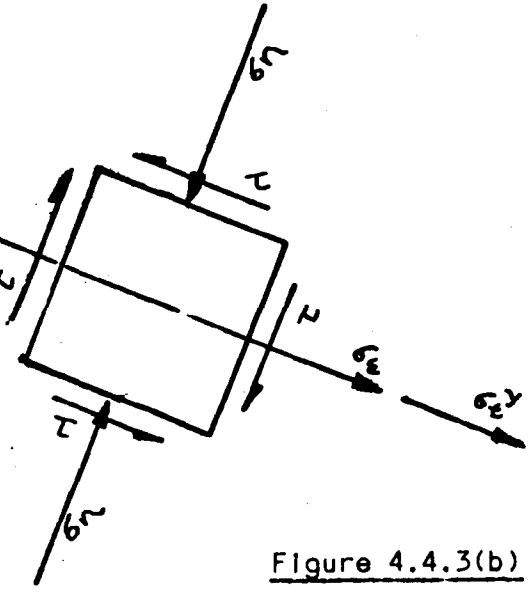

Figure 4.4.3(b)

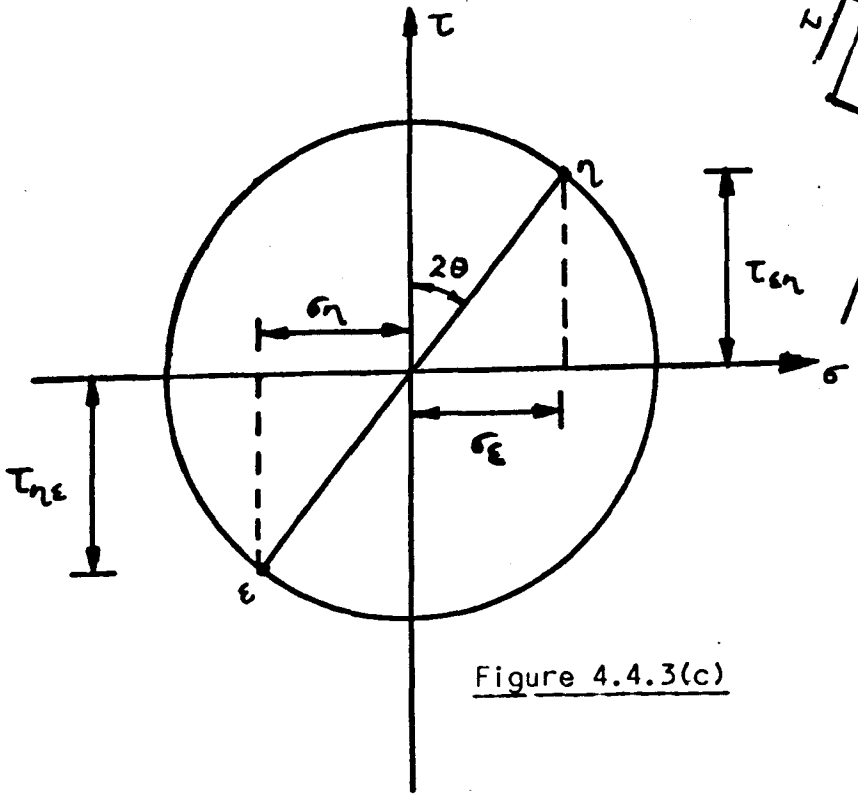

Figure 4.4.3(c)

(4.11) and (4.12) respectively, one can obtain

$$\sigma_t^y = -\frac{3}{2}\tau_{cr}.\sin 2\theta + \sqrt{\sigma_{yw}^2 + \tau_{cr}\left[\left(\frac{3}{2}\sin 2\theta\right)^2 - 3\right]} \qquad (4.13)$$

To support the validity of the lower bound solution it is necessary to show that the stress distribution throughout the structure is in equilibrium, balances the external loads and does not violate the yield condition.

It has been shown previously in this section that for the lower bound solution, the forces are in equilibrium. A set of forces can be obtained which will maintain equilibrium in the wedges 'AWB' and 'CUD' (Figure 4.4.4(a)) without violating yield. As shown in Figure 4.4.4(a) the yield band coincides with the internal plastic hinge positions at W and U. Because the shear force is zero at the internal plastic hinge position, the normal reactions at A and C will be zero as shown in Figure 4.4.4(b) and 4.4.4(c) respectively. Therefore the flange moment will remain constant and equal to the plastic moment between the flange portion 'W-A' and 'U-C' in the tension and compression flange respectively (Figure 4.4.4(b) and 4.4.4(c)) and hence it does not violate the yield condition.

If the yield band extends beyond W and U, then the moment acting between W and A in the tension flange and U and C in the compression flange will be reduced as shown in Figure 4.4.5(a) and 4.4.5(b) respectively. It can be seen from Figure 4.4.6 that even when the yield band extends beyond the tension diagonal band, the equilibrium of forces at any section P-P remains unchanged.

Thus the lower bound solution presented in this section is valid because in any case the equilibrium of internal and

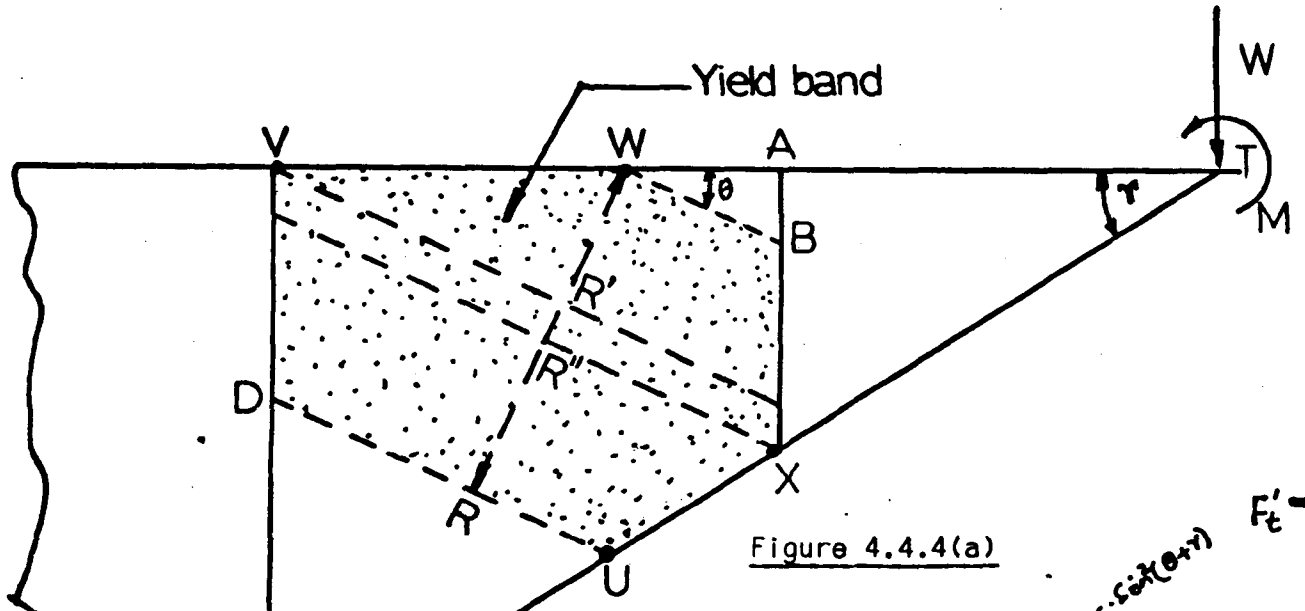

Figure 4.4.4(a)

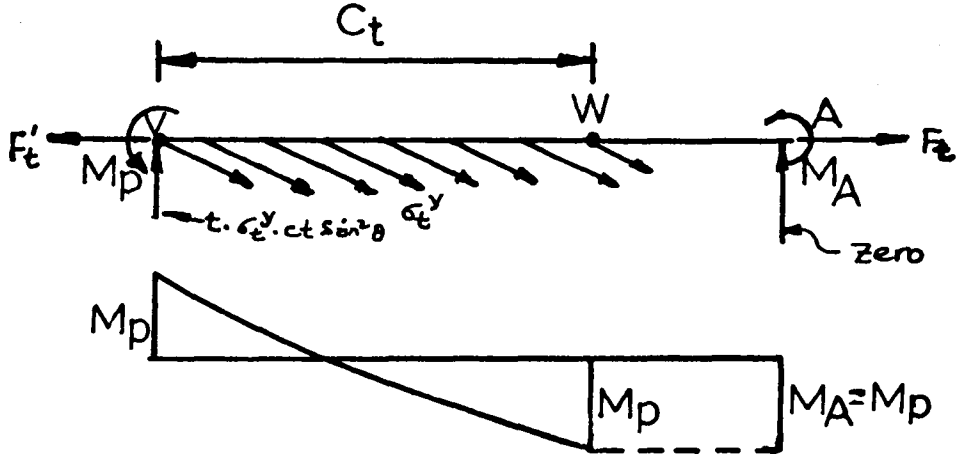

Figure 4.4.4(b)

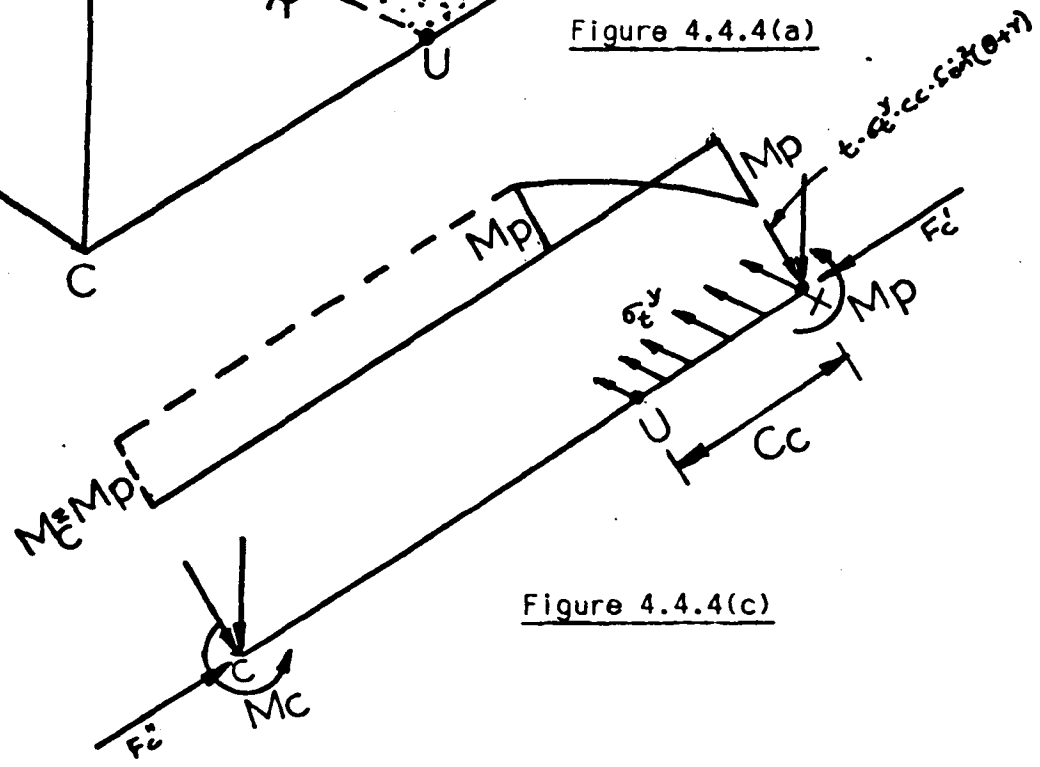

Figure 4.4.4(c)

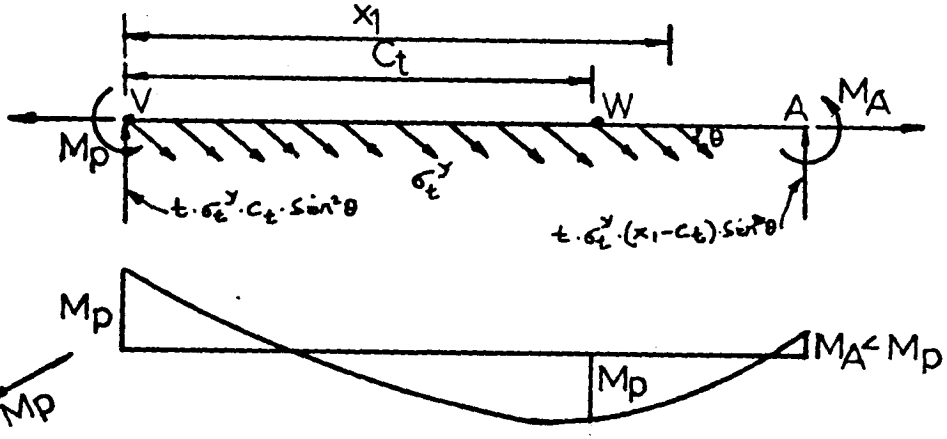

Figure 4.4.5(a)

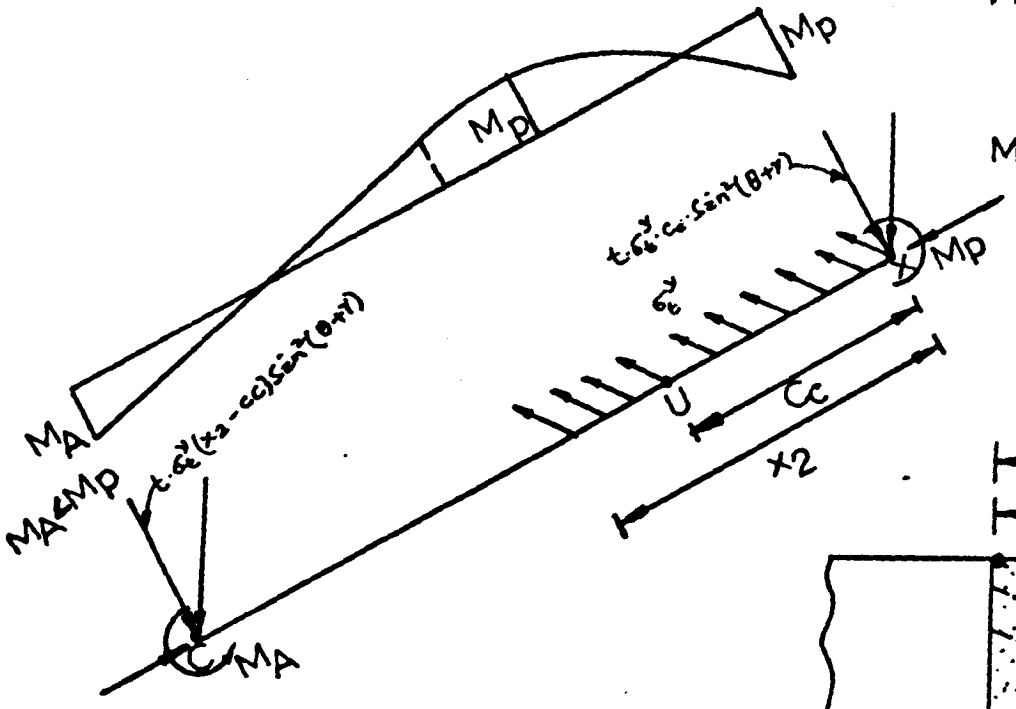

Figure 4.4.5(b)

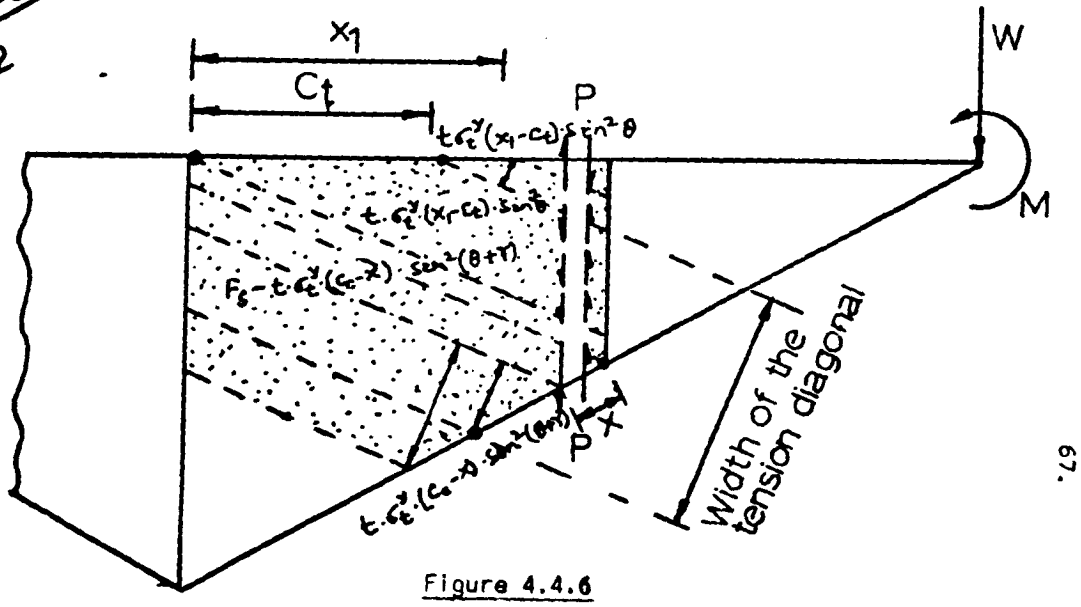

Figure 4.4.6

external forces are maintained and at the same time it does not violate the yield condition.

4.5 Upper Bound (Mechanism) Solution

Assume the rotations of the plastic hinges at V, W, X and U are θ_1, θ_2, θ_3 and θ_4 respectively as shown in Figure 4.5.1. For small value of β (Figure 4.5.1), the magnitude of θ_1, θ_2 and θ_3, θ_4 can be obtained from the geometrical relations of triangles VW'T and UX'T (Figure 4.5.1) respectively.

$$\theta_1 = \frac{(z - C_t)}{C_t} .\beta \tag{4.14}$$

$$\theta_2 = \left[\frac{z}{C_t}\right] .\beta \tag{4.15}$$

$$\theta_3 = \left[\frac{d_1}{C_c.\sin\gamma} + 1\right] .\beta \tag{4.16}$$

and $$\theta_4 = \frac{d_1}{C_c.\sin\gamma} .\beta \tag{4.17}$$

From the collapse mechanism in Figure 4.5.1, it is clear that the stresses acting on section U-V do no work, and therefore only those stresses acting on the inclined right hand web section (W-X) and the flanges will do work. The total work done can be divided into four parts as shown below:

(i) The internal virtual work done by the tensile membrane stresses acting on the tension flange (Figure 4.5.2(a)) will be equal to

$$-\frac{t.\sigma_t^y}{2}\left[C_t.\sin\theta\right]^2.\frac{(z - C_t)}{C_t} .\beta$$

This work will be negative because the displacement of the flange

takes place in the opposite direction to the direction of the forces (Figure 4.5.2(a)).

(ii) The internal virtual work done by the tensile membrane stresses acting on the compression flange (Figure 4.5.2(b) will be equal to

$$+\frac{t.\sigma_t{}^{y}}{2}\left[C_c.\sin(\theta+\gamma)\right]^2.\frac{d_1}{C_c.\sin\gamma}\ .\beta$$

(iii) The internal virtual work done by the tensile membrane stresses acting on the inclined web section W-X (Figure 4.5.2(c)) will be equal to

$$+\frac{t.\sigma_t{}^{y}}{2}\left[C_t\sin\theta + d_1\cos\theta - b\sin\theta\right].\left[(z-C_t).\sin\theta + \frac{d_1\sin(\theta+\gamma)}{\sin\gamma}\right].\beta = +\frac{t.\sigma_t{}^{y}}{2}.(WR'').\left[(z-C_t).\sin\theta + \frac{d_1\sin(\theta+\gamma)}{\sin\gamma}\right].\beta$$

(iv) The internal virtual work done due to rotations at the plastic hinges will be equal to

$$M_p(\theta_1+\theta_2+\theta_3+\theta_4)$$

$$= 2M_p\left[\frac{z}{C_t}+\frac{d_1}{C_c.\sin\gamma}\right].\beta$$

Therefore the total internal virtual work done will be equal to

$$2M_p.\left(\frac{z}{C_t}+\frac{d_1}{C_c.\sin\gamma}\right).\beta + \frac{t.\sigma_t{}^{y}}{2}\left[\frac{d_1\sin(\theta+\gamma)}{\sin\gamma}.(WR) + (z-C_t).\sin\theta(R'R'')\right].\beta$$

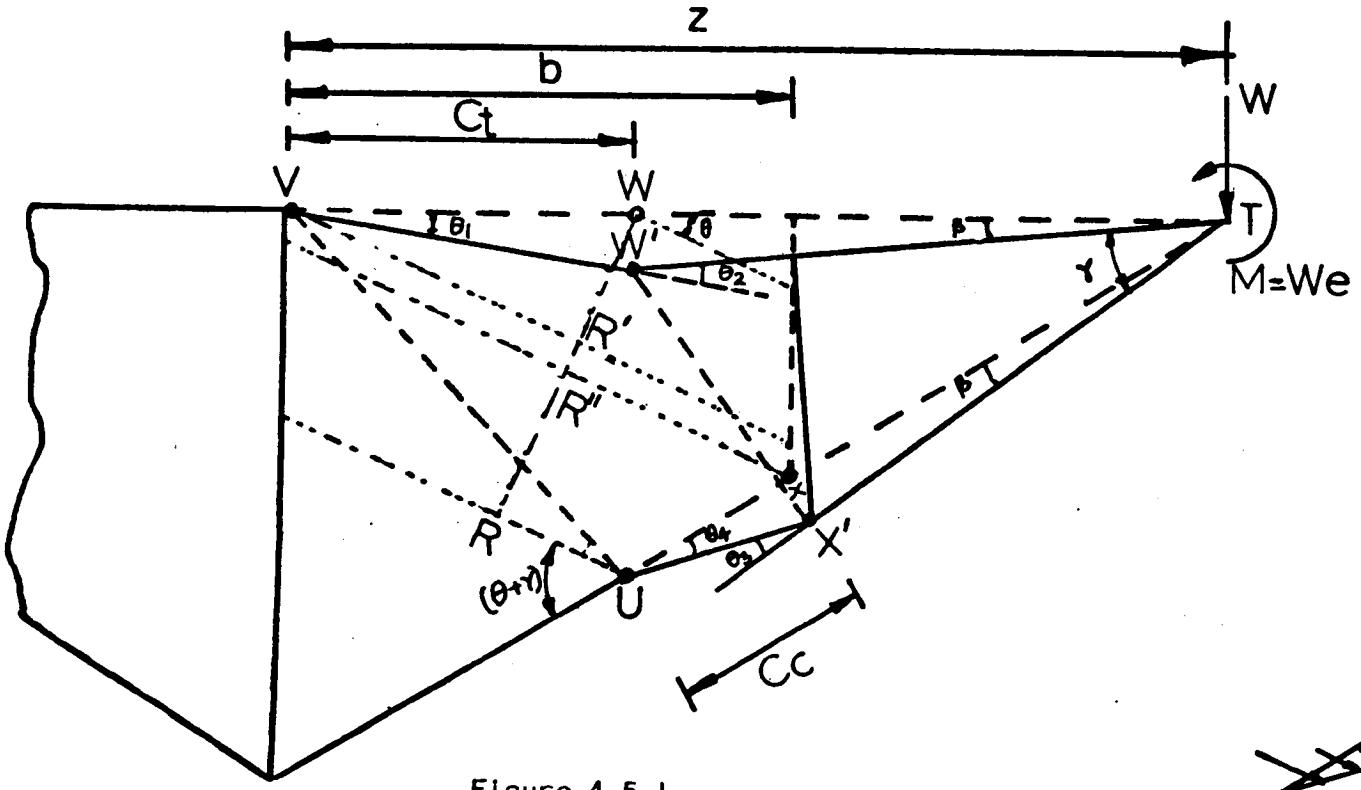

Figure 4.5.1

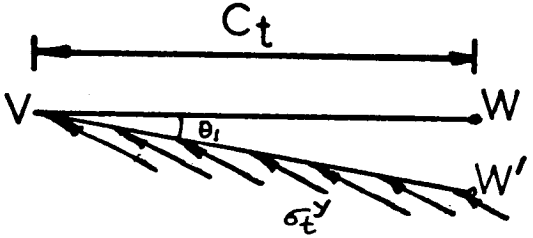

Figure 4.5.2(a)

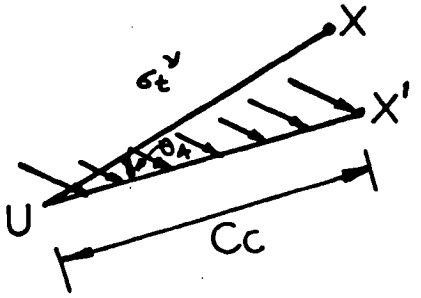

Figure 4.5.2(b)

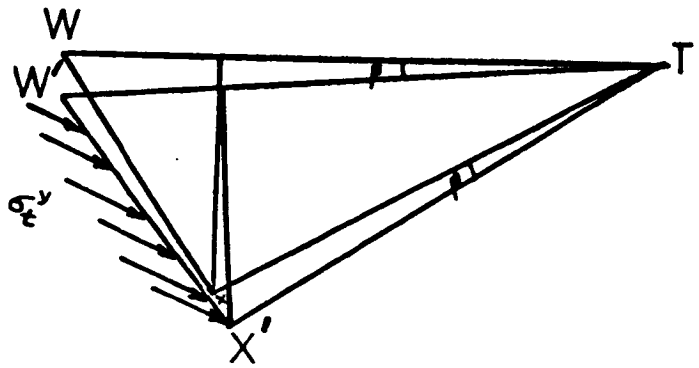

Figure 4.5.2(c)

External work done in the mechanism will be equal to $W \times 0 + M \times \beta = W.e.\beta$.

By equating the external and internal virtual work done one can obtain:

$$W = \frac{1}{e}\left[2M_p\left(\frac{z}{C_t} + \frac{d_1}{C_c.\sin\gamma}\right) + \frac{t.\sigma_t^y}{2}\left[\frac{d_1 \sin(\theta + \gamma)}{\sin\gamma}(WR) + (z - C_t)\cdot\sin\theta(R'R'')\right]\right] \quad (4.18)$$

The ultimate load will be equal to the load 'W' carried by the membrane field and the flanges, together with the shear load which causes buckling.

$$W_{ult} = W + V_{cr}$$

$$W_{ult} = \frac{1}{e}\left[2M_p\left(\frac{z}{C_t} + \frac{d_1}{C_c.\sin\gamma}\right) + \frac{t.\sigma_t^y}{2}\left[\frac{d_1 \sin(\theta + \gamma)}{\sin\gamma}(WR) + (z - C_t)\sin\theta(R'R'')\right]\right] + \tau_{cr}.\frac{(d_1+d_2)}{2}.t \quad (4.19)$$

A computer programme shown in Appendix I (AI.1) was written by the author to calculate the collapse loads, with full plastic moment capacity of the flanges, obtained from an Upper bound and Lower bound solutions for various values of 'θ' (inclination of the tensile membrane stress field).

4.6 Effect of Axial Forces on Plastic Moment Capacity of Flanges

It is evident from the analysis of forces of Figure 4.4.2 that the axial forces in the flanges of tapered beams are quite large and in particular, in the inclined compression flange the axial forces are very high. However, it will be shown later (Table 4.7.2) that for smaller eccentricity of load inside the tip, the plastic moment of the inclined compression flange

reduces quite significantly. Therefore, it is necessary to allow for the reduction in the plastic moment capacity of the flanges resulting from the presence of the axial forces.

The magnitude of axial forces in the tension and compression flanges can easily be calculated from equations (4.7) and (4.5) respectively, which were obtained from the Lower bound solution presented in section (4.4).

However, it is also possible to calculate the magnitude of the axial forces in the flanges from the ultimate load obtained from the equilibrium of forces and moments shown in Figure 4.6.1. This solution can include the effect of the horizontal (complementary) shear stresses. Because the effect of horizontal buckling stresses on the ultimate load is not significant and also the equation for the ultimate load becomes very complicated, in this section the axial forces in the tension and compression flange will be calculated from equations (4.7) and 4.5) respectively. However, the effect of vertical and horizontal buckling stress acting on the flanges will be taken into account while calculating the average flange stresses, as shown below.

The average axial force in compression flange contributed by the membrane stresses acting on the flange (Figure 4.6.2(a)) will be

$$= \frac{t.\sigma_t^y}{2} C_c.\sin(\theta + \gamma).\cos(\theta + \gamma) \qquad (4.20)$$

The average axial force in the compression flange contributed by the buckling stresses (Figure 4.6.2(b)) will be

$$= \tfrac{1}{2}\tau_{cr}.\sin 2\gamma.t.C_c \qquad (4.21)$$

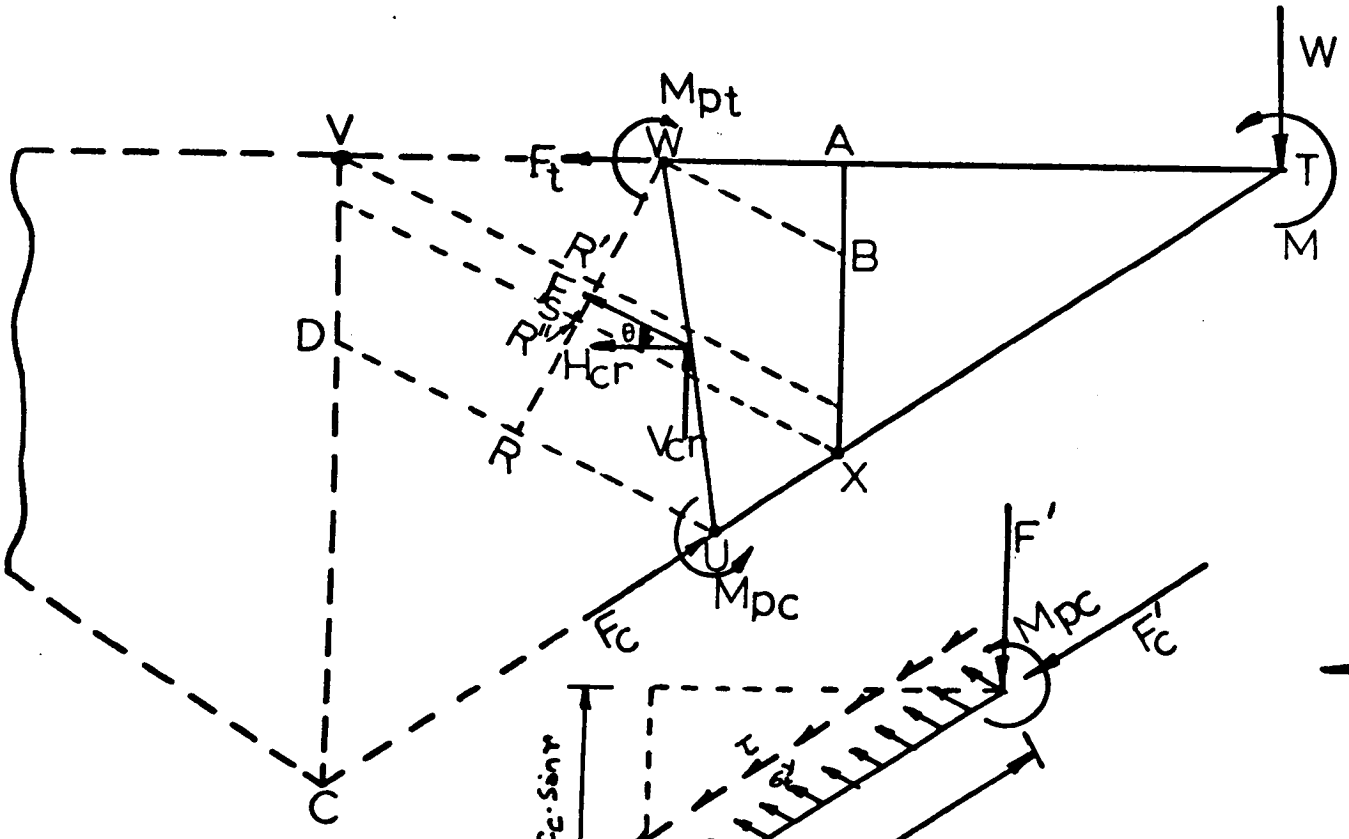

Figure 4.6.1

Figure 4.6.2(a)

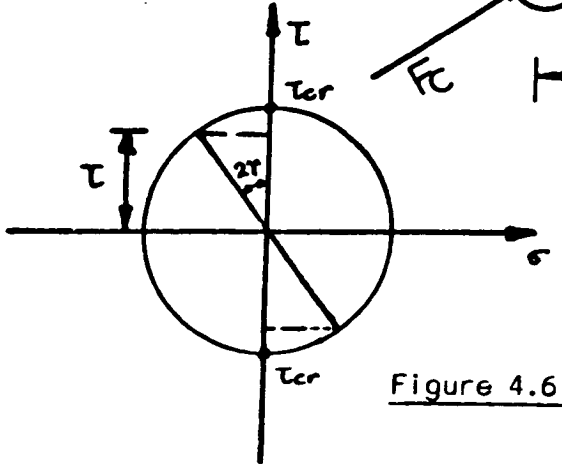

Figure 4.6.2(b)

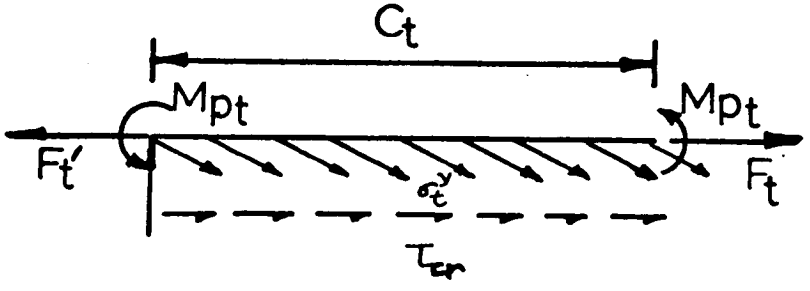

Figure 4.6.2(c)

Therefore the total average flange stress for the compression flange will be

$$\sigma_{cf} = \frac{F_c - [\sigma_t^y.\sin(\theta + \gamma).\cos(\theta + \gamma) + \tau_{cr}.\sin 2\gamma].\frac{t.C_c}{2}}{A_{cf}} \quad \ldots \quad (4.22)$$

The average axial force in the tension flange contributed by the membrane stresses acting on the flange (Figure 4.6.2(c)) will be

$$= t.\sigma_t^y.C_t.\sin\theta.\cos\theta \quad (4.23)$$

The average axial force in the tension flange contributed by the buckling stress will be

$$= \tfrac{1}{2}\tau_{cr}.t.C_t \quad (4.24)$$

Therefore the total average flange stress for the tension flange will be

$$\sigma_{tf} = \frac{F_t + [\sigma_t^y.\sin\theta.\cos\theta + \tau_{cr}].\frac{t.C_t}{2}}{A_{tf}} \quad (4.25)$$

To calculate the values of full plastic moment and the reduced plastic moment capacity of the flange due to the presence of axial forces, it was assumed that a section of that web plate (as shown in Figure (4.6.3(a))) acts with the flange. The expression shown below was used to calculate the depth of the web plate which acts with the flange as proposed by Rockey and Skaloud[22].

$$d_e = 30.t.\left[1 - \frac{2\tau_{cr}}{\tau_{yw}}\right] \quad (4.26)$$

At zero axial load, the neutral axis at full plasticity for the flange section is the equal area axis as shown in Figures 4.6.3(b) and 4.6.4(b) but if there is any axial force, the position of neutral axis will vary and will depend upon the magnitude of the axial tension or compression and the sign (hogging or sagging) of the bending moment. For the various positions of the neutral axis shown in Figures 4.6.3(b) to 4.6.3(e) and 4.6.4(b) to 4.6.4(e), the values of $\frac{N}{N_p}$ and $\frac{M}{M_p}$ were calculated for the flanges of all the girders used. Figure 4.6.5(a) to 4.6.5(d) show $\frac{M}{M_p}$ plotted against $\frac{N}{N_p}$ by using the n^{th} order Regression Analysis. The second order equations were obtained for all the flanges used and the corresponding coefficients of those equations were used to analyse the values of the reduced plastic moments of the flanges. Because the area of the web, which makes one axis of the flange section asymmetrical, is very small, the plots of $\frac{M}{M_p}$ against $\frac{N}{N_p}$ are apparently identical for hogging and sagging bending moment (Figure 4.6.6(a) to (d)).

Therefore, the relationships for reduced plastic moment of resistance of the flanges, obtained from the 'Regression Analysis' is given by:

$$M'_{pc} = M_p \times \left[1 - \left[0.8 \times \left(\frac{\sigma_{cf}}{\sigma_{yw}}\right)^2 + 0.2 \times \left(\frac{\sigma_{cf}}{\sigma_{yw}}\right) \right] \right] \qquad (4.26)$$

$$M'_{pt} = M_p \times \left[1 - \left[0.8 \times \left(\frac{\sigma_{tf}}{\sigma_{yw}}\right)^2 + 0.2 \times \left(\frac{\sigma_{tf}}{\sigma_{yw}}\right) \right] \right] \qquad (4.27)$$

Because the values of M'_{pc} and M'_{pt} will be different, the Lower bound Load will be given by the equation shown below:

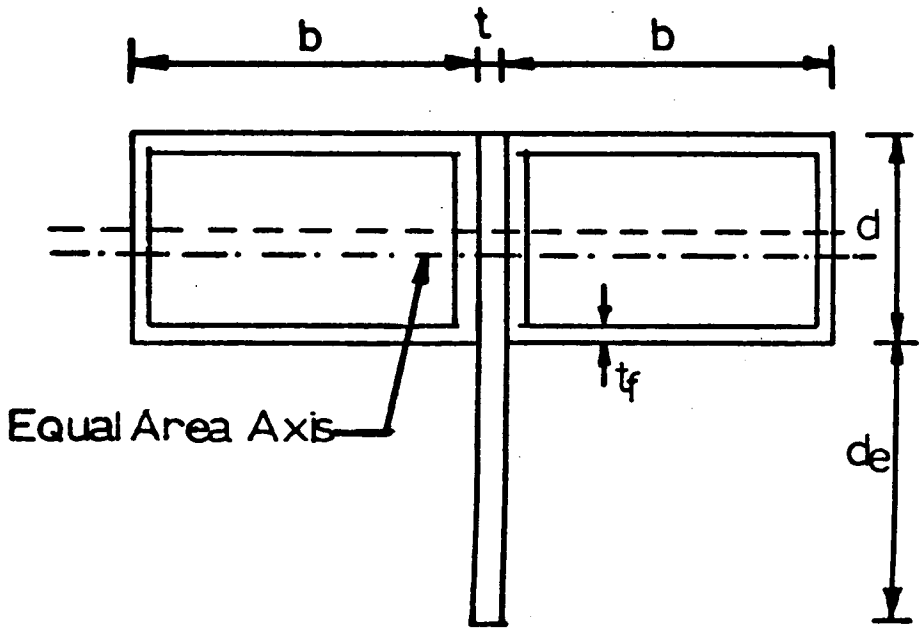

Figure 4.63(a)

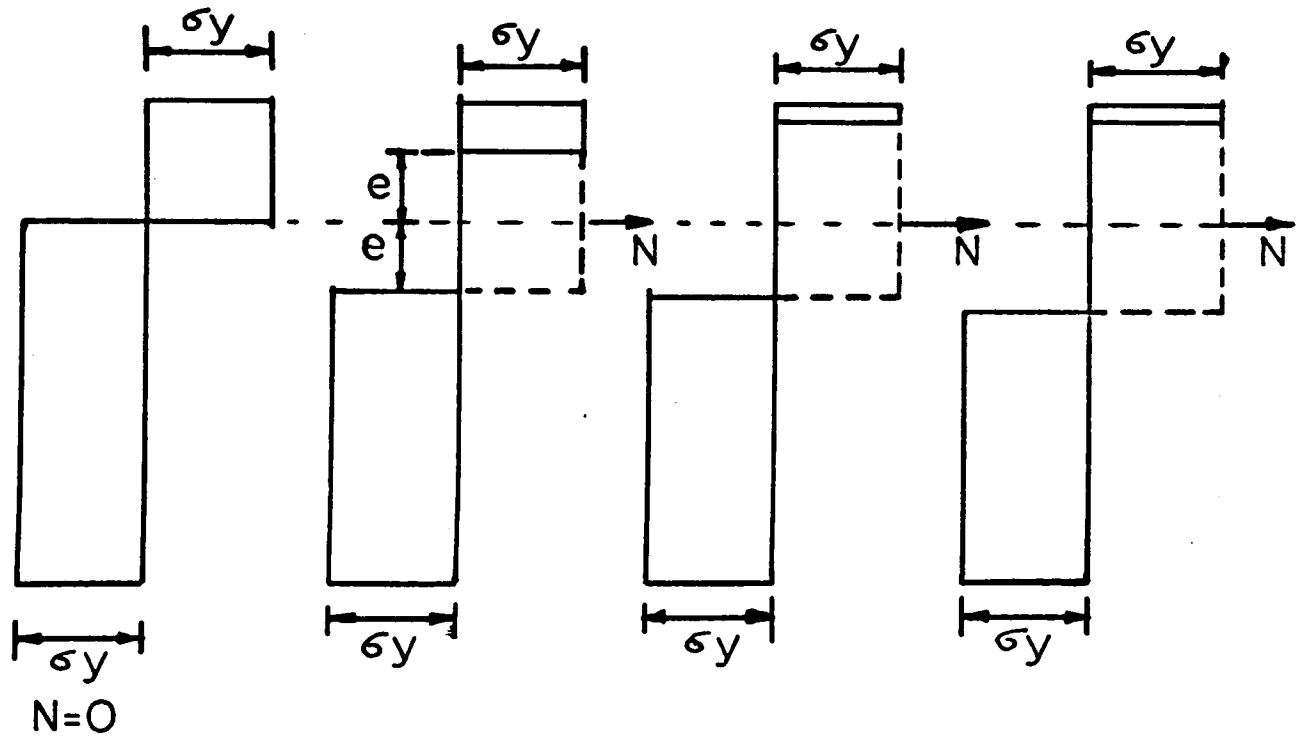

(b) (c) (d) (e)

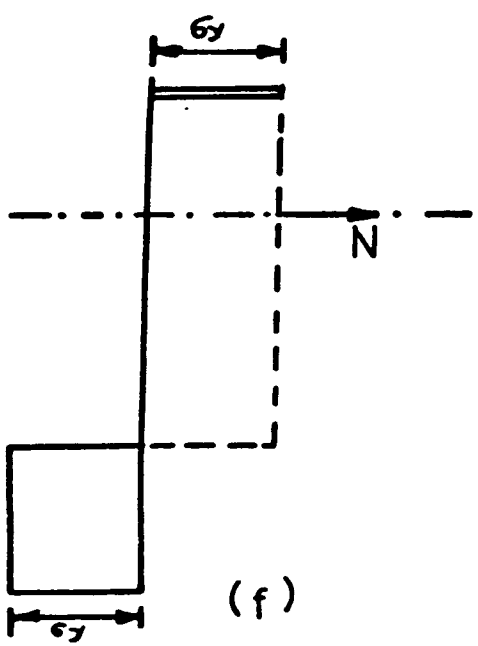

The stress distribution diagrams for

(i) Compression flange with hogging bending moment

(ii) Tension flange with sagging bending moment

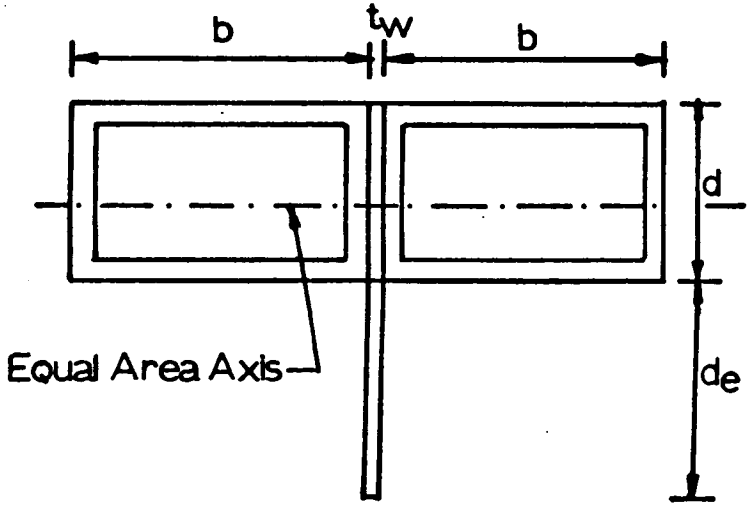

Figure 4.6.4(a)

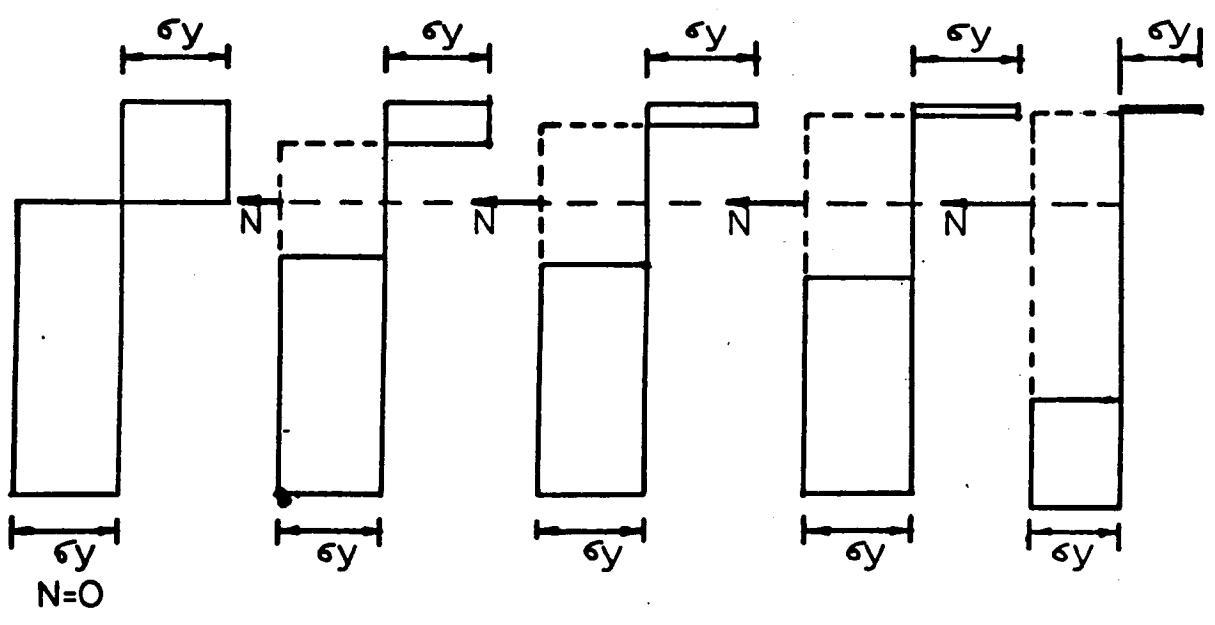

Figure 4.6.4(b)

Figure 4.6.4(c)

Figure 4.6.4(d)

Figure 4.6.4(e)

Figure 4.6.4(f)

The stress distribution diagrams for

(i) Compression flange with sagging bending moment
(ii) Tension flange with hogging bending moment

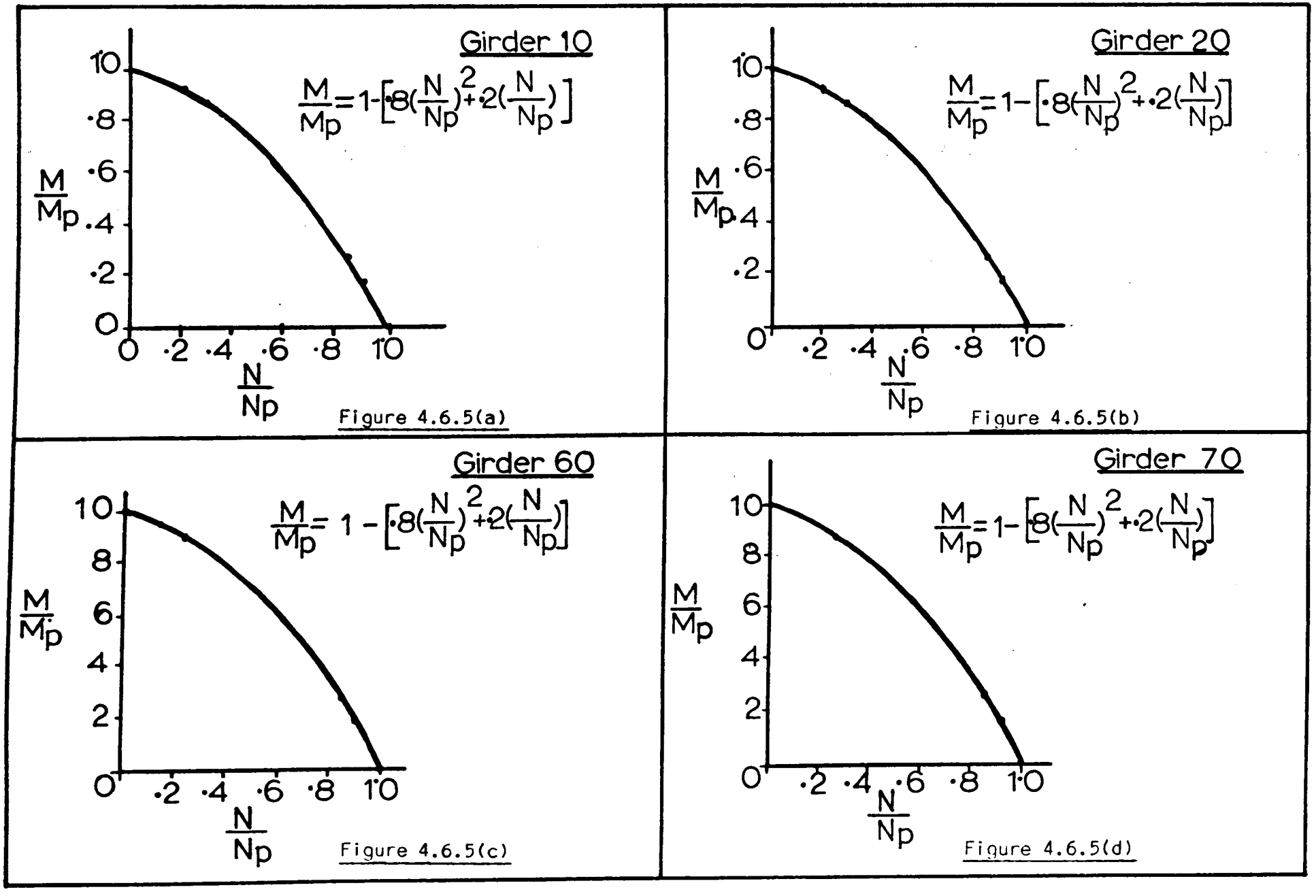

Figure 4.6.5(a)

Figure 4.6.5(b)

Figure 4.6.5(c)

Figure 4.6.5(d)

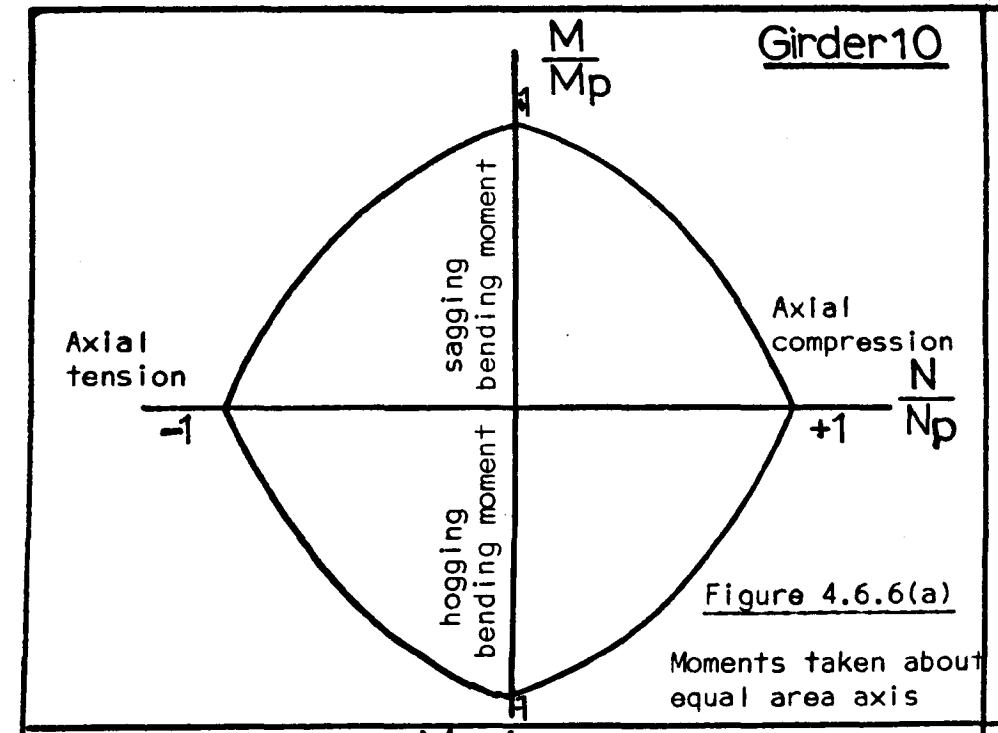

Figure 4.6.6(a)

Moments taken about equal area axis

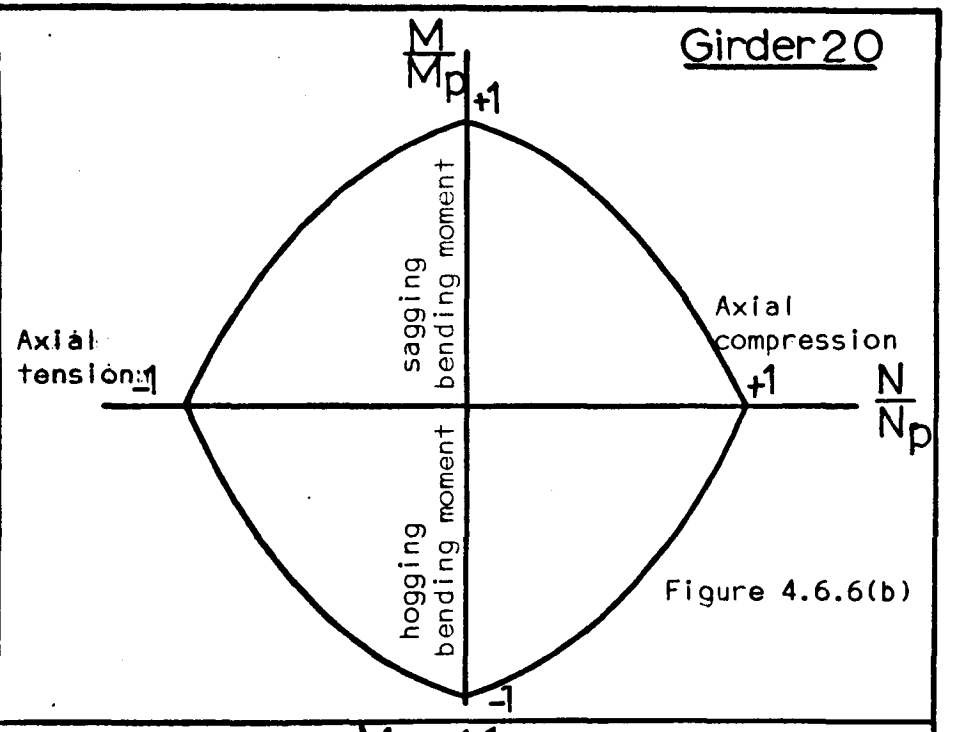

Figure 4.6.6(b)

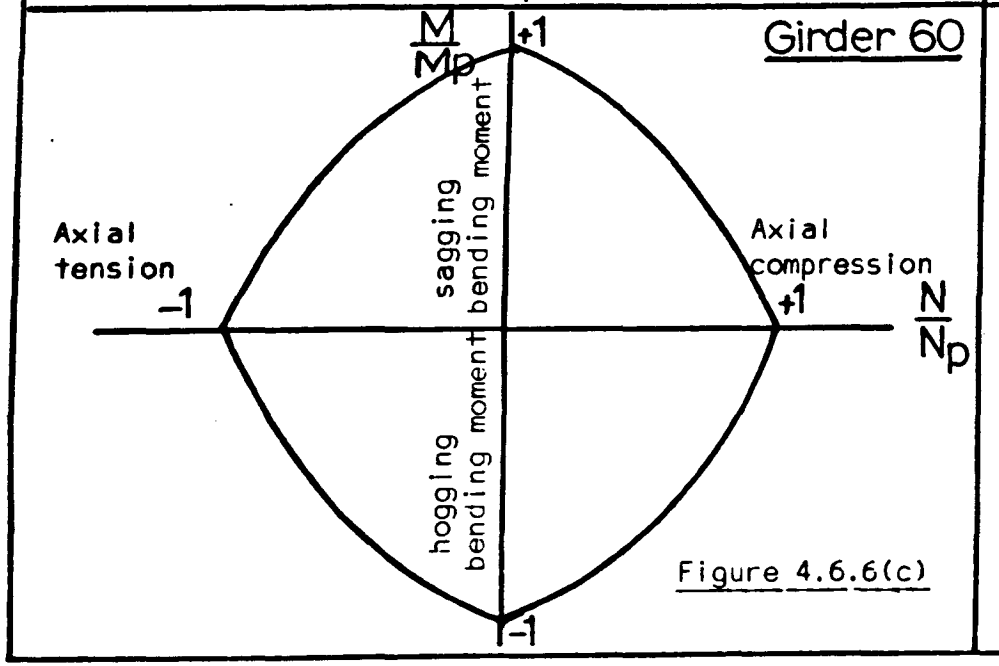

Figure 4.6.6(c)

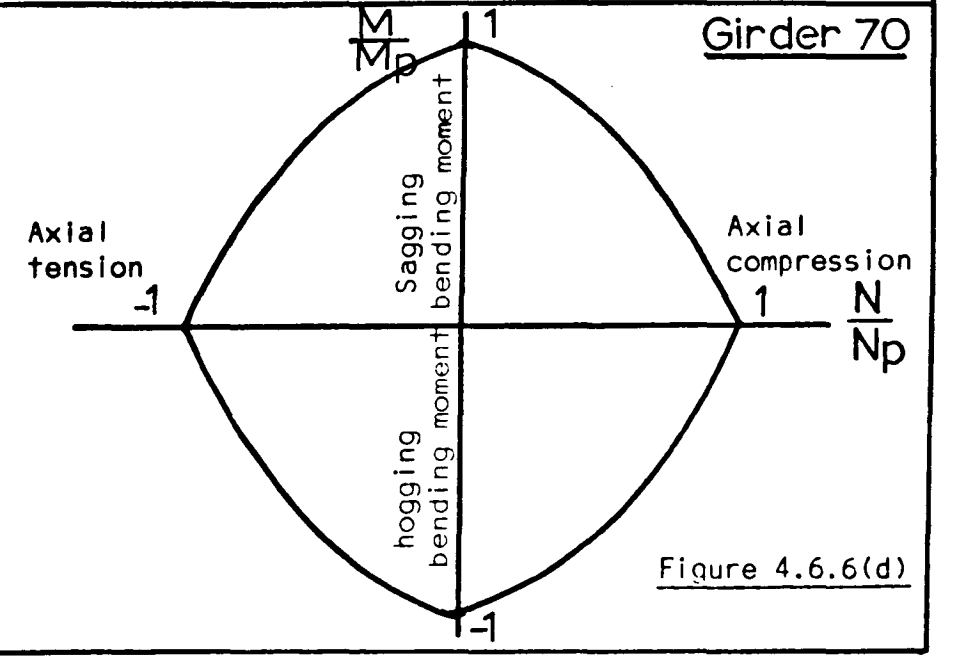

Figure 4.6.6(d)

$$W_{ult} = \frac{1}{e}\left[F_s\left[(z - C_t)\sin\theta + \frac{(WR)}{2}\right] + \left[M'_{pt} - M'_{pc}\right]\right] + V_{cr}$$

... (4.28)

A computer program, shown in 'Appendix I' (AI.2), was written by the author to analyse the collapse load by considering the reduced plastic moment capacity of the flanges for tapered beams loaded inside the tip.

4.7 Analysis and Discussions of the Theoretical Results

The variations of upper and lower bound loads with inclination of the tensile membrane stresses are shown in Figures 4.7.1 (a) to (g) where 'θ_m' is defined as the inclination which provides the maximum value of the upper and lower bound load. Figure 4.7.2 shows how the eccentricity of the load about the tip affects the ultimate loads obtained from consideration of the full plastic moment and the reduced plastic moment capacity of flanges. This figure shows that as the eccentricity of load about the tip decreases, the ultimate load for full plastic moment capacity of the flanges increases significantly.

It can be seen from the results presented in Table 4.7.1 that the upper and lower bound loads are identical for all girders loaded inside the tip.

The results presented in Table 4.7.2 show that as the eccentricity of loads about the tip becomes smaller the magnitude of axial forces in the tension and compression flanges becomes higher and accordingly the plastic moment capacity of the flanges is reduced, hence decreasing the ultimate load quite significantly (Figure 4.7.2).

As explained previously, the calculation of the web

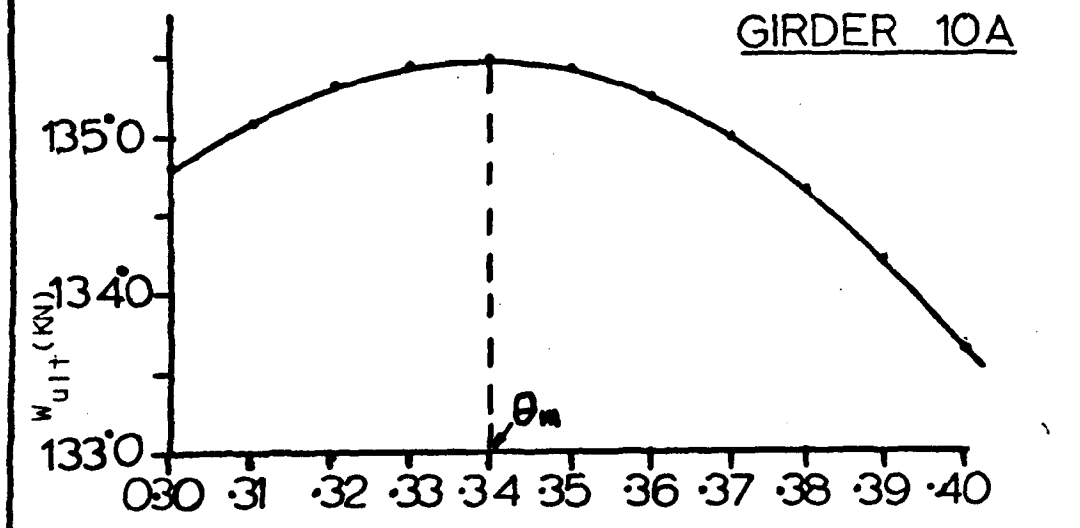

Inclination of membrane field 'θ' (rad.) Figure 4.7.1(a)

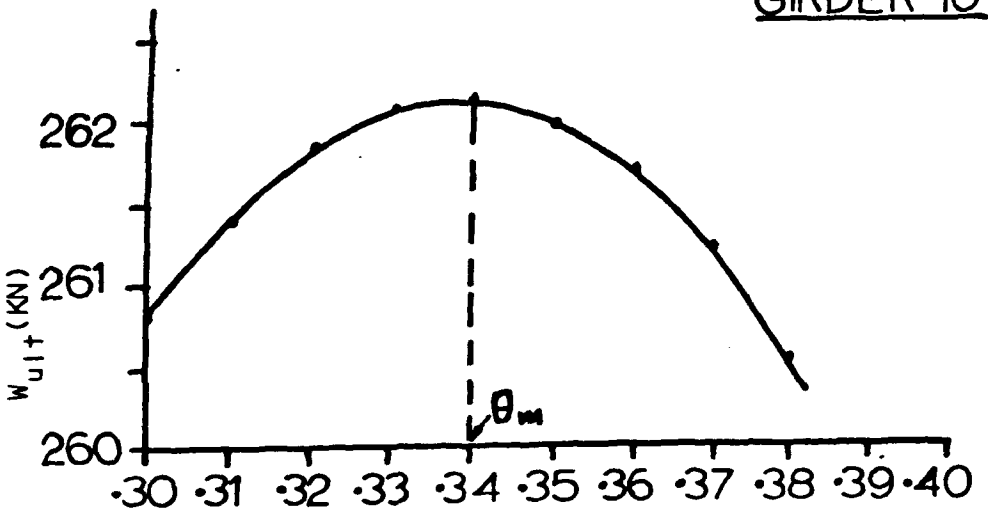

θ in rad. Figure 4.7.1(b)

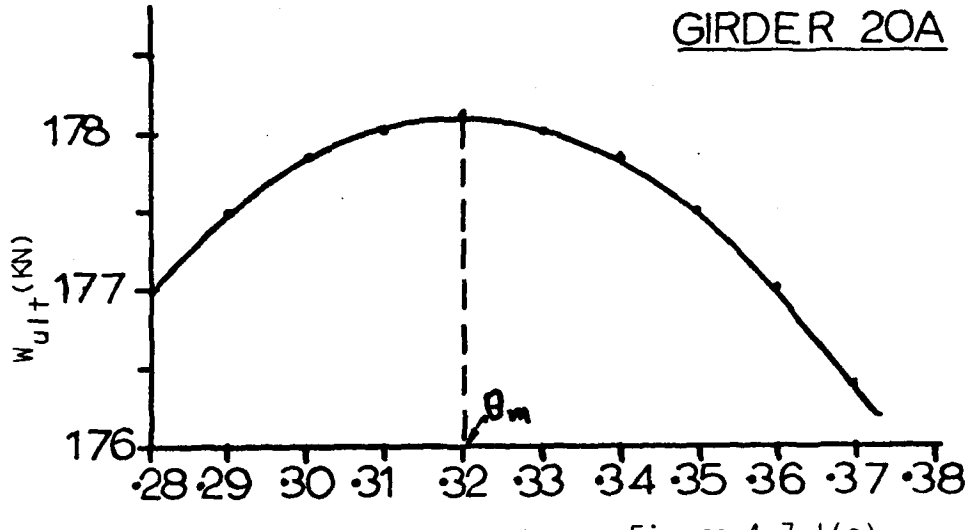

θ in rad. Figure 4.7.1(c)

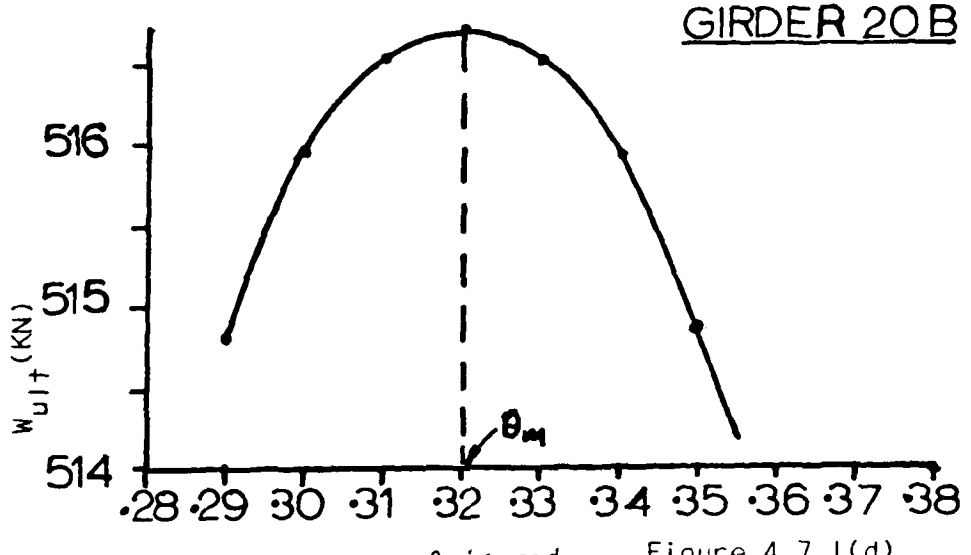

θ in rad. Figure 4.7.1(d)

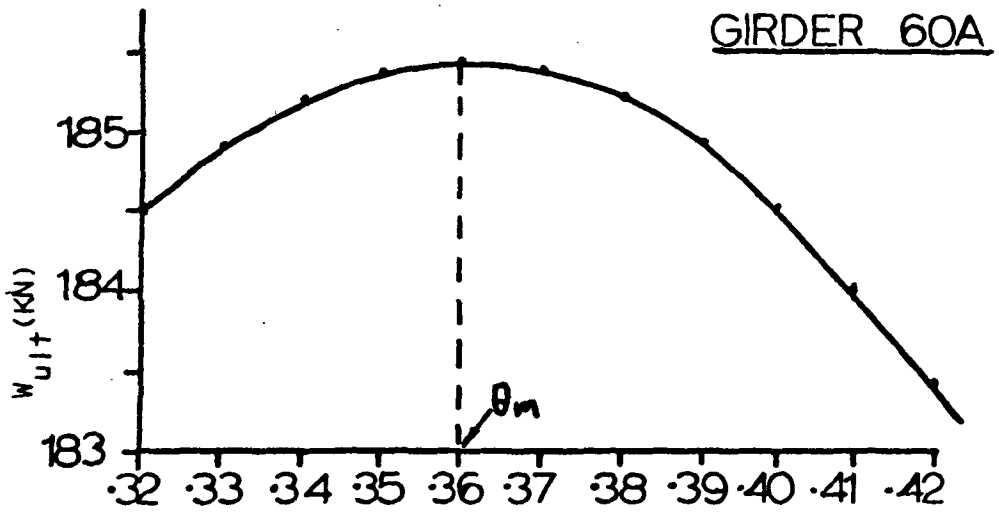

Figure 4.7.1(e)

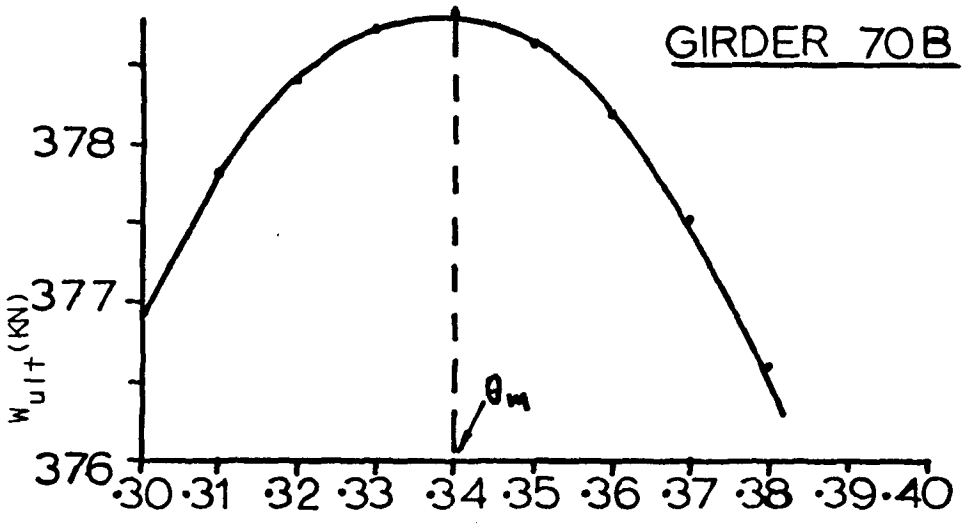

Figure 4.7.1(g)

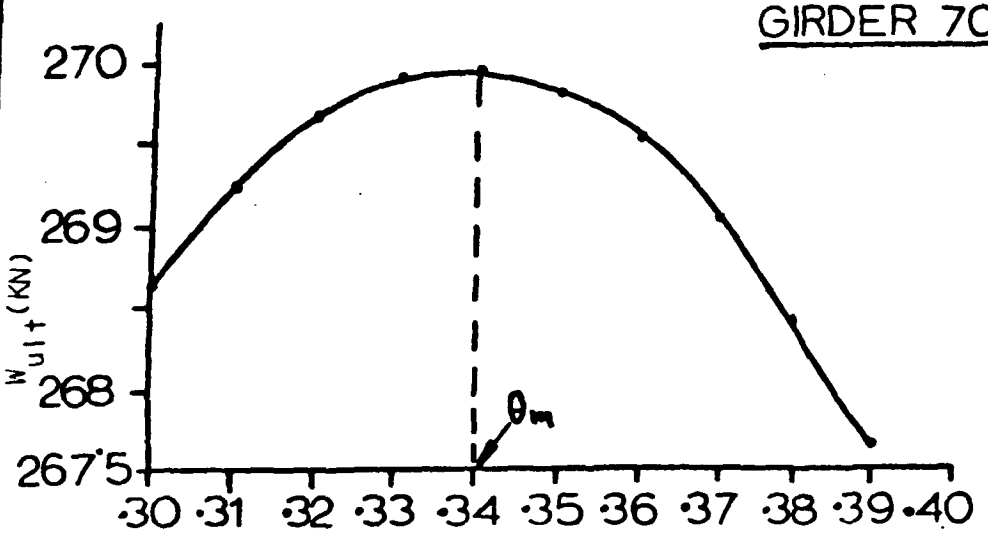

Figure 4.7.1(f)

Figure 4.7.1(a) to (g)

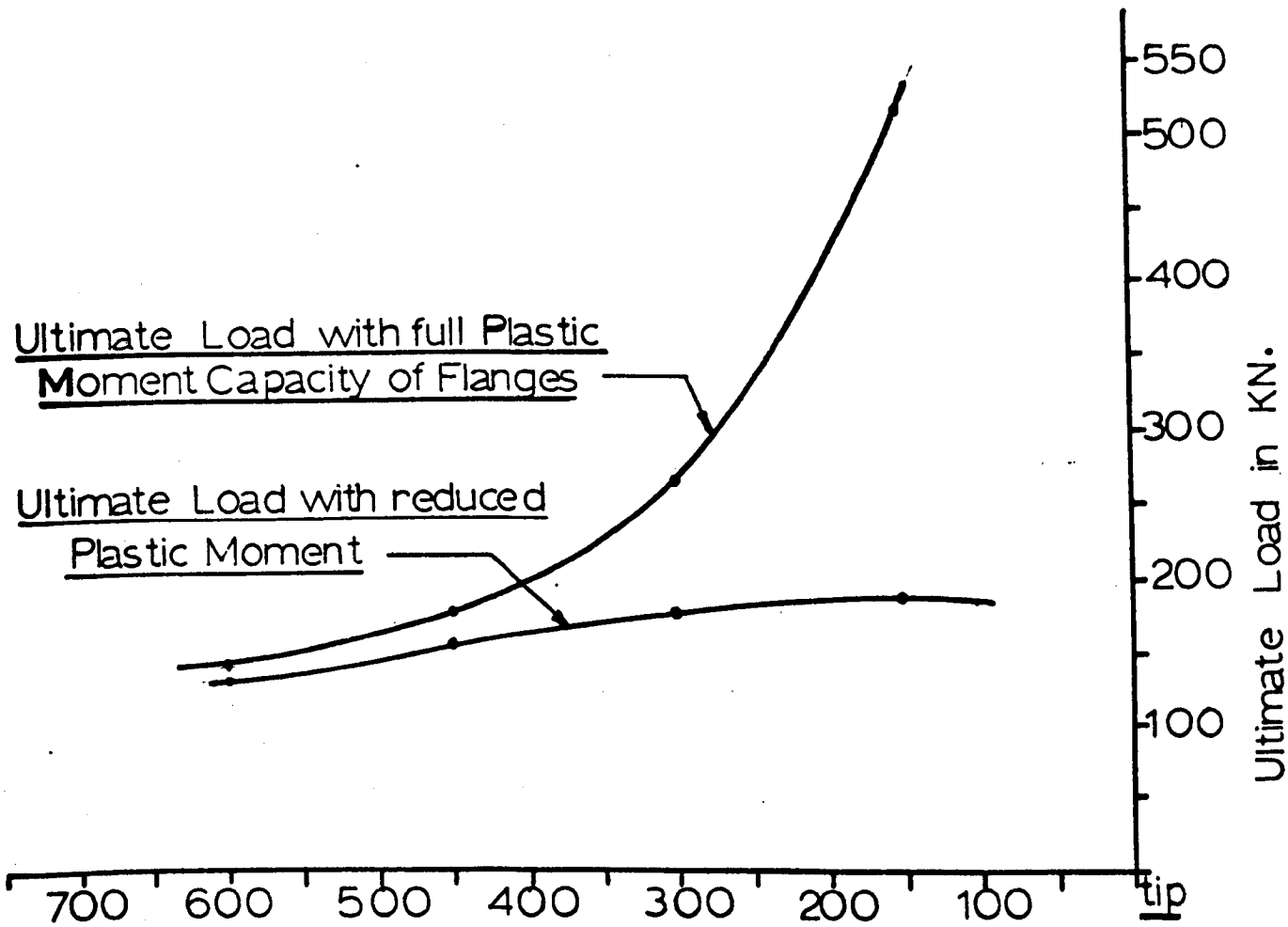
Ultimate Load with full Plastic Moment Capacity of Flanges
Ultimate Load with reduced Plastic Moment
550
500
400
300
200
100
Ultimate Load in KN.
700
600
500
400
300
200
100
tip
Eccentricity in mm.
Load inside the tip

Figure 4.7.2

Girder No.	Ratio d/t	θm (rad)	C_t (mm)	C_c (mm)	Buckling load of the panel (KN)	Lower bound load (with MP) (KN)	Upper bound load (with MP) (KN)	Ultimate load with reduced MP (KN)	Eccentricity about the tip (mm)
10 (A)	326	0.34	617 (606)	286 (257)	8.80	135.5	135.5	127	600
10 (B)	326	0.34	617 (488)	286 (151)	8.80	262.2	262.2	177	300
20 (A)	326	0.32	598 (560)	266 (207)	8.80	178.1	178.1	154	450
20 (B)	326	0.32	598 (342)	266 (0.0)	8.80	516.8	516.8	182	150
60 (A)	294	0.36	637 (626)	307 (279)	13.60	185.5	185.5	175	639
70 (A)	250	0.34	623 (581)	290 (224)	24.0	270.0	270.0	233	489
70 (B)	250	0.34	623 (490)	290 (147)	24.0	378.8	378.8	258	339

Table 4.7.1

N.B. The values of 'C_t' and 'C_c' shown in brackets are the values obtained from the reduced value of plastic moment capacity of the flanges.

Girder No.	Eccentricity about the tip (mm)	σ_{yw} (N/mm^2)	σ_{yf} (N/mm^2)	Full plastic moment MP (KN mm)	Axial comp. at collapse in comp. flange (KN)	Axial tension at collapse in tension flange (KN)	Reduced Plastic moment of comp. flange (KN mm)	Reduced plastic moment of tension flange (KN mm)
10 (A)	600	255	330	3870	152	31	3140	3733
10 (B)	300	255	330	3870	294	160	1088	2420
20 (A)	450	276	300	3518	220	58	2128	3091
20 (B)	150	276	300	3518	341	247	0.00	1148
60 (A)	639	283	386	5717	203	52	4693	5514
70 (A)	489	290	378	5773	308	74	3431	5014
70 (B)	339	290	378	5773	408	212	1483	3566

Table 4.7.2

buckling load is based on the equivalent rectangular panel of the same width and an average depth of the tapered panel (Figure 4.2.1(a)). However, it can be seen from the results presented in Table 4.7.1 that the buckling load of the panel is significantly lower than the plastic collapse load of the panel. Hence in order to simplify the solution of the plastic collapse of tapered beams, loaded inside the tip, equivalent rectangular panel of the same width and an average depth can be considered.

4.8 General Conclusions

On the basis of the analyses of theoretical results, the following conclusions can be drawn;

(i) The proposed collapse mechanism which consists of two plastic hinges in the tension flange and two plastic hinges in the compression flange (Figure 4.4.1) provides identical collapse loads from upper and lower bound solutions.

(ii) The axial forces in the tension and compression flanges which reduce the plastic moment capacities of the flanges have a significant effect on the ultimate load of tapered beams loaded inside the tip.

(iii) As the eccentricity about the tip decreases the ultimate load, with full plastic moment capacity of flanges, increases significantly (Figure 4.7.2) and theoretically it becomes infinity for zero eccentricity.

(iv) The buckling load of the web panel is significantly lower than the plastic collapse load of the panel. In assessing the buckling load for the plastic collapse load calculations of the tapered panel, an equivalent rectangular panel of same width and an average depth (Figure 4.2.1(a)) can be considered.

CHAPTER FIVE

THE COLLAPSE MODE OF FAILURE OF TAPERED BEAMS LOADED OUTSIDE THE TIP

5.1 Introductory Remarks

In this chapter a plastic collapse mode of failure for tapered steel beams loaded outside the tip is presented which provides an identical collapse load whether obtained from an upper bound or a lower bound solution. The effect of the axial forces on full plastic moment capacity of flanges are discussed and the collapse loads are predicted using these reduced values of plastic moment. Finally, the theoretical results are described and discussed and conclusions are drawn.

5.2 Possible Modes of Failure

As with the possible collapse modes of failure of tapered steel beams loaded inside the tip, explained in Chapter four, similarly the collapse modes of failure of tapered steel beams loaded outside the tip are divided into three phases.

Phase : 1 PURE SHEAR BEHAVIOUR

For a perfectly rectangular flat, web plate, there will be a uniform shear stress throughout the web panel prior to buckling. A principal tensile stress (σ_t) and a principal compressive stress (σ_c) of magnitude 'τ' will act at 45^o and 135^o respectively to the horizontal (Figure 5.22). This stress system which exists for the loading below the critical shear stress 'τ_{cr}' is known as the state of pure shear behaviour.

To assess the buckling load of the tapered panel loaded outside the tip, similar assumptions are made as explained in section 4.2 (Chapter four). The values of critical shear stresses

are calculated by using equation (4.1), (4.2) and (4.3) presented in the previous chapter.

Phase : 2 POST BUCKLED BEHAVIOUR

When the shear stress reaches the value of the critical shear stress, the panel buckles and it cannot sustain any increase in the compressive stress. After the panel has buckled, any additional load has to be carried by the tensile membrane stress 'σ_t' (Figure 5.2.1(b)) which develops along the tension diagonal. Because the beam is loaded outside the tip, the direction of the 'tip-moment' will be opposite to direction of 'tip-moment' when the load was inside the tip (Chapter Four). Due to change in the direction of 'tip moment' the tension and compression diagonals (considered in previous chapter) interchange. The tensile membrane stress imposes a lateral pull on the flanges and under this action, the flanges clearly bend inwards as shown in Figure 5.2.1(b).

Phase : 3 ULTIMATE BEHAVIOUR

On further loading the tensile membrane stress (σ_t) and the critical shear stress (τ_{cr}) produce yielding in the web. The membrane stress at yield is defined as σ_t^y. The panel fails when the plastic hinges have formed in the flanges which together with the yield zone 'UVWX' (Figure 5.2.1(c)) forms a plastic collapse mechanism. As explained in Chapter Four, the plastic yielding could extend beyond the boundaries 'UVWX', but the minimum requirements for a plastic mechanism to form is that the complete region 'UVWX' must yield.

5.3 Collapse Mechanism Proposed

The proposed collapse mechanism consists of two plastic hinges in the tension flange and two plastic hinges in the com-

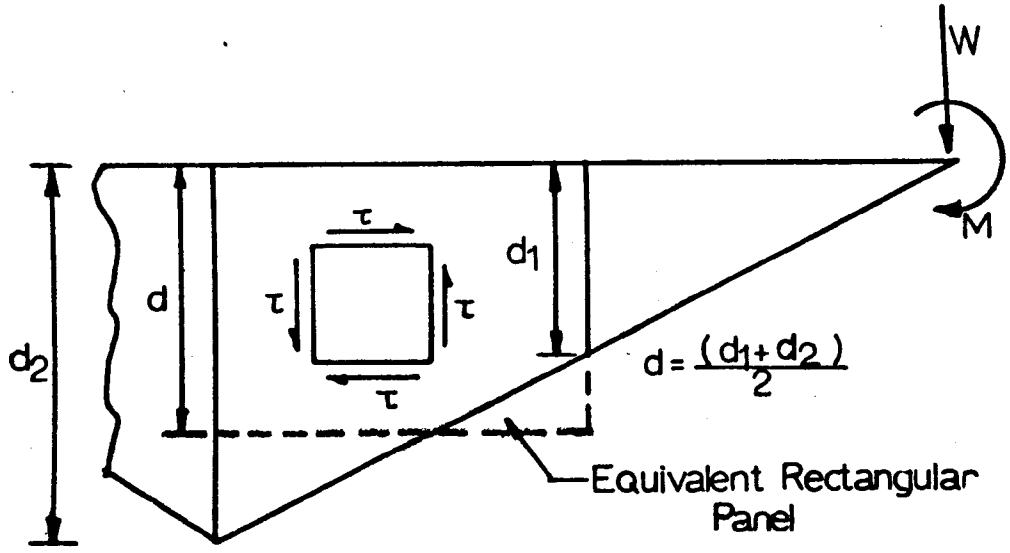

Phase : 1 $\tau < \tau_{cr}$ Figure 5.2.1(a)

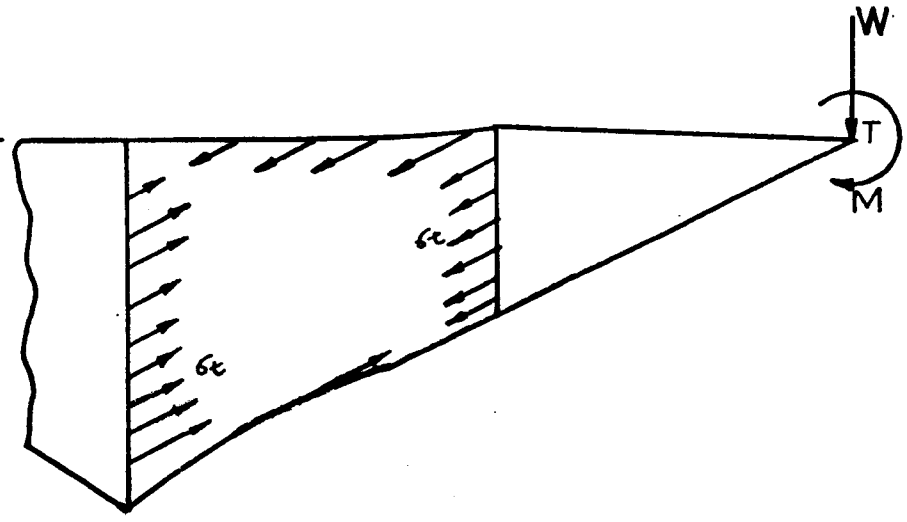

Phase : 2 $\tau \geq \tau_{cr}$ Figure 5.2.1(b)

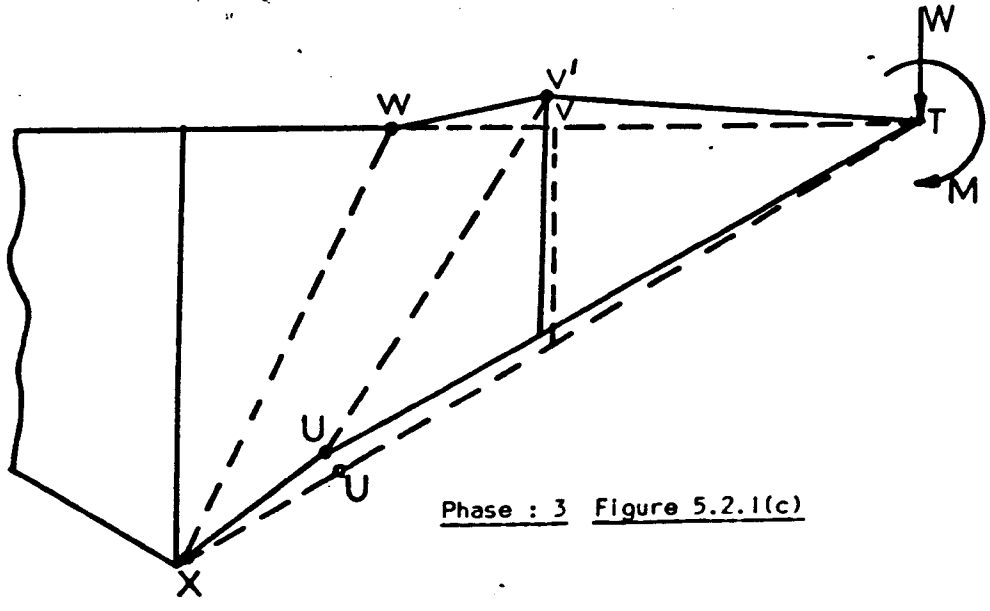

Phase : 3 Figure 5.2.1(c)

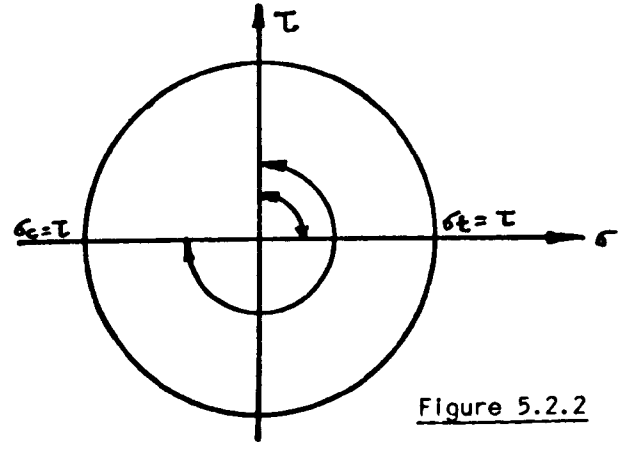

Figure 5.2.2

pression flange as shown in Figure 5.4.1. At collapse it is assumed that the wedge 'UVT' (Figure 5.2.1(c)) rotates about the tip in the direction of the 'tip moment', such that the vertical displacement of the tip is zero. Because the direction of tip moment is clockwise, so the wedge 'UVT' will rotate about the tip in clockwise direction as shown in Figure 5.2.1(c).

The failure load can be determined by considering the mechanism developed in 'phase : 3' (Figure 5.2.1(c)). As explained in Chapter Four, the region 'UVWX' can be considered cut out from the web plate and its action upon the flanges and the adjacent web material can be replaced by the inclined membrane stresses as shown in Figure 5.4.1.

5.4 Lower Bound (Equilibrium) Solution

As explained in section 4.4 of the previous chapter, the ultimate load condition will be considered to be composed of a critical shear stress condition plus the post buckled action. The forces in the post buckled range are shown in Figure 5.4.1. Consider a section 'W-U' passing through the two internal plastic hinges where the internal and external forces acting in the post buckled range are shown in Figure 5.4.2(a).

To satisfy the equilibrium of vertical forces and moments at 'W', the following equations are obtained:

$$\Sigma V = 0$$

$$W = F_c.\sin\gamma - F_s.\sin\theta$$

i.e. $$F_c\sin\gamma = W + F_s.\sin\theta \qquad (5.1)$$

$$F_c = [W + F_s.\sin\theta]/\sin\gamma \qquad (5.2)$$

ΣM at W = 0

$$W.(z - b + C_t) + F_s.\frac{WR}{2} + M + M_{pt} - M_{pc} - F_c.$$

$$\sin\gamma(z - b + C_t) = 0$$

After substituting the value of $F_c.\sin\gamma$ from equation (5.1) and letting $M_{pt} = M_{pc}$ (for full plastic moment capacity of flanges) the above equation can be expressed as:

$$W(z - b + C_t) + F_s.(\frac{WR}{2}) + W.e - (z - b + C_t).$$

$$\left[W + F_s.\sin\theta\right] = 0$$

i.e. $$W.e = F_s.\left[(z - b + C_t)\sin\theta - \frac{(WR)}{2}\right]$$

$$W = \frac{F_s}{e}\left[(z - b + C_t).\sin\theta - \frac{(WR)}{2}\right]$$

$$\therefore W_{ult} = \frac{F_s}{e}\left[(z - b + C_t).\sin\theta - \frac{(WR)}{2}\right] + V_{cr} \qquad (5.3)$$

The axial forces in the tension flange can be calculated from the horizontal equilibrium of forces, i.e.

$$F_t = \left[F_c.\cos(\gamma) - F_s.\cos\theta\right]$$

i.e. $$F_t = \left[W\cot\gamma - F_s.(\cos\theta - \cot\gamma.\sin\theta)\right] \qquad (5.4)$$

The positions of internal plastic hinges 'U' and 'W' can be obtained in similar way as explained in section 4.4 of the previous chapter, by considering the equilibrium of the beam section 'W-V' and X-U' respectively. By taking moments at 'V' and 'X' (Figures 5.4.2(b) and 5.4.2(c)) one can obtain the following equations respectively:

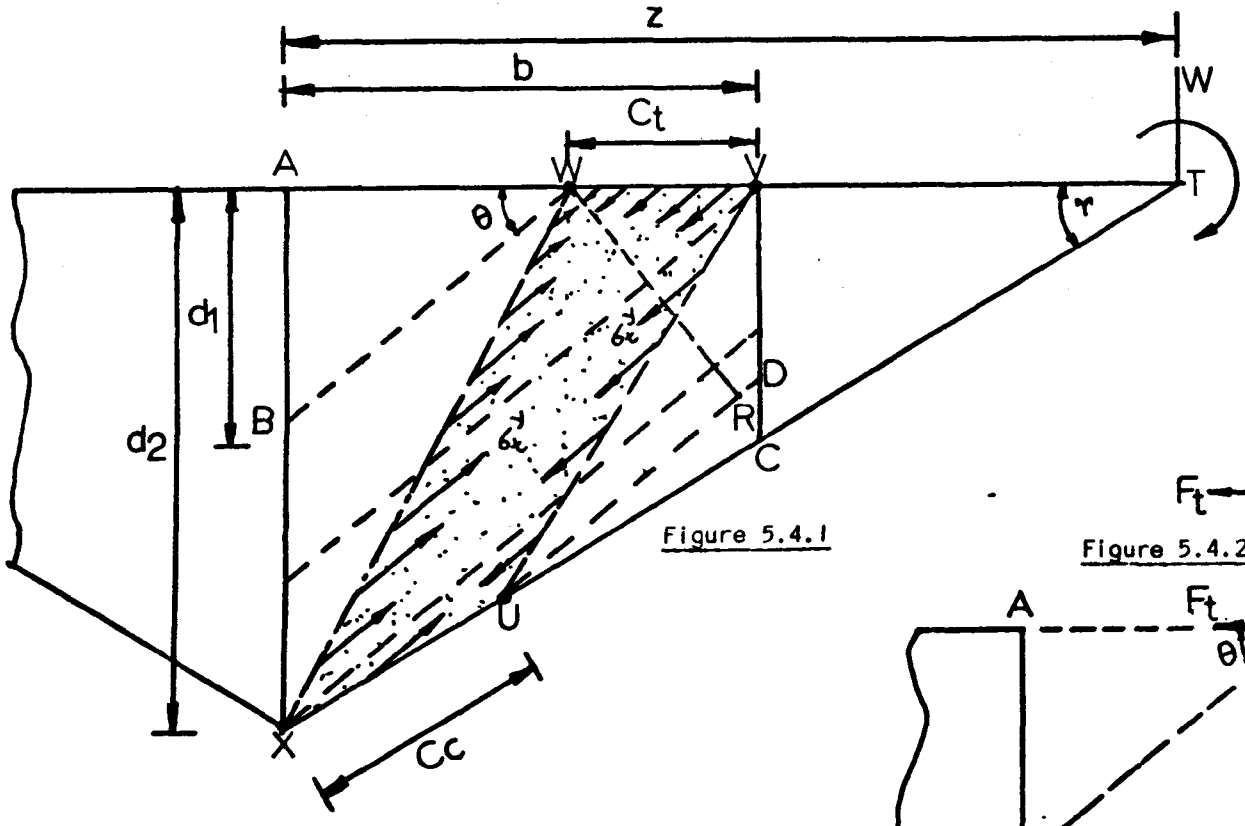

Figure 5.4.1

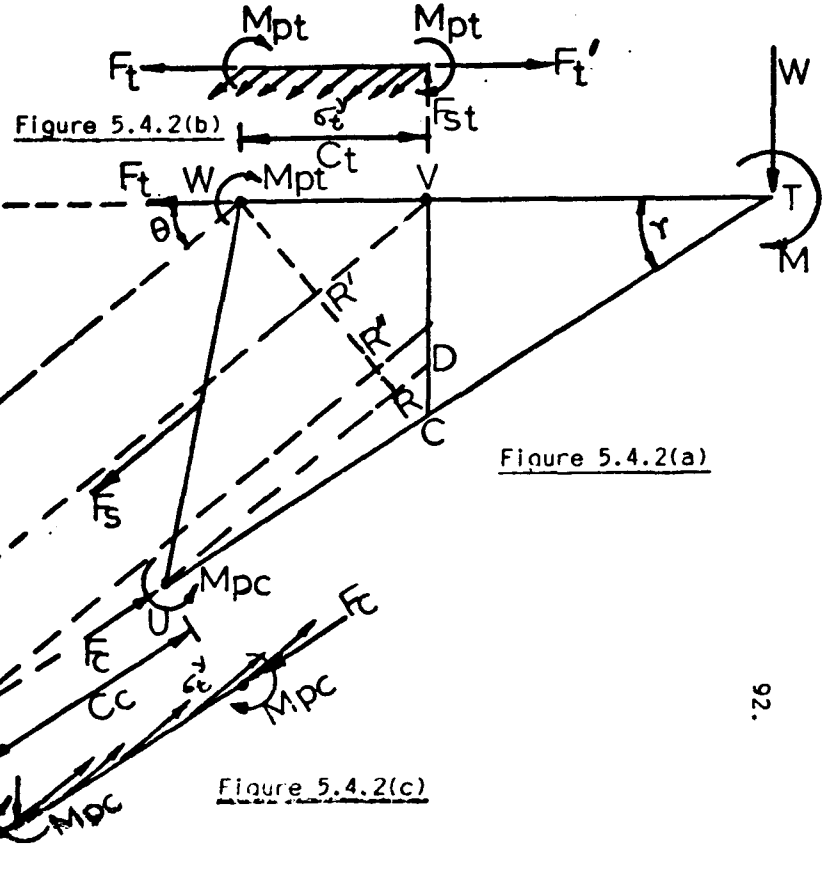

Figure 5.4.2(b)

Figure 5.4.2(a)

Figure 5.4.2(c)

$$C_t = \frac{2}{\sin\theta} \cdot \sqrt{\frac{M_{pt}}{t.\sigma_t^y}} \tag{5.5}$$

$$C_c = \frac{2}{\sin(\theta - \gamma)} \cdot \sqrt{\frac{M_{pc}}{t.\sigma_t^y}} \tag{5.6}$$

Equations (5.5) and (5.6) hold for all positive values of σ_t^y and for all values of 'C_t' and 'C_c' within the range of $0 < C_t < b$ and $0 < C_c < b \cdot \sec\gamma$ respectively.

The value of 'σ_t^y' is obtained by using equation (4.13) presented in the previous chapter.

As explained in Chapter Four (section 4.4) that to support the validity of the lower bound solution it is necessary to show that the stress distribution throughout the structures, is in equilibrium, balances the external loads and does not violate the yield condition. The lower bound solution presented previously in this section shows that the forces are in equilibrium. Similar to the previous case when the tapered beam was loaded inside the tip (Chapter Four), a set of forces can be obtained which will maintain equilibrium in the wedge 'AWB' and 'CUD' (Figure 5.4.3(a)) without violating yield. As shown in Figure 5.4.3(a) the yield band coincides with the internal plastic hinge position at 'W' and 'U'. Because the shear forces are zero at the internal plastic hinge positions, the normal reactions at A and C will be zero as shown in Figures 5.4.3(b) and 5.4.3(c) respectively. Therefore the flange moment will remain constant and equal to the plastic moment between the flange portion 'W-A' and 'U-C' in the tension and compression flange respectively (Figures 5.4.3(b) and 5.4.3(c)) and hence it does not violate the yield condition.

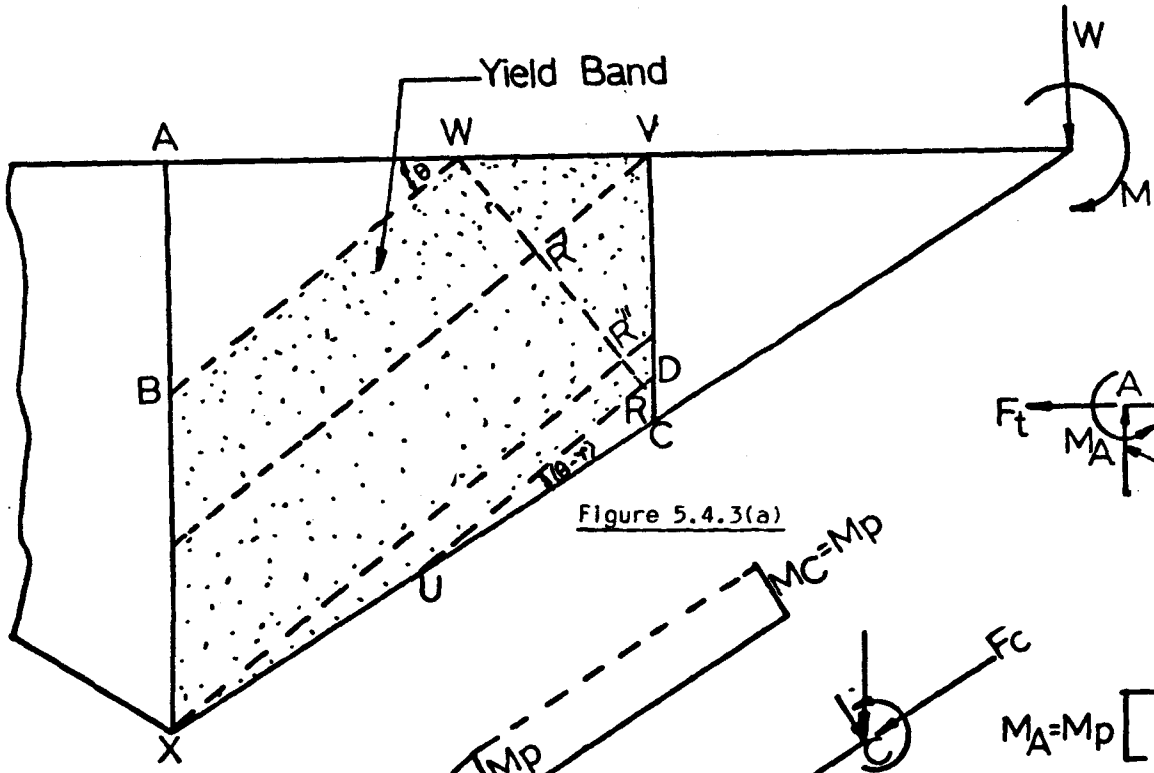

Figure 5.4.3(a)

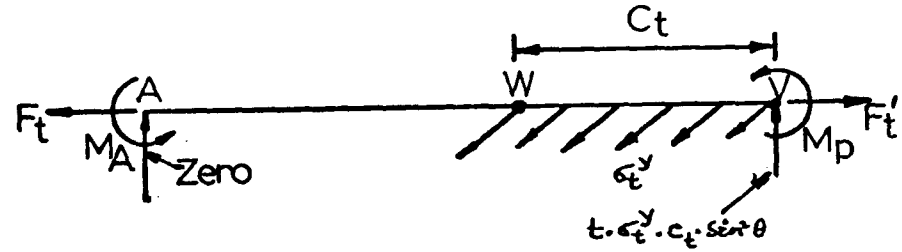

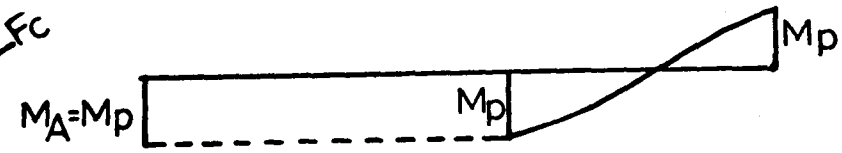

Bending Moment Diagram

Figure 5.4.3(b)

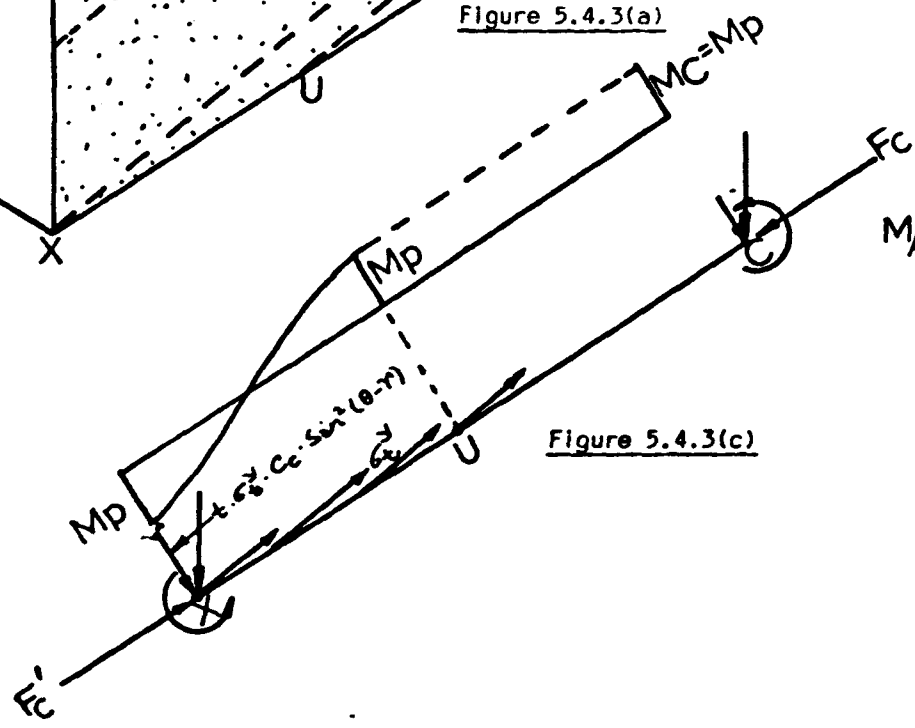

Figure 5.4.3(c)

If the yield band extends beyond 'W' and 'U' then the moment acting between 'W' and 'A' in the tension flange and 'U' and 'C' in the compression flange will be reduced as shown in Figures 5.4.4(a) and 5.4.4(b) respectively.

It can be seen from Figure 5.4.5 that even when the yield band extends beyond the tension diagonal band, the equilibrium of forces at any section P-P remains unchanged.

Thus the lower bound solution presented in this section is valid because in any case the equilibrium of internal and external forces are maintained and at the same time it does not violate the yield condition.

5.5. Upper Bound (Mechanism) Solution

Consider the rotations of plastic hinges at W, V, U and X are θ_1, θ_2, θ_3 and θ_4 respectively as shown in Figure 5.5.1. For small value of β (Figure 5.5.1), the magnitude of θ_1, θ_2, θ_3 and θ_4 can be obtained from the geometrical relations of triangles WV'T and XU'T (Figure 5.5.1) respectively.

$$\theta_1 = \frac{(z - b)}{C_t} . \beta \qquad (5.7)$$

$$\theta_2 = \frac{(z - b + C_t)}{C_t} . \beta \qquad (5.8)$$

$$\theta_3 = \frac{d_2}{C_c . \sin\gamma} . \beta \qquad (5.9)$$

and $$\theta_4 = \left[\frac{d_2}{C_c . \sin\gamma} - 1 \right] . \beta \qquad (5.10)$$

From the collapse mechanism shown in Figure 5.5.1, it is clear that the stresses acting on section W-X do no work, and therefore only those stresses acting on the inclined right hand

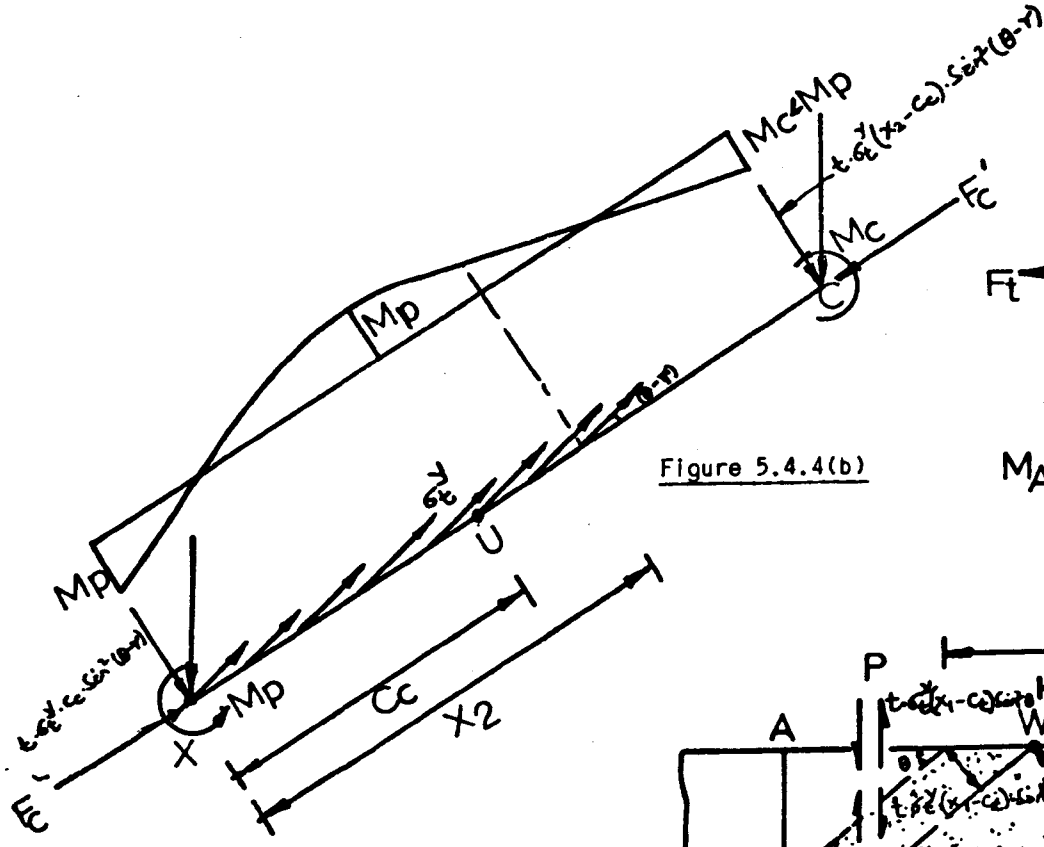

Figure 5.4.4(b)

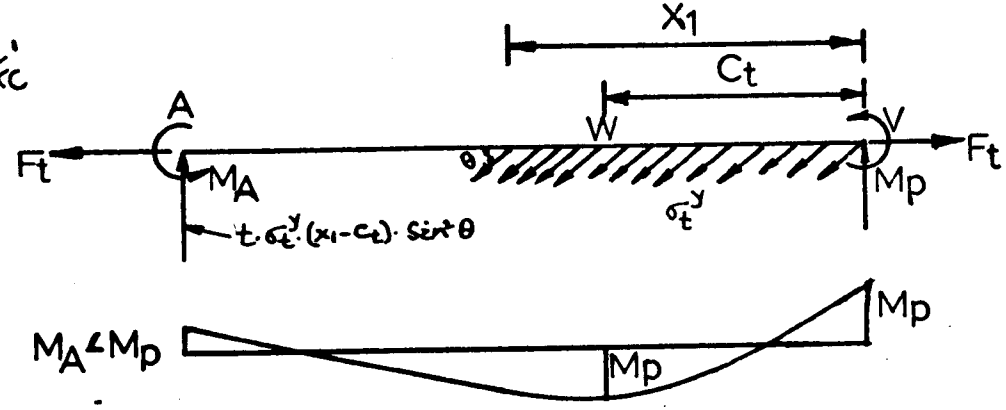

Figure 5.4.4(a)

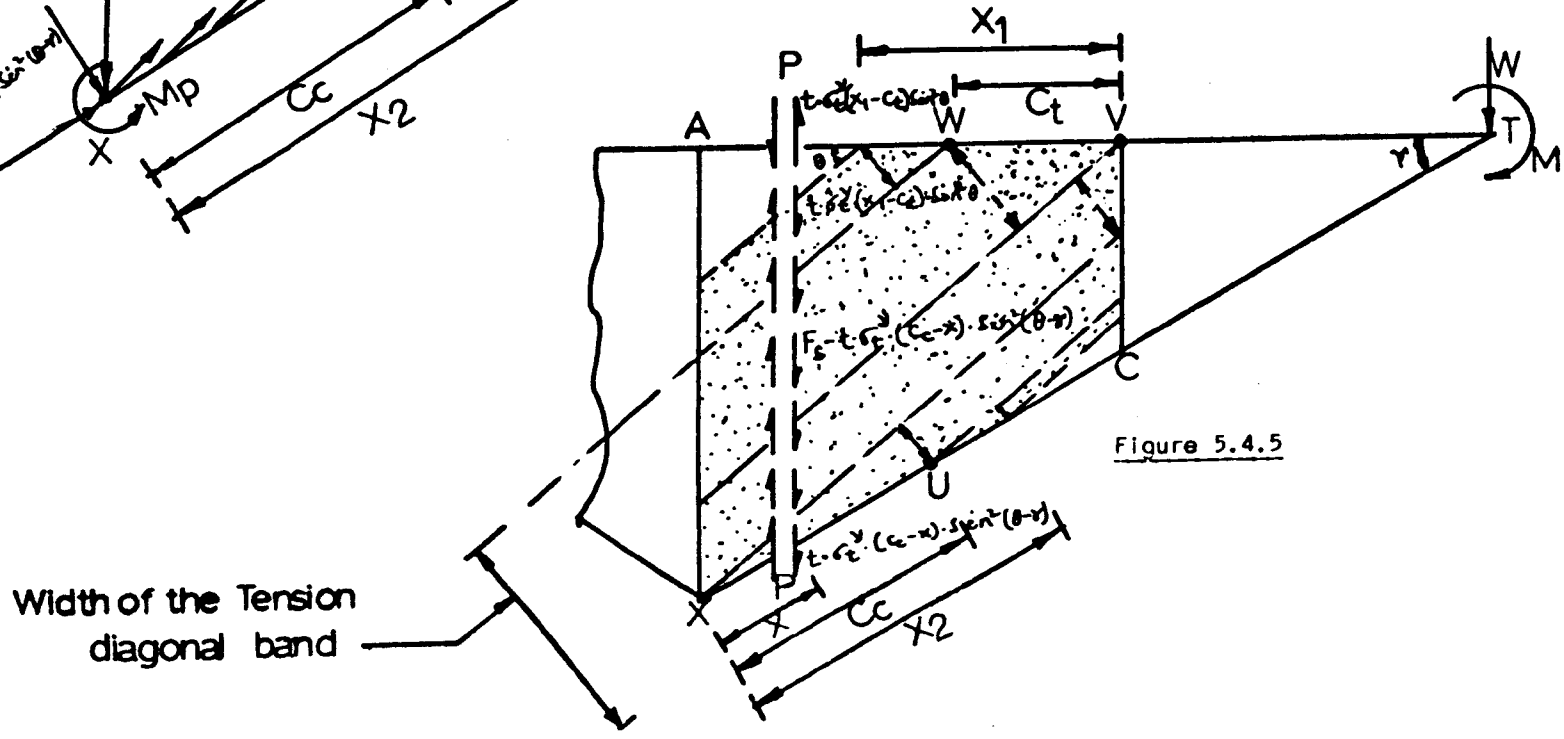

Figure 5.4.5

web section (U-V) and the flanges will do work.

The total virtual work done can be divided into four parts:

(i) work done by stresses acting on tension flange (Figure 5.5.2(a))

(ii) work done by stresses acting on compression flange Figure 5.5.2(b))

(iii) Work done by stresses acting on the inclined web section U-V (Figure 5.5.2(c))

(iv) work done due to rotations at the plastic hinges.

(i) Internal virtual work done by σ_t^y on the tension flange will be equal to:

$$+\frac{t.\sigma_t^y}{2}.\left[C_t.\sin\theta\right]^2\frac{(z-b)}{C_t}.\beta \qquad (5.11)$$

(ii) Internal virtual work done by σ_t^y on the compression flange will be equal to:

$$-\frac{t.\sigma_t^y}{2}\left[C_c.\sin(\theta-\gamma)\right]^2.\left[\frac{d_2}{C_c.\sin\gamma}-1\right].\beta \qquad (5.12)$$

This work will be negative because the displacement of the flange takes place in the opposite direction to the direction of the forces (Figure 5.5.2(b)).

(iii) The internal virtual work done by σ_t^y on the inclined web section U-V (Figure 5.5.2(c)) will be equal to:

$$+\frac{t.\sigma_t^y}{2}.\left[RR'\right].\left[(z-b).\sin\theta+\left[\frac{d_2}{\sin\gamma}-C_d\right].\sin(\theta-\gamma)\right].\beta \qquad \ldots (5.13)$$

where $RR' = \left[C_c.\sin(\theta-\gamma) + d_2\cos\theta - b.\sin\theta\right]$

(iv) The internal virtual work done due to rotations at the

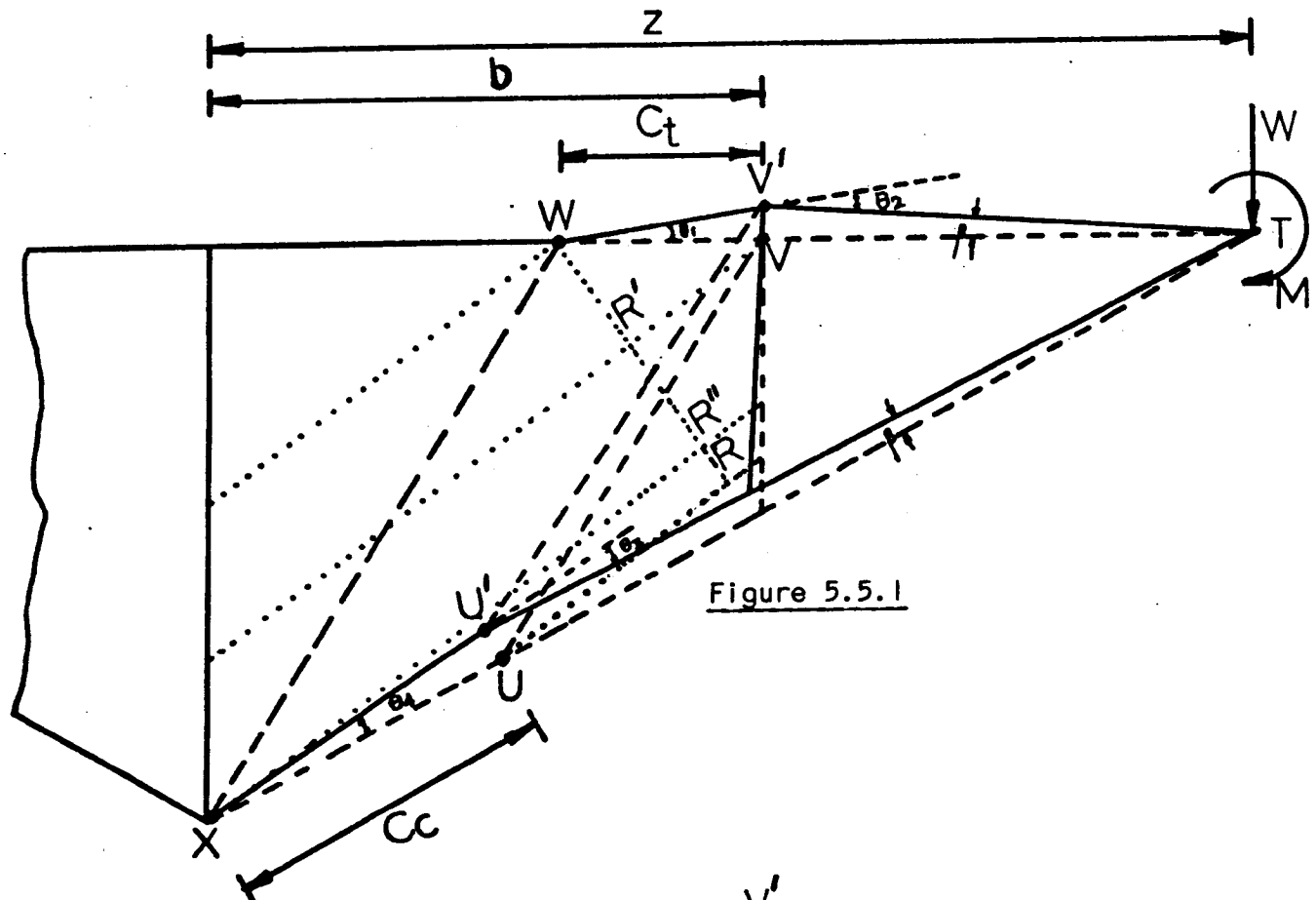

Figure 5.5.1

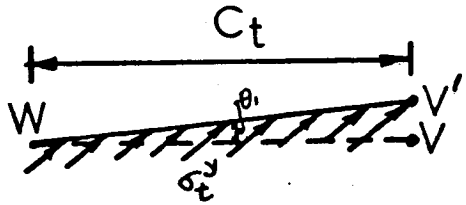

Figure 5.5.2(a)

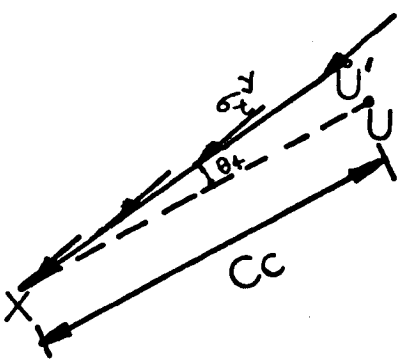

Figure 5.5.2(b)

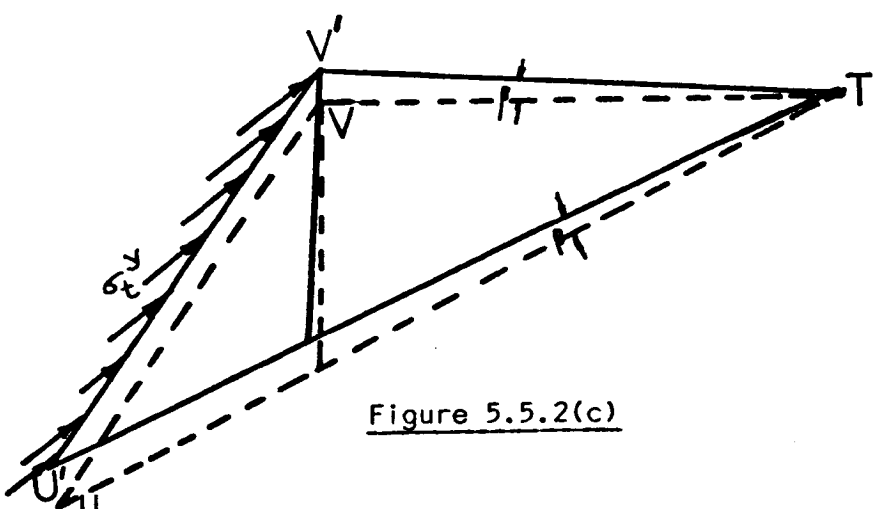

Figure 5.5.2(c)

plastic hinges will be equal to:

$$M_p(\theta_1 + \theta_2 + \theta_3) = 2M_p \cdot \left[\frac{(z - b)}{C_t} + \frac{d_2}{C_c.\sin\gamma}\right].\beta \qquad (5.14)$$

Therefore the total internal virtual work done will be equal to:

$$2M_p \cdot \left[\frac{(z - b)}{C_t} + \frac{d_2}{C_c.\sin\gamma}\right]\beta + \frac{t.\sigma_t^y}{2}\left[(z - b)\sin\theta.(WR)\right.$$

$$\left. + \left(\frac{d_2}{\sin\gamma} - C_c\right).\sin(\theta - \gamma).(d_2\cos\theta - b.\sin\theta)\right].\beta$$

External work done in the mechanism will be equal to:

$W \times 0 + M \times \beta = W.e.\beta.$

By equating the external and internal virtual work done one can obtain:

$$W = \frac{1}{e}\left[2M_p \cdot \left[\frac{(z - b)}{C_t} + \frac{d_2}{C_c.\sin\gamma}\right] + \frac{t.\sigma_t^y}{2}\left[(z - b)\sin\theta.(WR) + \right.\right.$$

$$\left.\left.\left(\frac{d_2}{\sin\gamma} - C_c\right).\sin(\theta - \gamma) \times (R'R'')\right]\right] \qquad (5.15)$$

The ultimate load will be equal to the load 'W' carried by the membrane field and the flanges, together with the buckling load.

Therefore $W_{ultimate} = W + V_{cr}$

$$W_{ult} = \frac{1}{e}\left[2M_p\left[\frac{(z - b)}{C_t} + \frac{d_2}{C_c.\sin\gamma}\right] + \frac{t.\sigma_t^y}{2}\left[(z - b).\right.\right.$$

$$\left.\left.\sin\theta.(WR) + \left(\frac{d_2}{\sin\gamma} - C_c\right).\sin(\theta - \gamma).(R'R'')\right]\right] + \frac{\tau_{cr}.(d_1 + d_2).t}{2}$$

... (5.16)

A computer program shown in Appendix 2 (A2.1) was written by the author to calculate the collapse loads, with full plastic moment capacity of flanges, obtained from an upper and lower bound solutions for various values of 'θ' (inclination of the tensile membrane stress field).

5.6 Effect of Axial Forces on Plastic Moment Capacity of Flanges

It can be noted from Table 5.7.2 that the axial forces in the flanges of tapered beams loaded outside the tip are quite large. It can also be noted (Table 5.7.2) that for smaller eccentricity of load outside the tip, the plastic moment of resistance of the inclined compression flange reduces quite significantly. Therefore it is necessary to allow for the reduction of the plastic moment capacity of the flanges resulting from the presence of the axial forces.

The magnitude of axial forces in the tension and compression flanges can be obtained from the equations (5.4) and (5.2) respectively. These equations for the axial forces do not include the effect of horizontal (complementary) shear stresses. However, it is possible to obtain the expressions for the axial forces in the flanges from the Figure 5.6.1, which can include the effect of complementary shear stresses. As mentioned before, the effect of complementary shear stresses on the ultimate load is not significant and also the equation for the ultimate load becomes very complicated. Therefore, it was decided to calculate the axial forces in the compression and tension flange (for tapered beams loaded outside the tip) by using equations (5.2) and (5.4) respectively.

However, the effect of vertical and horizontal shear stresses of the web acting on the flange will be taken into

account while calculating the average flange stresses, as indicated below.

The average force in the compression flange contributed by the membrane stresses acting on the flange (Figure 5.6.2(a)) will be equal to

$$\frac{t.\sigma_t^y}{2}.C_c.\sin(\theta - \gamma).\cos(\theta - \gamma) \qquad (5.17)$$

The average axial force in the compression flange contributed by the buckling stresses (Figures 5.6.2(a) and (b)) will be equal to:

$$\tfrac{1}{2}\,\tau_{cr}.\sin 2\gamma.t.C_c \qquad (5.18)$$

Therefore the total average flange stress for the compression flange will be equal to:

$$\sigma_{cf} = \frac{F_c - \left[\sigma_t^y.\sin(\theta - \gamma).\cos(\theta - \gamma) + \tau_{cr}.\sin 2\gamma\right].\frac{t.C_c}{2}}{A_{cf}} \qquad \ldots \quad (5.19)$$

The average axial force in the tension flange contributed by the membrane stresses acting on the flange (Figure 5.6.2(c)) will be

$$= t.\sigma_t^y.C_t \sin\theta.\cos\theta \qquad (5.20)$$

The average axial force in the tension flange contributed by the shear stresses acting on the flange (Figure 5.6.2(c)) will be

$$= \tfrac{1}{2}\,\tau_{cr}.t.C_t \qquad (5.21)$$

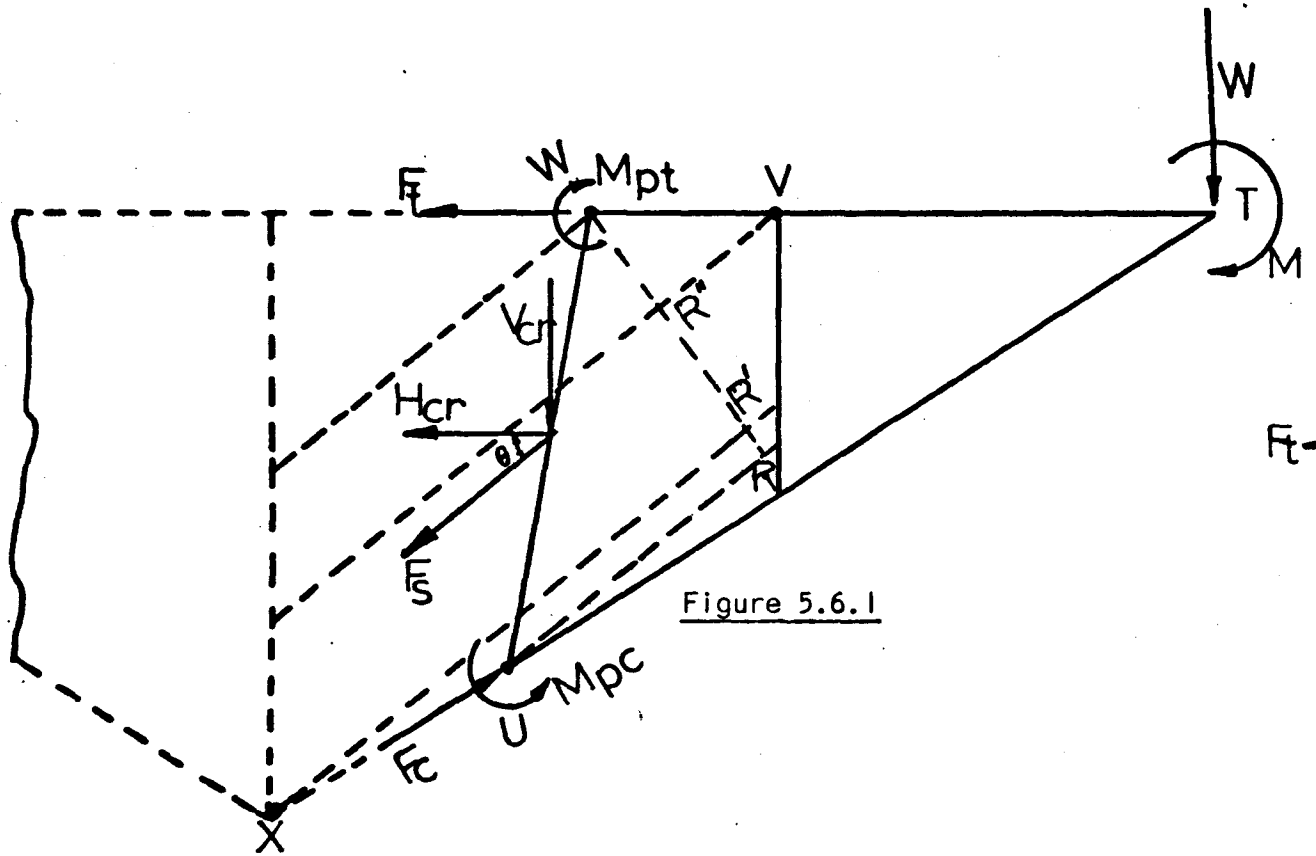

Figure 5.6.1

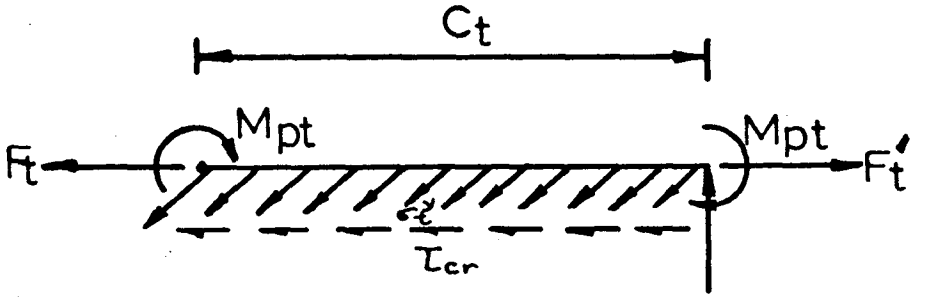

Figure 5.6.2(c)

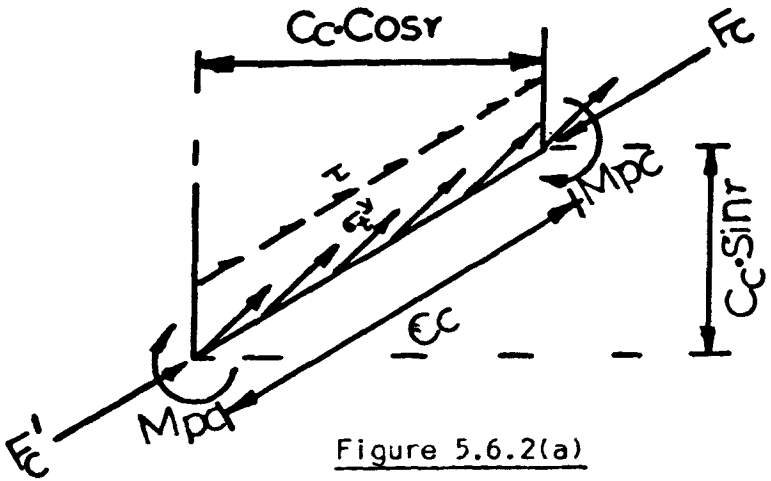

Figure 5.6.2(a)

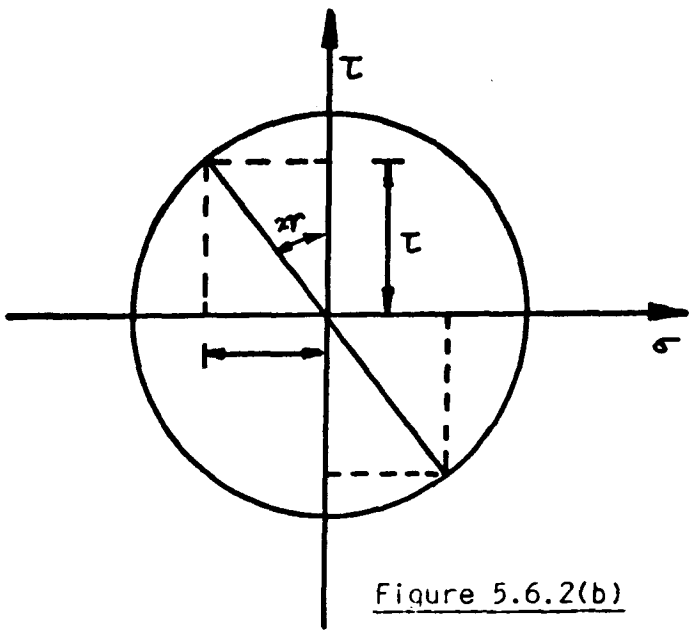

Figure 5.6.2(b)

Therefore the total average flange stresses for the tension flange will be:

$$\sigma_{tf} = \frac{F_t + \left(\sigma_t^Y.\sin\theta.\cos\theta + \tau_{cr}\right).\frac{t.C_t}{2}}{A_{tf}} \qquad (5.22)$$

The assumptions, procedures and other details for calculating the full plastic moment and the reduced plastic moment capacity of the flanges of all the tapered beams loaded outside the tip are the same as described and discussed in the previous chapter (section 4.6). Therefore the values of reduced plastic moments of the compression and the tension flanges are calculated from equations (4.26) and (4.27) respectively.

However, the plotted graphs of $\frac{M}{M_p}$ against $\frac{N}{N_p}$ for hogging and sagging moments(for all girders loaded outside the tip) are shown in Figures 5.6.3(a) to 5.6.3(c).

Because the values of reduced plastic moment capacity of tension flange (M'_{pt}) and compresssion flang (M'_{pc}) will be different, the lower bound load will be given by the equation shown below:

$$W_{ult} = \frac{1}{e}.\left[F_s.\left[(z - b + C_t).\sin\theta - \frac{(WR)}{2}\right] - \left[M'_{pt} - M'_{pc}\right]\right] + V_{cr} \qquad (5.23)$$

A computer program, shown in Appendix 2 (A2.2), was written by the author to analyse the collapse load by considering the reduced plastic moment capacity of the flanges for tapered beams loaded outside the tip.

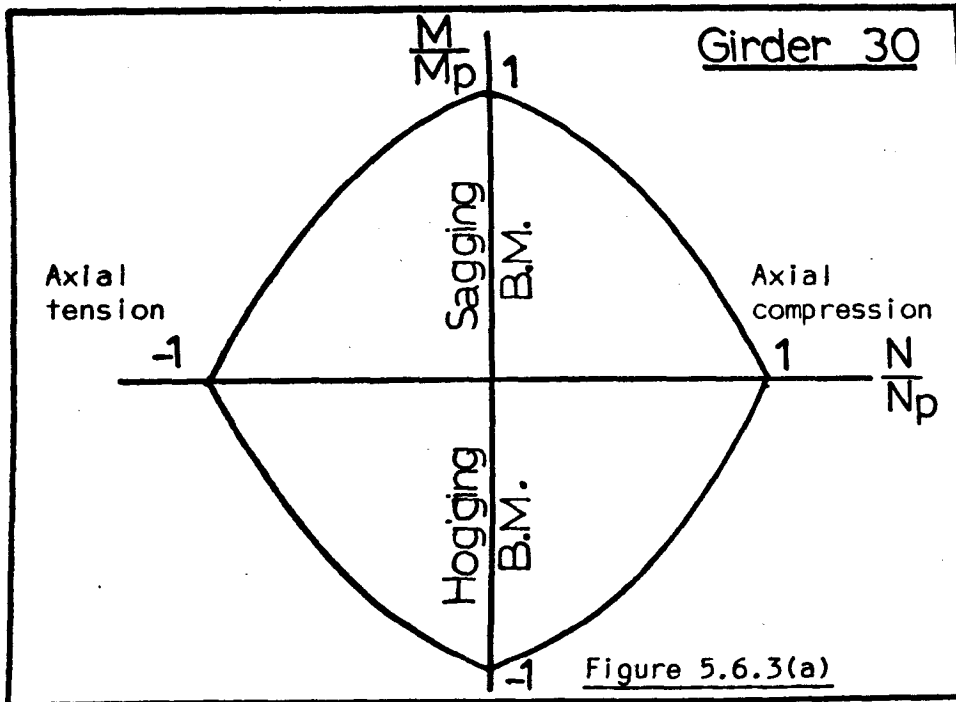

Figure 5.6.3(a)

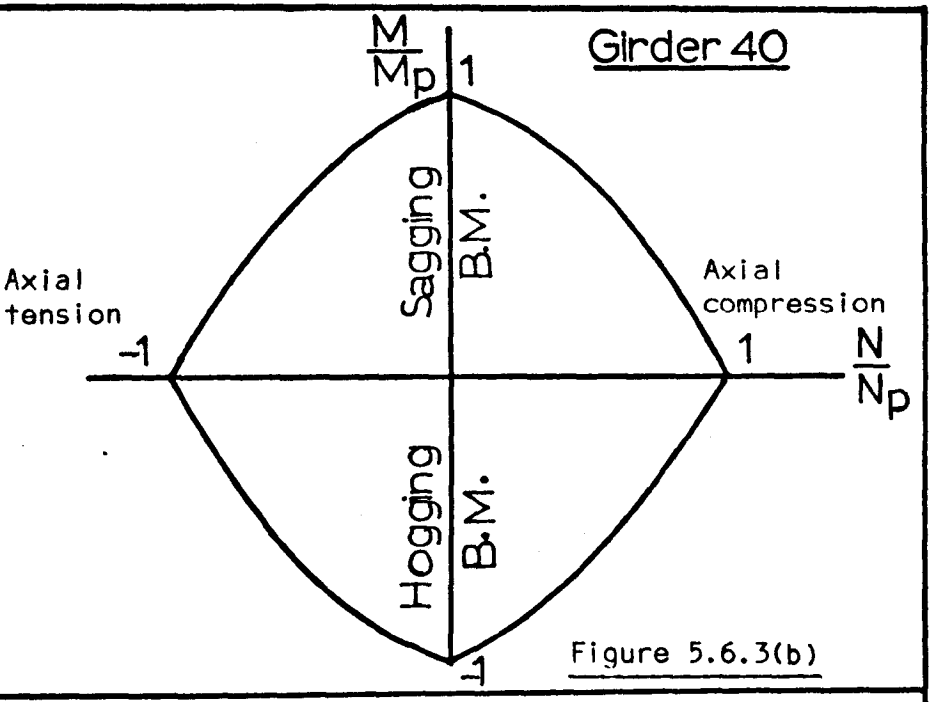

Figure 5.6.3(b)

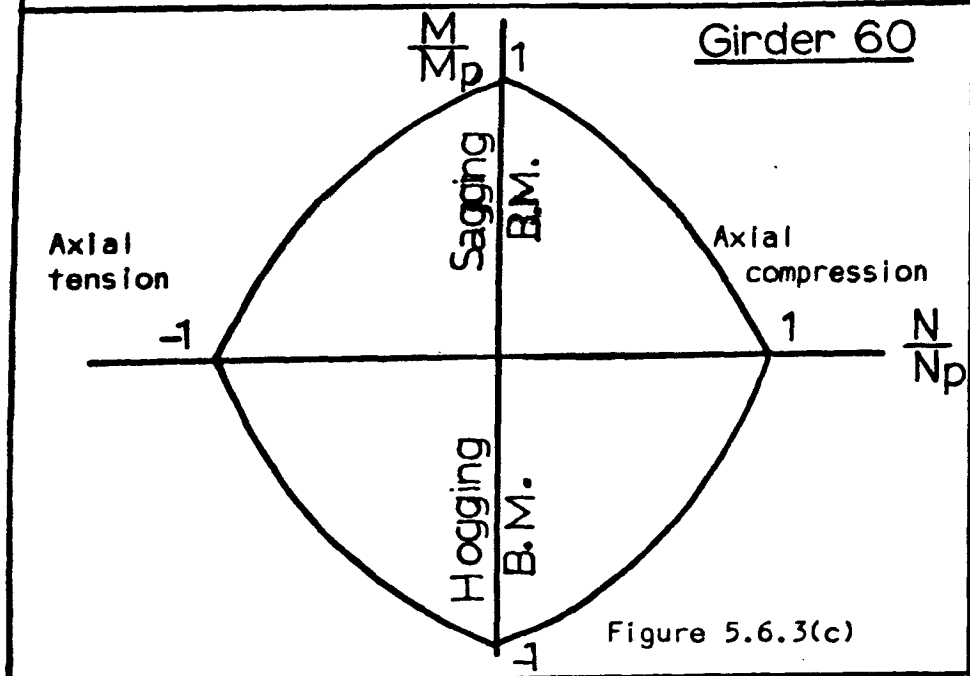

Figure 5.6.3(c)

5.7 Analysis and Discussions of the Theoretical Results

The analysis of results obtained from the collapse mechanism proposed in this chapter shows that the collapse loads with full plastic moment capacity of the flanges are the same, obtained from both the upper and lower bound solutions as shown in Table 5.7.1.

The variations of upper and lower bound loads with inclinations of the tensile membrane stresses are shown in Figure 5.7.1(a) to 5.7.1(d) where 'θ_m' is defined as the inclination which provides the maximum value of the upper and lower bound load.

The results presented in Table 5.7.2 show that as the eccentricity of loads about the tip becomes smaller, the ultimate load for full plastic moment capacity of the flanges increases significantly. Figure 5.7.2 shows how the eccentricity of the load about the tip affects the ultimate loads obtained from the consideration of the full plastic moment and the reduced plastic moment capacity of flanges.

It can be noticed from the results presented in Table 5.7.2 that as the eccentricity of load about the tip decreases, the magnitude of axial forces in the tension and compression flanges increases and accordingly the plastic moment capacity of the flanges is reduced, hence decreasing the ultimate load quite significantly (Figure 5.7.2).

As explained in the previous chapter, the calculation of the buckling load of the tapered panel is based on the equivalent rectangular panel of the same width and an average depth (Figure 5.2.1(a)). However, it can be seen from the results presented in Table 5.7.2 that the buckling load of the panel is very low compared with the plastic collapse load of

Girder No.	D/t ratio $d=\frac{d_1+d_2}{2}$	θ_m (rad.)	C_t (mm)	C_c (mm)	Lower bound load with MP (KN)	Upper bound load with full plastic moment (MP) (KN)	Ultimate load with reduced plastic moment (KN)	Eccentricity (mm)
30 (A)	294	0.73	313 (205)	777 (320)	162.80	162.80	97.40	461
30 (B)	294	0.73	313 (153)	777 (0.0)	440.80	440.80	133.40	161
40 (A)	294	0.74	333 (200)	808 (280)	241.00	241.00	124.90	311
60 (B)	294	0.74	337 (230)	820 (391)	201.00	201.00	124.99	461

Table 5.7.1

N.B. The values of 'C_t' and 'C_c' shown in brackets are the values obtained from the reduced value of plastic moment capacity of the flanges.

GIRDER 30A

Figure 5.7.1(a)

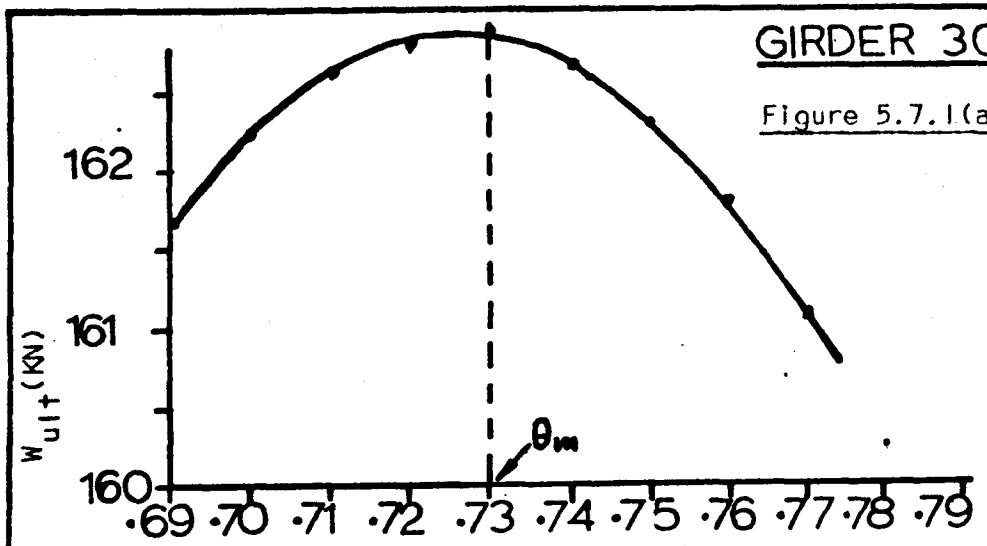

Inclination of membrane stress field 'θ' in radians

GIRDER 40A

Figure 5.7.1(c)

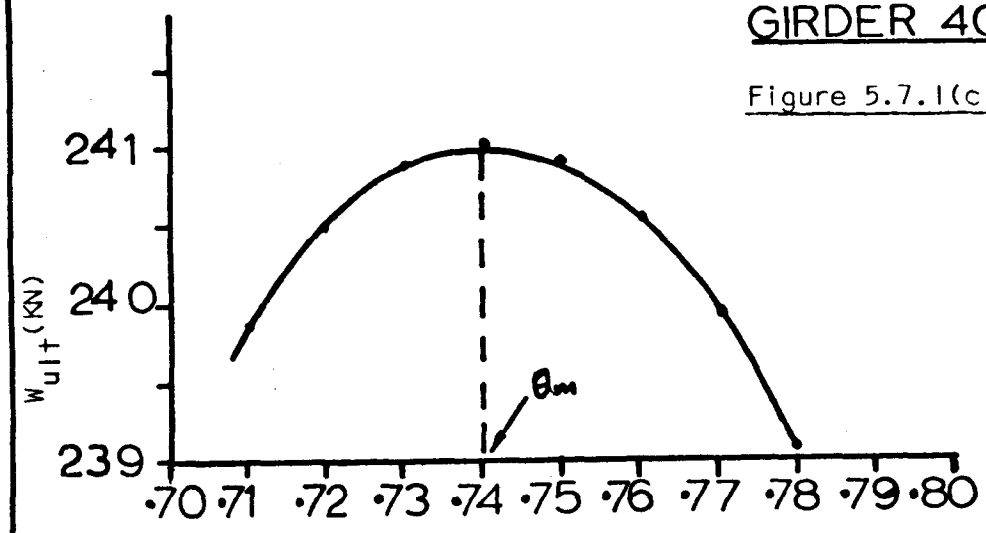

θ in radians

GIRDER 30B

Figure 5.7.1(b)

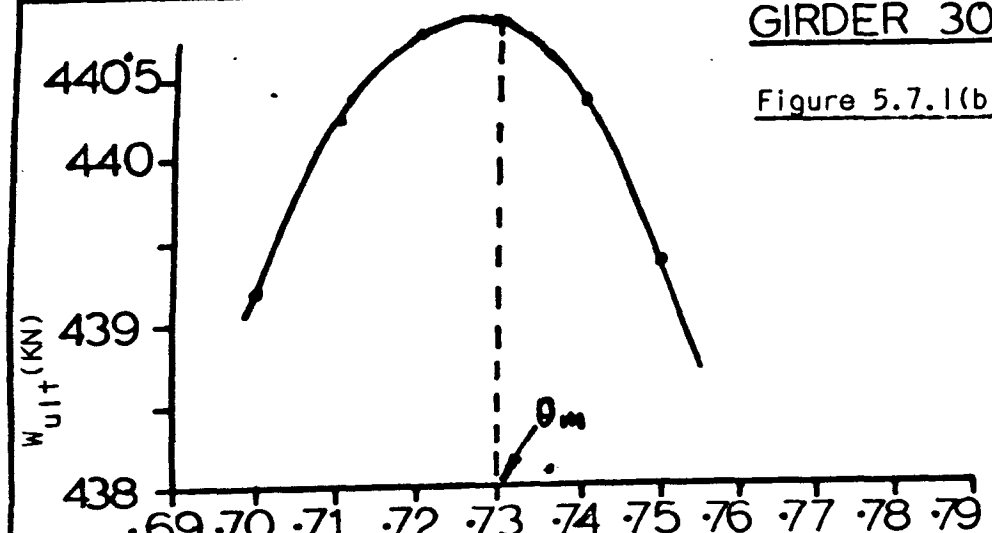

θ in radians

GIRDER 60B

Figure 5.7.1(d)

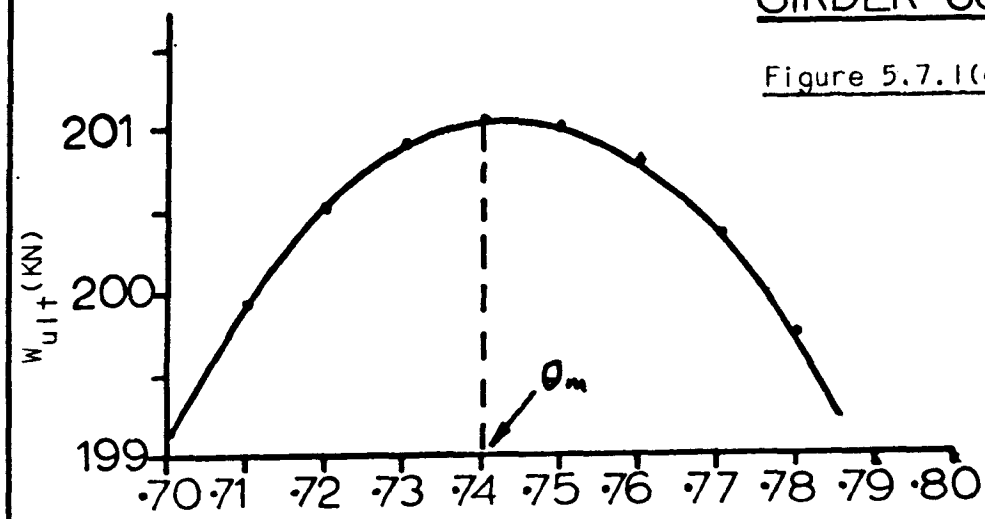

θ in radians

Girder No.	Eccentricity about the tip (mm)	σ_{yw} (N/mm^2)	σ_{yf} (N/mm^2)	Full plastic moment MP (KN mm)	Axial comp. at collapse in comp. flange (KN)	Axial tension at collapse in tension flange (KN)	Reduced plastic moment of comp. flange (KN mm)	Reduced plastic moment of tension flange (KN mm)	Buckling load of the panel
30 (A)	461	249	310	4159	322	222	706	1787	13.60
30 (B)	161	249	310	4159	339	272	0.00	999	13.60
40 (A)	311	239	324	4612	368	272	555	1663	13.60
60 (B)	461	283	386	5717	426	297	1302	2642	13.60

Table 5.7.2

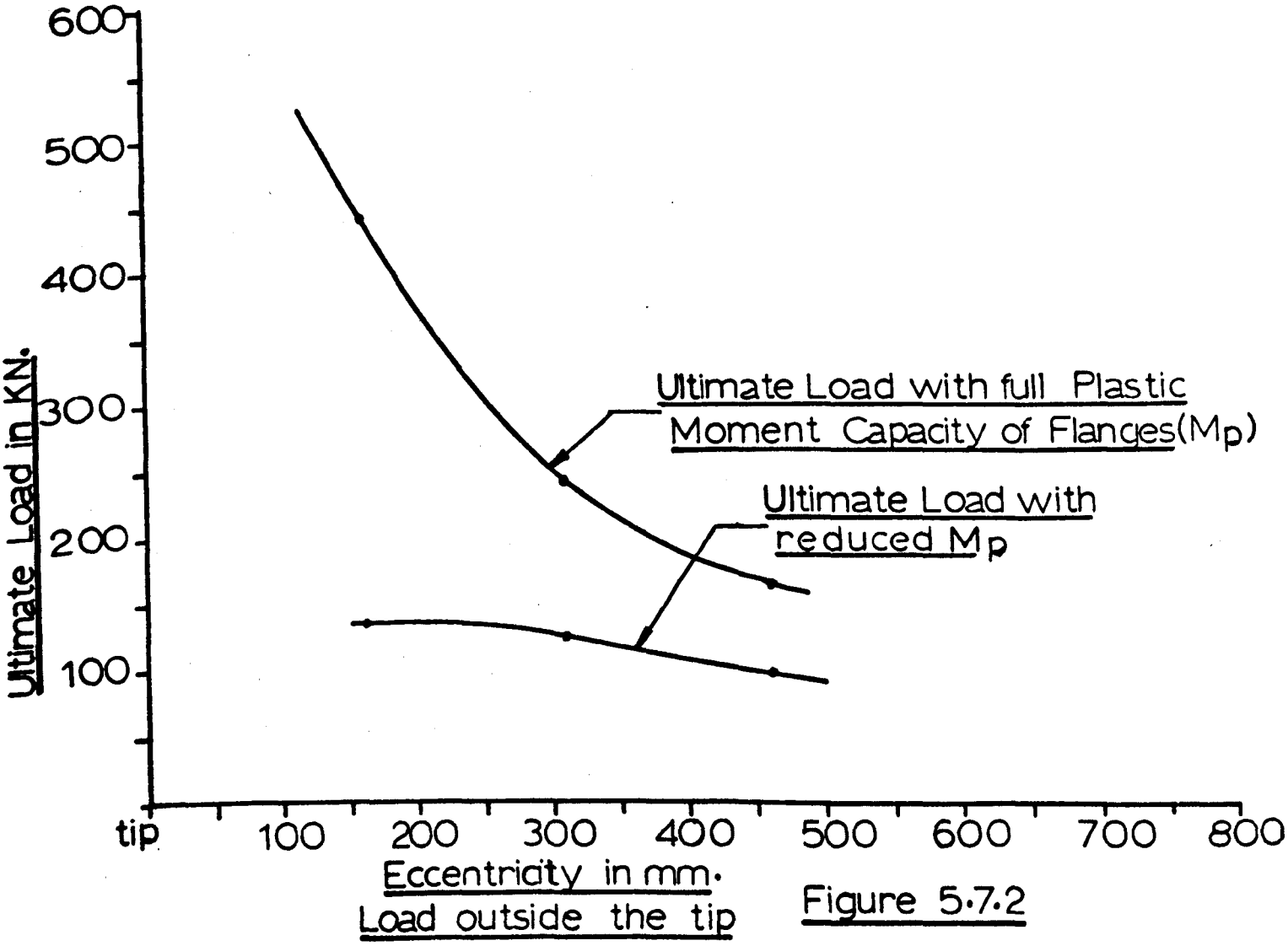
600
500
400
300
200
100
Ultimate Load in KN.
Ultimate Load with full Plastic Moment Capacity of Flanges(Mp)
Ultimate Load with reduced Mp
tip
100
200
300
400
500
600
700
800
Eccentricity in mm.
Load outside the tip

Figure 5.7.2

the panel and hence to provide the simplicity to the solution of the plastic collapse of tapered beams loaded outside the tip, equivalent rectangular panel of the same width and an average depth can be considered.

5.8 General Conclusions

On the basis of the analyses of theoretical results, the following conclusions can be drawn:

(i) The proposed collapse mechanism which consists of two plastic hinges in the tension flange and two plastic hinges in compression flange (Figure 5.4.1) provides identical collapse loads from upper and lower bound solutions.

(ii) The axial forces in the tension and compression flanges which reduces the plastic moment capacity of the flanges have a significant effect on the ultimate load of tapered beams loaded outside the tip.

(iii) The buckling load of the web panel is significantly low with compared to the plastic collapse load of the panel, therefore to assess the buckling load for the plastic collapse load calculations of the tapered panel, an equivalent rectangular panel of the same width and an average depth (Figure 5.2.1(a)) can be considered.

(iv) As the eccentricity of loads about the tip becomes smaller, the ultimate load, with full plastic moment capacity of flanges, increases significantly (Figure 5.7.2).

CHAPTER SIX

THE COLLAPSE MODE OF FAILURE OF TAPERED BEAMS LOADED AT THE TIP

6.1 Introductory Remarks

In this chapter a plastic collapse mode of failure for tapered steel beams loaded at the tip is presented. The collapse loads are predicted and the theoretical results are described and discussed and finally conclusions are drawn.

6.2 Collapse Mechanism Proposed

As described and discussed in Chapter Two (section 2.5), when a tapered beam is loaded at the tip, the elastic shear stresses in the web will be zero, because the tip moment is zero.

However, if there is no shear stress in the web panel, the collapse mode of failure of the beam will be entirely different to the collapse modes when the beam is loaded inside or outside the tip.

Furthermore, because there is no shear stress in the web, tensile membrane stresses will not form in the web panel. In 'Appendix 3' it is analytically varified that the magnitude of the tensile membrane stress must be zero.

Because, there is no tensile membrane stress in the web, the webs will not play any significant role in carrying the load for the plastic collapse of the beam. Therefore the load is carried solely by the flanges which act as members of a truss and hence the web can be neglected while calculating the collapse load of the panel. A section of the web is assumed to act with the flange as described in Chapter Four and shown in

Figure 4.6.3. It will of course be recognised that the web stiffens the flange to some extent (although by a reduced amount if there are large imperfections), and this prevents the flange buckling and allows the flange to yield.

At the collapse, when flange material yields, the beam fails with three hinge rotations of the inclined compression flange and one hinge rotation of the tension flange. Therefore the proposed collapse mechanism consists of one plastic hinge in the tension flange and three plastic hinges in the compression flange as shown in Figure 6.3.1(a). At collapse it is assumed that the wedge 'WXT' rotates in the direction of load giving a large deflection of the tip (Figure 6.2.1).

However, from the geometrical considerations the magnitude of axial forces in the compression flange is higher than the axial forces in the tension flange. Hence for the identical flange properties for both the flanges, the collapse occurs when the compression flange yields or buckles (i.e. when the web either provides negligible resistance to the flange buckling or has large imperfections). For the case when the web provides resistance to the flange buckling, the failure load can be determined by considering a section through 'X-V' (Figure 6.3.1(a)) and resolving the forces vertically and horizontally.

6.3 Lower Bound (Equilibrium) Solution

Consider a section 'X-V' passing through the two plastic hinges where the internal and external forces acting on the section at collapse are shown in Figure 6.3.1(b).

To satisfy the equilibrium of vertical and horizontal forces, the following equations are obtained:

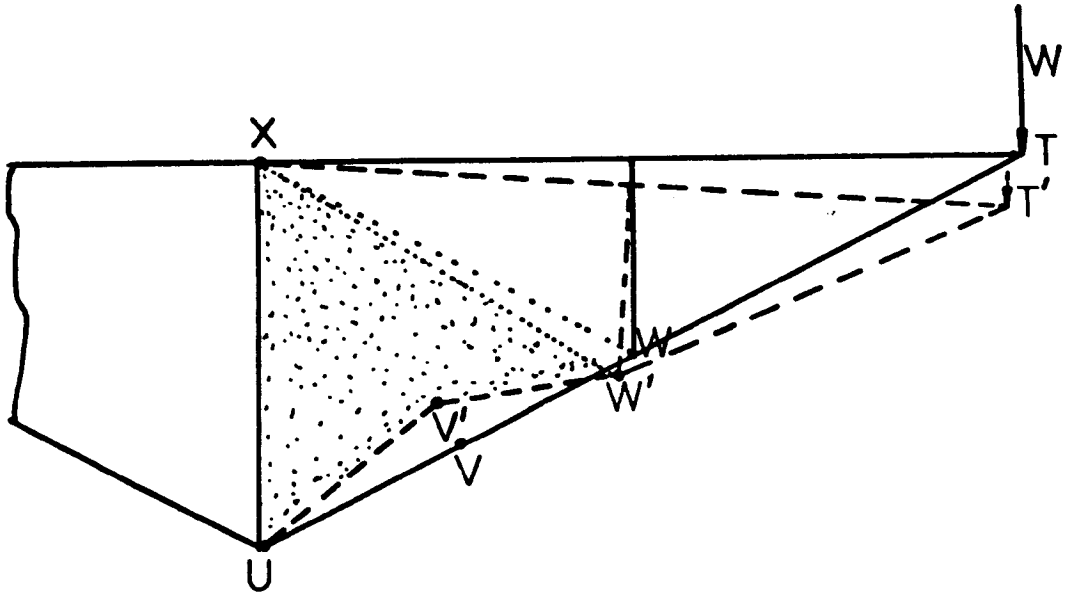

Figure 6.2.1

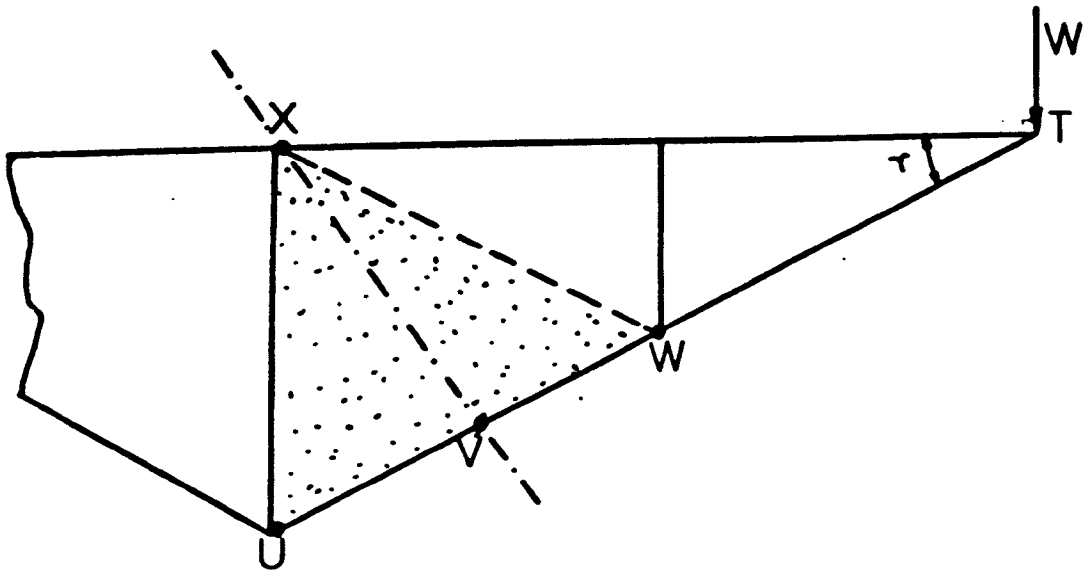

Figure 6.3.1(a)

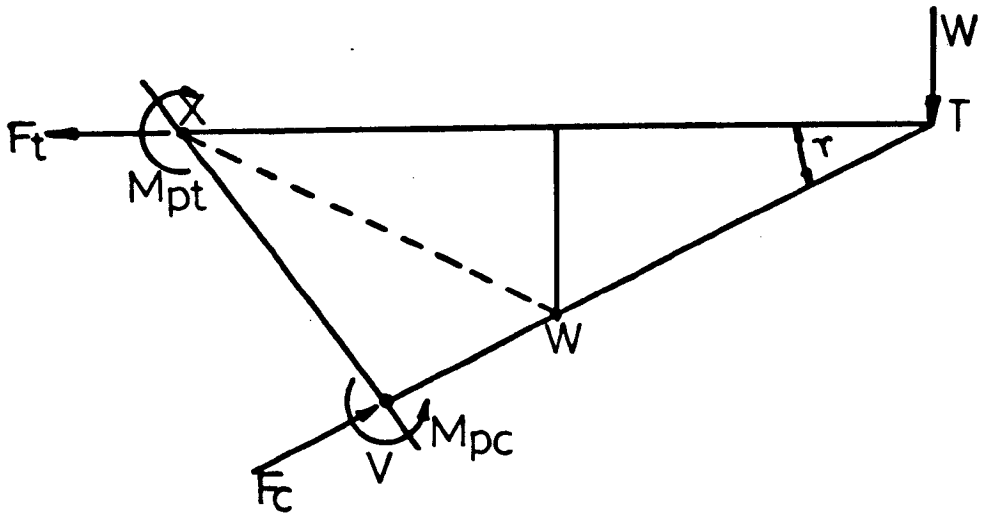

Figure 6.3.1(b)

$$F_c . \sin\gamma = W \tag{6.1}$$

$$F_c . \cos\gamma = F_t \tag{6.2}$$

At yield, $F_c = (\sigma_{yf} \times A_{cf})$ (6.3)

$$\therefore W = (\sigma_{yf} \times A_{cf}) \times \sin\gamma \tag{6.4}$$

and $$F_t = (\sigma_{yf} \times A_{cf}) \times \cos\gamma \tag{6.5}$$

As described in Chapter Four (section 4.6), a section of the web plate was considered to act with the flange section and the depth of the web plate which acts with the flange was calculated from equation (4.26). Similar assumptions are made in this chapter, therefore at yield the axial force 'F_c' will be given by:

$$F_c = (\sigma_{yf} \times A_{cf} + \sigma_{yw} \times A_w) \tag{6.6}$$

Accordingly, the values of 'W' and 'F_t' will be given by equations (6.7) and (6.8) respectively.

$$W = (A_{cf} \times \sigma_{yf} + A_w \times \sigma_{yw}) \times \sin\gamma \tag{6.7}$$

and $$F_t = (A_{cf} \times \sigma_{yf} + A_w \times \sigma_{yw}) \times \cos\gamma \tag{6.8}$$

6.4 Analysis and Discussions of the Theoretical Results

As explained in the previous section, the axial force in the compression flange will always be greater than the axial force in the tension flange. Therefore the calculation of the collapse loads of the beams are based on the yield of the compression flange. The collapse loads, axial tension and axial compression of the flanges presented in Table 6.4.1 are calculated from equations (6.7), (6.8) and (6.6) respectively.

Girder No.	d/t ratio	A/c of the flange (mm^2)	σ_{yf} yield stress of the flange material (N/mm^2)	Area of the web considered to act with flange (mm^2)	σ_{yw} yield stress of the web (N/mm^2)	Inclination of the comp. flange (radians)	Axial tension in the tension flange (KN)	Axial comp. in comp. flange (KN)	Collapse load at the tip (KN)
40 (B)	294	1101	324	63	239	0.46	333.10	371.80	165.0
50 (A)	294	1105	317	59	232	0.46	326.0	364.0	162.0
50 (B)	294	1105	317	59	232	0.46	326.0	364.0	162.0

Table 6.4.1

6.5 General Conclusions

The following conclusions can be drawn about the collapse behaviour of tapered beams loaded at the tip:

(i) The shear stresses in the web panel are approximately zero.

(ii) The tensile membrane stresses in the web do not develop.

(iii) At the collapse, when flange material yields, the tapered beam fails with three hinge rotations of the compression flange and one hinge rotation of the tension flange.

(iv) The webs of tapered beams loaded at the tip do not play any significant role in carrying the load.

CHAPTER SEVEN

EXPERIMENTAL STUDIES

7.1 Introductory Remarks

This chapter is concerned with the objectives, fabrications, instrumentation and collapse behaviour of steel beams having tapered webs. Each of the beam specimens was investigated as a balanced cantilever beam. Experimental investigations were divided into three test series. In Test Series One, the beam was loaded inside the tip; in Test Series Two, the beam was loaded outside the tip, and in Test Series Three the beam was loaded at or near the tip. Because all the calculations were based on the central dimensions, it was decided to measure the eccentricity of loads (inside and outside the tip) from the central tip as shown in Figures 7.1.1(a) and 7.1.1(b).

7.2 General aim of the experimental studies

Although the main aim of the experimental work was to study the collapse mode of failure and to assess the ultimate load of steel beams having tapered webs, other objectives were to investigate:

(a) The buckling pattern of the web panel by measuring the 'out of plane deflection' of the web.

(b) The presence of the tensile membrane stress field in the web, and to assess its inclination.

(c) The validity of the assumption of 'no tip deflection' for the tapered beams loaded inside and outside the tip.

7.3 Method of Fabrication

It was necessary to use very thin mild steel plate for the web panel to ensure that the critical shear stress 'τ_{cr}' was not

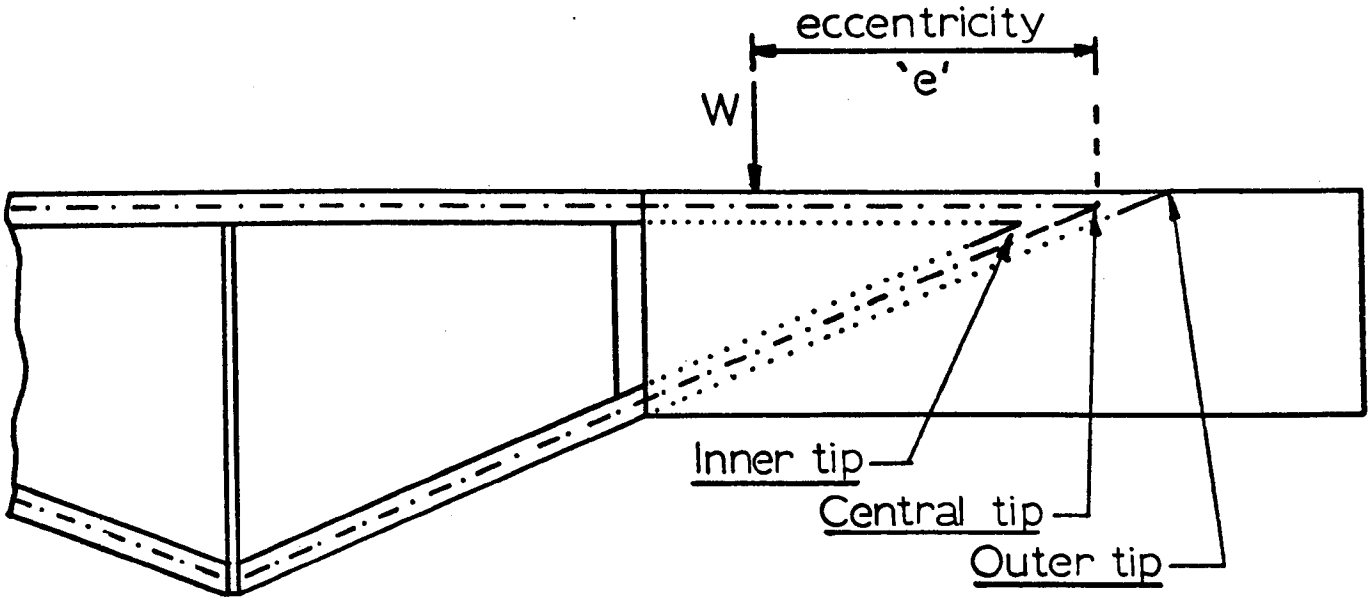

Figure 7.1.1a. Beam Loaded inside the tip

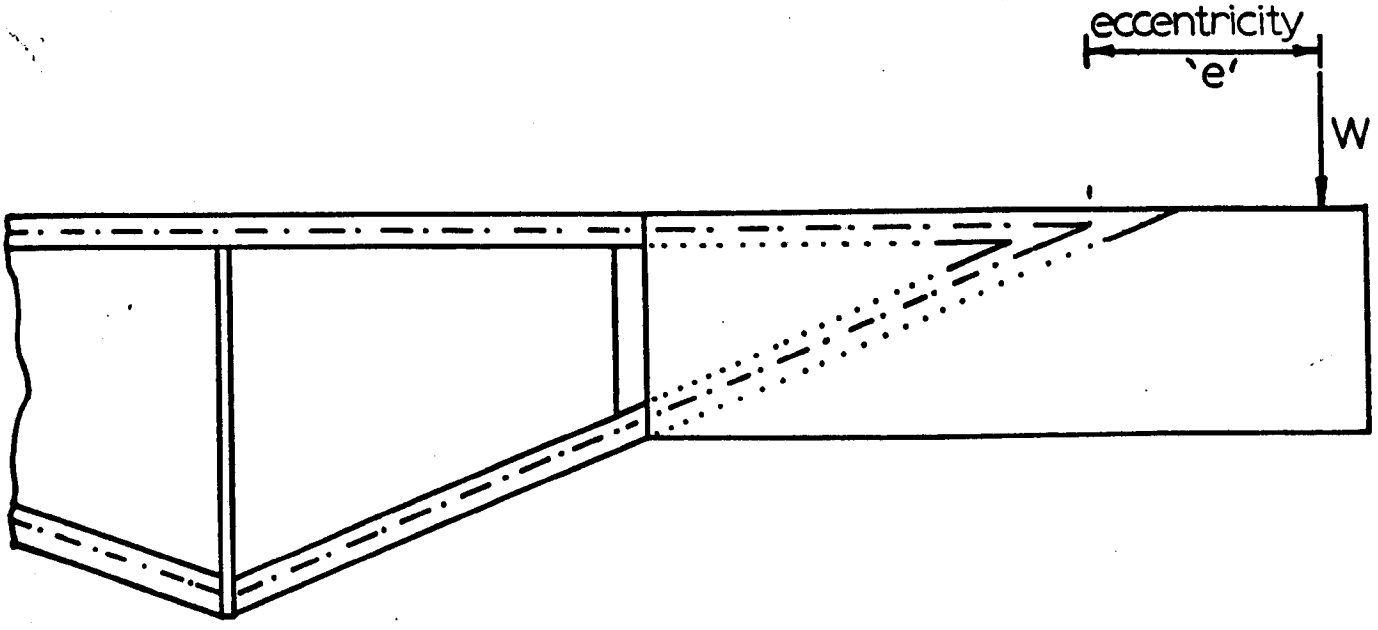

Figure 7.1.1b Beam Loaded outside the tip

so large as to cause the web to yield before it buckled, preventing the formation of the tensile membrane stress field and other post buckling behaviour of the web panel. The web thicknesses varied from 1.5 mm to 2.0 mm for all tapered beam specimens. In order to facilitate testing, tapered beams were fabricated with two identical panels back to back. To reduce the possibility of out of plane failure due to lateral torsional instability, the flanges were fabricated from rectangular rolled hollow sections. First two girders, number 10 and 20, were fabricated from two 50.8 x 25.4 mm Rectangular Hollow Sections of wall thickness 3.2 mm welded back to back on their shorter face with the 1.5 mm thick web plate in the middle (a cross-section of a girder is shown in Figure 7.6.3(a)). The end panels supporting the central tapered panel of the girder were made stronger to ensure that these should not fail before the tapered panel. For the end panels, 3.2 mm thick web plate was used. The cross-section of the flange was the same throughout the length of the girder. Figure 7.3.1 shows the positions of welds and the transverse stiffeners in the central and end panels. The central panel of girders other than girder no. 10 and 20 were fabricated from two 50 x 30 mm R.H.S. of wall thickness 3.2 mm welded back to back on their shorter face with the web plate in the middle. 356 mm x 127 mm x 33 kg/m Universal Beams were used as the end panels. Special precautions were taken while connecting the ends of the universal beams to the central panel. It was ensured that the webs of the universal beams and the central tapered panels were in the same vertical plane and were rigidly connected to each other to get continuous connection between panels so that the applied bending moment and shear force from the end panel could be transferred accurately to the central panel. Figure 7.3.2 shows the positions of welds and other details for the girders numbered 30, 40, 50, 60

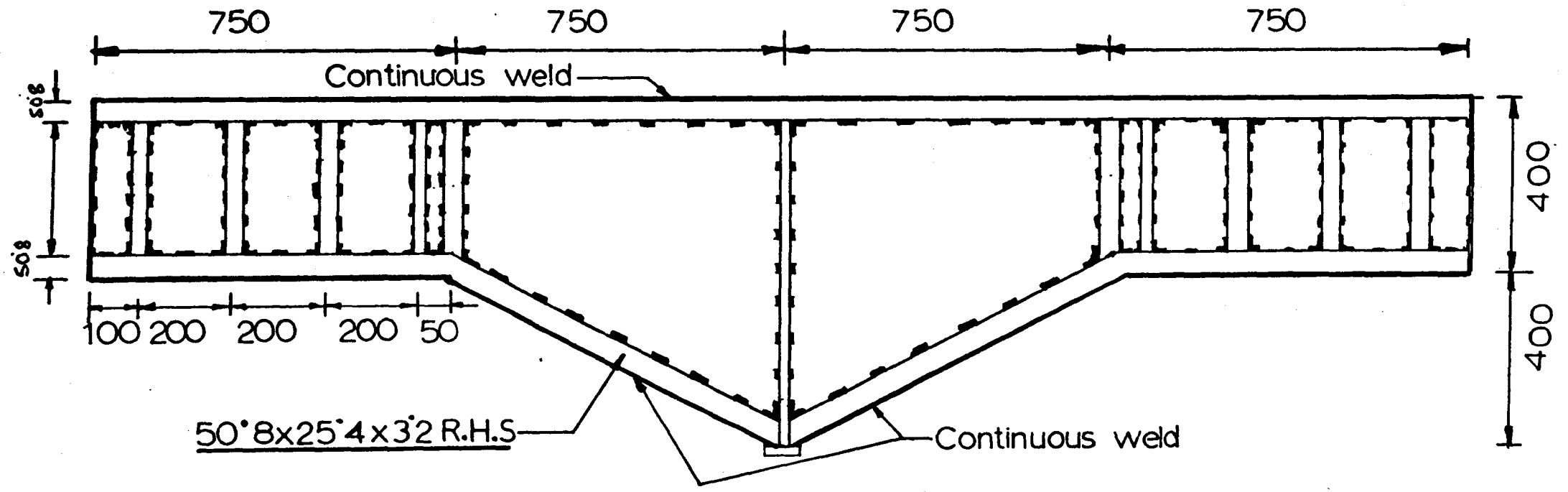

Figure 7.3.1

Typical view of the tapered girder(No. 10 & 20) showing the positions of welds and vertical stiffeners

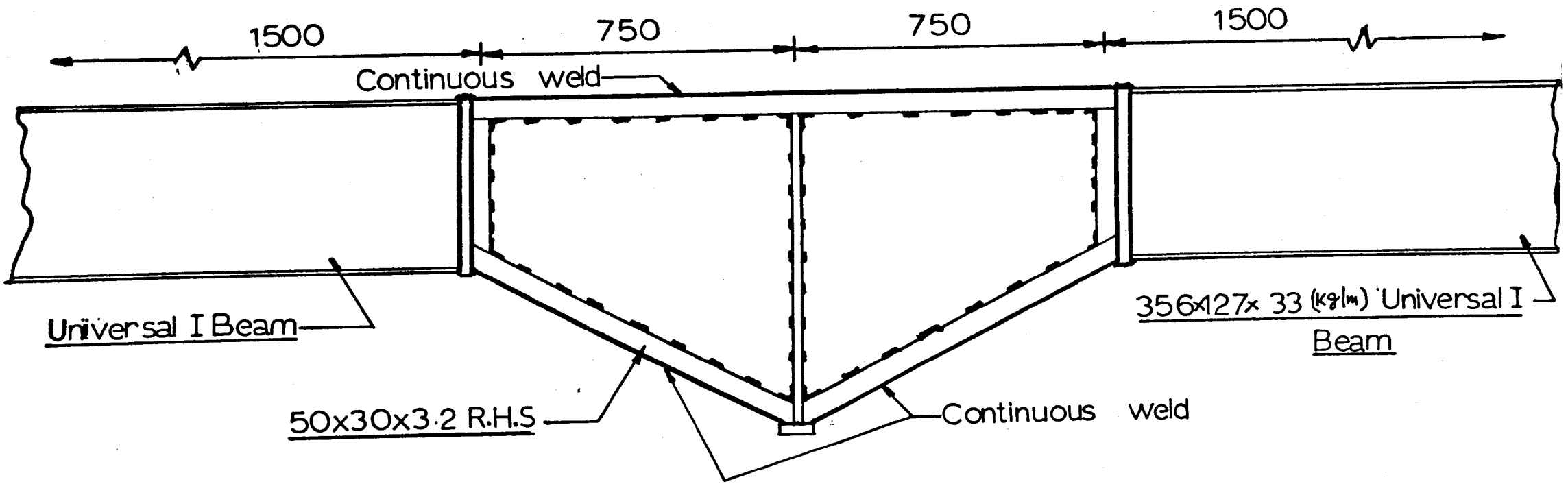

Figure 7.3.2

Typical view of the tapered girders (No.30-70) showing the positions of welds and vertical stiffeners

and 70.

Although care was taken during the fabrication, initial buckling of the webs was unavoidable due to its small thickness.

7.4 Material Tests

A number of test specimens were made from the same lengths of steel plates and Rectangular Hollow Sections used for the fabrication of tapered beams (according to B.S.18(6)). The specimens were tested in an 'Instron' machine. The typical stress/strain curves plotted by using the readings obtained from the tension test are shown in Appendix 5 (A5.1). To obtain accurately the yield stress of the materials, it was later decided to test the specimens prepared from the coupons obtained from the unyielded parts of each tested tapered beam specimens on a 'Housfield Tensometer'. The values of yield stresses obtained for the web and flange materials are shown in Tables 8.2.4(a), 8.3.4(a) and 8.4.7. The typical curves obtained from the Hounsfield Tensometer test for the web and flange materials are shown in Appendix 5 (A5.2).

The plastic moment of resistance of the flanges was obtained from the product of yield stress of the material and the plastic modulus about the equal area axis of the cross section of the flanges. The values of plastic moment of resistance of the flanges is shown in Tables 8.2.4(a), 8.3.4(a) and 8.4.7.

7.5 Test rig and test procedure

7.5.1 Test rig:

The test rig was designed to meet the following requirements:

(i) The tapered beam specimens could be supported to give the required magnitude of eccentricity (up to 600 mm) about the tip.

(ii) Lateral restraints to the tension and compression flanges of the beam could be provided at any point along their length to

prevent lateral torsional instability and to provide free rotation in the plane of the beam.

(iii) Loading increments were arranged such that the pre-buckling and the post-buckling behaviour of beams could be studied.

The overall test arrangement is illustrated in Figure 7.5.1 and 7.5.2 and a pictorial view of the set up is shown in Plate 1. The beam specimen was inverted in the rig. A rectangular steel plate of thickness 1" was welded on the apex of the tapered section to give a flat platform for loading the beam at the top. Load was applied by a hydraulic jack. The beam was simply supported at the bottom of the tension flange. The support at each end incorporated a load cell. One end was supported on rollers and a ball seating, and the other end was supported on a knife-edge. As shown in Plate 2(a) the lateral supports consisted of a ball-bearing roller attached to a rigid frame bolted to the laboratory floor. Lateral supports were provided at the section A-A, B-B and C-C as shown in Figure 7.5.2 and at the end panels. These supports permitted free rotation in the plane of loading but prevented both lateral displacement and longitudinal twist.

A dial gauge frame was designed to measure the out of plane deflections of the web panels relative to the boundaries. This frame was clamped to the top inclined flange and was held by a pair of springs to the bottom flange. As shown in Figure 7.5.3 the dial gauge frame consisted of five columns. The first three columns from the larger end held six dial gauges and the other two columns held five and four respectively to form a rectangularly spaced grid.

The initial imperfections were measured with a device (shown in Plate 2(b)) which consisted of a vertical steel rod of

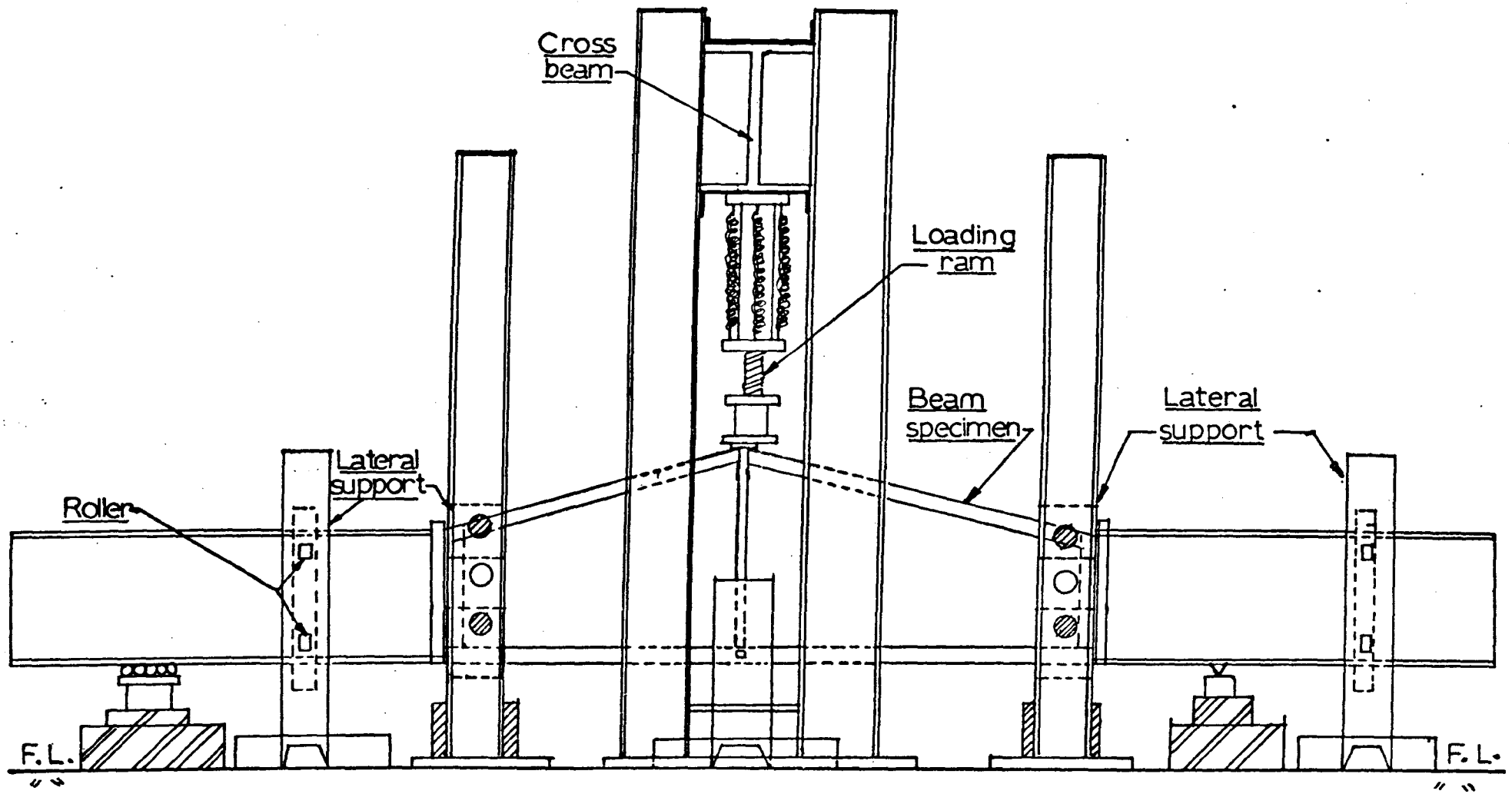
Cross beam
Loading ram
Beam specimen
Lateral support
Lateral support
Roller
F. L.
F. L.

Figure 7.5.1

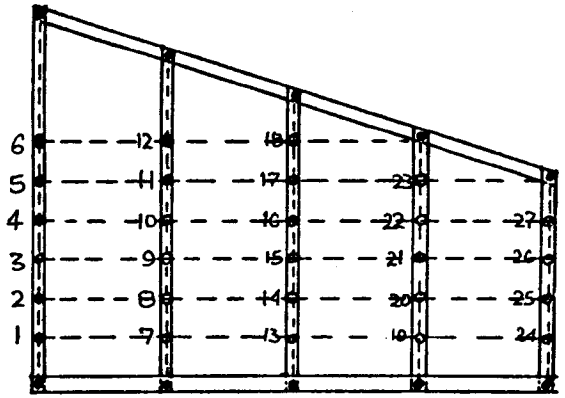

Figure 7.5.3
Dial gauge frame

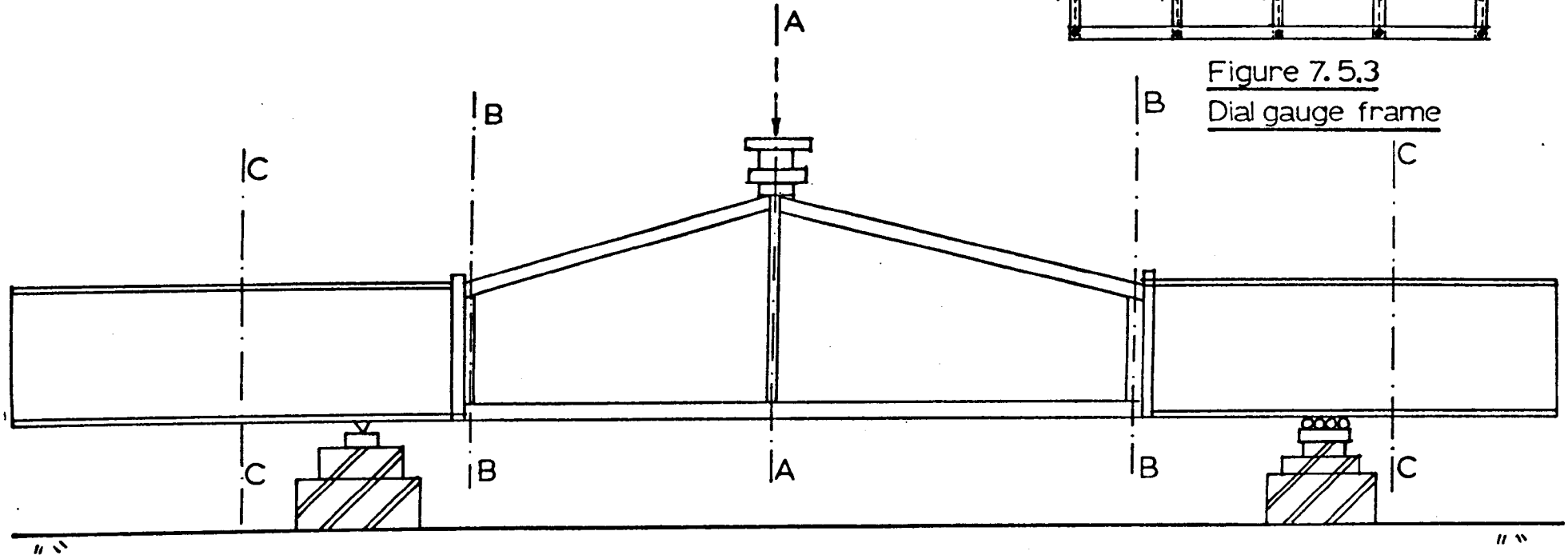

Figure 7.5.2

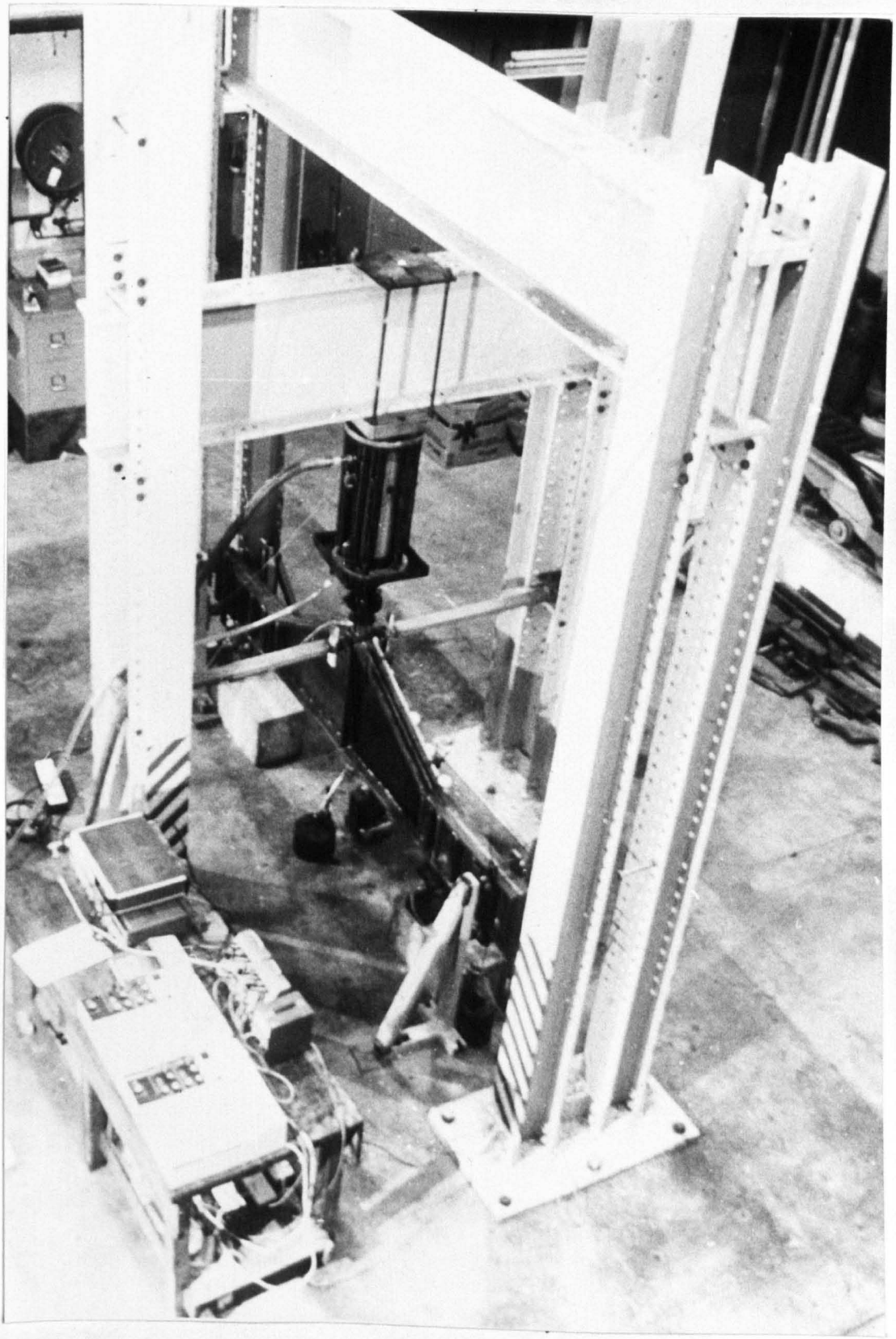

Plate-1

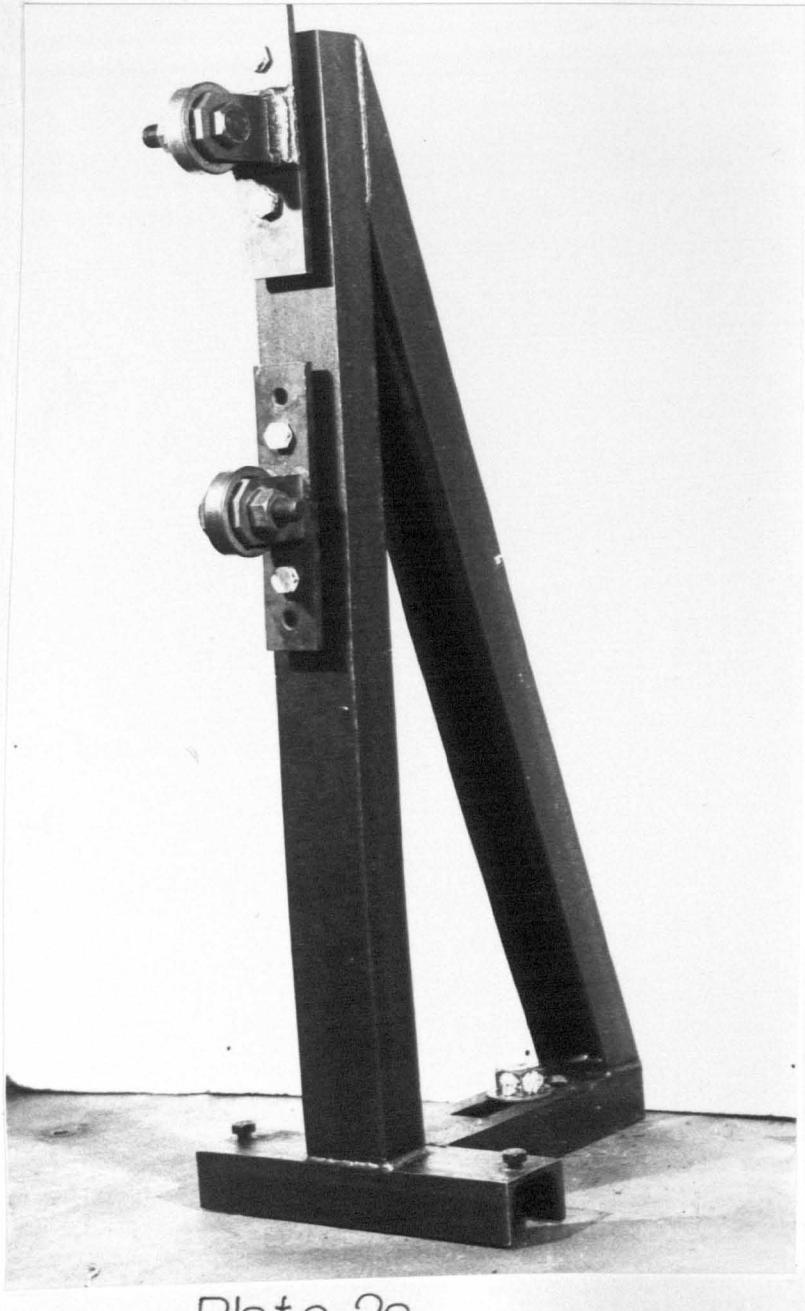

Plate 2a

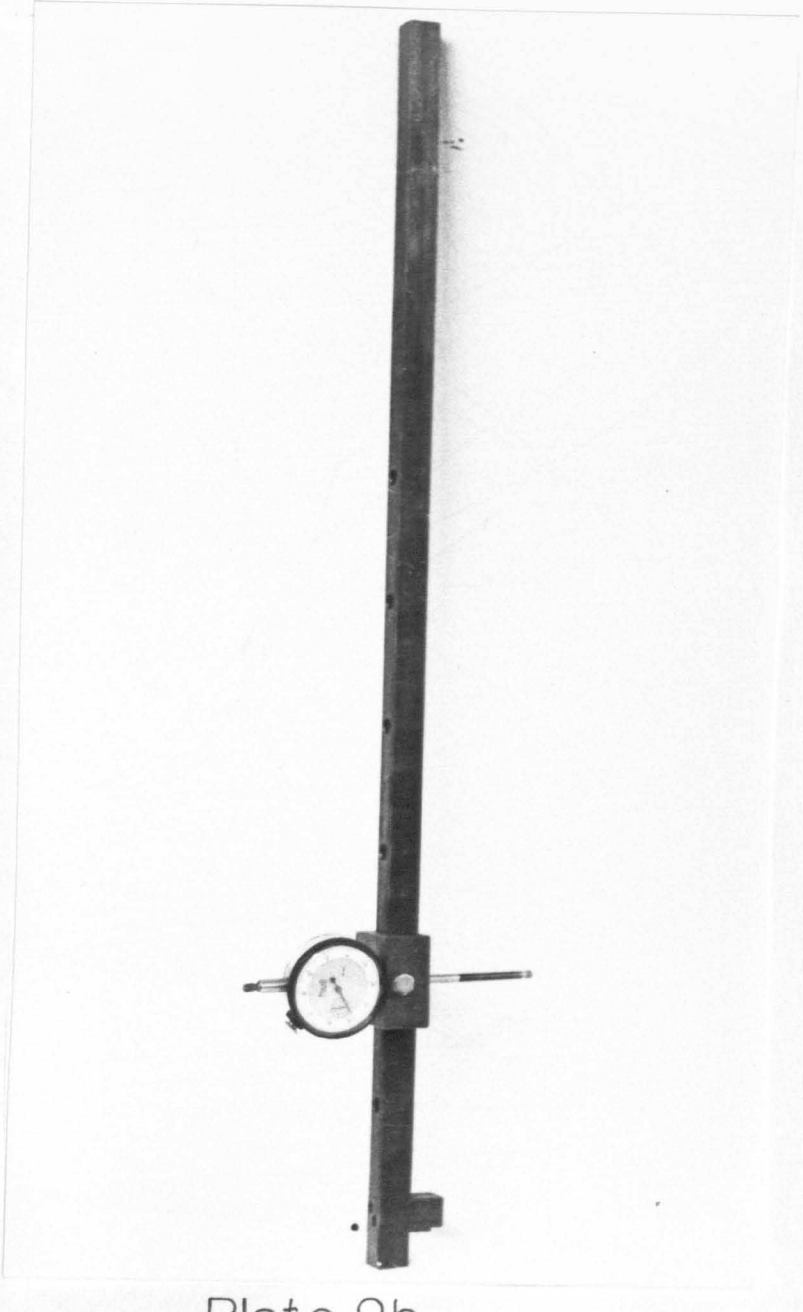

Plate 2b

cross-section 20 mm square and 700 mm high. Six circular holes of diameter 10 mm were drilled along the centre line of the rod at the same spacings as the holes in a column of the dial gauge frame shown in Figure 7.5.3. A cubic steel block of 18 mm side was joined perpendicularly to the inner face of the vertical rod near its lower end. This cube was designed to sit on top of the tension flange. The lower part of the vertical rod rested against the tension flange and the upper part rested against the inclined compression flange in the same manner as the dial gauge frame. It could be placed at points on the web panel corresponding to the vertical columns of the dial gauge frame. A steel block machined to hold a dial gauge could slide along the rod. Before mounting the dial gauge frame to the web panel the positions of each column of the dial gauge frame were marked and the initial profiles (initial imperfections) were measured (using the profile measuring device) at each dial gauge positions.

The load was applied by a hydraulic jack and measured by an electric load cell. Load increments were applied to the specimen by monitoring the voltage output (on a digital voltmeter) from the support load cell of the panel being tested. Loads from all three load cells were also recorded by pen-recorders. In the first experiments, the beam was loaded by a hand-operated hydraulic jack. Later on, it was decided to use the L.O.S. hydraulic control system to load the beam because at the collapse it was very difficult to maintain the load on the panel by using a hand-jack. The testing installation of the L.O.S. system provided a precise means of controlling individual loading rams under various conditions of load or deformation. The installation comprised of a double pump unit, passing oil to a distributor on which

is mounted a high flow servo valve. The servo valve controls the flow of oil to the loading rams. The loading rams were connected to the distributor by means of quick release leakfree couplings and flexible hoses. The loading ram was mounted beneath the cross beam of the test rig as shown in Figure 7.5.1.

After the first six experiments it was decided to record the central deflection with respect to the central load on an X-Y plotter. A Linear Variable Differential Transformer (L.V.D.T.) was mounted at the bottom of the tension flange to record the central deflection and was connected to the X-channel of the X-Y plotter. The load from the central load cell was recorded on Y-channel.

A number of dial gauges were mounted underneath the tension flange to measure the deflections at various points. The positions of these dial gauges varied according to the positions of the supports.

7.5.2 Test Procedure

Prior to actual testing, the beam was loaded and unloaded in the elastic range to ensure smooth working of the rig and to check the functioning of the rosettes and strain gauges.

After taking the initial readings of all the instruments, the load was applied in equal increments in the elastic range of loading. Readings of strain gauges and rosettes were taken by punched paper tape output at each increment of load. Readings of all dial gauges mounted to the web panel and bottom of the tension flange were taken also. The stress coat on the web panel was inspected for any cracking in the resin coating which would indicate the formation of the tensile membrane stress field in the web panel. In the inelastic range, when the plastic

hinges in the flanges were distinct, the dial gauge frame was removed. The beam specimen was loaded up to the collapse in certain increments of load, and the readings of strain gauges and rosettes were recorded by punched paper tape output.

The test was continued until either the load dropped 10 to 15% below the peak load or the central deformations became large.

7.6 Instrumentation

In the first experiment of girder number 10, electrical resistance strain gauges were used to measure the longitudinal and shear strains in the tension and compression flanges. Figures 7.6.1(a) and 7.6.1(b) show the positions of strain gauges in the tension and compression flanges on both faces A and B of the panel respectively. FLA-6-11 type foil gauge of 6 mm gauge length manufactured by Tokyo Sokki Kenkyujo Co. Ltd. were used. The gauge factor and resistance of the strain gauges were 2.10 and (120 ± 0.3) Ω respectively.

Nine 45° rosettes (FRA-6-11 type) were used on both faces 'A' and 'B' of the web panel to measure the principal and shear strains at various points. The positions of rosettes on both faces A and B of the web panel are shown in Figures 7.6.2(a) and 7.6.2(b) respectively. The gauge length and resistance were 6 mm and (120 ± 0.5) Ω respectively. As shown in Figures 7.6.2(a) and 7.6.2(b) the rosettes numbered 1 and 10 were bonded exactly at the same point and opposite to each other on faces A and B respectively. Similarly rosettes numbered 2, 3, 4, 5, 6, 7, 8 and 9 were bonded opposite to rosettes numbered 11, 12, 13, 14, 15, 16, 17 and 18 on either side of the web panel respectively.

Also, for the first experiment of girder number 50, thirty-

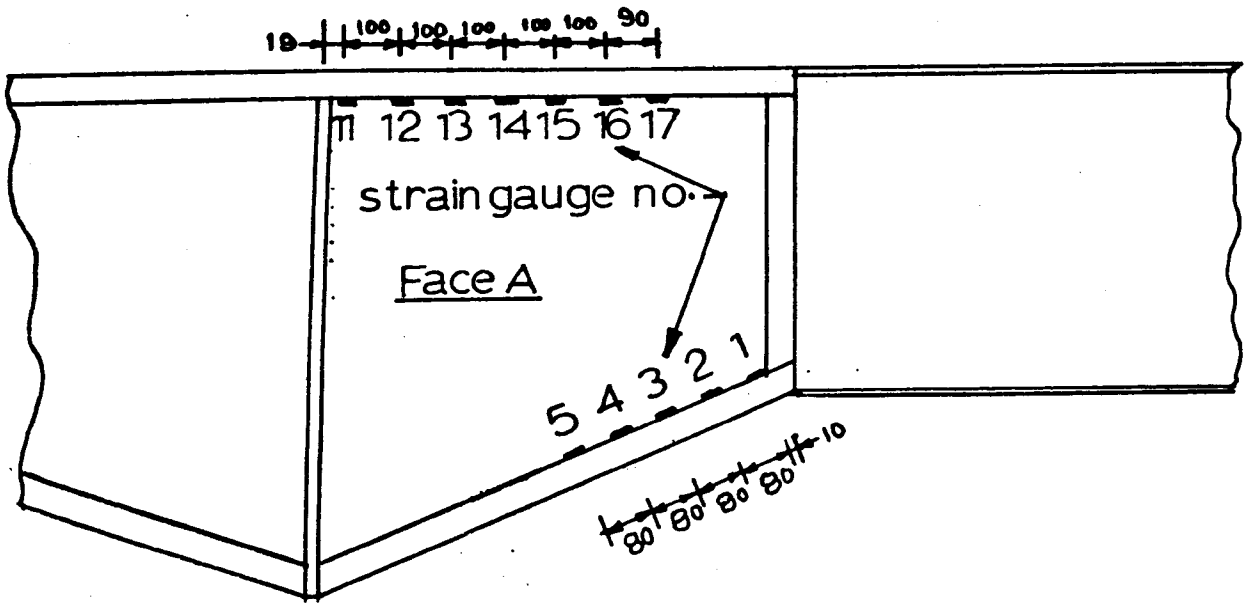

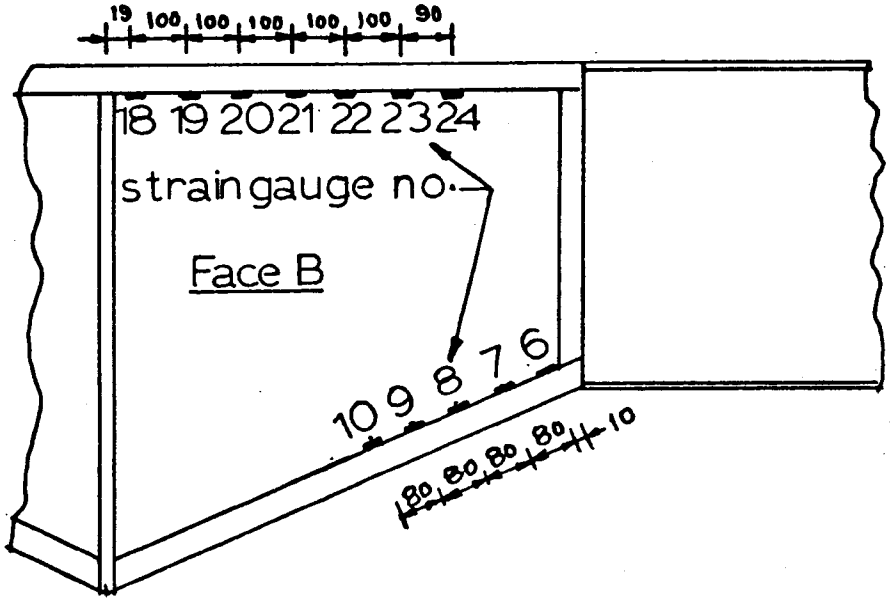

Positions of the strain gauges in the tension and compression flanges

Figure 7.6.1(a)

Figure 7.6.1(b)

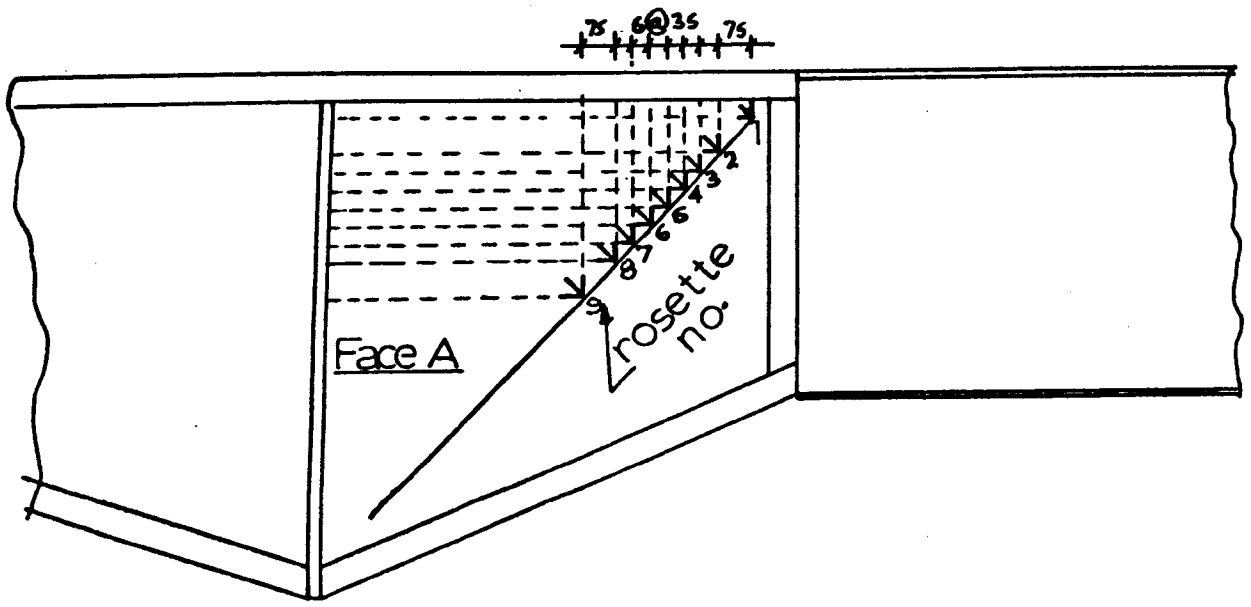

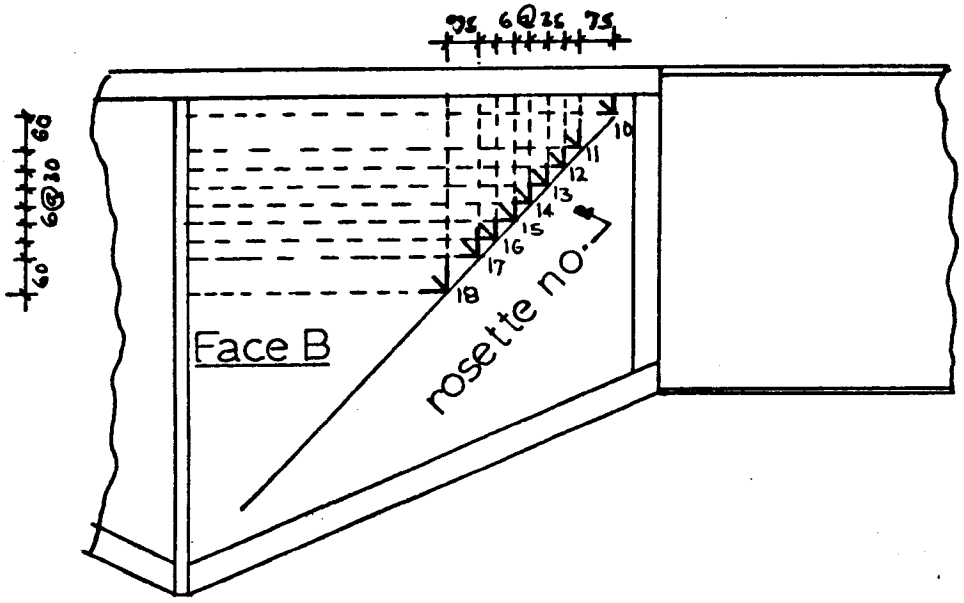

Positions of the rosettes in the web panel

Figure 7.6.2(a)

Figure 7.6.2(b)

six PL-10 foil electrical resistance strain gauges were used to measure the bending, shear and longitudinal strains of the tension and compression flanges. The positions of the sets of strain gauges at six different sections in the tension and compression flanges are shown in Figure 7.6.3(b). Six strain gauges were used at each section of the tension and compression flanges as shown in Figure 7.6.3(a).

Rosettes and strain gauges were bonded in place with "MBOND - 200" and protected with polyurethane varnish.

A "SCHLUMBERGER" data logging system in combination with a paper tape punch were used to record the strain gauge, rosette and load cell readings. 'SCHLUMBERGER' data logging system comprises of a digital voltmeter fitted with a fan-out unit, data-transfer unit, strain gauge power supply unit and an analogue scanner unit. The data logging system consists of ninety channels numbered from 50 to 139 for strain gauges and three channels numbered from 140 to 142 for load cells.

A computer program, shown in 'Appendix 4' was written by the author to analyse the paper tape output and to calculate the axial forces and stresses in the flanges and the principal and shear strains of the web panel.

The web panel of girder number 10, experiment number 1 was coated with 'Brittle Lacquer'. The minimum strain for cracks to develop was 500 micro strain. Later on, for all other experiments, it was decided to use 'Plumber's Resin' as a stress coat to the web panels. The recommended method of applying a stress coat of Plumber's Resin suggested that the panel should be heated from the bottom using an acetylene torch and a coat of resin was applied to the top surface.

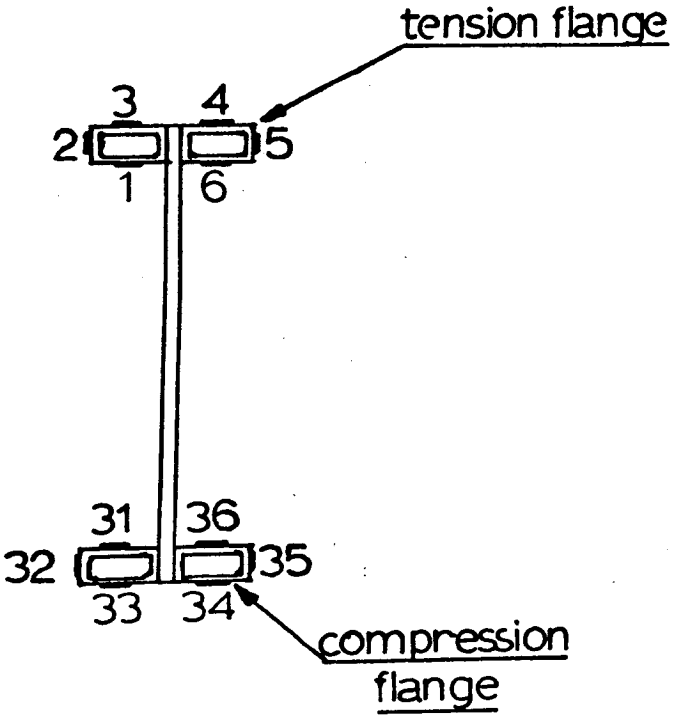

Figure 7.6.3(a)

Section at A-A

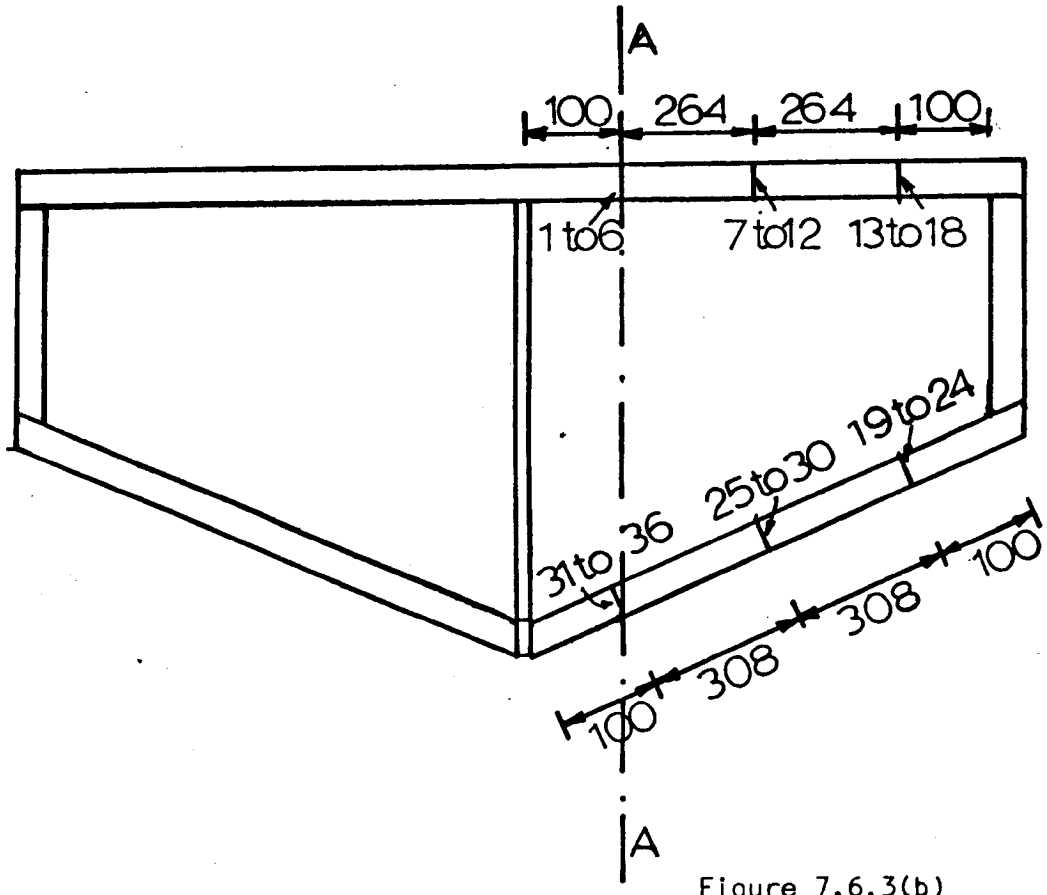

Figure 7.6.3(b)

7.7 Tapered beams loaded inside the tip (Test Series One)

7.7.1 Introductory Remarks

Seven tests on tapered beam specimens loaded inside the tip were carried out to examine the collapse mode of failure and their ultimate strengths. All beam specimens consisted of two symmetrical tapered web panels and each panel was tested separately. For the first experiment of any beam loaded inside the tip, the panel chosen was the one which was supported nearer to the central load. The other panel of the beam was supported at the point where the eccentricity from the tip was minimum and the theoretical predicted load was higher than the first panel. It was possible to test the first panel up to its collapse without significant yield of the second panel. Before the second experiment of any beam, the collapsed panel was stiffened by welding a 2" x ½" steel plate machined to fit exactly to the inner face of the panel and along the tension diagonal, as shown in Figure 7.7.1. The stiffened panel provided sufficient strength to the collapsed panel and it was possible to test the second panel for any eccentricity about the tip.

7.7.2 Observations

It was difficult to estimate the exact buckling load of the web panel due to the fact that the webs of the tapered beams were not flat before the tests. However, during the tests, it was observed that at certain load levels the web panels buckled.

In the post buckled range, cracks in the resin showed the formation of the tensile membrane stress field along the tension diagonal. It was also observed that some of the plastic hinges in the compression flange were very distinct and the yielding of the compression flange extended all along its length. On the

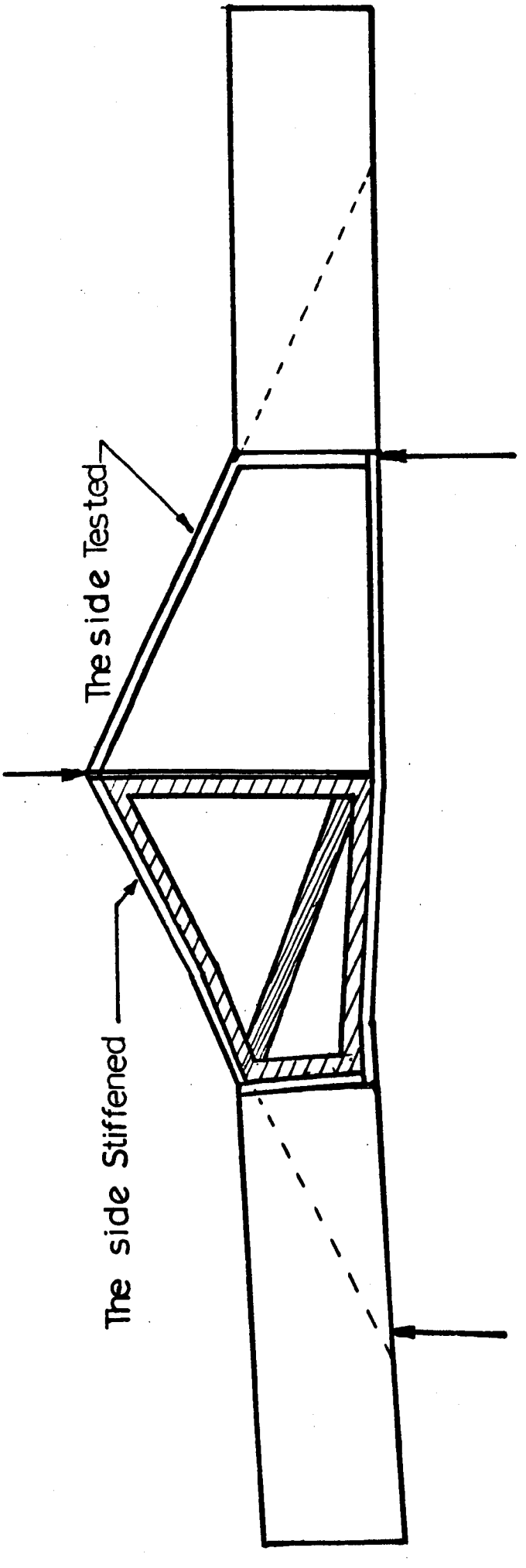

A typical stiffened panel after collapse (beam loaded inside the tip

Figure 7.7.1

other hand, only one plastic hinge in the tension flange near the central stiffener was distinct, and there was very little impression of yielding in the tension flange. However, in the next chapter it is shown that by plotting the profile of the tension and compression flanges it was possible to easily detect the position of plastic hinges in the tension and compression flanges.

Apart from the analyses of the rosette readings, to be shown in the next chapter, it has been observed here that the web panel yielded completely in the region bounded by the plastic hinges in the tension and compression flanges.

As the eccentricity of loads about the tip was decreased, the lateral instability of beams became more critical. Eventually, small eccentricity of load about the tip not only caused the compression flange to yield all along its length, but also caused more lateral instability problems. However, these lateral instabilities were prevented by providing sufficient lateral supports.

7.7.3 General Conclusions

On the basis of physical inspections and observations, the following conclusions can be drawn:

(i) The cracks in the resin confirm that, in the post buckling stage, the tensile membrane stresses develop along the short diagonal of the web panel.

(ii) The collapse mechanism consists of two plastic hinges in the compression flange near the smaller end of the panel and two plastic hinges in the tension flange.

(iii) The web panel between the two inclined boundaries, joining the plastic hinges in the tension and compression flanges, yields

completely.

(iv) As the eccentricity of the load about the tip of the panel decreases, the tendency for general yielding of the compression and tension flange spreads.

7.8 Tapered beams loaded outside the tip (Test series - two)

7.8.1 Introductory Remarks

Four tests on tapered beam specimens loaded outside the tip were carried out to examine the collapse mode of failure and their ultimate strengths. All the beam specimens consisted of two panels and each panel was tested separately. In the first experiment on each of the four beams loaded outside the tip, the panel chosen was the one which had the support farthest from the centre. In other words, the second panel was supported at a point where the eccentricity about the tip was small and therefore the theoretical collapse load was higher than for the first panel. It was possible to test the first panel up to its collapse without significant yield of the second panel. However, it was noticed that the web of the second panel still buckled, but there was very little post buckling effect on the second panel. The collapsed panel was stiffened by welding 2" x ½" steel plates machined to fit exactly along the inner face of the flanges and along the tension diagonal as shown in Figure 7.8.1.

Because the 'tip moment' changes sign when the support position is changed from inside to outside the tip, the tension and compression diagonals interchange.

7.8.2 Observations

Apart from the change in direction of the tension diagonal, the observations were similar to the previous case as explained in section 7.7.2. Also, the yielding of compression flanges as

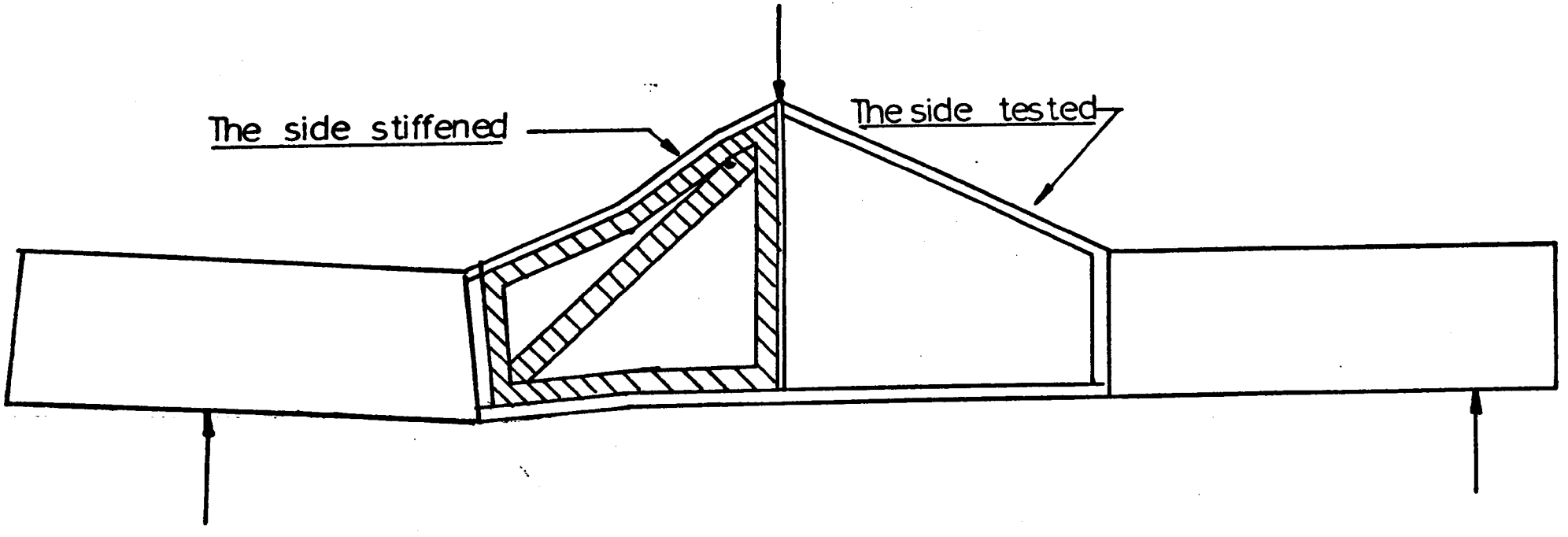

A typical stiffened panel after collapse (beam loaded outside the tip)

Figure 7.8.1

well as the lateral instability problems for small eccentricity of loads about the tip were similar as explained in section 7.7.2.

7.8.3 General Conclusions

On the basis of physical inspections and observations, the following conclusions can be drawn:

(i) The direction of the tension diagonal for the case when the beam was loaded outside the tip is opposite to the direction of the tension diagonal when the beam was loaded inside the tip.

(ii) The cracks in the resin confirm that in the post buckling stage the tensile membrane stresses develop along the long diagonal of the tapered web panel.

(iii) The web area between the two inclined boundaries, joining the plastic hinges in the tension and the compression flanges yields completely.

(iv) As the eccentricity of the load about the tip of the panel decreases, the yielding of the compression and tension flange increases.

7.9 Tapered beams loaded at the tip (Test series - Three)

7.9.1 Introductory Remarks

Three tests on tapered beam specimens loaded at the tip were carried out to examine the collapse mode of failure and their ultimate strengths. Three different positions of support at the tip were chosen. In the first experiment the beam was supported near the central tip, in second experiment it was supported near the inner tip, and in the third experiment it was supported near the outer tip. Because the beam was loaded symmetrically having its supports at the tip, it was not possible to test the first panel up to its collapse without the yielding of the second panel. So it was decided to stiffen one panel by

welding 2" x ½" steel plates machined to fit exactly to the inner face of the flanges and along the short diagonal as shown in Figure 7.9.1(a). After the first experiment the plates welded to the stiffened panel were cut out of the panel and the collapsed panel was stiffened in a similar way as shown in Figure 7.9.1(b). Precautions were taken while cutting the welds of the stiffening plates from the uncollapsed panel so as not to damage the flange tube.

7.9.2 Observations

During the experiment, it was observed that up to the load level of about 35% of the collapse load, there was no crack in the stress coat (Plumber's resin) nor any sign of buckling of the web panel.

However, when the flange material started yielding with some impression of the formation of the plastic hinges in the tension and compression flange, a large diagonal band 'X-U-V-W-X' (Figure 8.4.8) along the diagonal 'X-W' formed in the web panel. This diagonal band was entirely different from the previous tensile diagonal band when the tapered beams were loaded inside and outside the tip.

Although the 'out-of-plane' deflections of the web were large, there was still no sign of the presence of tensile membrane stresses in the web. It was observed that the plastic deformation in the compression flange extended all along its length. There were three plastic hinges in the compression flange and one plastic hinge in the tension flange.

However, it was clear that the panel failed due to three hinge rotations and overall plastic deformation of the compression flange together with one hinge rotation of the tension flange.

A typical stiffened panel (beam loaded at the tip)

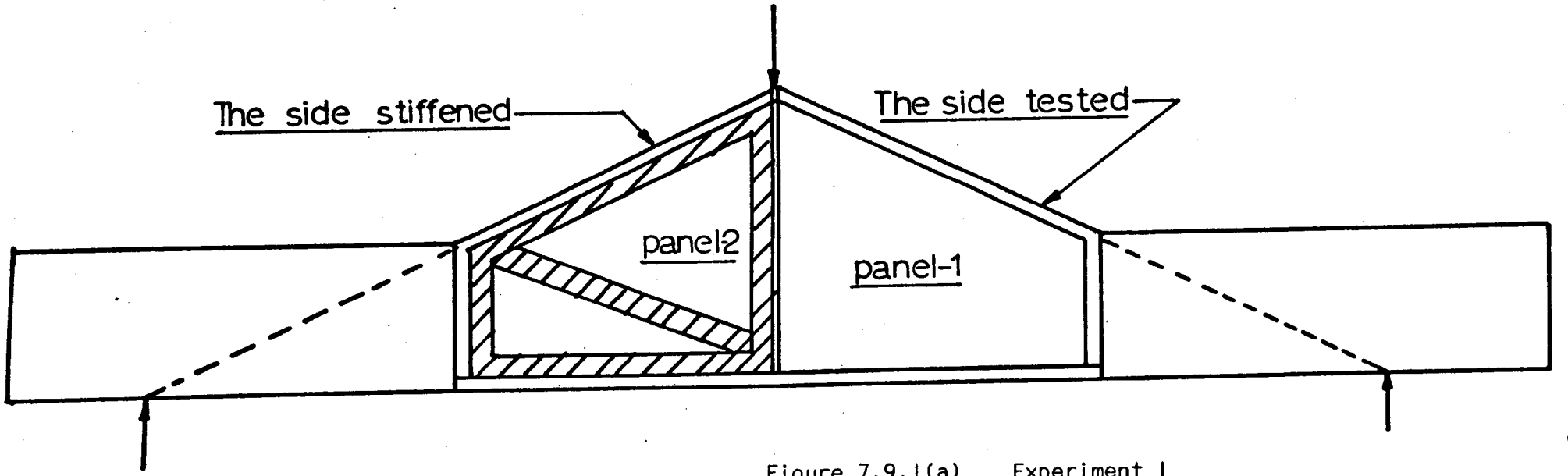

Figure 7.9.1(a) Experiment 1

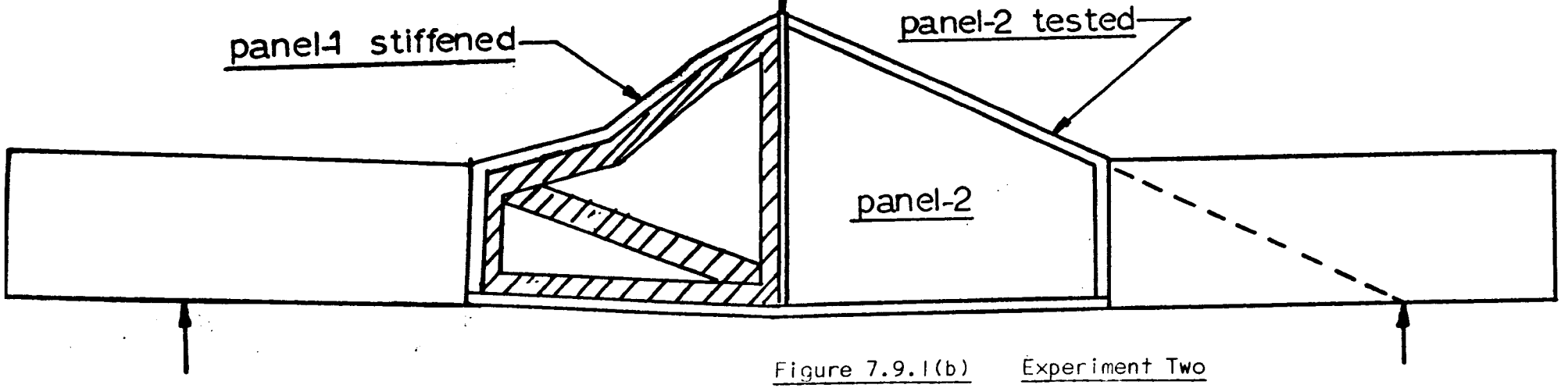

Figure 7.9.1(b) Experiment Two

Also, there was no crack in the stress coat, which indicated clearly that the tensile membrane stresses were not present in the web.

The lateral instability problems were more critical in comparison with the cases when girders were loaded inside and outside the tip. It was quite clear that the girders loaded at or near the tip would have failed due to lateral instability if sufficient lateral supports were not provided.

7.9.3 General Conclusions

On the basis of physical inspections and observations, the following conclusions can be drawn for the tapered beams loaded at tip:

(i) The collapse mechanism consists of three plastic hinges in the compression flange and one plastic hinge in the tension flange.

(ii) The tensile membrane stresses do not form in the web panel.

(iii) The plastic collapse occurs due to the plastic yield and three hinge rotations of the compression flange and one hinge rotation of the tension flange.

(iv) The collapse loads and the modes of failures were identical for all the three cases; that is, when the beams were loaded near the inner tip, near the central tip and near the outer tip.

CHAPTER EIGHT

RESULTS OF THE EXPERIMENTAL STUDIES AND THEIR COMPARISON WITH THE THEORETICAL PREDICTIONS

8.1 Introductory Remarks

The purpose and details of the experimental programmes were given in the previous chapter. The results of those experiments are described, discussed and compared with the theoretical predictions in this chapter. Conclusions are drawn about the plastic collapse mode of failure of tapered beams and their ultimate strengths.

8.2 Tapered beams loaded inside the tip (Test Series One)

8.2.1 Introductory Remarks

As explained in Chapter Seven, in Test Series One, seven experiments were performed to examine the ultimate strengths and the collapse mode of failure of tapered beams loaded inside the tip. The dimensions of the girders tested and the material properties are presented in Table 8.2.4(a). In this chapter, the results of one experiment (Girder - 60) will be used to plot the out-of-plane deflections of the web panel and the deflected profile of the tension and compression flanges. The plotted profiles of the remaining experiments are shown in Appendix 6.

8.2.2 Out-of-plane deflections of the web panels

The out-of-plane deflections of the webs were measured by the profile measuring device as illustrated in section 7.5.1. The readings for the initial imperfections, the out-of-plane deflections at 26%, 44% and 63% of the collapse load and the final deflected profile of the web panel of the girder (Girder - 60) are presented in Table 8.2.1. The column numbers and the

dial gauge numbers shown in the table are in the same order as shown in Figure 7.5.3. The contours of the initial imperfections are shown in Figure 8.2.1. The contour lines showing the formation of the tension band along the tension diagonal of the web panel at the three loads mentioned previously (26%, 44% and 63% of the collapse load) are shown in Figures 8.2.2, 8.2.3 and 8.2.4 respectively. Also, the contour lines showing the final deflected profile of the web panel are shown in Figure 8.2.5. In Figure 8.2.6 the deflections of various points of the web panel are shown at the three different loads (mentioned previously). The deflected profiles of the web panels of all other experiments are shown in Appendix - 6.

It can be seen from Figure 8.2.6 that the out-of-plane deflections of the web increase with the increase of load on the panel.

Because the panel was supported laterally at the position of column number five of the dial gauge frame (Figure 7.5.3), the out-of-plane deflections of the web panel during the experiment along the 5th column (Tables 8.2.1, 8.3.1 and 8.4.1) were not recorded.

8.2.3 Analysis of the strain gauges and rosettes readings

In the first experiment on girder number - 10, as explained in section 7.6, twenty-four strain gauges were used to measure the longitudinal and shear strain in the tension and compression flange. Also, eighteen rosettes were used to measure the principal and shear strains at various points of the web panel.

Figures 8.2.7(a) and 8.2.7(b) show the strain gauge readings in the tension and compression flanges respectively at 25%, 50%, 75%, 90% and 100% of the collapse load. It can be seen

Column number	Dial gauge number	Initial imperfections	Profile at 26% of the collapse load (mm)	Profile at 44% of the collapse load (mm)	Profile at 63% of the collapse load (mm)	Final profile after collapse (mm)
1	1	-2.94	-2.79	-2.56	-2.23	4.40
	2	-2.66	-2.54	-2.34	-2.56	0.90
	3	-1.23	-1.27	-1.21	-1.71	-0.11
	4	-2.30	-2.32	-2.30	-2.84	-1.09
	5	-3.10	-3.05	-2.96	-3.38	-1.21
	6	-3.22	-3.17	-3.09	-3.33	-0.73
2	7	-2.46	-3.90	-4.96	-11.89	-26.09
	8	-3.57	-3.83	-3.99	-6.30	4.56
	9	-4.21	-2.51	-2.35	-6.61	2.87
	10	-4.89	-4.08	-3.14	-7.02	-4.82
	11	-4.90	-4.38	-4.33	-6.73	-4.33
	12	-3.09	-2.90	-3.18	-4.30	-1.69
3	13	+1.79	1.04	0.68	0.58	10.54
	14	+2.81	1.06	0.41	-5.49	-19.28
	15	+2.84	2.90	4.62	3.84	16.87
	16	+1.83	3.77	7.34	7.43	2.13
	17	+0.42	3.51	4.27	3.08	-1.24
	18	1.04	-0.35	-0.27	-0.73	-0.05
4	19	-2.38	-2.64	-2.45	-1.94	4.22
	20	-2.70	-6.04	-6.27	-7.01	5.94
	21	-1.98	-9.08	-9.71	-14.13	-19.43
	22	-1.25	-4.45	-3.90	-3.17	10.78
	23	-0.19	-0.17	0.21	0.60	1.05
5	24	+1.27				0.90
	25	+0.13				-0.31
	26	-2.54				0.05
	27	-1.58				-11.52

Table 8.2.1

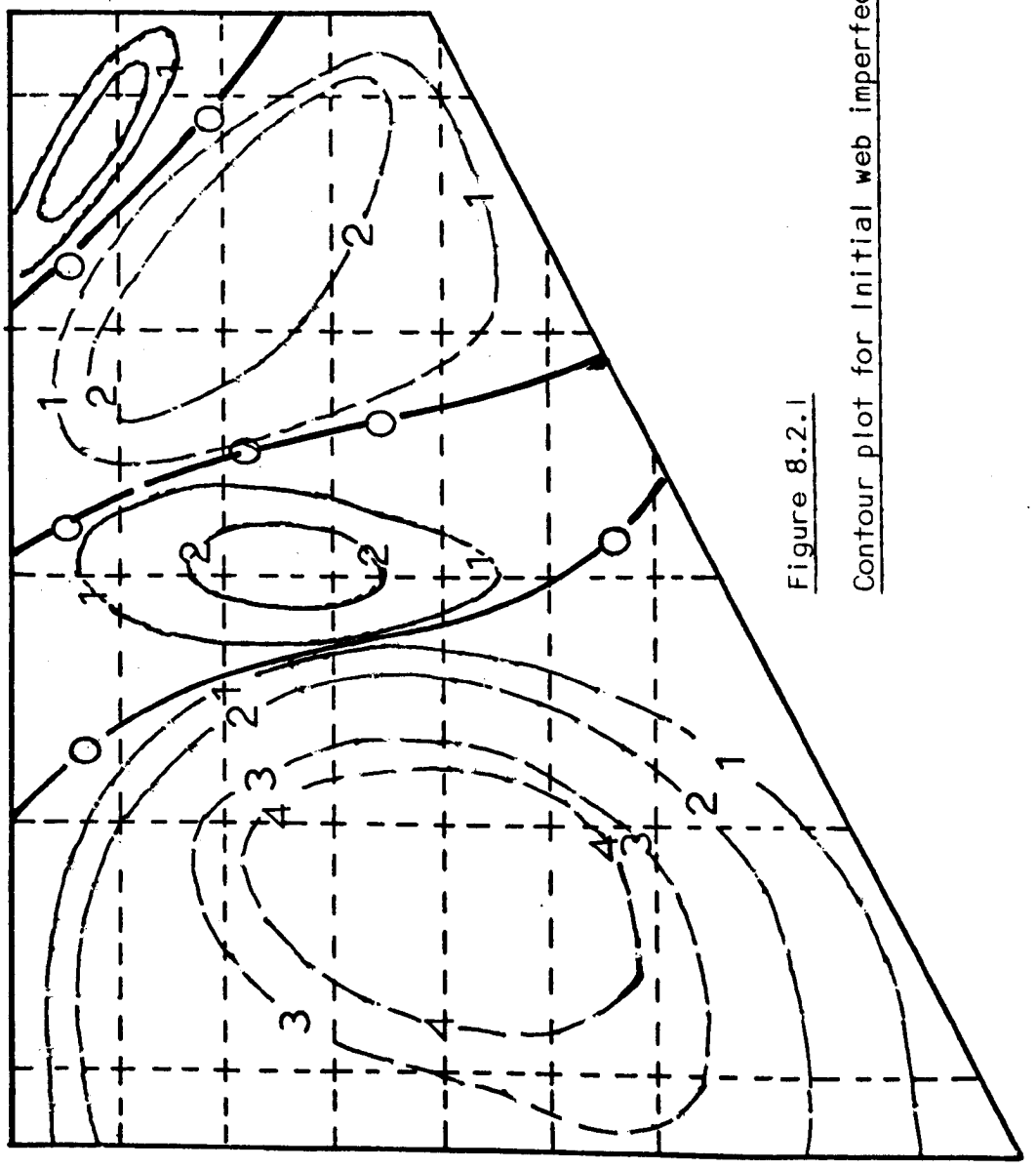

Figure 8.2.1

Contour plot for Initial web imperfection (Girder - 60A)

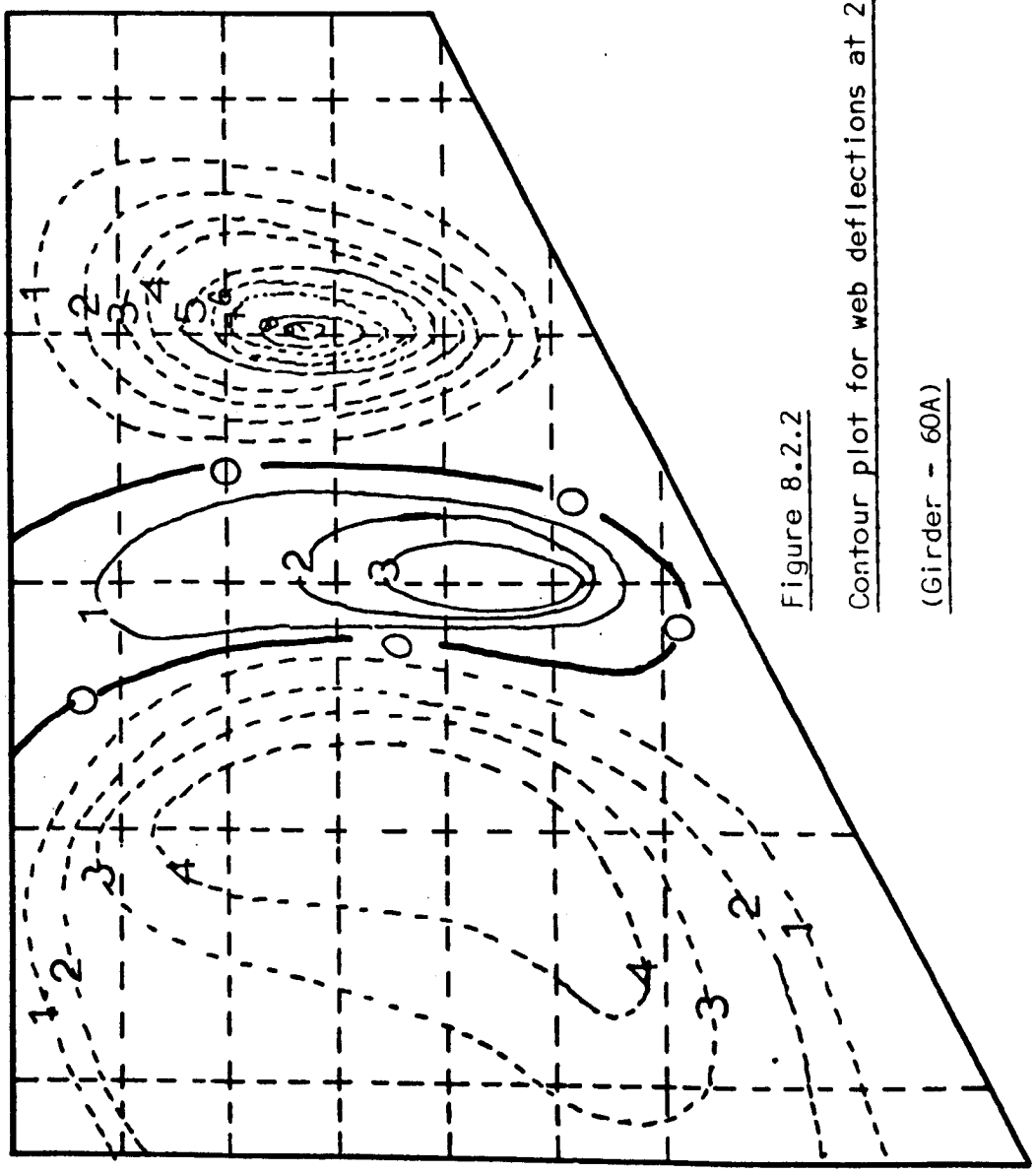

Figure 8.2.2

Contour plot for web deflections at 26% of the collapse load

(Girder - 60A)

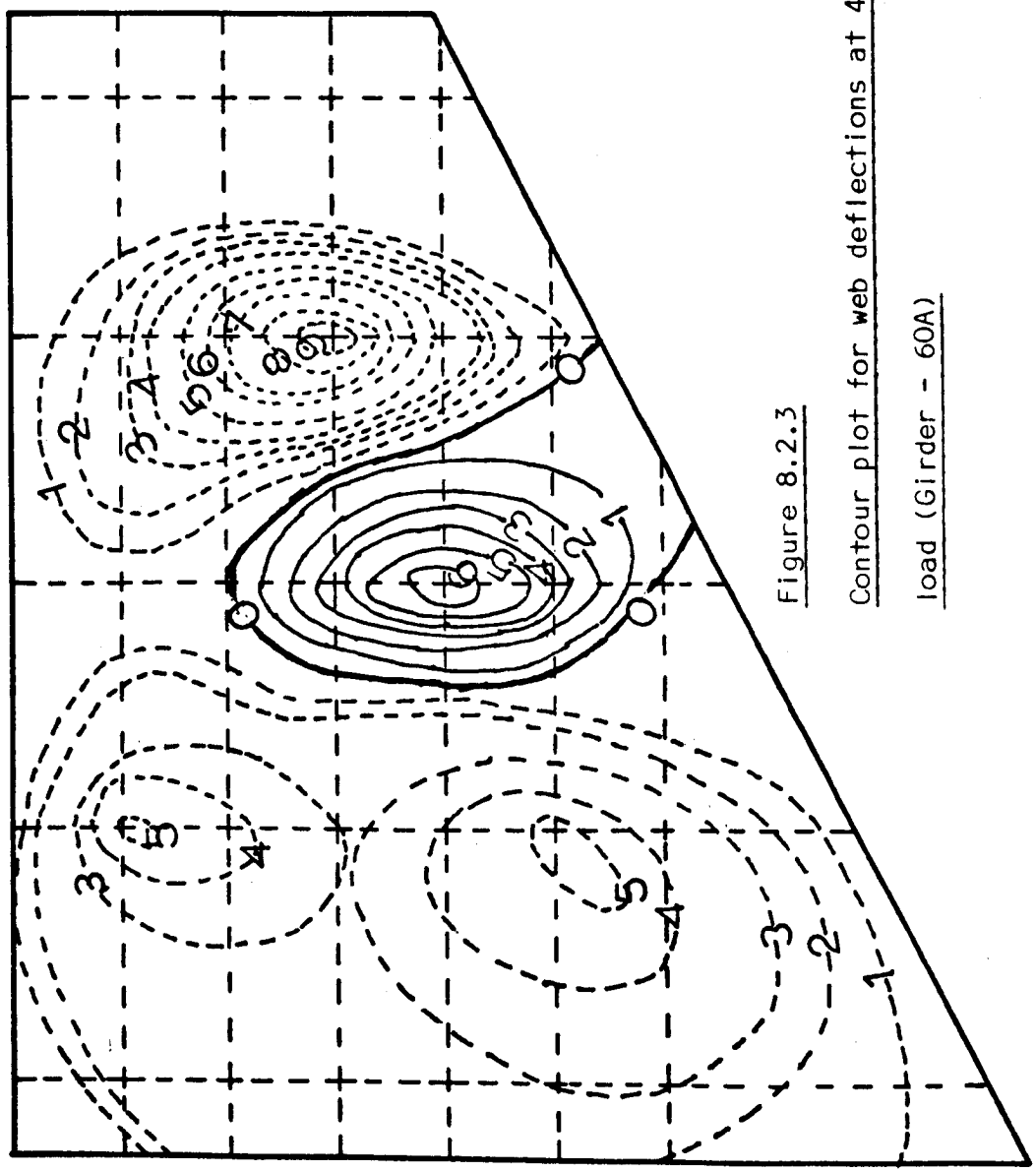

Figure 8.2.3

Contour plot for web deflections at 44% of the collapse load (Girder - 60A)

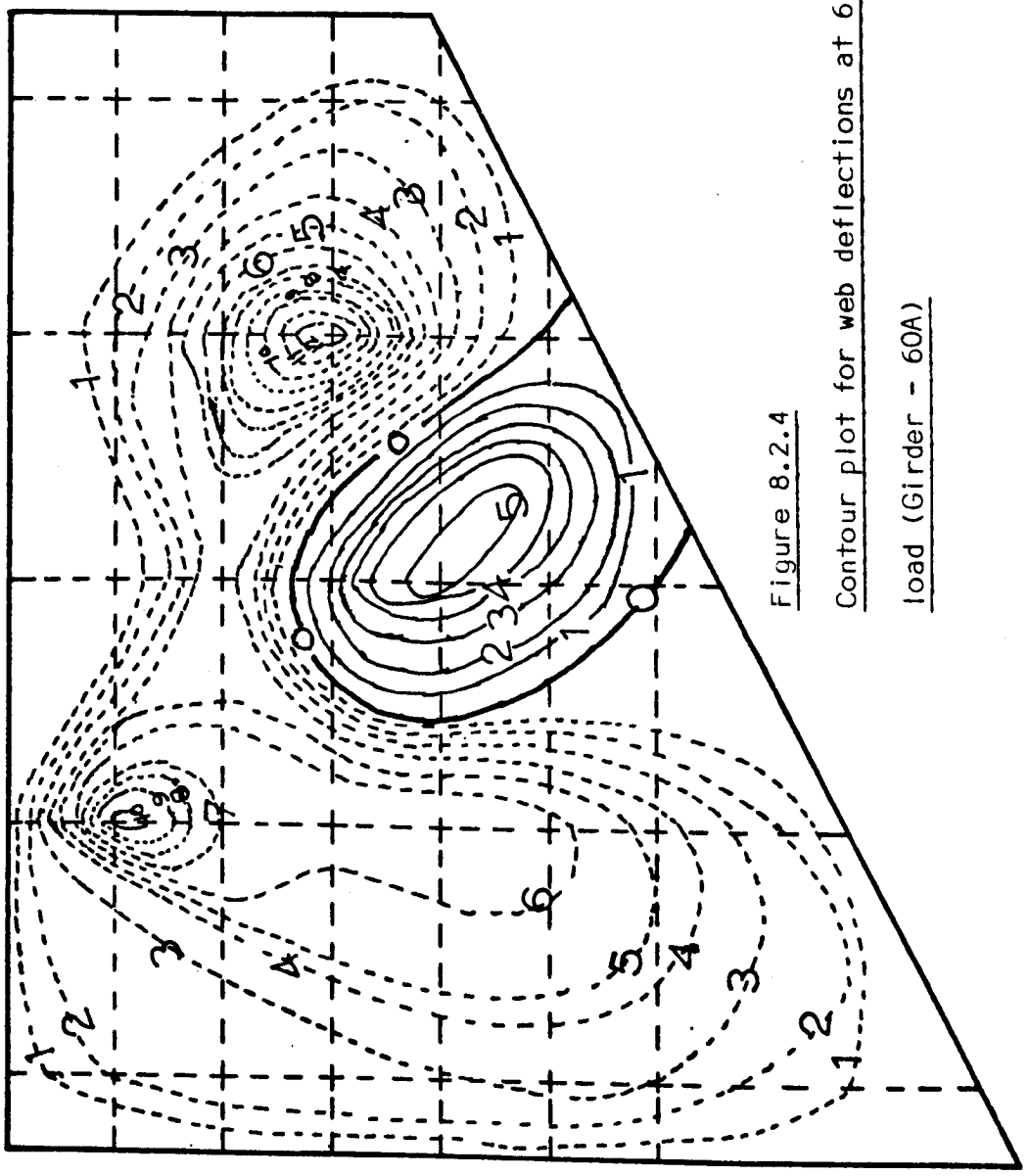

Figure 8.2.4

Contour plot for web deflections at 63% of the collapse load (Girder - 60A)

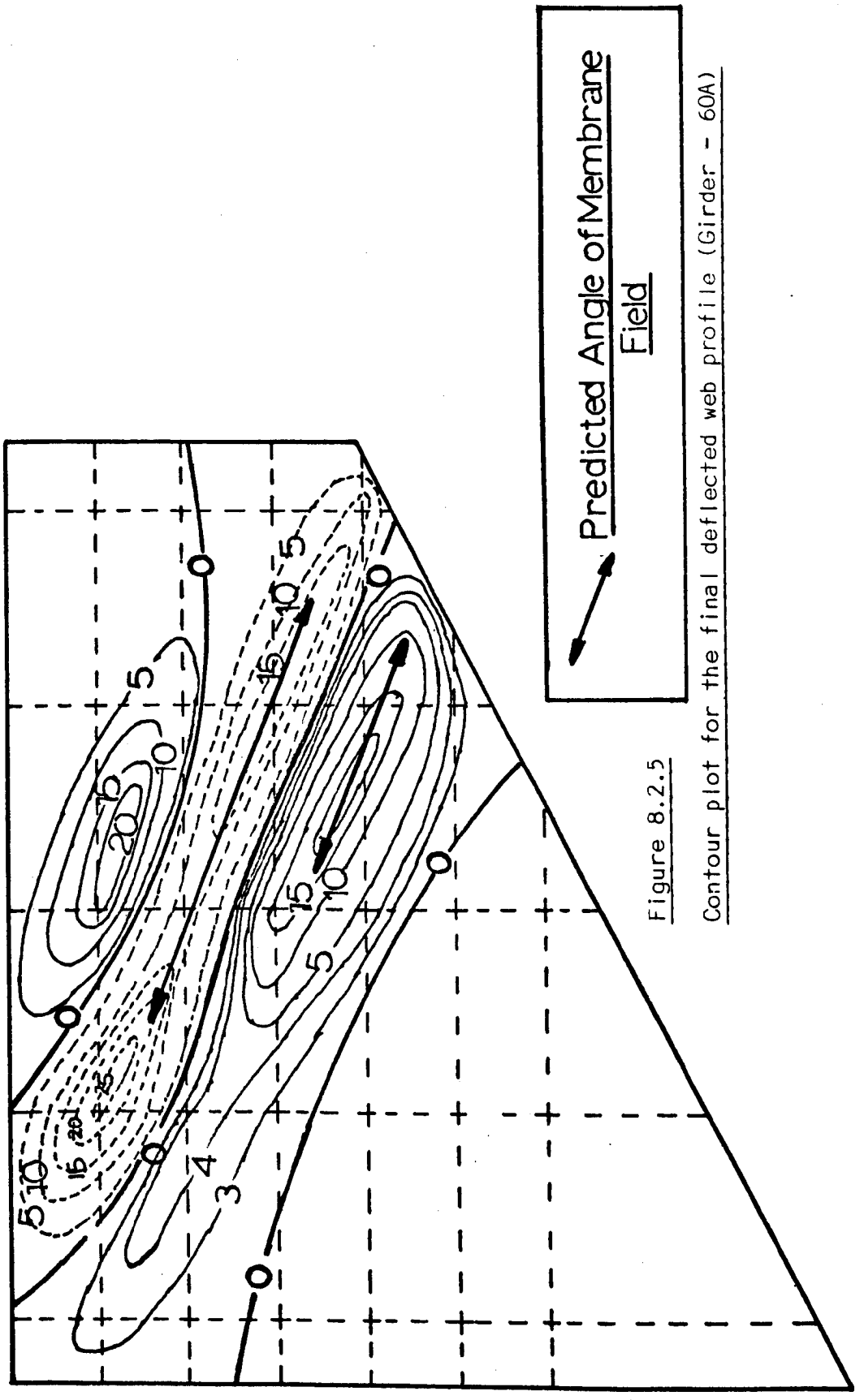

Figure 8.2.5

Contour plot for the final deflected web profile (Girder - 60A)

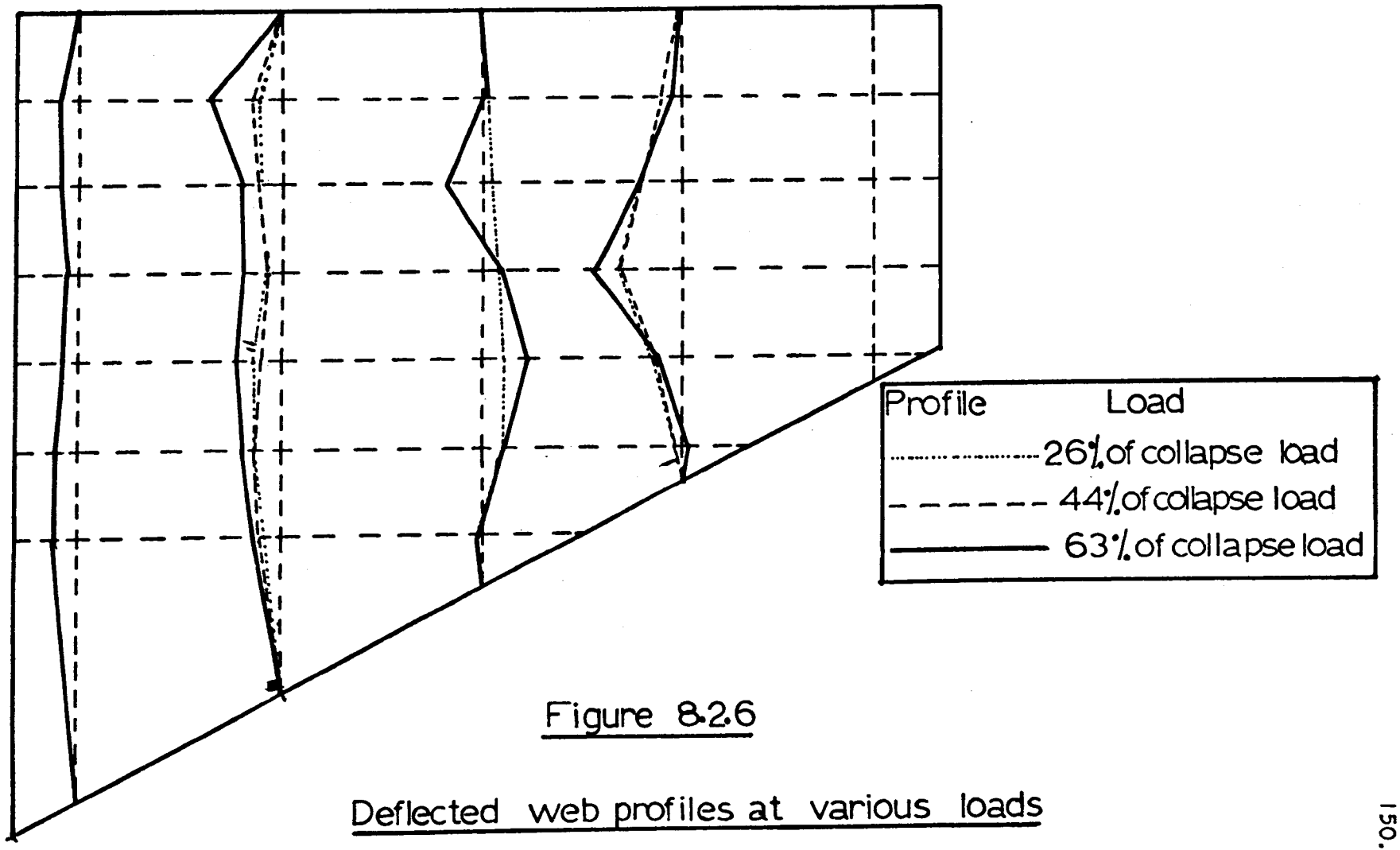

Figure 8.2.6

Deflected web profiles at various loads

that at the collapse load, the strain levels at the points shown in the tension and compression flange have attained their yield values.

The variations of the strains across the tension band at various points of the web measured by the rosettes at 25%, 50%, 75% and 90% of the collapse load of the panel are shown in Figure 8.2.8. The plottings of the strains in Figure 8.2.8 clearly illustrate the magnitude of strains at various points and the width and inclination of the tensile band. It can be seen that the strains at every point across the tension band have exceeded yield.

8.2.4 Deflected profile of the tension and compression flanges

8.2.4.1 Deflected profile of the tension flange

Before placing the tapered beam specimen in the test rig, it was inverted and placed on a lathe-bed so that the central vertical stiffener was perfectly vertical. The measurements for the initial and final vertical profile of the tension flange were taken by setting a dial gauge at chosen points along its length. The dial gauge was fixed with a magnetic base to the lathe bed and so for each point a constant datum level was maintained. A set of readings for the initial and final profiles of the tension flange of Girder number - 60, is presented in Table 8.2.2.

8.2.4.2 Deflected profile of the Compression flange

To obtain the deflected profile of the compression flange, a straight-edged steel rod was clamped to the flange as shown in Figure 8.2.9 and the offsets were measured by a Vernier depth gauge which slid along the straight edge. A set of readings for the final profile of the compression flange is presented in

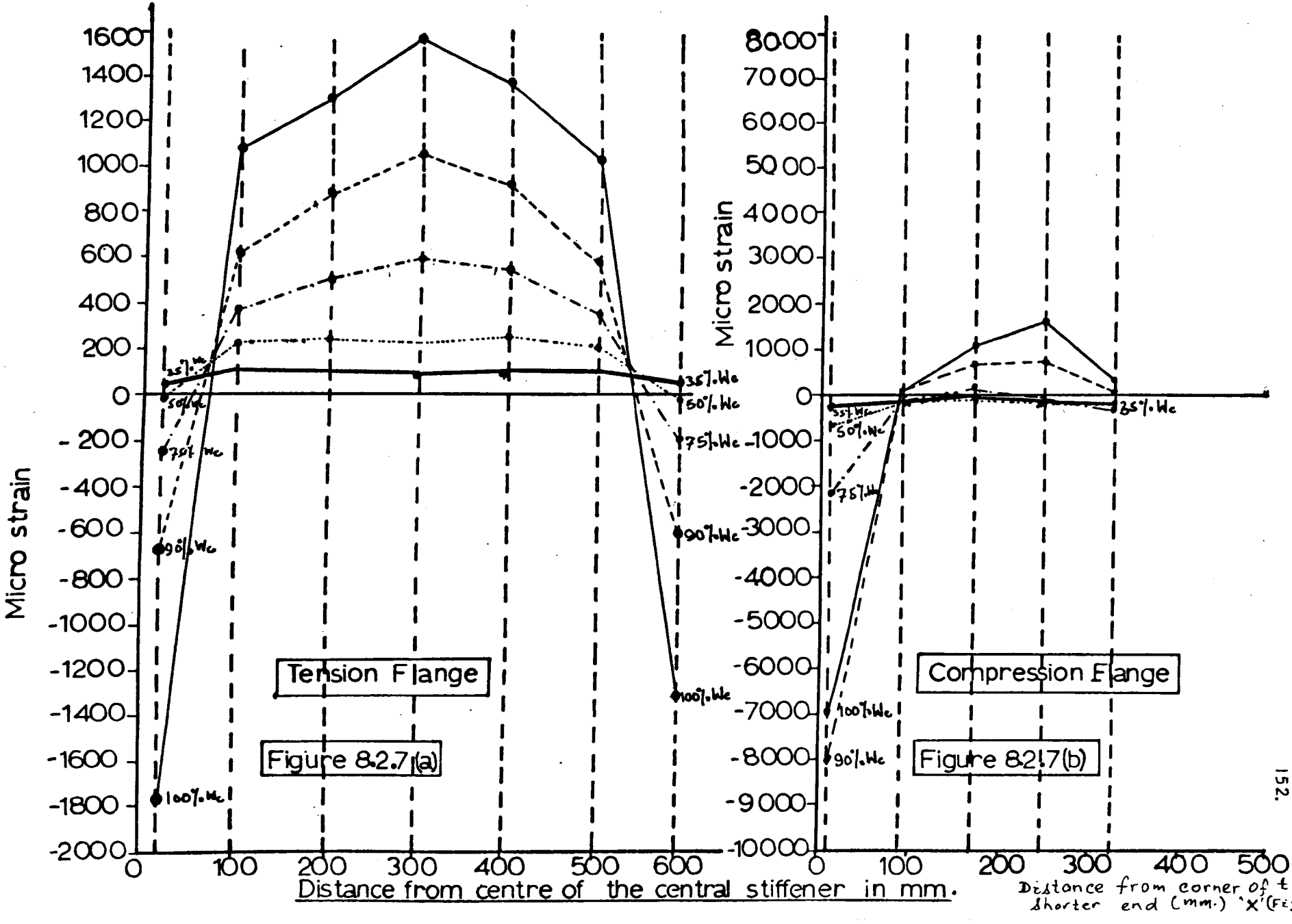
Micro strain
1600
1400
1200
1000
800
600
400
200
0
-200
-400
-600
-800
-1000
-1200
-1400
-1600
-1800
-2000
35% We
50% We
75% We
90% We
100% We
Tension Flange
Figure 8.2.7(a)
0
100
200
300
400
500
600
Distance from centre of the central stiffener in mm.
Micro strain
8000
7000
6000
5000
4000
3000
2000
1000
0
-1000
-2000
-3000
-4000
-5000
-6000
-7000
-8000
-9000
-10000
35% We
50% We
75% We
90% We
100% We
Compression Flange
Figure 8.2.7(b)
0
100
200
300
400
500
Distance from corner of the shorter end (mm.) 'x' (Figure 8.2.9)

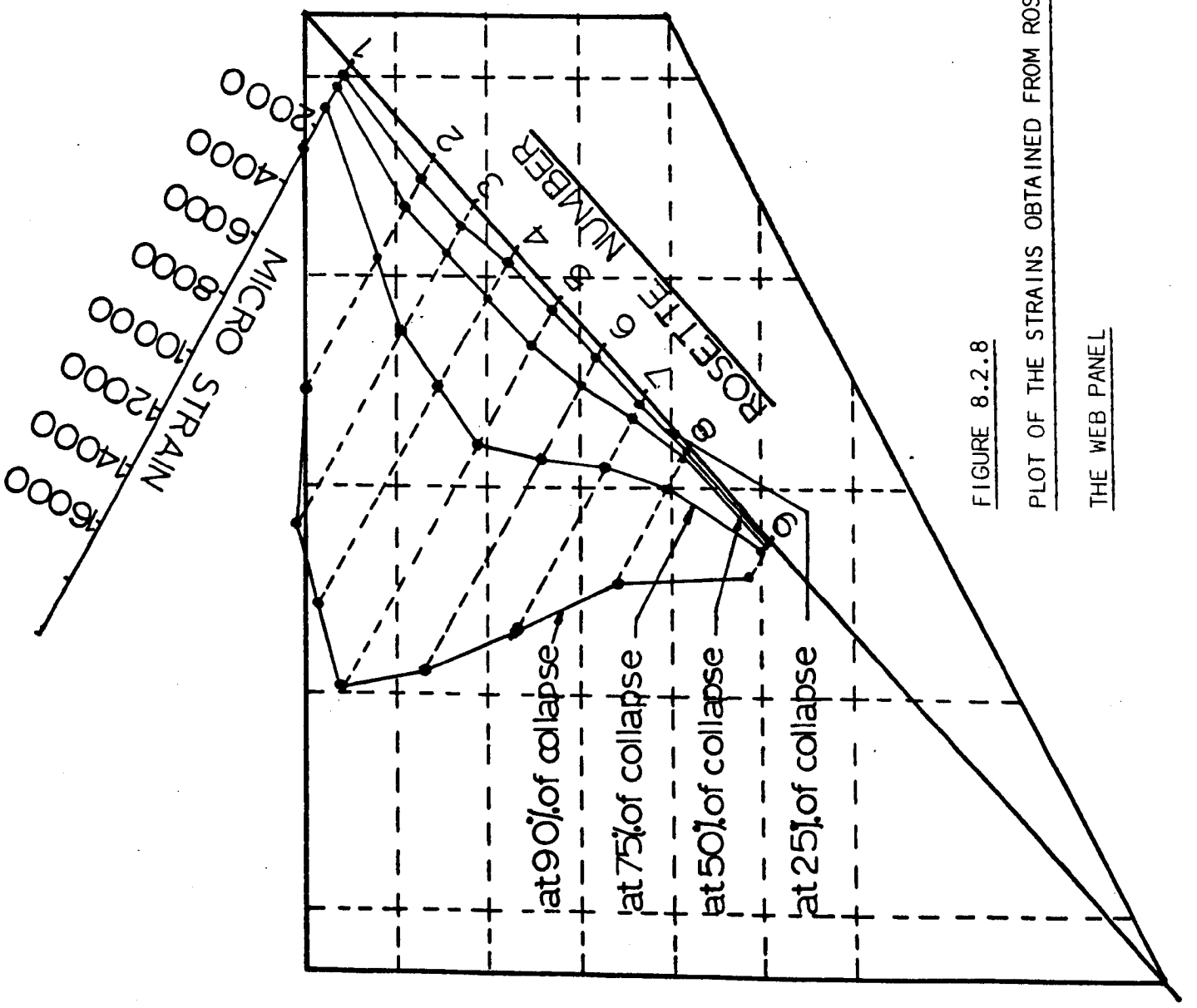

FIGURE 8.2.8

PLOT OF THE STRAINS OBTAINED FROM ROSETTES READINGS IN THE WEB PANEL

Distance from ℄ of the central stiffener (mm)	Initial profile (mm)	Final profile (mm)	Distance from ℄ of the central stiffener (mm)	Initial profile (mm)	Final profile (mm)
0	0.00	0.00	1150	0.94	15.11
50	0.17	2.23	1200	0.88	12.98
100	0.34	5.63	1250	1.17	10.72
150	0.47	9.30	1300	1.00	8.84
200	0.49	13.03	1350	0.79	6.63
250	0.38	16.71	1400	0.72	4.50
300	0.33	20.45	1450	0.71	2.12
350	0.35	23.93	1500	0.70	0.06
400	0.32	27.17	1550	0.62	-2.16
450	0.39	30.10	1600	0.60	-4.24
500	0.41	32.57	1650	0.72	-6.46
550	0.44	34.52	1700	0.84	-8.65
600	0.47	35.58	1750	0.84	-10.85
650	0.51	35.58	1800	0.93	-13.31
850	1.27	28.32	1850	1.02	-15.47
900	1.04	26.21	1900	1.05	-
950	1.03	24.11	1950	0.91	-
1000	1.05	21.94	2000	0.91	-
1050	1.00	19.80	2050	0.47	-
1100	0.94	17.49	2100	0.63	-

Table 8.2.2

Table 8.2.3.

8.2.4.3 Plotting the deflected profile of the tension and compression flange

The deflected profile of the tension and compression flange was plotted by using the readings given in Tables 8.2.2 and 8.2.3, and is shown in Figure 8.2.10.

It can be noticed from this figure that the wedge 'WXYZ' rotates about the tip and that the tip does not deflect vertically.

8.2.5 Central load deflections of the tapered beam specimen

As explained in Chapter Seven, an L.V.D.T. was mounted at the bottom of the tension flange to record the central deflection, which was plotted with respect to the central load on an X-Y plotter. Figure 8.2.11 shows the plotted curve.

It can be seen from Figure 8.2.11 that at failure (collapse) the beam was subjected to large central deformations.

8.2.6 Comparison of the collapsed panel with the proposed theoretical collapse mechanism

At about 55% of the collapse load, the cracks in resin (Plate 3) show clearly the formation of the tensile membrane stresses along the tension diagonal of the panel. The photographs (plates 4 and 5) as well as the plotted profile shown in Figure 8.2.10 of the collapsed panel show clearly the two plastic hinges in the tension flange and the two plastic hinges in the compression flange. Also, the profiles of the tension and compression flanges (Figure 8.2.10) show that the collapse mechanism occurs with rotation of the wedge 'WXYZ' about the tip. It can be seen that the proposed theoretical collapse mode of failure as illustrated in Chapter

Distance (X) (mm)	Vernier readings (δ) (mm)	Deflected profile (mm)	Distance (X) (mm)	Vernier readings (δ) (mm)	Deflected profile (mm)
0	19.00	0.00	400	34.80	15.80
25	19.90	0.90	425	33.90	14.90
50	21.70	2.70	450	32.90	13.90
75	23.90	4.90	475	32.00	13.00
100	25.70	6.70	500	30.90	11.90
125	27.80	8.80	525	29.90	10.90
150	29.70	10.70	550	28.90	9.90
175	31.60	12.60	575	27.80	8.80
200	33.30	14.30	600	27.00	8.00
225	35.00	16.00	625	25.80	6.80
250	36.30	17.30	650	24.70	5.70
275	36.90	17.90	675	23.60	4.60
300	37.20	18.20	700	22.50	3.50
325	37.10	18.10	725	21.50	2.50
350	36.40	17.40	750	20.40	1.40
375	35.70	16.70	775	19.30	0.30

Table 8.2.3. Final profile of the Compression flange

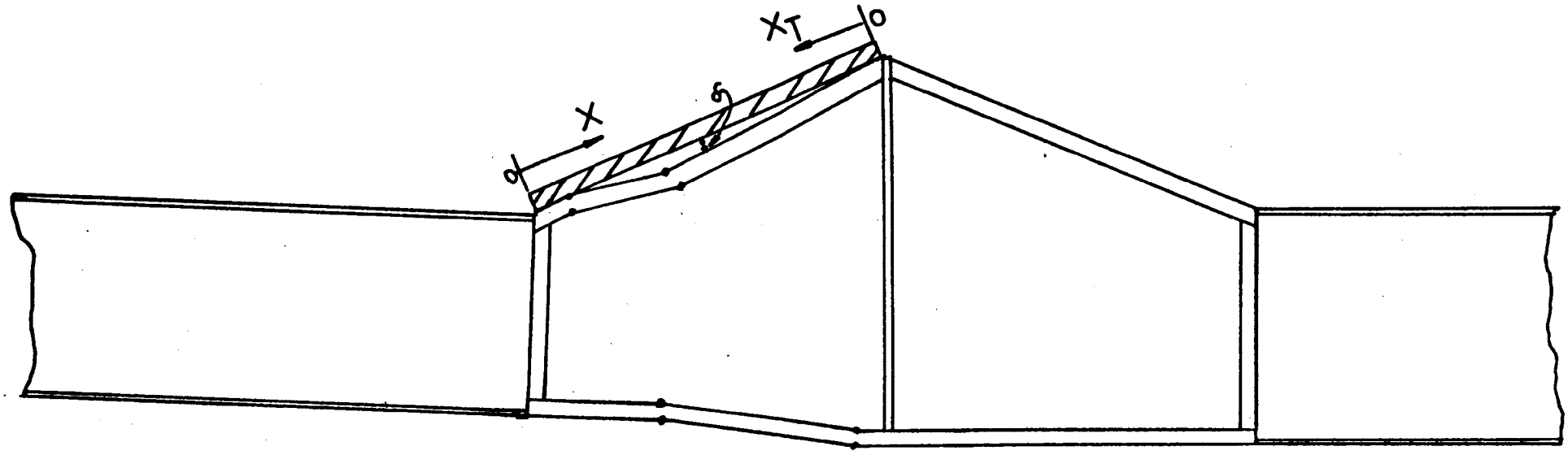

Figure 8.2.9

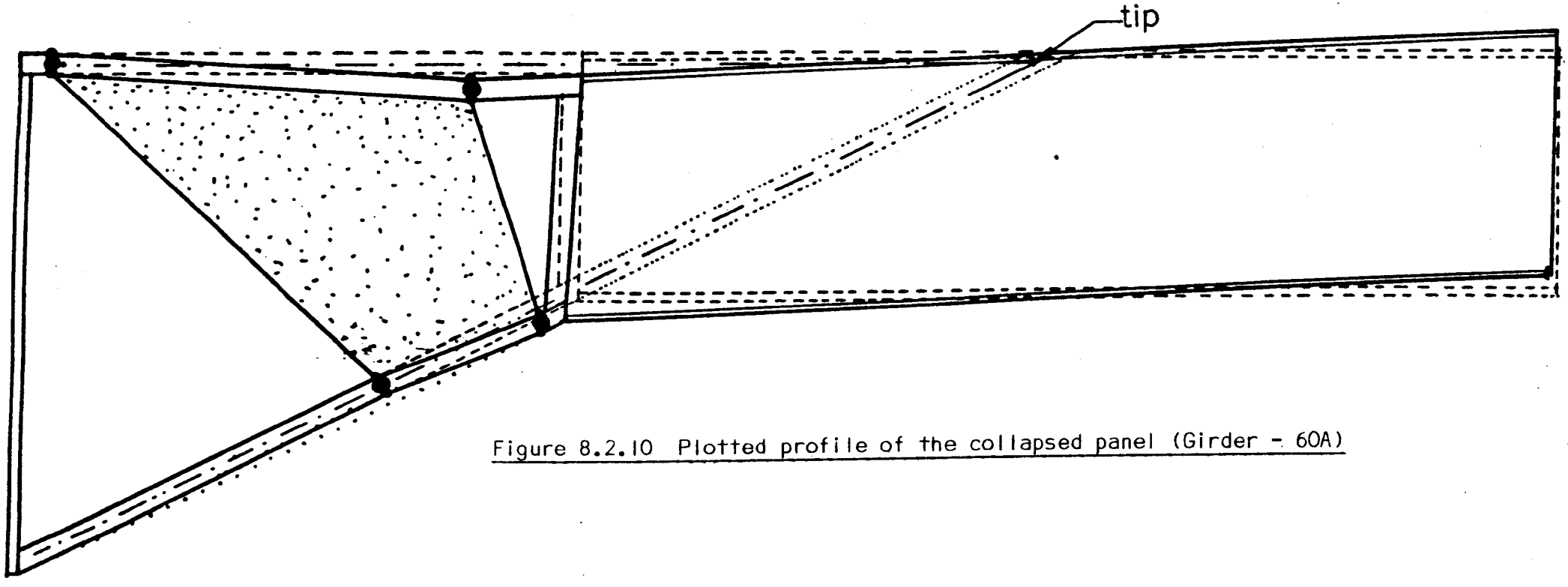

Figure 8.2.10 Plotted profile of the collapsed panel (Girder - 60A)

CENTRAL LOAD - DEFLECTION CURVE OBTAINED FROM AN X-Y PLOTTER

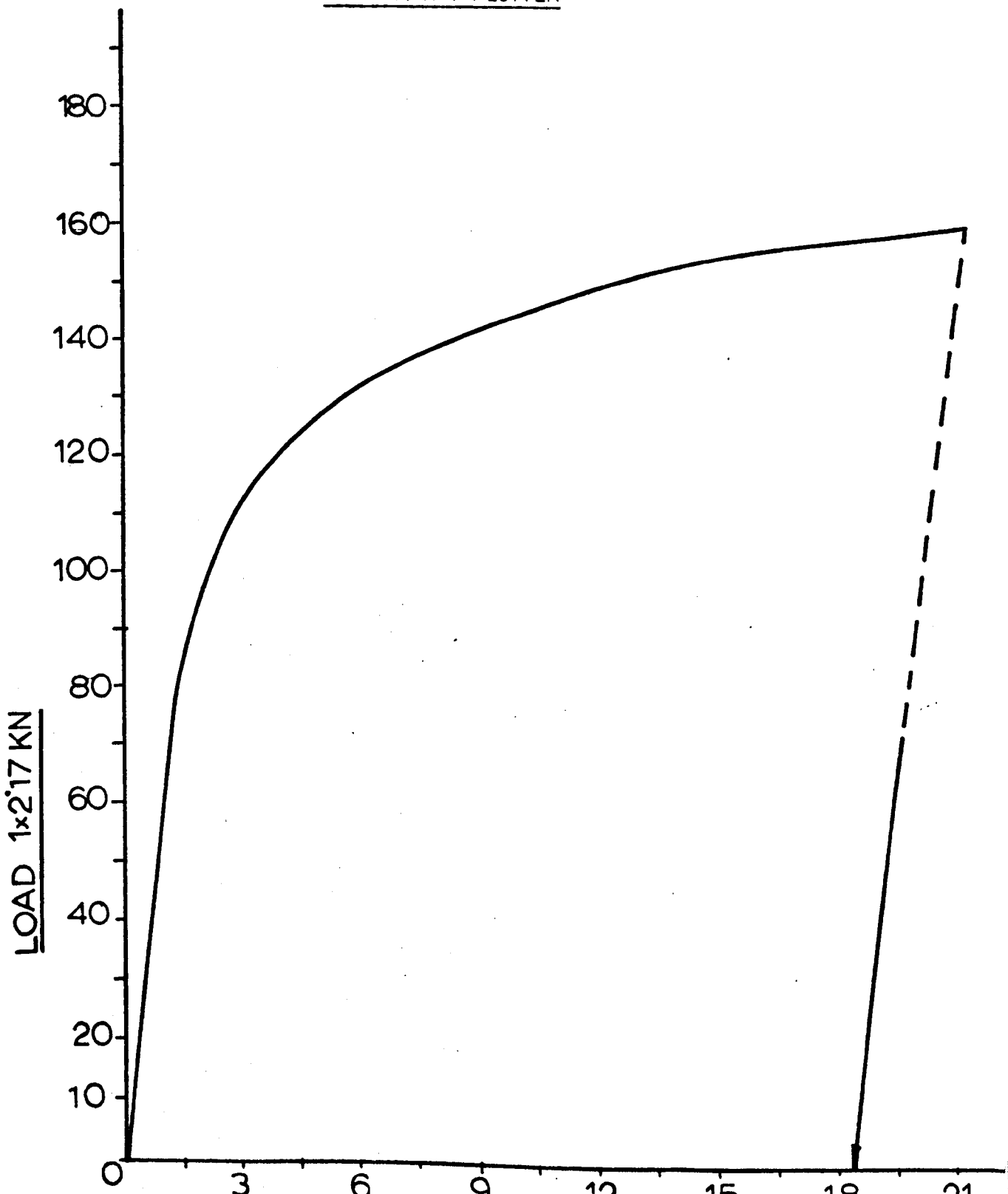

Figure 8.2.11

Plate 3


GIRDER-60
E=566 MM.
SIDE-A
LOAD-105 KN

Plate 4


GIRDER-60
E=566 MM.
SIDE-A
AFTER COLLAPSE
L

Plate 5

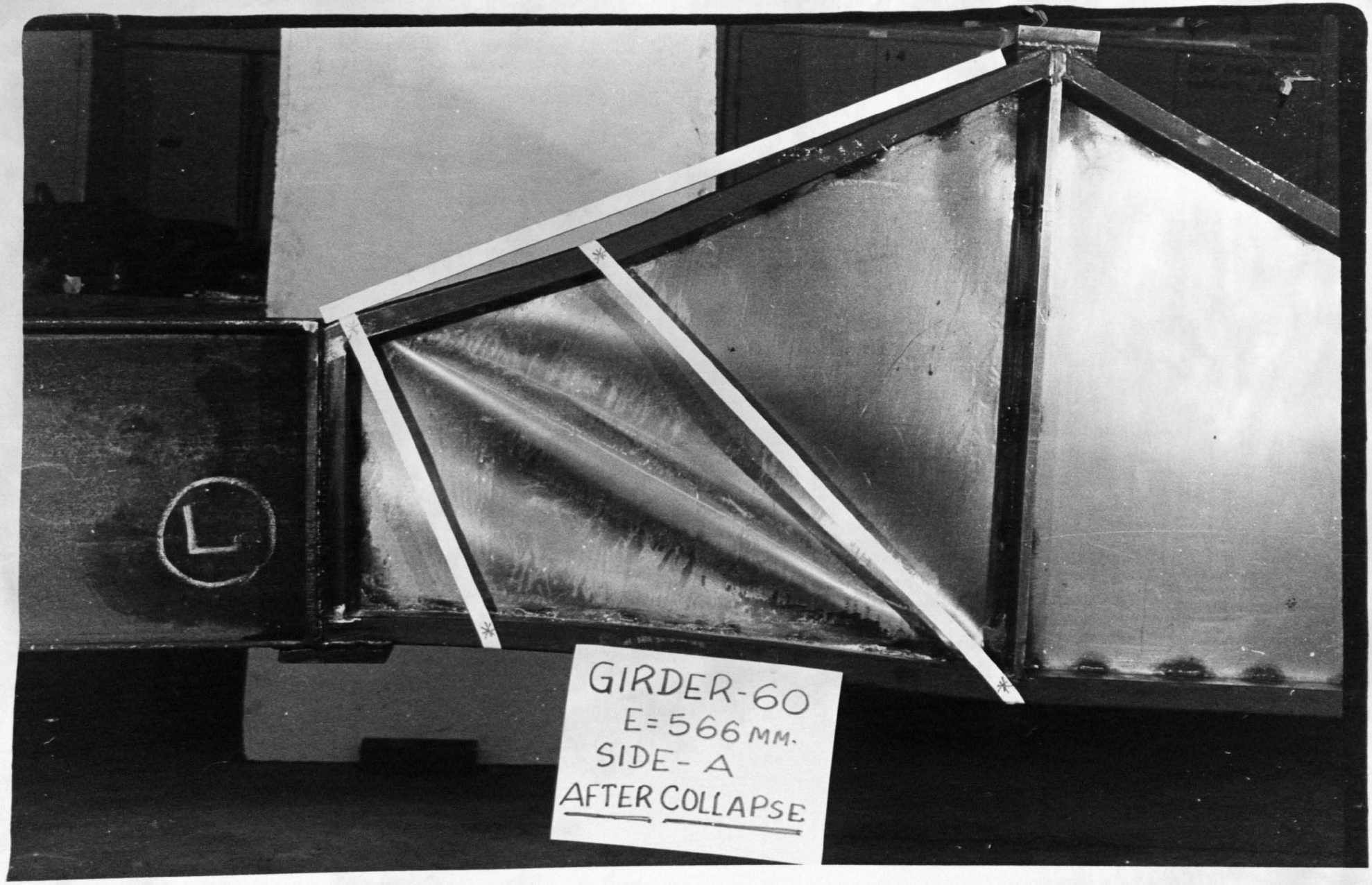
GIRDER-60
E=566 MM.
SIDE-A
AFTER COLLAPSE

Four is identical with the experimental collapse mode.

The analysis of the rosette readings plotted in Figure 8.2.8 shows that the web portion 'UVWX' has yielded completely at 90% of the collapse load. In other words, failure occurs when the plastic hinges in the flanges have formed, which, together with the yield zone 'UVWX' form a plastic mechanism. It is appreciated that the plastic yielding could extend beyond the boundaries 'UVWX', but the minimum requirement, that the complete region 'UVWX' must yield for a mechanism to develop, was achieved.

Table 8.2.4(b) shows the comparison between the experimental and predicted theoretical collapse loads of all the tapered beam specimens loaded inside the tip. The experimental collapse loads are within 8% of the predicted collapse loads.

It can be seen from Figure 8.2.5 that the predicted inclination of the tensile stress field (θ_m) is in good agreement with the inclination of the tension field indicated by the plotted contour lines.

8.2.7 General Conclusions

On the basis of the analyses of results, the following conclusions can be drawn:

(i) The collapse of the tapered beam specimen occurs when the plastic hinges form in the flanges which together with the yield zone 'UVWX' (Figure 8.2.10) forms a plastic mechanism.

(ii) At the plastic collapse of the girder, the wedge (WXYZ - Figure 8.2.10) rotates anticlockwise (in the direction of the 'tip-moment') about the tip such that the vertical deflection at the tip is zero.

(iii) The experimental collapse loads of tapered beams loaded

Girder No.	d_1 (mm)	d_2 (mm)	b (mm)	t (mm)	σ_{yw} N/mm^2	σ_{yf} N/mm^2	τ_{cr} N/mm^2	Z_{pf} (mm^3)
10 (A)	301	677	750	1.5	255	330	12	11726
10 (B)	301	677	750	1.5	255	330	12	11726
20 (A)	301	677	750	1.5	276	300	12	11726
20 (B)	301	677	750	1.5	276	300	12	11726
60** (A)	315	685	750	1.7	283	386	16	14812
70 (A)	315	685	750	2.0	290	378	24	15272
70 (B)	315	685	750	2.0	290	378	24	15272

Table 8.2.4(a)

** Girder considered in this chapter to analyse the results.

Girder No.	θ_m (rad)	M_p (KN.mm)	'e' (mm)	Lower bound load with full M_p (KN)	Upper bound load with full M_p (KN)	Lower bound load with reduced M_p (KN)	Experimental collapse loads (KN)	$\frac{W_{ult}\ (Predicted)}{W_{experiment}}$
10 (A)	0.34	3870	600	136	136	127	125	1.01
10 (B)	0.34	3870	300	262	262	177	169	1.04
20 (A)	0.32	3518	450	178	178	154	144	1.06
20 (B)	0.32	3518	150	517	517	182	180	1.01
60* (A)	0.36	5717	639	186	186	175	190	0.92
70 (A)	0.34	5773	489	270	270	233	252	0.92
70 (B)	0.34	5773	339	379	379	258	275	0.93

Table 8.2.4(b)

inside the tip give good agreement with the theoretical loads calculated by considering the reduced plastic moment of the flanges.

(iv) The inclinations of the tensile membrane stress field indicated by the contour lines of the out-of-plane deflections of the web are in good agreement with the theoretical values.

8.3 Tapered beams loaded outside the tip (Test Series Two)

8.3.1 Introductory Remarks

As specified in Chapter Seven, in Test Series Two, four experiments were performed to examine the ultimate strengths and the collapse mode of failure of tapered beams loaded outside the tip. The dimensions of the girders tested and the material properties are presented in Table 8.3.4(a). In this section, the results of one experiment (Girder - 60, panel - 2) will be used to plot the out-of-plane deflections of the web panel and the deflected profile of the tension and compression flanges.

8.3.2 Out-of-plane deflections of the web panel

The technique for the measurements of the out-of-plane deflections of the web panels is given in Chapter Seven. The readings of the initial imperfections, the out-of-plane deflections at 31%, 63% and 91% of the collapse load and the final deflected profile of the web panel of the girder (Girder - 60) are presented in Table 8.3.1. The contours of the initial imperfections are shown in Figure 8.3.1. The contour lines showing the formation of the tension band along the tension diagonal of the web panel at the three loads mentioned previously (31%, 63% and 91% of the collapse load) are shown in Figures 8.3.2, 8.3.3 and 8.3.4 respectively. Also the contour lines showing the final deflected profile of the web panel are plotted

Column number	Dial gauge number	Initial imperfections (mm)	Profile at 31% of the collapse load (mm)	Profile at 63% of the collapse load (mm)	Profile at 91% of the collapse load (mm)	Final profile after collapse (mm)
1	1	+0.07	0.07	0.11	0.20	0.18
	2	+0.02	0.02	0.02	0.13	0.10
	3	−1.34	-1.42	-1.01	-1.58	-0.02
	4	+0.13	-0.06	-0.26	0.04	0.88
	5	+0.17	0.02	0.18	0.71	0.45
	6	0.38	-0.23	0.25	0.72	-0.23
2	7	−1.62	-1.91	-2.42	-2.55	-0.54
	8	-3.14	-3.71	-5.91	-5.60	-0.62
	9	-3.56	-4.83	-8.80	-7.61	-1.97
	10	-2.90	-4.71	-9.09	-7.31	-3.26
	11	-0.56	-2.06	-5.35	-3.96	-2.57
	12	+1.40	-2.20	-1.52	-1.93	-4.23
3	13	+0.43	1.20	-0.99	-0.73	2.18
	14	-1.58	-0.62	-6.67	-7.39	0.26
	15	-3.65	-3.17	-10.78	-12.90	-8.12
	16	-4.86	-4.94	-10.88	-15.65	-10.89
	17	-3.32	-3.20	-5.71	-6.51	8.70
	18	-0.82	-0.75	-1.07	1.83	18.00
4	19	+2.30	3.55	4.66	1.55	-1.77
	20	+3.55	5.39	10.61	7.15	-4.42
	21	+1.93	3.04	9.48	11.62	22.88
	22	-1.88	-1.57	1.47	4.10	21.22
	23	-1.21	-1.20	-0.74	-0.68	-2.15
5	24	-1.48				8.92
	25	-0.39				5.85
	26	-2.04				1.20
	27	-1.57				-1.53

Table 8.3.1

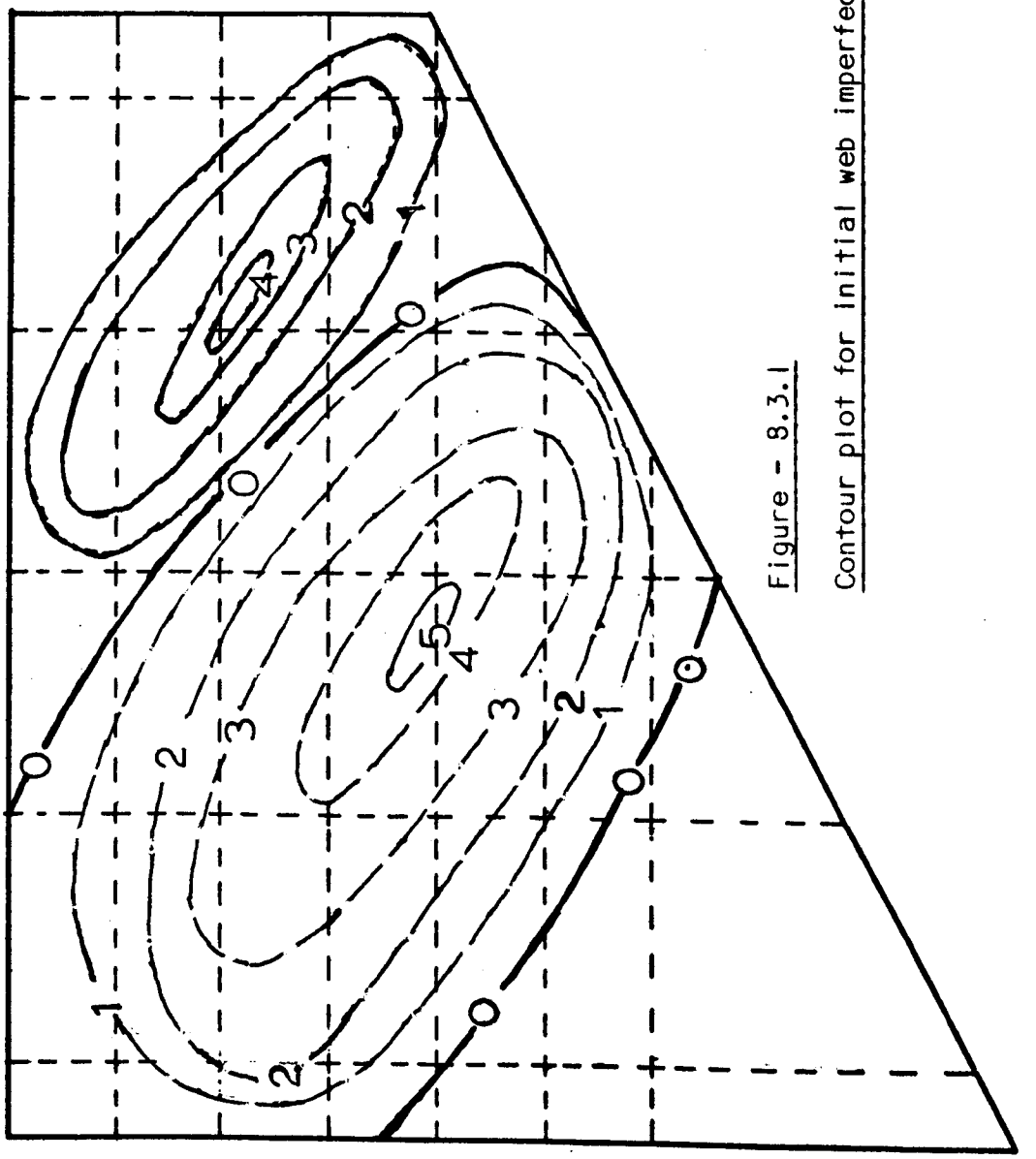

Figure - 8.3.1

Contour plot for initial web imperfections (Girder - 60B)

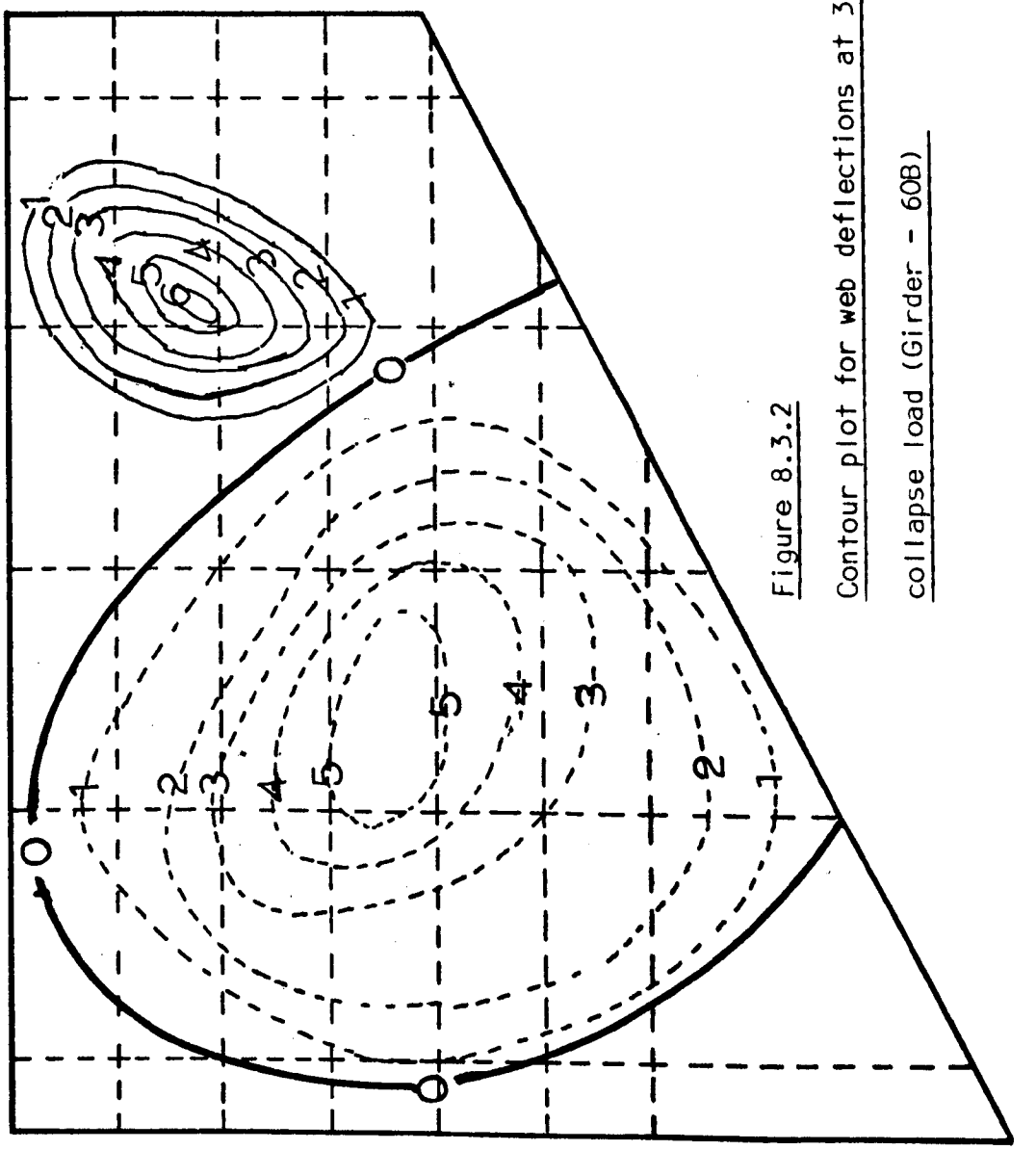

Figure 8.3.2

Contour plot for web deflections at 31% of the collapse load (Girder - 60B)

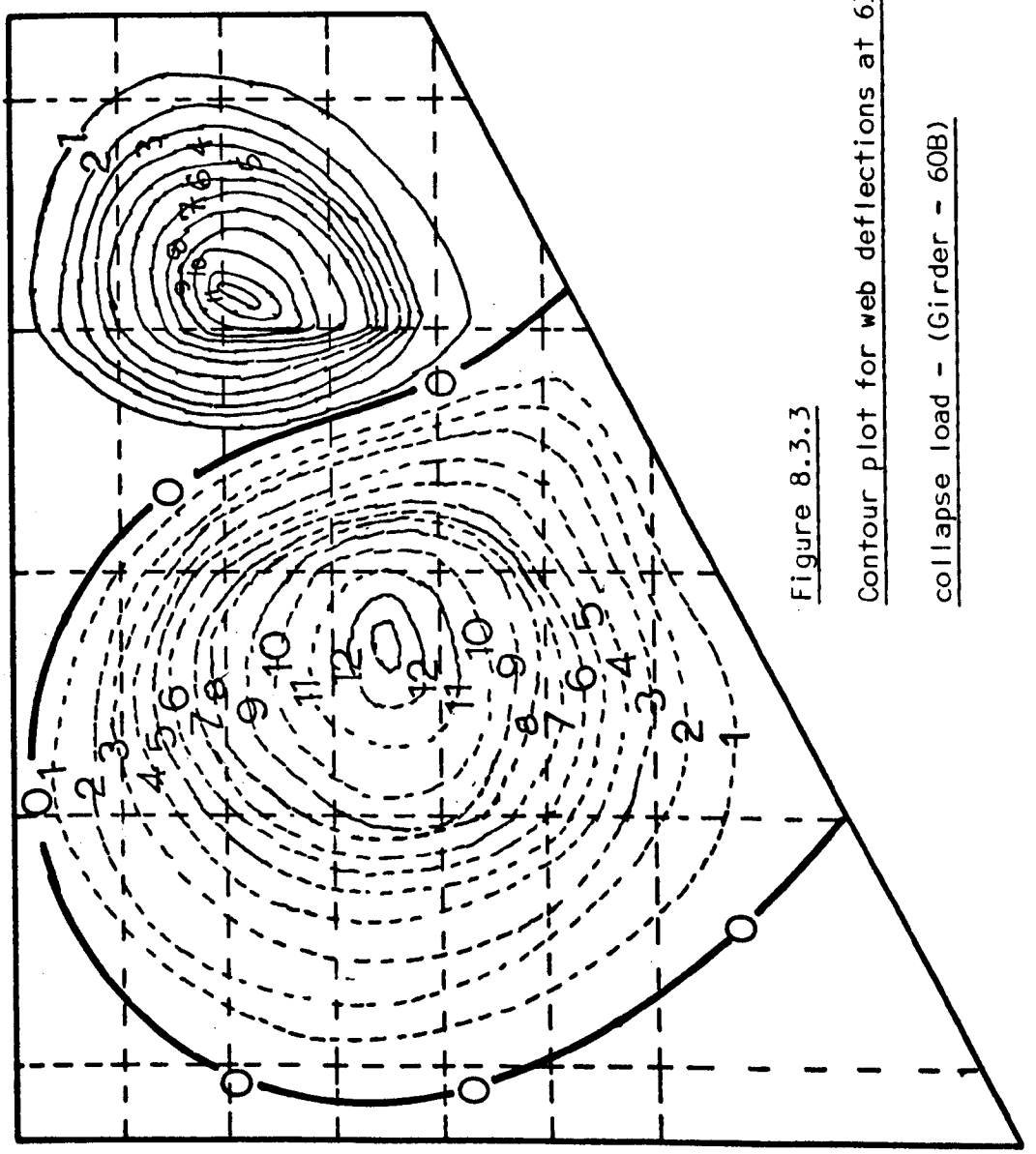

Figure 8.3.3

Contour plot for web deflections at 63% of the collapse load - (Girder - 60B)

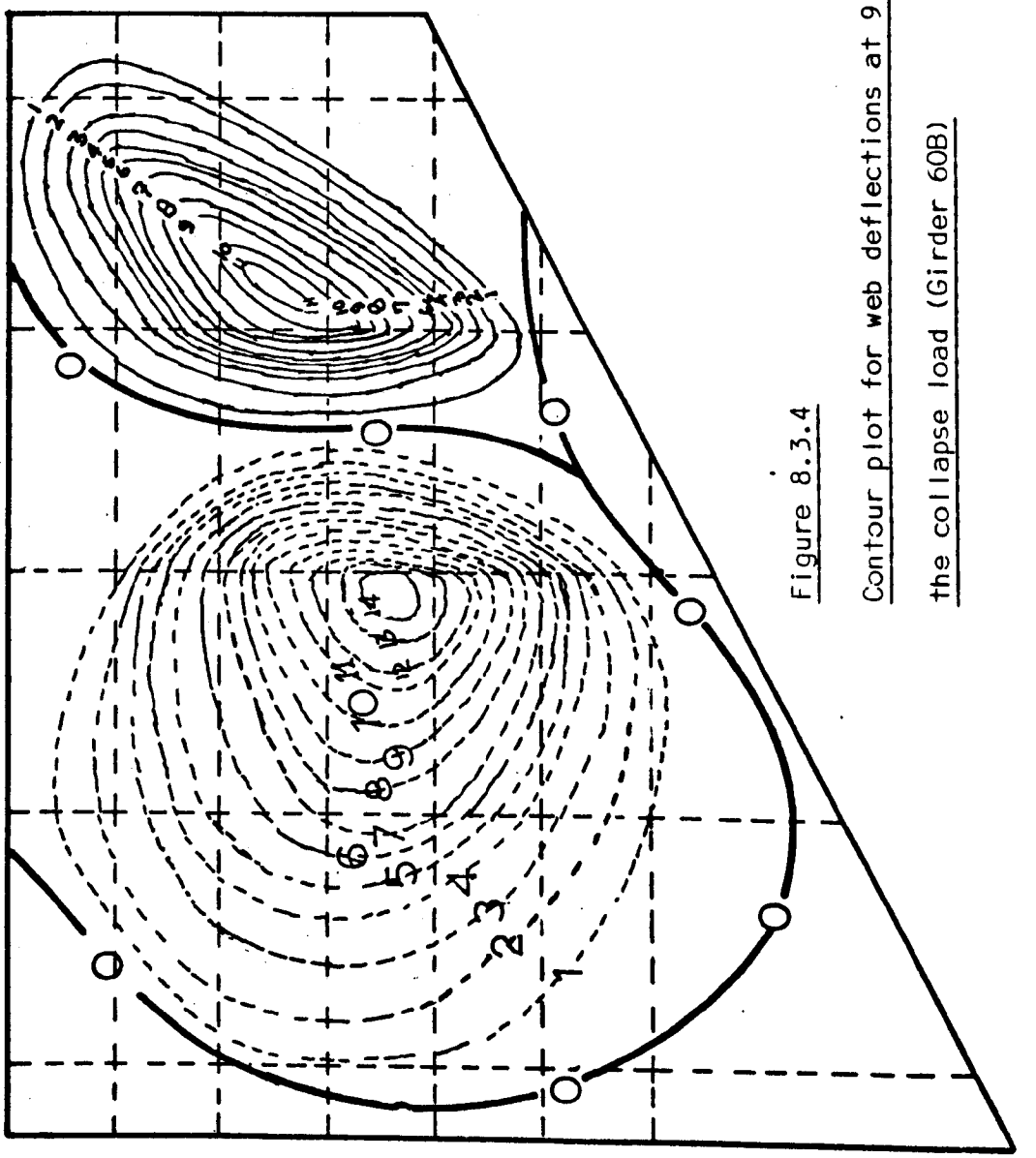

Figure 8.3.4

Contour plot for web deflections at 91% of the collapse load (Girder 60B)

in Figure 8.3.5. In Figure 8.3.6 the profiles of the web panel are plotted for the three different panel loads as mentioned previously. The contours showing the deflected profiles of the web panels of all other experiments are shown in Appendix 7.

It is clear from Figure 8.3.5 that when a tapered beam is loaded outside the tip, the tension diagonal is along the long diagonal, whereas the tension diagonal was along the short diagonal of the tapered panel for the case when the beam was loaded inside the tip.

8.3.3 Deflected profile of the tension and compression flanges

The techniques for the measurements of the profile of the tension and compression flange are explained in section 8.2.4. A set of readings for the initial and final profile of the tension flange is presented in Table 8.3.2.

The profile of the compression flange was measured in the same way as explained in section 8.2.4. A set of readings for the final profile of the compression flange is presented in Table 8.3.3.

The final profiles of the tension and compression flange were plotted by using the readings in Tables 8.3.2 and 8.3.3 and are shown in Figure 8.3.7.

It can be noticed from Figure 8.3.7 that the wedge 'WXYZ' rotates about the tip. The slight vertical deflection of the tip occurred because this experiment was the second experiment on the girder (Girder 60, panel no. 2), and in the first experiment this panel was supported near the tip.

8.3.4 Central load deflections of the tapered beam specimen

The central deflection was recorded with respect to the central load in the same way as explained previously. The

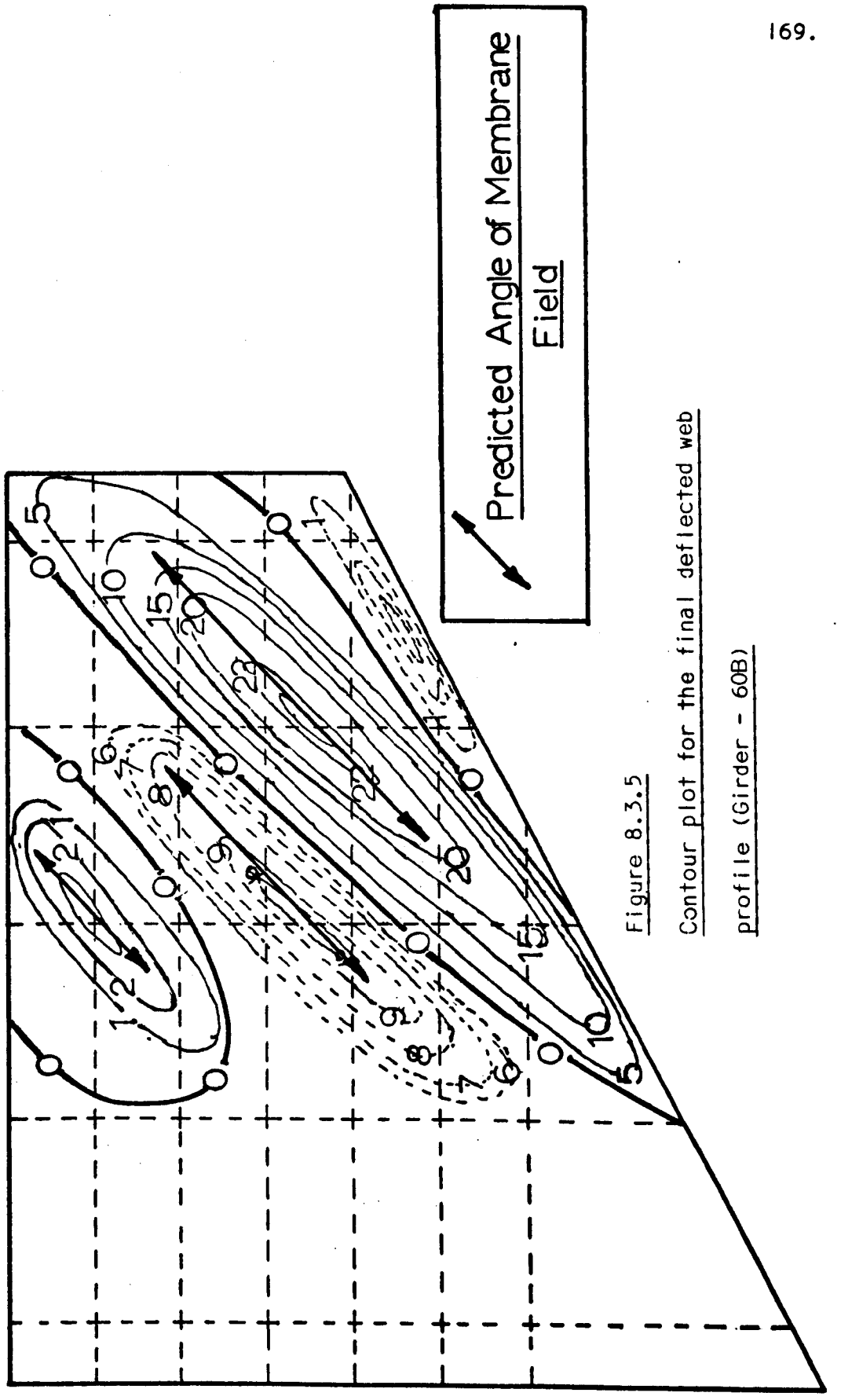

Figure 8.3.5

Contour plot for the final deflected web profile (Girder - 60B)

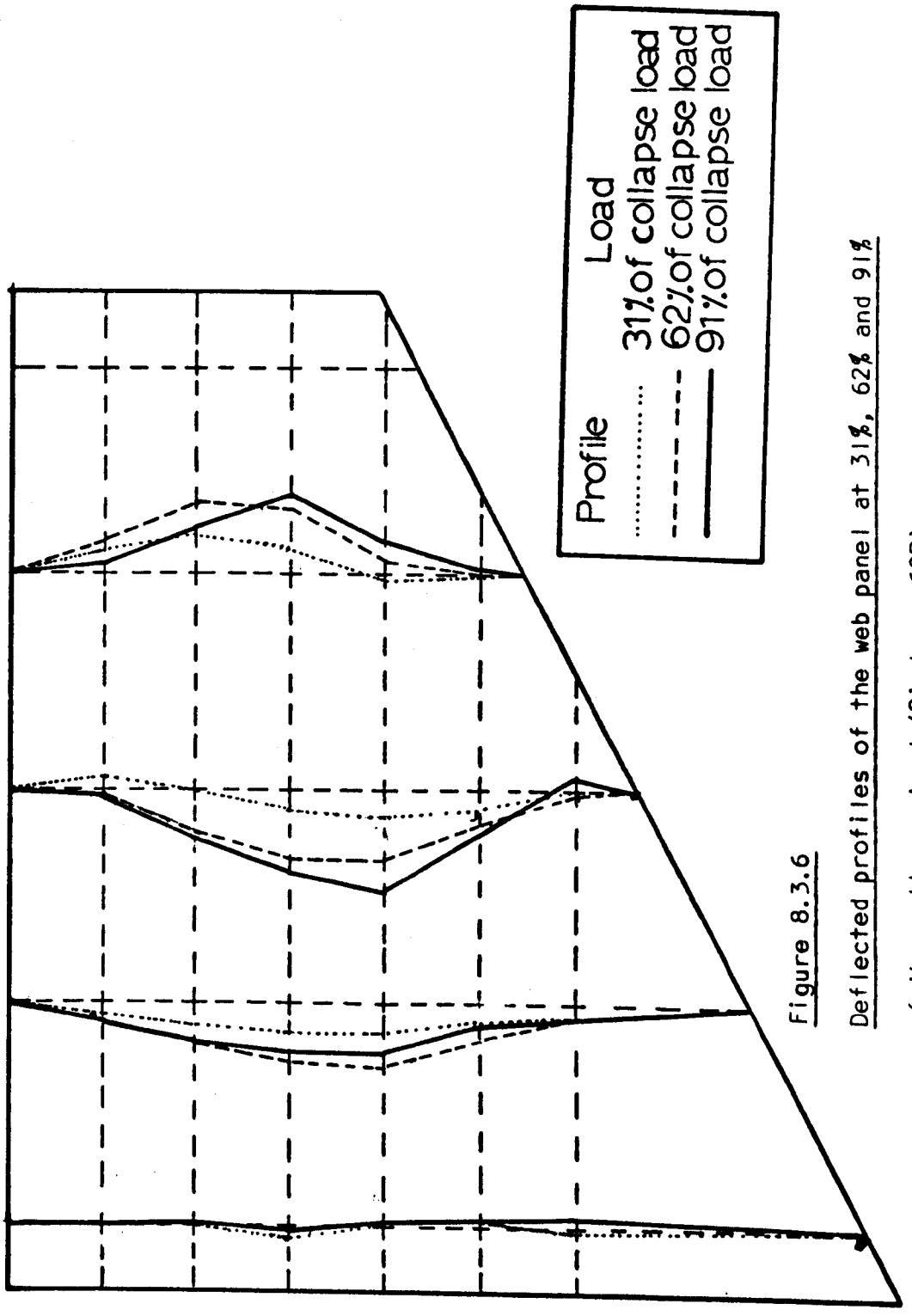

Figure 8.3.6

Deflected profiles of the web panel at 31%, 62% and 91% of the collapse load (Girder - 60B)

Distance from ℄ of the central stiffener (mm)	Initial profile (mm)	Final profile (mm)	Distance from ℄ of the central stiffener (mm)	Initial profile (mm)	Final profile (mm)
0	0.00	0.00	1100	3.22	-0.12
50	-0.58	-0.35	1150	3.31	1.76
100	-0.48	-0.63	1200	3.47	4.20
150	-0.08	-1.14	1250	3.57	5.66
200	0.13	-1.51	1300	3.78	7.76
250	0.29	-1.94	1350	3.90	9.32
300	0.03	-2.15	1400	4.05	11.21
350	0.51	-3.03	1450	4.27	13.21
400	0.69	-3.85	1500	4.37	15.04
450	0.71	-4.72	1550	4.57	16.84
500	0.91	-6.19	1600	4.65	18.77
550	1.06	-7.91	1650	4.81	20.56
600	1.15	-9.79	1700	4.92	22.13
650	1.36	-11.85	1750	5.05	23.96
700	1.48	-13.25	1800	5.17	25.90
800	2.78	-11.51	1850	5.27	27.81
850	2.61	-9.62	1900	5.43	29.67
900	2.77	-7.75	1950	5.44	31.77
950	2.86	-5.75	2000	5.67	33.28
1000	2.99	-4.00	2050	5.80	35.12
1050	3.06	-1.97			

Table 8.3.2

Distance (X) (mm)	Vernier readings (δ) (mm)	Deflected profile (mm)	Distance (X) (mm)	Vernier readings (δ) (mm)	Deflected profile (mm)
0	21.30	1.68	400	33.20	13.58
25	22.96	3.34	425	31.38	11.76
50	24.60	4.98	450	28.50	8.88
75	26.50	6.88	475	26.50	6.88
100	28.04	8.42	500	24.50	4.88
125	29.60	9.98	525	22.80	3.18
150	31.20	11.58	550	21.30	1.68
175	32.60	12.98	575	20.20	0.58
200	34.02	14.40	600	19.62	0.00
225	35.30	15.68	625	19.62	0.00
250	36.60	16.98	650	19.62	0.00
275	37.30	17.68	675	19.94	0.32
300	37.80	18.18	700	20.42	0.80
325	37.46	17.84	725	20.86	1.24
350	36.50	16.88	750	21.20	1.58
375	35.10	15.48			

Table 8.3.3

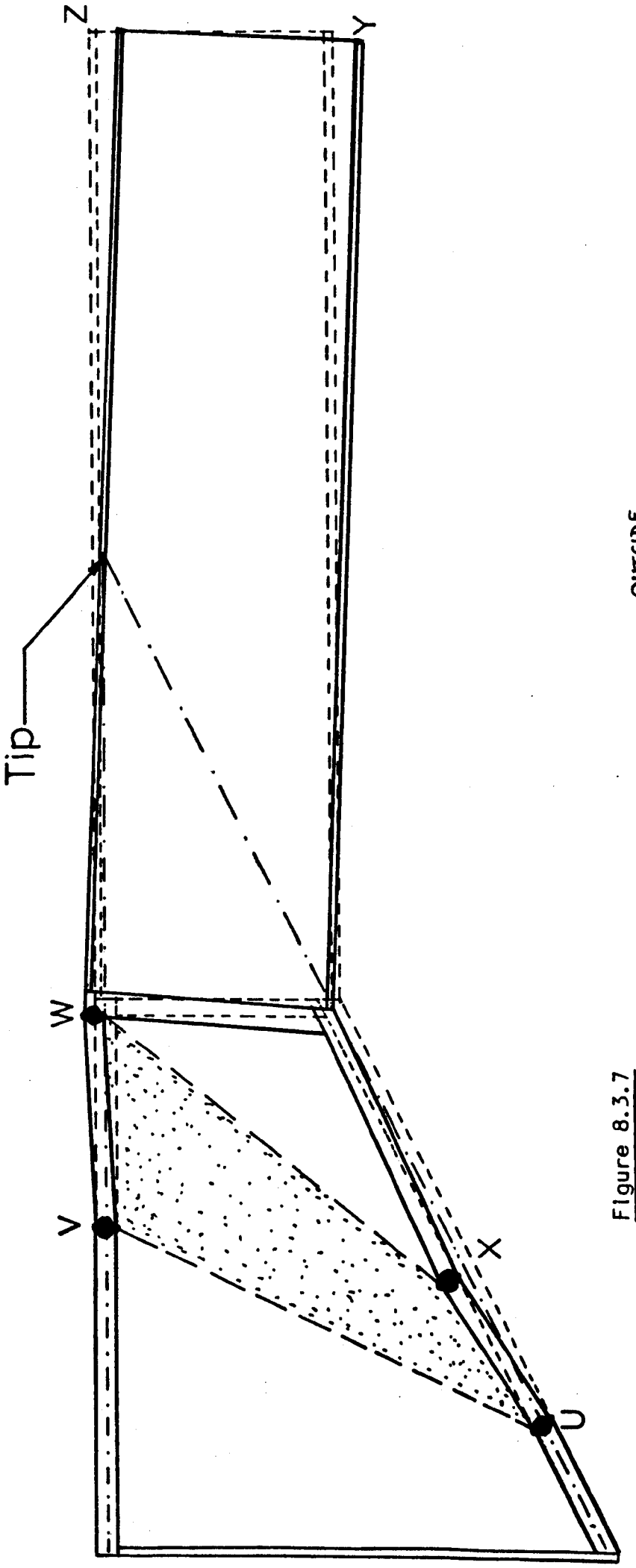

Figure 8.3.7

PLOTTED PROFILE OF THE COLLAPSED PANEL (BEAM LOADED ^ THE TIP)

GIRDER - 60B

plotted curve is shown in Figure 8.3.8 from which it can be noticed that at collapse the beam has failed giving large central deflections.

8.3.5 Comparison of the collapsed panel with the proposed theoretical collapse mechanism

The photographs (plates 6 and 7) and the plotted profile (Figure 8.3.7) of the collapsed panel show clearly the two plastic hinges in the tension flange and the two plastic hinges in the compression flange. The plotted profile of the flanges (Figure 8.3.7) also shows that the collapse mechanism occurs with rotation of the wedge 'WXYZ' about the tip. It can be seen that the proposed theoretical collapse mode of failure as illustrated in Chapter Five is identical with the experimental collapse mode.

Although the measurement of strains in the webs and the flanges was not carried out in this test series, due to the cost involved, it is clear from the photographs (plates 6 and 7) and Figure 8.3.7 that the web portion of the wedge 'UVWX' has yielded completely.

In the same way as explained in section 8.2.5, the failure of the girder occurs when the plastic hinges in the flanges form, which, together with the yield zone 'UVWX' form a plastic mechanism.

The comparison between the experimental and the theoretical collapse loads of all the tapered beam specimens loaded outside the tip is presented in Table 8.3.4(b). The experimental collapse loads are within 9% of the predicted collapse loads.

It can be seen from Figure 8.3.5 that the predicted

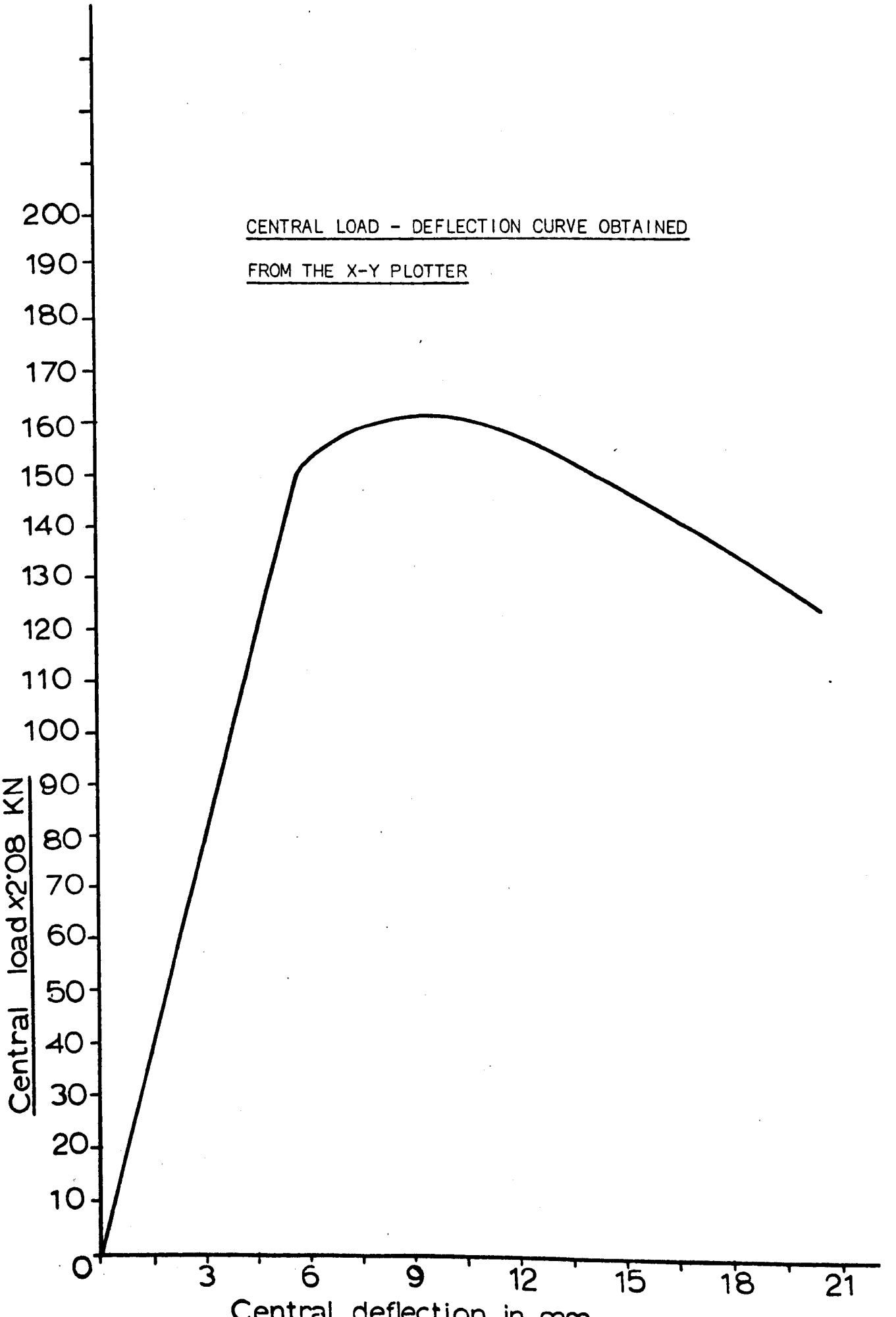
CENTRAL LOAD - DEFLECTION CURVE OBTAINED
FROM THE X-Y PLOTTER
Central load x2'08 KN
0
10
20
30
40
50
60
70
80
90
100
110
120
130
140
150
160
170
180
190
200
3
6
9
12
15
18
21
Central deflection in mm.

Figure 8.3.8

Plate 6


GIRDER-60
TEST SERIES-IIA
SIDE-B
AFTER COLLAPSE
R

Plate 7


GIRDER-60
TEST SERIES-II A
SIDE-A
AFTER COLLAPSE

Girder No.	d_1 (mm)	d_2 (mm)	b (mm)	t (mm)	σ_{yw} (N/mm^2)	σ_{yf} (N/mm^2)	τ_{cr} (N/mm^2)	Z_p (mm^3)
30 (A)	315	685	750	1.7	249	310	16	13416
30 (B)	315	685	750	1.7	249	310	16	13416
40 (A)	315	685	750	1.7	239	324	16	14236
60 (B)	315	685	750	1.7	283	386	16	14812

Table 8.3.4(a)

Girder No.	θ_{mm} (rad)	M_p (KN.mm)	e (mm)	Lower bound load with full M_p (KN)	Upper bound load with full M_p	Lower bound load with reduced M_p (KN)	Experimental collapse loads (KN)	$\frac{W_{ult}\ (Predicted)}{W_{experiment}}$
30 (A)	0.73	4159	461	163	163	97	89	1.08
30 (B)	0.73	4159	161	441	441	133	121	1.09
40 (A)	0.74	4612	311	241	241	125	115	1.08
60 (B)	0.74	5717	461	201	201	125	126	0.99

Table 8.3.4(b)

inclination of the tensile stress field (θ_m) is in good agreement with the inclination of the tension field indicated by the plotted contour lines.

8.3.6 General Conclusions

On the basis of the analyses of results, the following conclusions can be drawn:

(i) The collapse of the tapered beam specimen loaded outside the tip occurs when the plastic hinges form in the flanges which together with the yield zone 'UVWX' (Figure 8.3.7) forms a plastic mechanism.

(ii) At the plastic collapse of the girder, the wedge (WXYZ - Figure 8.3.7) rotates clockwise (in the direction of the tip-moment) about the tip such that the vertical deflection at the tip is zero.

(iii) The experimental collapse loads of the tapered beams loaded outside the tip give good agreement with the theoretical loads calculated by considering the reduced plastic moment of the flanges.

(iv) The inclinations of the tensile membrane stress field indicated by the contour lines of the out-of-plane deflections of the web are in good agreement with the theoretical values.

8.4 Tapered beams loaded at the tip (Test Series Three)

8.4.1 Introductory Remarks

In Test Series Three, as explained in Chapter Seven, three experiments were performed to examine the ultimate strengths and the collapse mode of failure of tapered beams loaded at the tip. The dimensions of the girders tested and the material properties are presented in Table 8.4.7. In this section, the results of one experiment (Girder - 50,

panel - 1) will be used to plot the out-of-plane deflections of the web panel and the deflected profiles of the flanges.

8.4.2 Out-of-plane deflections of the web panel

The technique for the measurements of the out-of-plane deflections of the web panels is explained in Chapter Seven. The readings of the initial imperfections, the out-of-plane deflections at 30%, 60% and 91% of the collapse load and the final deflected profile of the web panel of the girder (Girder - 50) are presented in Table 8.4.1. The contours of the initial imperfections are shown in Figure 8.4.1. The contour lines showing the out-of-plane deflections of the web at the three loads mentioned previously are shown in Figures 8.4.2, 8.4.3 and 8.4.4 respectively. Also the contour lines showing the final profile of the web panel are plotted in Figure 8.4.5. In Figure 8.4.6 the profiles of the web panel are plotted for the three different panel loads as mentioned previously. The contours showing the deflected profile of the web panels of all other experiments are shown in Appendix 8.

8.4.3 Analysis of the strain gauge readings

In the first experiment on Girder number 50, as explained in Chapter Seven (7.6), thirty-six strain gauges were used to measure the bending, shear and longitudinal strains of the tension and compression flanges.

The theoretical and experimental values of the axial forces in the tension and compression flanges are presented in Tables 8.4.2 and 8.4.3 respectively. The experimental values of the axial forces are calculated from the measured strains in the flanges by using the corresponding values of stresses from the stress-strain curve of the tension tests of the flange material.

Column number	Dial gauge number	Initial profile (mm)	Profile at 30% of the collapse load (mm)	Profile at 60% of the collapse load (mm)	Profile at 91% of the collapse load (mm)	Final profile after collapse (mm)
1	1	−2.54	-2.63	-2.71	-2.25	6.20
	2	-3.12	-3.16	-3.16	-2.39	6.84
	3	-2.48	-2.39	-2.22	-1.19	7.08
	4	-3.68	-3.51	-3.26	-2.15	6.43
	5	-3.38	-3.15	-2.84	-2.00	4.97
	6	-3.99	-3.72	-3.39	-3.13	2.80
2	7	-2.48	-2.84	-3.35	-4.25	-14.92
	8	-4.56	-5.27	-6.23	-7.15	-21.82
	9	-4.82	-5.41	-6.26	-6.85	-20.86
	10	-5.10	-5.46	-6.06	-6.19	-17.55
	11	-4.92	-4.94	-5.12	-4.26	-8.54
	12	-4.56	-4.19	-3.81	-1.43	7.02
3	13	+2.14	2.54	3.09	0.71	0.79
	14	+2.92	2.95	3.07	-0.53	2.23
	15	+3.28	2.83	2.32	-1.31	2.63
	16	+2.97	2.34	1.63	-3.25	-9.11
	17	+1.54	1.17	0.95	-1.31	-11.18
	18	+0.24	0.14	0.12	0.04	-2.11
4	19	−0.53	-0.35	-0.11	-2.50	0.08
	20	+0.42	0.60	0.95	-1.45	-2.27
	21	+2.16	1.97	1.84	-1.94	-12.27
	22	+2.93	2.42	1.80	-3.06	-13.93
	23	+1.09	0.89	0.58	-1.41	-14.93
5	24	+0.10				0.78
	25	-2.64				1.09
	26	-3.33				1.87
	27	-1.94				4.92

Table 8.4.1

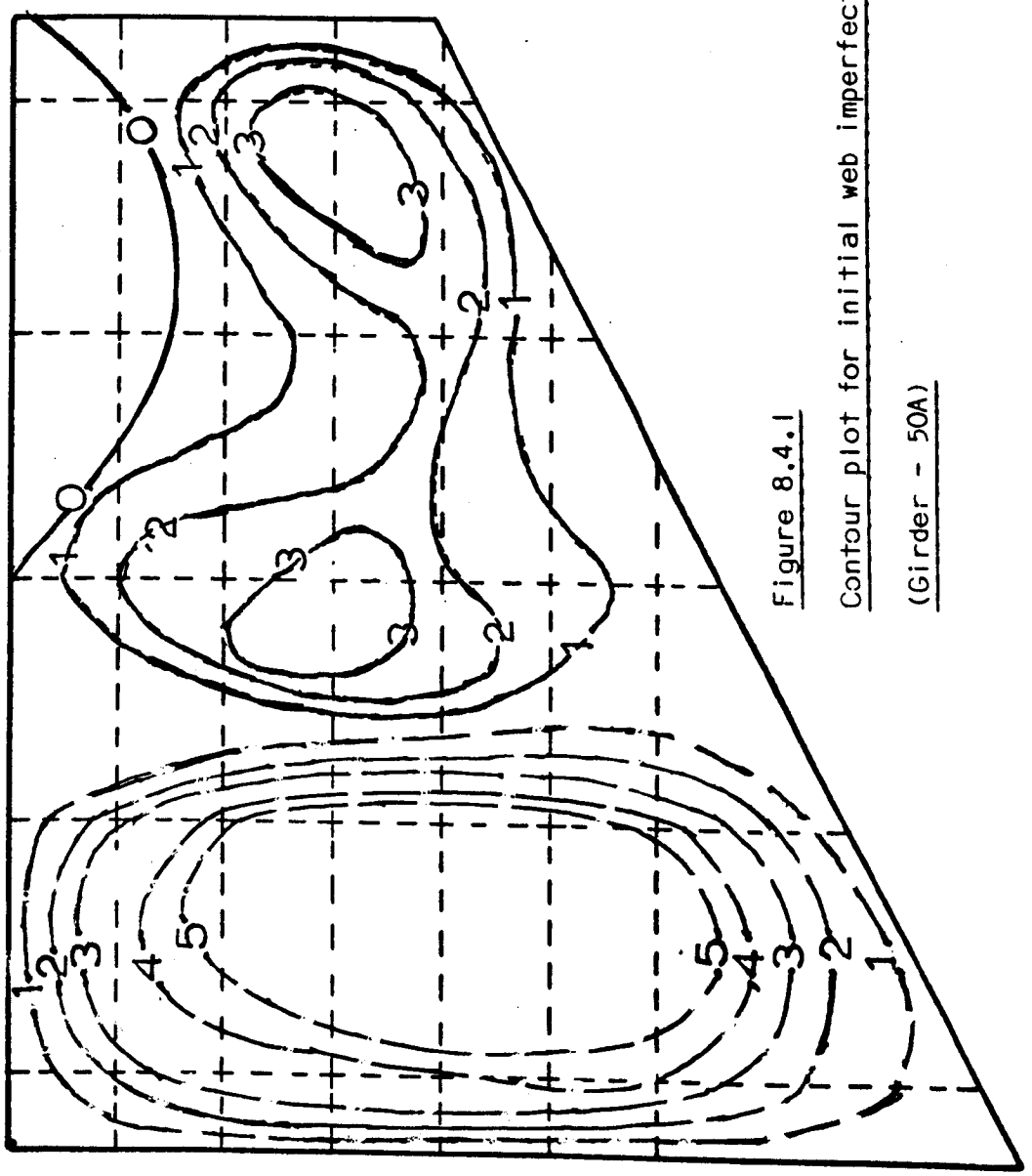

Figure 8.4.1

Contour plot for initial web imperfections

(Girder - 50A)

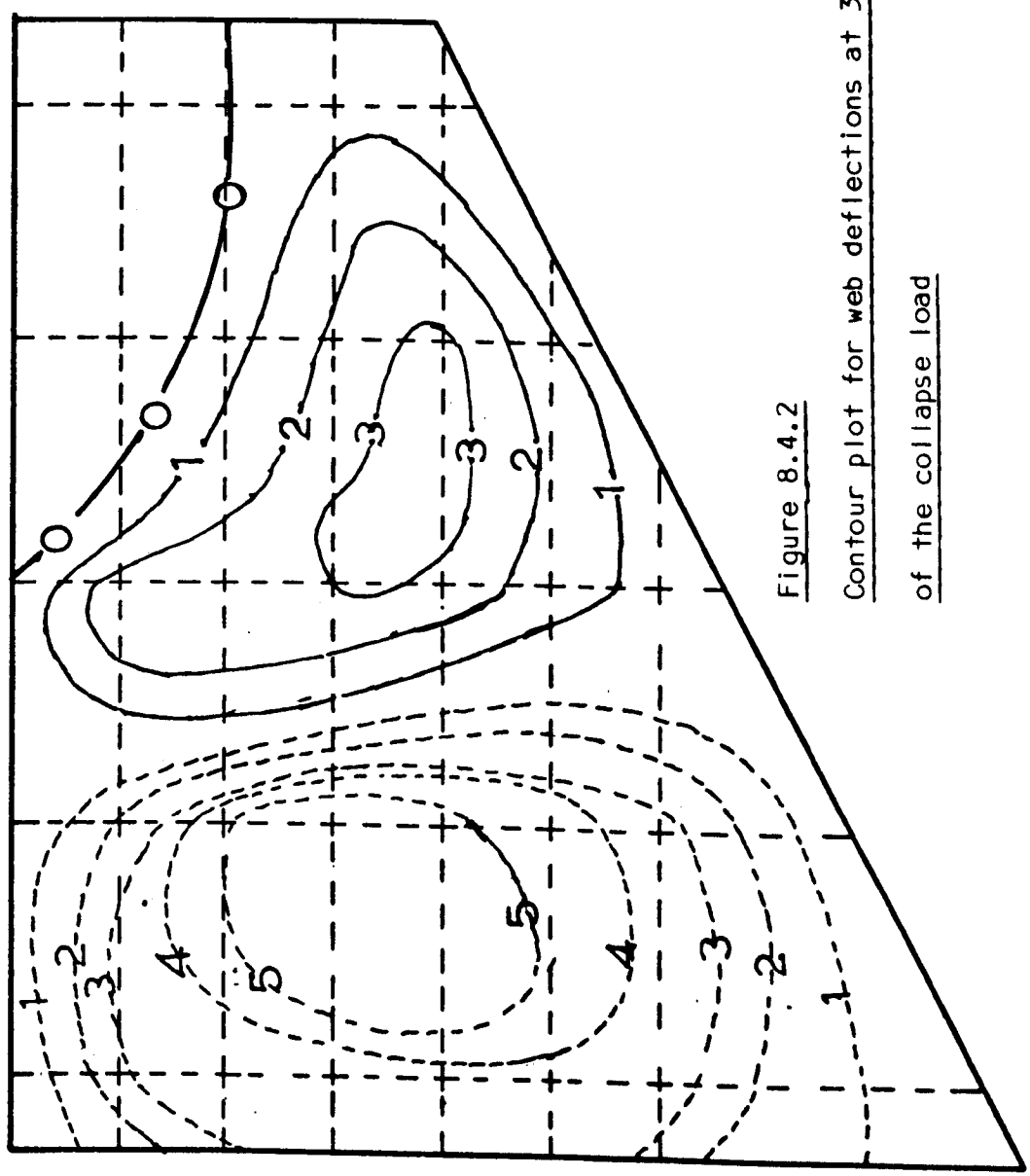

Figure 8.4.2

Contour plot for web deflections at 30% of the collapse load

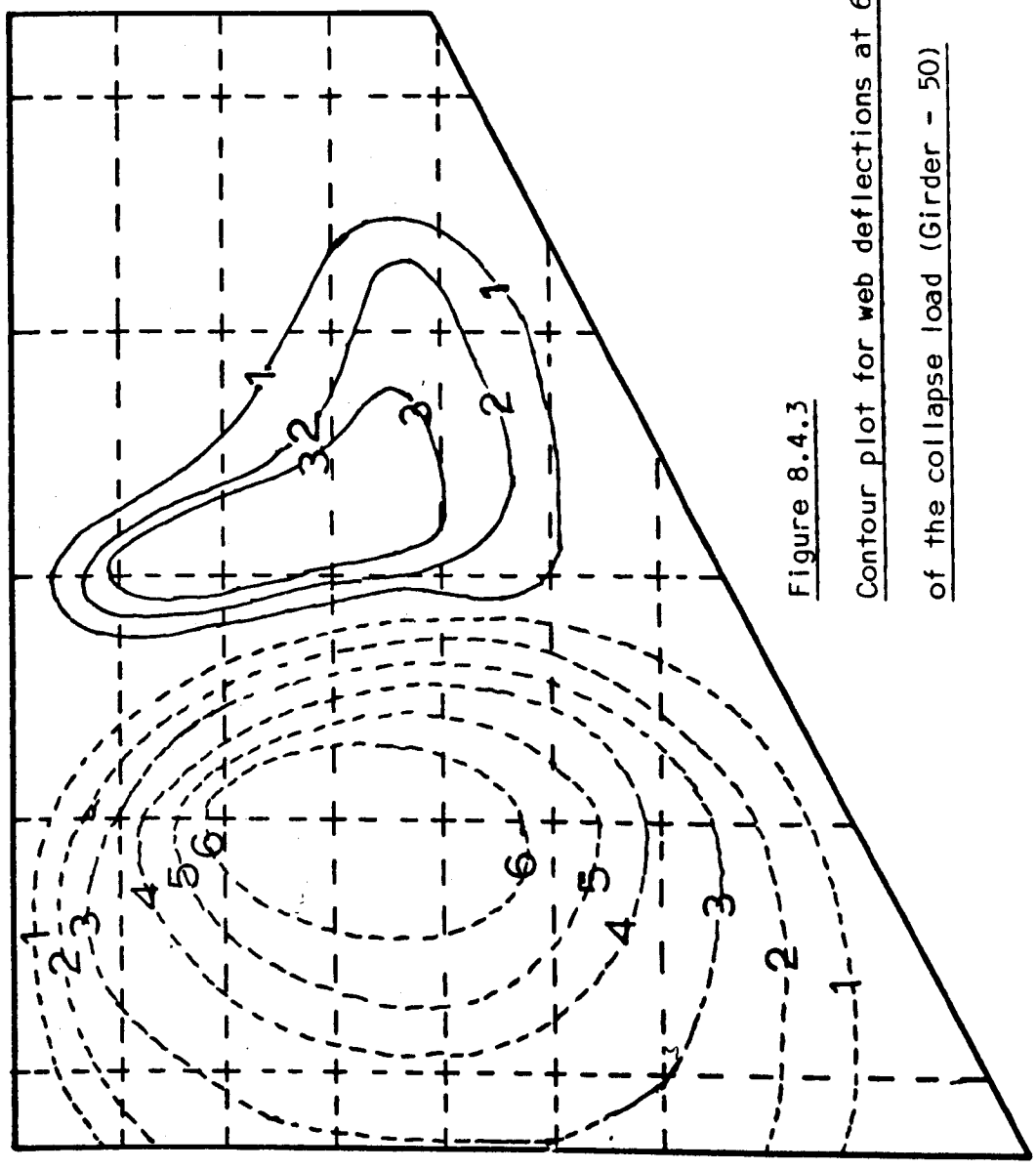

Figure 8.4.3

Contour plot for web deflections at 60% of the collapse load (Girder - 50)

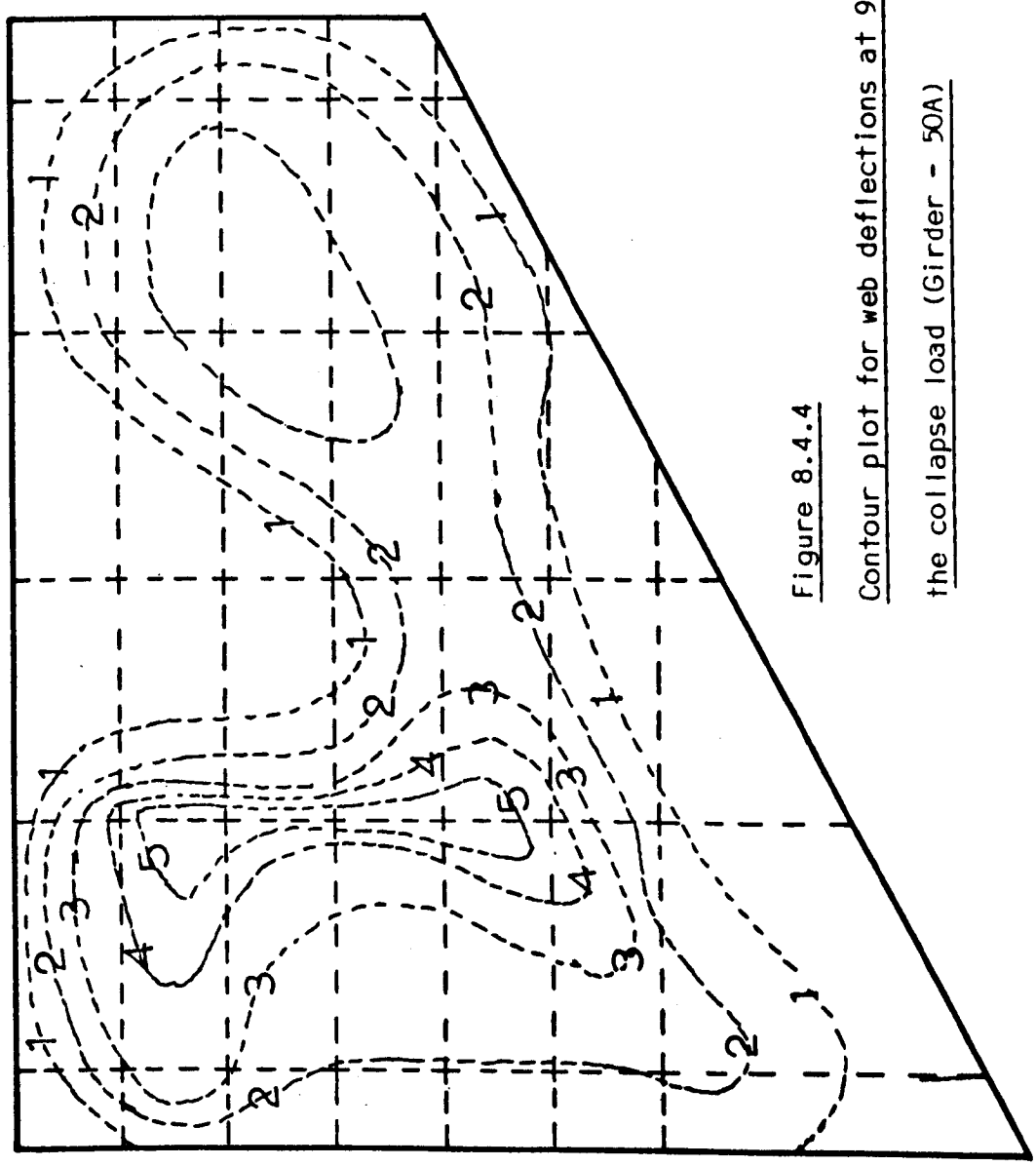

Figure 8.4.4

Contour plot for web deflections at 91% of the collapse load (Girder - 50A)

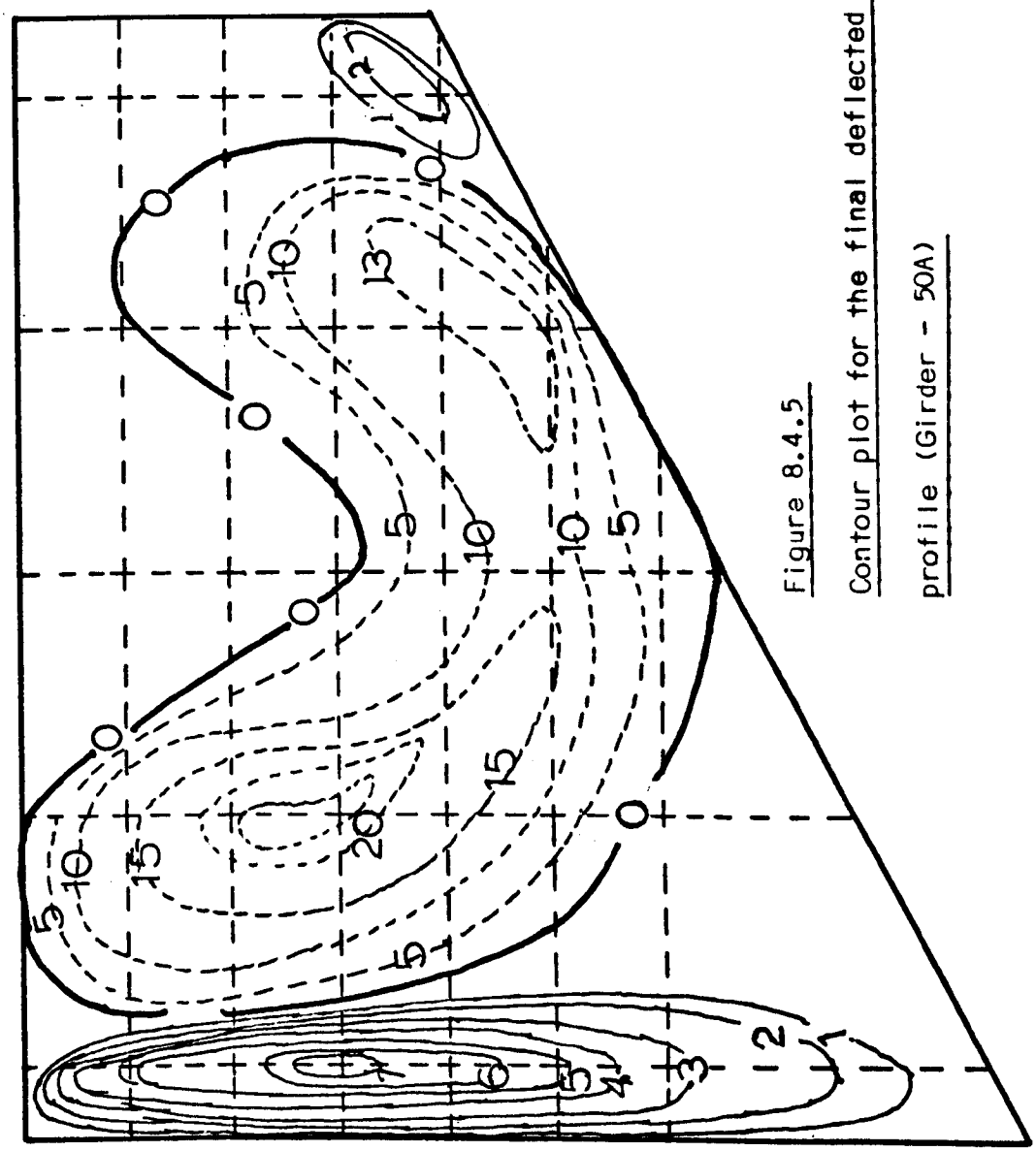

Figure 8.4.5

Contour plot for the final deflected web profile (Girder - 50A)

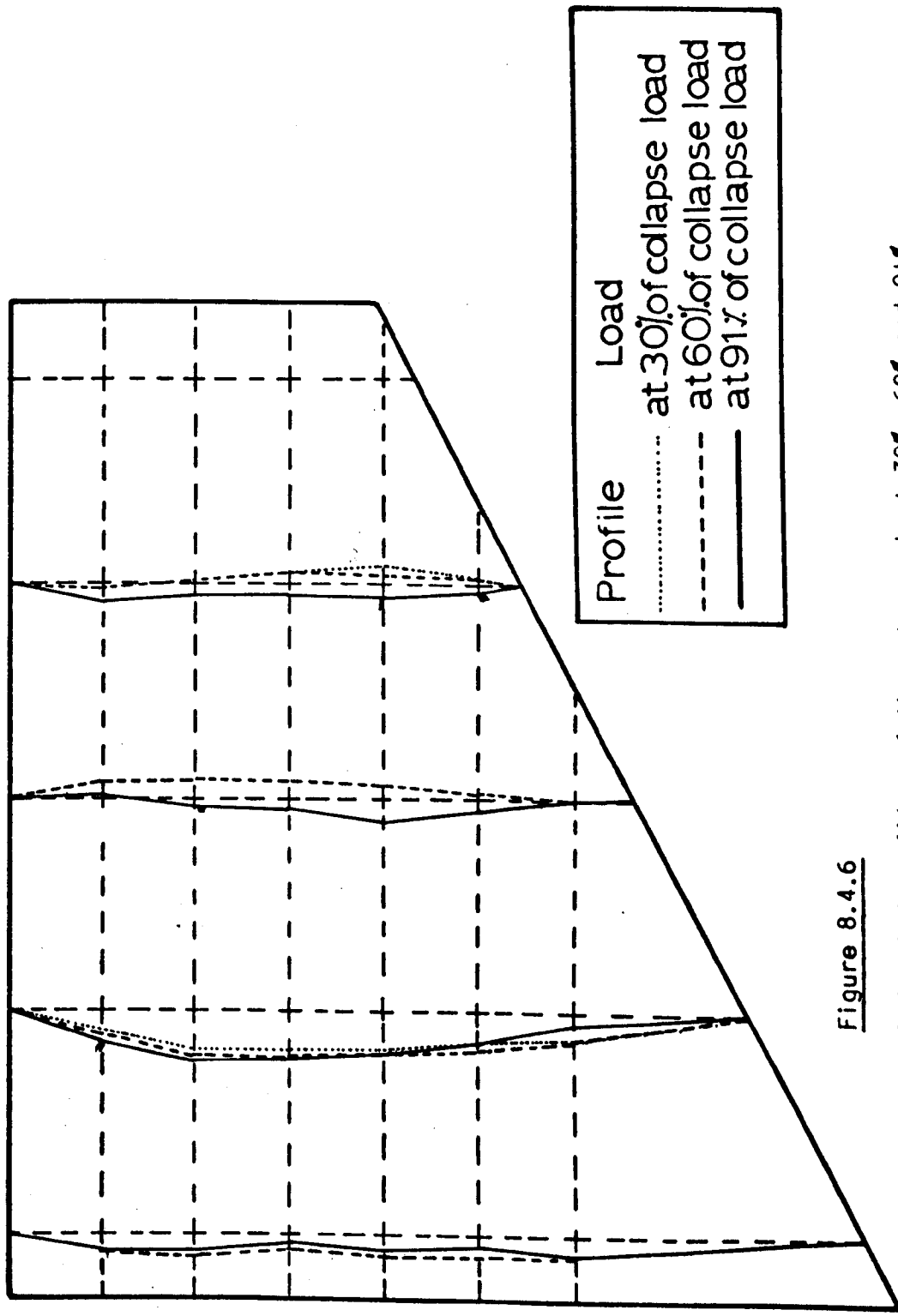

Figure 8.4.6

Deflected profiles of the web panel at 30%, 60% and 91% of the collapse load (Girder 50A)

Panel load in (KN)	Average strain in the tension flange (micro strain)	Corresponding stress from the tension test (N/mm^2)	Axial tension (Stress x Area) (KN)	Theoretical Axial force (KN)
50	459	94	96	101
75	742	145	148	151
100	1030	200	204	202
124	1336	250	255	250
147	1800	328	335	297
159	2592	344	351	321

Table 8.4.2

Panel load (KN)	Average strain in the comp. (micro strain)	Corresponding stress from the tension test (N/mm^2)	Axial compression (KN)	Theoretical axial comp. (KN)
50	471	96	98	113
75	733	140	143	169
100	1104	210	214	225
124	1587	300	306	279
147	4038	352	359	331
159	5397	355	362	358

Table 8.4.3

The experimental values of the axial forces in the tension and compression flanges are plotted against their theoretical values in Figure 8.4.7.

8.4.4 Deflected profiles of the tension and compression flanges

The techniques for the measurements of the profiles of the tension and compression flanges are explained in section 8.2.4. A set of readings for the final profiles of the tension and compression flange is presented in Tables 8.4.4 and 8.4.5 respectively. The deflected profiles of the tension and compression flanges were plotted from these readings and are shown in Figure 8.4.8.

It can be observed from Figure 8.4.8 that there are three plastic hinges in the compression flange and one plastic hinge in the tension flange. It is also clear from Figure 8.4.8 that due to three hinge rotation of the compression flange, the wedge 'WX-ZP' has large rotation in the direction of the load, giving a large vertical deflection of the tip 'T'.

8.4.5 Central Load - Deflection of the Tapered Beam Specimen

The central deflection was recorded with respect to the central load on an X-Y plotter as explained previously. The plotted curve is shown in Figure 8.4.9. It can be seen from the figure that the beam has failed giving large central deflections.

8.4.6 Comparison of the Collapsed Panel with the Proposed Theoretical Collapse Mechanism

The photograph (plate8) and the plotted profile (Figure 8.4.8) of the collapsed panel show clearly that there are

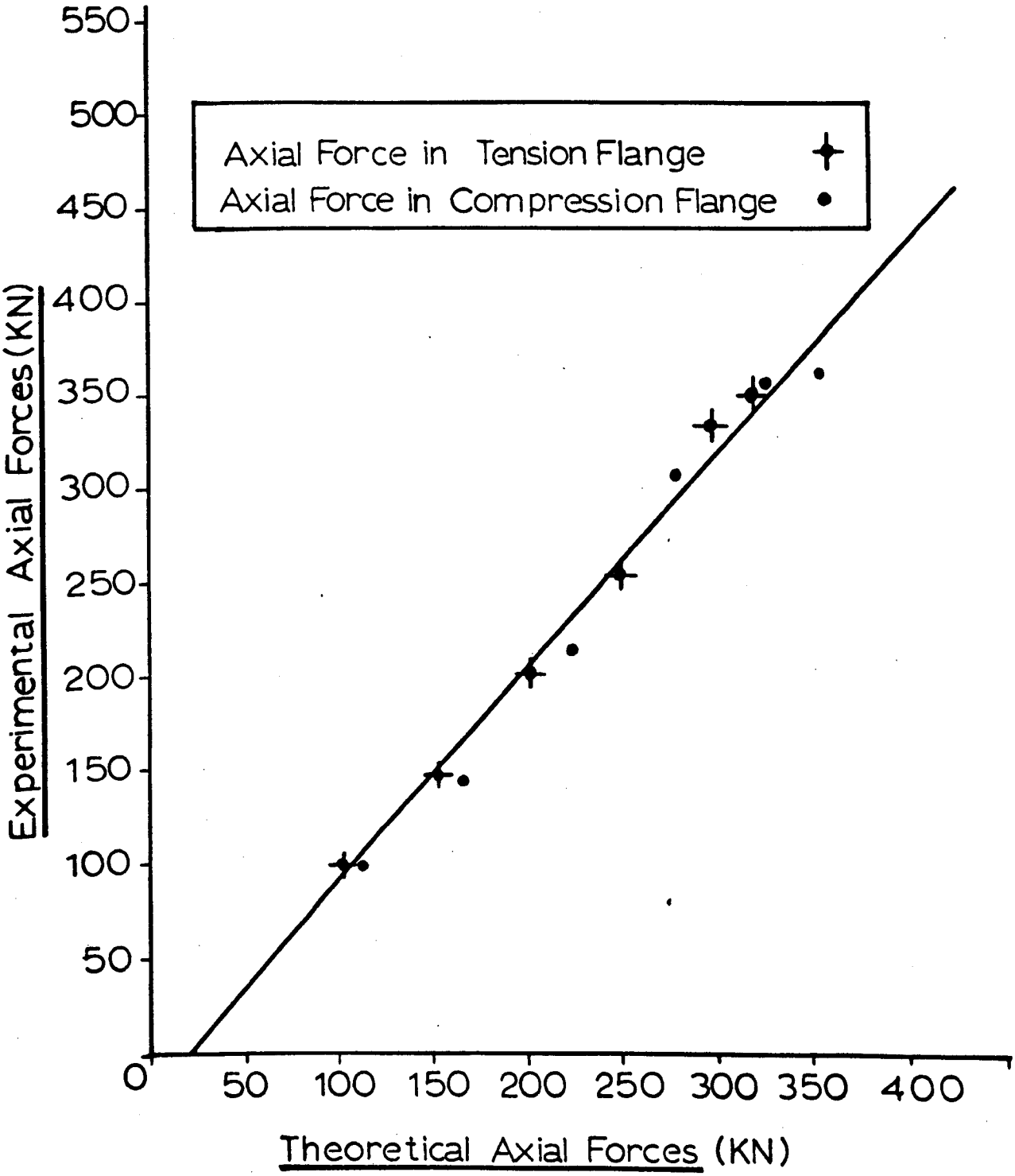
Axial Force in Tension Flange
Axial Force in Compression Flange
Experimental Axial Forces (KN)
Theoretical Axial Forces (KN)
0
50
100
150
200
250
300
350
400
450
500
550

Figure 8·4·7

Distance from ℄ of the central stiffner (mm)	Final profile of the tension flange (mm)	Distance from ℄ of the central stiffner (mm)	Final profile of the tension flange (mm)
0	0.00	700	28.61
50	0.40	850	37.40
100	1.11	950	43.19
200	3.77	1050	48.91
300	7.68	1150	54.75
400	11.96	1250	60.76
500	16.96	1450	82.84
600	23.01	1550	88.76
650	26.12	1650	94.24

Table 8.4.4 Final Profile of the tension flange

Distance X_t (figure 8.2.9) (mm)	Deflections (δ) (mm)	Distance (X_t) (in mm)	Deflections (mm)
50	1.50	500	34.00
100	4.00	550	28.00
150	6.50	600	20.50
200	7.50	650	11.50
250	8.50	700	5.50
300	12.00	750	0.00
350	18.50	800	0.00
400	27.00	850	0.00
450	34.00	900	0.00

Table 8.4.5 Final profile of the compression flange

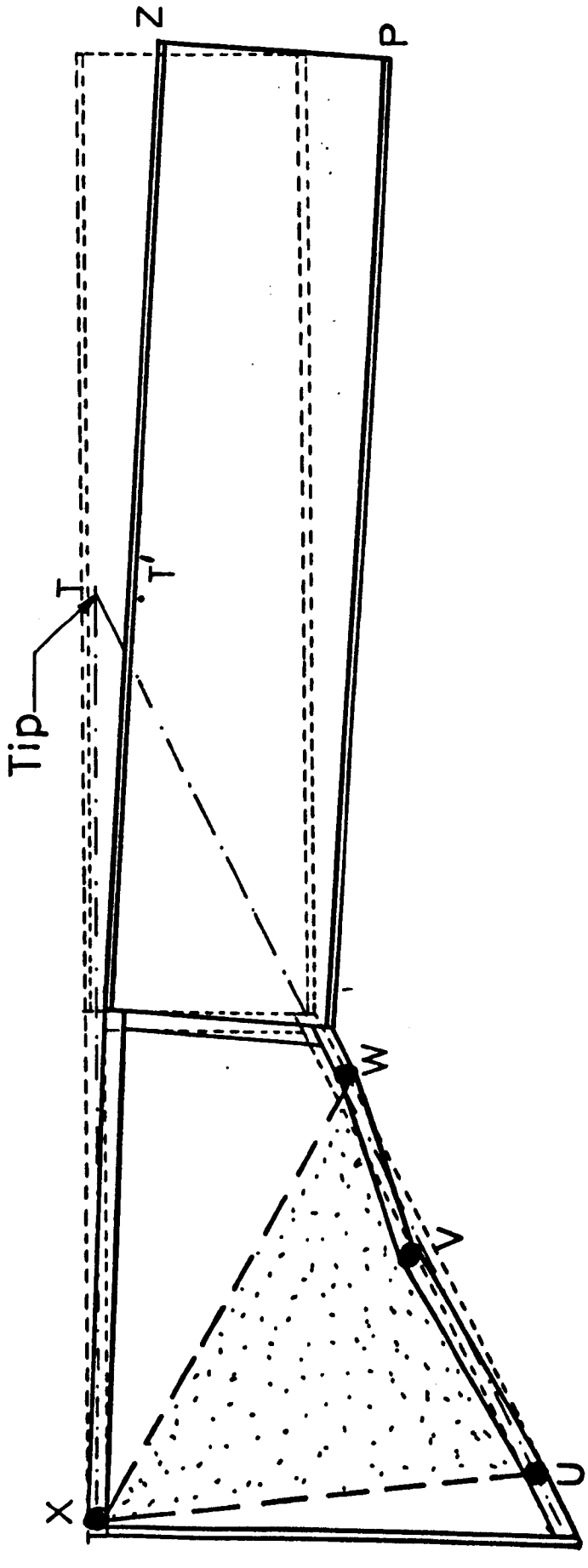

Figure 8.4.8

PLOTTED PROFILE OF THE COLLAPSED PANEL (BEAM LOADED AT THE TIP)

CENTRAL LOAD - DEFLECTION CURVE

OBTAINED FROM THE X-Y PLOTTER

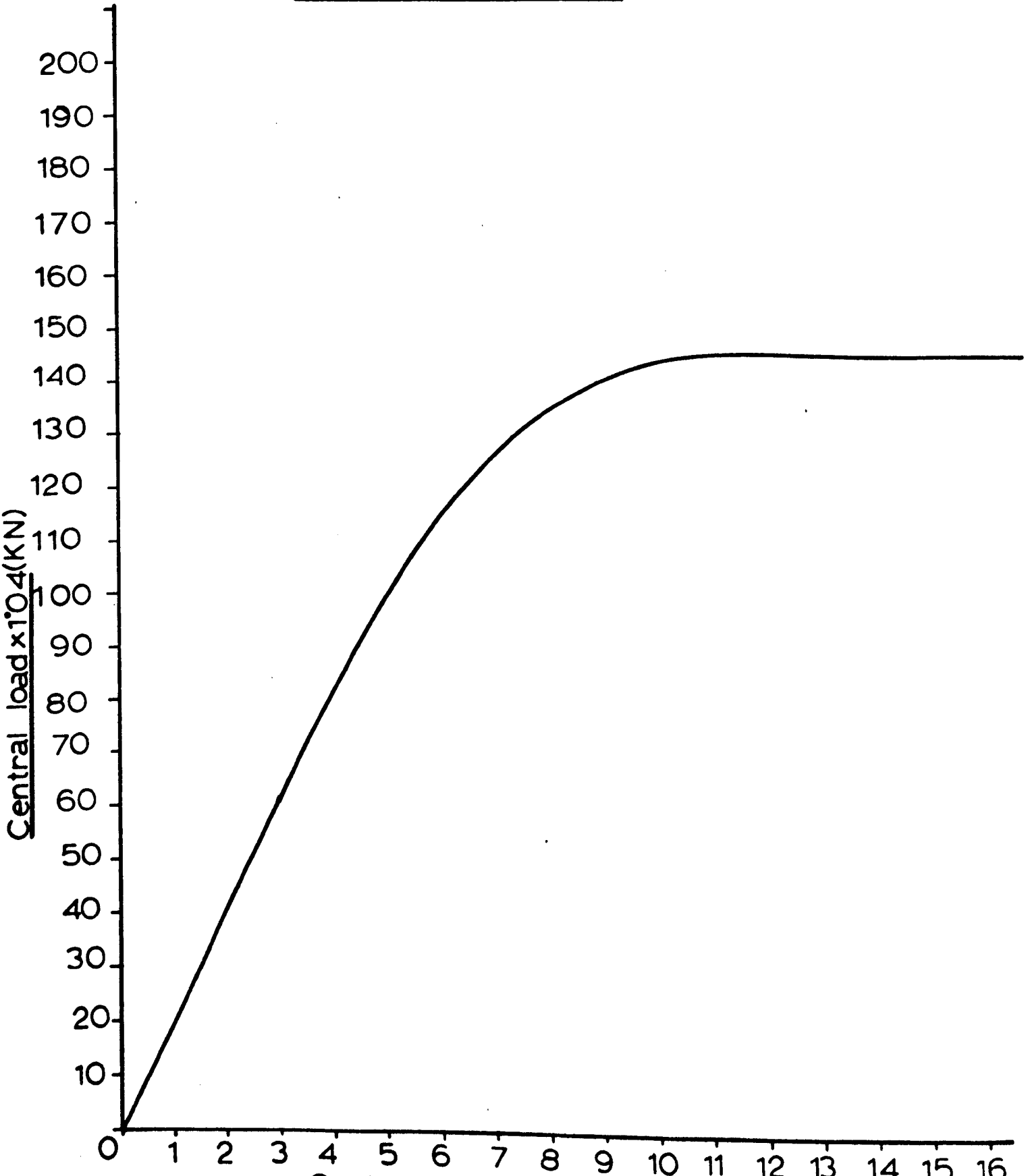

Figure 8.4.9

Plate 8


GIRDER-50
t = 36 mm
Collapse load = 155 kN

three plastic hinges in the compression flange and one plastic hinge in the tension flange.

Although a very limited number of experiments was carried out to examine the collapse mode of failure of tapered beams loaded at the tip, it is clear that the beam specimen fails with the overall plastic yield and three hinge rotations of the compression flange and one hinge rotation of the tension flange as assumed in the theoretical collapse mechanism. It is also clear from Figure 8.4.8 that the wedge 'WXT' rotates in the direction of load giving a large tip deflection which varifies the assumption made in the theoretical collapse mechanism.

The three hinge rotations of the compression flange caused the flange to bend inward, which produced a large 'out-of-plane' deflection of the web causing a large diagonal band. However, as mentioned in Chapter Seven also, there was no sign of the presence of tensile membrane stresses in the web.

The comparison between the experimental and the theoretical collapse loads of all the tapered beam specimens loaded at the tip is presented in Table 8.4.6. The experimental collapse loads are within 1% of the predicted collapse loads.

Girder No.	Axial force in tension flange (KN)	Axial force in compression flange (KN)	Theoretical collapse load (Predicted) (KN)	Experimental collapse load (KN)	Theoretical collapse load (Predicted) / Experimental collapse load
40(B) Loaded at outer tip	333	372	165	167	0.99
50(A) Loaded at central tip	326	364	162	164	0.99
50(B) Loaded at inner tip	326	364	162	164	0.99

Table 8.4.6

Girder No.	d_1 (mm)	d_2 (mm)	b (mm)	t (mm)	σ_{yw} (N/mm^2)	σ_{yf} (N/mm^2)	τ_{cr} (N/mm^2)	Z_p (mm^3)
40(B)	315	685	750	1.7	239	324	16	14236
50(A)	315	685	750	1.7	232	317	16	14236
50(B)	315	685	750	1.7	232	317	16	14236

Table 8.4.7

8.4.7 General Conclusions

On the basis of the analyses of the results, the following conclusions can be drawn about the collapse behaviour of tapered steel beams loaded at the tip:

(i) The collapse of the beam specimen occurs when the compression flange yields and the beam fails with three hinge rotations of the compression flange and one hinge rotation of the tension flange. This verifies the proposed theoretical collapse mechanism.

(ii) The experimental collapse loads of the beams are within 1% of the predicted theoretical collapse loads.

(iii) The three hinge rotations of the compression flange cause the flange to bend inward (Figure 8.4.8), and this produces large 'out-of-plane' deflections of the web. Hence the diagonal band becomes large.

(iv) No tensile membrane stresses form in the web.

CHAPTER NINE

SUMMARY OF CONCLUSIONS AND SUGGESTIONS FOR FUTURE RESEARCH

9.1 Summary of Conclusions

9.1.1 Tapered Beams Loaded Inside the Tip

(I) Although the estimates of buckling load of tapered web plates based on an equivalent rectangular web (Figure 4.2.1(a)) are likely to be inaccurate, this assumption can be made as the buckling loads of the panels (studied in this thesis) are significantly lower than the corresponding plastic collapse loads of beams. However, the buckling load may be significant for various d/t (depth/thickness) ratios (other than those studied in this thesis) and therefore accurate predictions are necessary.

(II) The collapse mechanism of tapered steel beams loaded inside the tip consists of two plastic hinges in the tension flange and two plastic hinges in the compression flange (Figure 4.4.1). The collapse occurs when the plastic hinges form in the flanges which together with the yield zone 'UVWX' (Figure 8.2.10) forms a pistic collapse mechanism.

(III) The pattern of cracks in the stress coat (Plumber's resin) and the plotted profiles of the web panel, in the post buckled range, confirm that the tensile membrane stresses develop diagonally depending upon the direction of the 'tip-moment'.

In this case, when the beams are loaded inside the tip, the direction of the 'tip-moment' is anticlockwise and the membrane stresses develop along the short diagonal of the tapered web panel.

(iv) The collapse mechanism (Figure 4.4.1) provides identical collapse loads (for any value of the inclination of the tensile membrane stresses) from upper and lower bound solutions.

(v) At the plastic collapse of the girder, the web between the two inclined boundaries 'U-V' and 'W-X' (Figure 8.2.10), joining the plastic hinges in the tension and the compression flanges yields completely and the wedge 'WXYZ' (Figure 8.2.10) rotates in the direction of the 'tip-moment' (anticlockwise) about the tip such that the vertical deflection of the tip is zero.

(vi) As the eccentricity of the load about the tip decreases, the ultimate load (with full plastic moment capacity of flanges) increases significantly (Figure 4.7.2).

(vii) The axial forces in the flanges of tapered beams are quite large, especially in the inclined compression flange. These axial forces in the tension and compression flanges, reduce the plastic moment capacities of flanges, and have a significant effect on the collapse load. Therefore, while calculating the collapse load of tapered beams loaded inside the tip, it is essential to consider the reduced plastic moment capacity of flanges due to the presence of axial forces in the flanges.

(viii) Yielding of the flange material beyond the portion between the plastic hinges could occur because, when the plastic hinges form in the flanges, the plastic moment extends throughout the flange (Figures 4.4.4(b) and 4.4.4(c)).

(ix) The experimental collapse loads of tapered beams loaded inside the tip give good agreement with the theoretically predicted collapse loads (calculated by considering the reduced plastic moment capacity of the flanges).

(x) The inclinations of the tensile membrane stress field indicated by the plotted contour lines of the 'out-of-plane' deflections of the web are in good agreement with the theoretical predictions.

9.1.2 Tapered Beams Loaded Outside the Tip

(i) As the buckling load of the web panel (studied in this thesis) is significantly lower than the plastic collapse load of the panel, to predict the buckling load for the plastic collapse load of the tapered panel, an equivalent rectangular panel of the same width and an average depth (Figure 5.2.1(a)) can be considered.

(ii) The collapse mechanism of tapered steel beams loaded outside the tip consists of two plastic hinges in the tension flange and two plastic hinges in the compression flange (Figure 5.4.1). The collapse occurs when the plastic hinges form in the flanges which together with the yield zone 'UVWX' (Figure 8.3.7) forms a plastic collapse mechanism.

(iii) The direction of the 'tip-moment' for this case (beams loaded outside the tip) is opposite to the direction of the 'tip-moment' when the beam was loaded inside the tip, and because of this change in direction of the tip-moment, the tension and compression diagonals interchange.

The crack-patterns in the stress coat and the plotted profiles of the web panel, in the post buckled range, confirm that the tensile membrane stresses develop along the log diagonal of the tapered web panel.

(iv) The collapse mechanism (Figure 5.4.1) provides identical collapse loads (for any value of the inclination of the tensile membrane stresses) whether obtained from upper or lower bound

solutions.

(v) At the plastic collapse of the girders, the web between the two inclined boundaries ('U-V' and 'W-X' (Figure 8.3.7)), joining the plastic hinges in the tension and compression flanges yields completely, and the wedge 'WXYZ' rotates clockwise (in the direction of the 'tip-moment') about the tip such that the vertical deflection of the tip is zero.

(vi) As the eccentricity of load about the tip decreases, the ultimate load, with full plastic moment capacity of flanges, increases significantly (Figure 5.7.2).

(vii) The axial forces in the tension and compression flanges which reduces the plastic moment capacity of the flanges have a significant effect on the ultimate load of tapered beams loaded outside the tip and therefore it is necessary to consider the reduced values of the plastic moment capacity of the flanges while calculating the collapse load of the beam.

(viii) At the stage when the plastic hinges form in the flanges, the yielding of the flange can extend all along its length (Figures 5.4.3(b) and 5.4.3(c)).

(ix) The experimental collapse loads of tapered beams loaded outside the tip give good agreement with the predicted theoretical collapse loads calculated by considering the reduced plastic moment capacity of the flanges.

(x) The inclinations of the tensile membrane stresses measured from the plotted contour lines of the 'out-of-plane' deflections of the web panels are in good agreement with the theoretical predictions.

9.1.3 Tapered Beams Loaded at the Tip

(i) For the tapered beams loaded at the tip, the shear stresses in the webs are approximately zero because the 'tip-moment' is zero.

(ii) Tensile membrane stresses in the web panel do not form.

(iii) The collapse mechanism of tapered steel beams loaded at the tip consists of one plastic hinge in the tension flange and three plastic hinges in the compression flange (Figure 8.4.8). The collapse occurs when the compression flange yields and the beam fails with three hinge rotations of the compression flange and one hinge rotation of the tension flange.

(iv) Because the three hinge rotations of the compression flange causes the flange to bend inward (Figure 8.4.8) which produces large 'out-of-plane' deflections of the web giving a large diagonal band.

(v) Because the shear stress in the web is zero and the tensile membrane stresses do not form in the web, the webs of tapered beams loaded at the tip do not play any significant role in carrying the load.

(vi) The experimental collapse loads of the tapered steel beams loaded at the tip are within one per cent of the predicted theoretical collapse loads which are based on the yield of the compression flange.

(vii) The collapse loads and the mode of failure of tapered beams loaded near the inner, central and outer tips are identical.

9.2 Suggestions for Future Research

1. Further investiation to extend the validity of the proposed collapse mechanisms for its suitability for inclusion in the relevant code of practice for the ultimate load design of tapered

steel beams.

2. Investigations to provide a more accurate method assessing the buckling load of the tapered web panel.

3. Investiation into the collapse load behaviour of tapered steel beams with a soffit of large radius of curvature in relation to its depth.

4. Investigation into the collapse load behaviour of tapered steel beams having

   (a) Transversely reinforced webs, and

   (b) Longitudinally reinforced webs.

5. Investigation into the lateral instabilities of tapered web panel for various depth/thickness ratios.

6. Investigation to choose the appropriate slope of the inclined compression flange which may provide the least lateral instability and also minimise the yielding caused by large axial forces in the flanges.

REFERENCES

1. Lee, G.C., Morrell, M.L. and Ketter, R.L., "Design of Tapered Members", Welding Research Council Bulletin, No. 173, June 1972.

2. Lee, G.C. and Morrell, M.L., "Application of AISC Design Provisions for Tapered Members", Engineering Journal, American Institute of Steel Construction, vol. 12, No. 1, 1st Quarter, 1975, pp. 1-13.

3. Morrell, M.L. and Lee, G.C. "Allowable Stress for Web-Tapered Beams with Lateral Restraints", Welding Research Council Bulletin, No. 192, February 1974, pp. 1-12.

4. Chong, K.P., Swanson, W.D. and Matlock, R.B., "Shear Analysis of Tapered Beams", Journal of the Structural Division, Proc. of the A.S.C.E., ST9, September 1976, pp. 1781-1788.

5. Kitipornchai, S. and Trahair, N.S., "Elastic Stability of Tapered I-Beams" Journal of the Structural Division, Proc. of the A.S.C.E., ST3, March 1972, pp. 713-728.

6. Davies, G., Lamb, R.S. and Snell, C. "Stress Distribution in Beams of Varying Depth", The Structural Engineer, No. 11, vol. 51, November 1973, pp. 421-434.

7. Butler, D.J. and Anderson, G.B., "The Elastic Buckling of Tapered Beam-columns", Welding Journal, vo. 42, No. 1, January 1963, p. 29.

8. Krefeld, W.J., Butler, D.J. and Anderson, G.B., "Welded Cantilever Wedge Beams", Welding Journal, vol. 38, No. 3, 1959, p. 97.

9. Prawel, S.P.Jr., Morrell, M.L. and Lee, G.C., "Bending and Buckling Strength of Tapered Members", Welding Research Journal Suppl., February 1974.

10. Wilson, J.M. "On Specifications for Strength of Iron Bridges", Trans. A.S.C.E., vol. 15, Part I, 1886, pp. 401-403.

11. Wagner, H., "Flat Sheet Metal Girder with Very Thin Metal Web", N.A.C.A. Tech. Memo. Nos. 604, 605 and 606, (1931).

12. Basler, K. and Thurlimann, M., "Strength of Plate Girders in Bending", Journal of the Structural Division, Proc. of the A.S.C.E., ST6, August 1961, vol. 87, pp. 153-181.

13. Basler, K., "Strength of Plate Girders in Shear", Journal of the Structural Division, Proc. of the A.S.C.E., ST7, October 1961, pp. 151-180.

14. Basler, K., "Strength of Plate Girders under Combined Bending and Shear", Journal of the Structural Division, Proc. of the A.S.C.E., ST7, October 1961, pp. 181-197.

15. Gaylord, E.H., "Discussions on Shear Strength of Plate Girders", Journal of the Structural Division, Proc. of the A.S.C.E., ST2, vol. 88, 1962, p. 151.

16. Fujii, T., "On an Improved Theory for Dr. Basler's Theory", Proc. 8th Congress, IABSE, New York, September 1968, pp. 477-487.

17. Rockey, K.C. and Skaloud, M., "Influence of Flange Stiffness upon the Load Carrying Capacity of Webs in Shear", Proc. 8th Congress IABSE, New York, September 1968, pp. 429-439.

18. Rockey, K.C., "Factors Influencing Ultimate Behaviour of Plate Girders", BCSA, Conference on Steel Bridges, London, June 1968, pp. 31-38.

19. Owen, D.R.J., Rockey, K.C., Skaloud, M., "Ultimate Load Behaviour of Longitudinally Reinforced Web Plate Subjected to Pure Bending", IABSE 1970, pp. 113-148.

20. Rockey, K.C., "Aluminium Plate Girders", Paper presented at the Symposium, Aluminium in Structural Engineering, held by Institution of Structural Engineers, June 1963, published in the Proceedings of Symposium, June 1964, p. 80-98.

21. Rockey, K.C. and Skaloud, M., "Ultimate Behaviour of Plate Girders Loaded in Shear", Structural Engineer, January 1972, No. 1, vol. 50.

22. Rockey, K.C. and Skaloud, M., "The Ultimate Load Behaviour of Plate Girders Loaded in Shear", Proc. IABSE Colloquium, Design of Plate and Box Girders for Ultimate Strength, London 1971, p. 1-19.

23. Ostapenko, A. and Chern, C., Ultimate Strength of Longitudinally Stiffened Plate Girders under Combined Loads", Proc. IABSE Colloquium, Design of Plate and Box Girders for Ultimate Strength, London 1971, p. 301-313.

24. Komatsu, S., "Ultimate Strength of Stiffened Plate Girders Subjected to Shear", Proc. IABSE Colloquium, Design of Plate and Box Girders, London 1971, p. 49-65.

25. Calladine, C.R., "A Plastic Theory for Collapse of Plate

Girders under Combined Shearing Force and Bending Moment", The Structural Engineer, April 1973, No. 4, vol. 51.

26. Porter, D.M., Rockey, K.C. and Evans, H.R., "The Collapse Behaviour of Plate Girders Loaded in Shear", The Structural Engineer, August 1975, No. 8, vol. 53, pp. 313-325.

27. Rockey, K.C., Evans, H.R. and Porter, D.M., "A Design Method for Predicting the Collapse Behaviour of Plate Girders", Proceedings, The Institute of Civil Engineers, Part 2, vol. 65, March 1978, pp. 85-112.

28. Basler, K., Yen, B., Mueller, J.A. and Thurlimann, B., "Web Buckling Tests on Welded Plate Girders", Welding Research Council Bulletin Series, September 1960.

29. Massonnet, C.H., "Stability Consideration in the Design of Plate Girders", Journal of the Structural Division, Proc. of A.S.C.E., vol. 86, January 1960, pp. 71-97.

30. Cooper, P.B., "Bending and Shear Strength of Longitudinally Stiffened Plate Girders", Fitz Engineering Lab. Report, No. 304.6, Lehigh University, September 1965, p. 140.

31. Fujii, T., "A Comparison between the Theoretical and Experimental Results for the Ultimate Shear Strength of Plate Girders", Proc. Colloquium on Design of Plate and Box Girders for Ultimate Strength, I.A.B.S.E., London, 1971, pp. 161-171.

32. Furguson, P.M., "Recent Trends in Ultimate Strength Design", Journal of the Structural Division, Proc. of the A.S.C.E., ST1, January 1961, pp. 57-71.

33. Heyman, J., "Plastic Design of Frames", vol. 1, The University Press, Cambridge.

34. Heyman, J., "Plastic Design of Frames", vol. 2, The University Press, Cambridge.

35. Guyon, Y., "Beams of Variable Depth", Pre-Stress Concrete Contractors Record and Municipal Engineering, London, 1953, pp. 367-375.

36. Timoshenko, S. and Goodier, J.N., "Theory of Elasticity", McGraw-Hill Book Co. Inc. New York, NY 1951, pp. 96-99.

37. Beach, H.T., "A Theory for Spacing Stiffeners in Plate Girders", Engineering News, vol. 39, No. 20, May 1898, p. 322.

38. Wilson, J.M., "Spacing Stiffeners in Plate Girders", Engineering News, vol. 40, No. 6, August 1898, p. 69.

39. Turneaure, F.E., "Tests of the Stress in Plate Girder Stiffeners", Engineering News, vol. 40, No. 12, September 1898, p. 186.

40. Turner, C.A.P. and Shinner, F.G., "Spacing Stiffeners in Plate Girders", Engineering News, vol. 40, No. 25, December 1898, p. 399.

41. Beach, H.T., "Spacing Stiffeners in Plate Girders", Engineering News, vol. 41, No. 7, February 1899, p. 106.

42. Rode, H.H., "Beitrag Zur Theorie der Knickerscheinungen", Wilhelm Engelmann Verlag, Leipzig, 1916 (Dissertation), and Eisenbau, vol. 7, 1916, p. 121, 157, 210, 239 and 296.

43. Rockey, K.C., "The Influence of Flange Stiffness upon the Post-Buckled Behaviour of Web Plates Subjected to Shear", Engineering, 20 December 1957, p. 788.

44. Rockey, K.C. and Jenkins, F., "Behaviour of Webplates of Plate Girders Subjected to Pure Bending", The Structural Engineer, May 1957, pp. 176-188.

45. Rockey, K.C., "Web Buckling and the Design of Webplates", The Structural Engineer, February 1958, pp. 45-60.

46. Fujii, T., Fukumoto, Y., Nishino, F. and Okumura, T., "Research Works on Ultimate Strength of Plate Girders and Japanese Provisions on Plate Girder Design", Proc. IABSE Colloquium, Design of Plate and Box Girders for Ultimate Strength, London 1971, p. 21-40.

47. Chern, C. and Ostapenko, A., "Ultimate Strength of Plate Girders under Shear", Fritz Engineering Laboratory Report No. 328.7, Lehigh University, U.S.A., August 1969.

48. Cook, I.T. and Rockey, K.C., "Shear Buckling of Rectangular Plates with Mixed Boundary Conditions", Aeronautical Quarterly, vol. 14, November 1963, pp. 349-356.

49. El-Gaaly, M.A., "Buckling of Tapered Plates Under Pure Shear", Proc. Conf. Steel Structures, Timisora, Romania, October 1973.

50. Rockey, K.C., Evans, H.R. and Porter, D.M., "Ultimate Load Capacity of Stiffened Webs Subjected to Shear and Bending", International Conference on Steel Box Girder Bridges organised by the Institute of Civil Engineers, February 1973.

51. Porter, D.M., Rockey, K.C., "The Collapse Behaviour of Plate Girders Loaded in Shear", University College, Cardiff, Report No. PRE/1/1.

52. Evans, H.R., Porter, D.M. and Rockey, K.C., "The Collapse Behaviour of Plate Girders Subjected to Shear and Bending", University College, Cardiff, Report.

53. Rockey, K.C., Evans, H.R. and Porter, D.M., "A Design Method for Predicting the Collapse Behaviour of Plate Girders", University College, Cardiff, Report.

54. Bergman, S.G.A., "Behaviour of Buckled Rectangular Plates under the action of Shearing Forces", Stockholm, 1948.

55. Skaloud, M., "Ultimate Load and Failure Mechanism of Thin Webs in Shear", Proc. IABSE Colloquium, Design of Plate and Box Girders for Ultimate Strength, London 1971, pp. 115-129.

56. Torsten Hoglund, "Simply Supported Long Thin Plate I-Girder without Web Stiffeners Subjected to Distributed Transverse Load", Proc. IABSE Colloquium, Design of Plate and Box Girders for Ultimate Strength, London, 1971, p. 85-97.

57. Rockey, K.C., "An Ultimate Load Method for the Design of Plate Girders", Proc. IABSE Colloquium, Design of Plate and Box Girders, London, 1971, p. 253-268.

58. Evans, H.R., Porter, D.M. and Rockey, K.C., "Ultimate Load Behaviour of Plate and Box Girder Webs", International Conference on Steel Plated Structures, Session 3, Paper 14.

59. Rockey, K.C., "The Design of Web Plates for Plate and Box Girders - A State of Art Report", Session 4, Paper 19.

60. Rockey, K.C. and Valtinat, G., "Design and Calculation of Vertical Stiffeners in Plate Girders", unpublished paper.

61. Lee, G.C. and Szabo, B.A., "Torsional Response of Tapered I-Girders", Journal of the Structural Division, Proc. of the A.S.C.E., ST5, October 1967, pp. 233-252.

62. Pratap, G. and Vardan, T.K., "Finite Deflection of Tapered Cantilevers", Journal of the Engineering Mechanics Division, A.S.C.E., EM3, pp. 549-552.

63. Johnston, B.G., "Guide to Stability Design Criteria for Metal Structures", Structural Stability Research Council, Third Edition, pp. 152-188.

64. Gaylord, E.H. and Gaylord, C.N., "Design of Steel Structures", McGraw-Hill Book Company.

65. Neal, B.G., "The Plastic Methods of Structural Analysis", Chapman and Hall Limited, London.

66. Wyatt, M.J., "Taper and Shear Lag Effects in Box Structures", Ph.D. Thesis, Department of Civil Engineering, University of Nottingham, May 1975.

67. Lamb, R.S., "Stress Distribution in Tapered Concrete Beams", Ph.D. Thesis, Department of Civil Engineering, University of Nottingham, October 1971.

68. Murray, N.W., "Buckling of Stiffened Panels Loaded Axially and

in Bending", The Structural Engineer, August 1973, No. 8, vol. 51, pp. 285-300.

69. Rockey, K.C., Evans, H.R. and Porter, D.M., "Tests on Longitudinally Reinforced Plate Girders Subjected to Shear", 2nd International Colloquium on Stability of Steel Structures, Preliminary Report, Liege, Belgium, April 1977, pp. 295-304.

70. Rockey, K.C., "An Ultimate Load Method of Design for Plate Girders", Development in Bridge Design and Construction, Edited by K.C. Rockey, J.L. Bannister and H.R. Evans, Crosby Lockwood, 1971, pp. 487-504.

71. Rockey, K.C. and Cook, I.T., "Shear Buckling of Clamped and Simply Supported Infinitely Long Plates Reinforced by Transverse Stiffeners and a Central Longitudinal Stiffener", Aeronautical Quarterly, vol. 13, p. 95, May 1962.

72. Cook, I.T. and Rockey, K.C., "Shear Buckling of Clamped and Simply Supported Infinitely Long Plates Reinforced by Transverse Stiffeners", Aeronautical Quarterly, vol. 13, pp. 41, February 1962.

73. B.S. 18, Part 2, Part 3, and Part 4, 1971, "Methods for Tensile Testing of Metals".

74. Hounsfield Tensometer Instruction Manual, Tensometer Limited, Croydon, Surrey.

75. Horne, M.R., "Plastic Theory of Structures", Thomas Nelson and Sons Limited, London.

76. Rockey, K.C., Porter, D.M. and Evans, H.R., "Ultimate Load Capacity of the Webs of Thin-walled Members", Second Specialty Conference on Cold-Formed Steel Structures, Held in St. Louis, Missouri, October 1973, Current Research and Design Trends, pp. 169-200.

77. Morris, L.J. and Packer, J.A., "Stability of Steel Structures", 2nd International Colloquium on Stability of Steel Structures, Preliminary Report, Liege, Belgium, April 1977, pp. 295-304.

78. Akhtar, S., "Elastic and Elastic-Plastic Stability of Haunched I-Section Beams", Ph.D. Thesis, University of Manchester, Faculty of Science, Department of Civil Engineering, November 1974.

79. Horne, H.R. and Ajmani, J.L., "The Post-Buckling Behaviour of Laterally Restrained Columns", The Structural Engineer, vol. 49, No. 8, August 1971, pp. 346-352.

80. Khan, M.Z. and Walker, A.C., "Buckling of Plates Subjected to Localised Edge Loadings", The Structural Engineer, vol. 50, No. 6, June 1972, pp. 225-232.

81. Ostapenko, A., Chern, C. and Parsanejad, S., "Ultimate Strength Design of Plate Girders", Development in Bridge Design and Construction, Edited by K.C. Rockey, J.L. Bannister and H.R. Evans, Crosby Lockwood, 1971, pp. 505-518.

82. Skaloud, M., "Prepared Discussions in Regard to the Ultimate Load Behaviour of Webs in Shear", Proc. IABSE Colloquium, Design of Plate and Box Girders, London 1971, pp. 173-178.

APPENDIX 1

A1. Listing of Computer Programs for the Calculation of Collapse Loads for Tapered Beams Loaded Inside the Tip

A1.1 Computer Program for Upper and Lower Bound Loads with Full Plastic Moment Capacity of Flanges

```
      MASTER VUL13
      REAL M
  100 READ(5,200)B,M,SI,T,DI,D2,EI,C
  200 FORMAT(8F0.0)
      IF(B.EQ.99.9) CALL EXIT
      WRITE(6,800)
  800 FORMAT(1H,5X,'XI'20X,'CT',20X,'CC',20X,'WLI',20X,'WUI')
      XI=0.20
      DO 400 I=1,35
      XI=XI+0.01
      S=(SQRT(((SI)**2)+C*(((1.5*SIN(2*XI))**2)-3)))-(1.5*C*SIN(2*XI))
      Z=(D2*B)/(D2-DI)
      A=ATAN((D2-DI)/B)
      D4=(DI+D2)/2
      CT=(2/SIN(XI))*(SQRT(M/(S*T)))
      CC=(2/SIN(XI+A))*(SQRT(M/(S*T)))
      SS3=CT*SIN(XI)+CC*SIN(XI+A)+DI*COS(XI)-B*SIN(XI)
      SIS2=DI*COS(XI)-B*SIN(XI)
      VCR=C*T*D4
      FS=(T*S*SS3)
      PI=((Z-CT)*SIN(XI))+(SS3/2)
      QI=2.0*M*((Z/CT)+(DI/(CC*SIN(A))))
      Q2=(Z-CT)*SIN(XI)*SIS2
      Q3=((DI*SIN(XI+A)*SS3)/SIN(A))
      WLI=((FS*PI)/EI)+VCR
      WUI=((QI+(S*T*(Q2+Q3)*0.5))*(1.0/EI))+VCR
      WRITE(6,801)XI,CT,CC,WLI,WUI
  801 FORMAT(1H,6X,FS.2,15X,F8.2,15X,F8.2,15X,F15.3,15X,F15.3
  400 CONTINUE
      WRITE(6,895)
  895 FORMAT(1H1,30X,'**************************************')
      WRITE(6,898)M,B,EI
  898 FORMAT(1H,30X,'M=',F15.2,1X,'B=',F6.2,'EI=',F6.2)
      WRITE(6,900)
  900 FORMAT(1H,30X,'**************************************')
      GO TO 100
      END
```

A1.2 Computer Program for the Collapse Loads with Reduced Plastic Moment Capacity of Flanges

```
      MASTER VULII
      REAL M
  100 READ(5,200)M,SI,T,DI,D2,EI,XI,C,ATF,SYF,B,CI,C2
  200 FORMAT(13F0.0)
      IF(M.EQ.99.9) CALL EXIT
      ACF=ATF
      S=(SQRT(((SI)**2)+C*(((1.5*SIN(2*XI))**2)-3)))-(1.5*C*SIN(2*XI))
      Z=(D2*B)/(D2-DI)
      A=ATAN((D2-DI)/B)
      D4=(DI+D2)/2
      CT=(2/SIN(XI))*(SQRT(M/(S*T)))
      CC=(2/SIN(XI+A))*(SQRT(M/(S*T)))
      SS3=CT*SIN(XI)+CC*SIN(XI+A)+DI*COS(XI)-B*SIN(XI)
      FS=(T*S*SS3)
      VCR=C*T*D4
      PI=((Z-CT)*SIN(XI))+SS3/2)
      AI=S*SIN(XI+A)*COS(XI+A)+2*C*SIN(A)*COS(A)
      A2=S*SIN(XI)*COS(XI)+C
      WLI=((FS*PI)/EI)
      A9=0.00
      GO TO 250
  777 CONTINUE
      WLI=(WLI+ACC)/2.00
      IF(A9.LT.9.0) GO TO 250
      WLI=(WLI+ACC)/2.00
      IF (A9.LE.20.0) GO TO 250
      WLI=(WLI+ACC)/2.00
      WLI=(WLI+ACC)/2.00
      IF(EI.GT.300.0) GO TO 250
      WLI=(WLI+ACC)/2.0
      WLI=(WLI+ACC)/2.0
      WLI=(WLI+ACC)/2.0
  250 FCI=(WLI-(FS*SIN(XI)))/SIN(A)
      IF(FCI.LT.0.00)FCI=0.00
      FTI=FCI*COS(A)-FS*COS(XI)
      IF(FTI.LT.0.00)FTI=0.00
      SCF=(FCI-((AI*CC*T)/2.0))/ACF
      STF=(FTI+((A2*T*CT)/2))/ATF
      X2=SCF/SYF
      IF(X2.LT.0.00)X2=0.00
      IF(X2.GT.1.00)X2=1.00
      RMPC=M*(1.0-((CI*((X2)**2))+C2*X2))
  500 X3=STF/SYF
      IF(X3.LT.0.00)X3=0.00
      IF(X3.GT.1.00)X3=1.00
      RMPT=M*(1.0-((CI*((X3)**2))+C2*X3))
  600 CT=(2/SIN(XI))*(SQRT(RMPT/(S*T)))
      CC=(2/SIN(XI+A))*(SQRT(RMPC/(S*T)))
      SS3=CT*SIN(XI)+CC*SIN(XI+A)+DI*COS(XI)-B*SIN(XI)
      ACC=WLI
      FS=(T*S*SS3)
      PI=((Z-CT)*SIN(XI))+(SS3/2)
      WLI=(((FS*PI)+(RMPT-RMPC))/EI)
```

```
      PDIF=ABS((ACC-WLI)*100.00/ACC)
      A9=A9+1.0
      IF(A9.GT.200) CALL EXIT
      WRITE(6,800)S,SS3,VCR
  800 FORMAT(1H1,10X,'S=',F10.3,10X,'SS3=',F10.3,'VCR=',F10.3)
      WRITE(6,810)FS,FCI,FTI
  810 FORMAT(1H,10X,'FS=',F10.3,10X,'FCI=',F10.3,'FTI=',F10.3)
      WRITE(6,820)X2,SCF,RMPC
  820 FORMAT(1H,10X,'X2=',F5.3,10X,'SCF=',F8.3,10X,'RMPC=',F15.3)
      WRITE(6,830)X3,STF,RMPT
  830 FORMAT(1H, 10X,'X3=', F5.3,10X,'STF=',F8.3,10X,'RMPT=',F15.3)
      WRITE(6,840)CT,CC,EI
  840 FORMAT(1H,10X,'CT=',F10.3,10X,'CC=',F10.3,10X,'EI=',F5.1)
      WRITE(6,850)WLI,ACC,PDIF
  850 FORMAT(1H,10X,'WLI=',F15.3,10X,'ACC=',F15.3,10X,'PDIF=',F7.2)
      WRITE(6,860)A9
  860 FORMAT(1H,10X,'A9='F5.0)
      IF(PDIF-1.0)778,777,777
  778 WLT=WLI+VCR
      WRITE(6,350)
  350 FORMAT(1H1,30X,'*******************************************')
      WRITE(6,880)
  880 FORMAT(1H,1X,'XI',14X,'WLT',10X,'FCI',13X,'SCF',12X,'RMPC',12X,'F
     ITI',12X,'STF',10X,'RMPT')
      WRITE(6,890)XI,WLT,FCI,SCF,RMPC,FTI,STF,RMPT
  890 FORMAT(1H,F4.2,7(3X,F12.2))
      WRITE(6,895)
  895 FORMAT(1H1,30X,'***************************************')
      WRITE(6,898)M,B,EI
  898 FORMAT(1H,30X,'M=',F15.2,1X,'B=',F6.2,'EI=',F6.2)
      WRITE(6,899)Z,A
  899 FORMAT(1H,30X,'Z=',F7.1,5X,'A=',F4.2)
      WRITE(6,900)
  900 FORMAT(1H,30X,'***************************************')
      GO TO 100
      END
```

APPENDIX 2

A2. Listing of Programs for the Calculation of Collapse Loads for Tapered Beams Loaded Outside the Tip

A2.1 Computer Program for Upper and Lower Bound Loads with Full Plastic Moment Capacity of Flanges

```
      MASTER VUL03
      REAL M
  100 READ(5,200)B,M,SI,T,DI,D2,EI,C
  200 FORMAT(8F0.0)
      IF(B.EQ.99.9) CALL EXIT
      WRITE(6,800)
  800 FORMAT(1H,5X,'XI',20X,'CT',20X,'CC',20X,'WLI',20X,'WUI')
      XI=0.64
      DO 400 I=1,35
      XI=XI+0.01
      S=(SQRT(((SI)**2)+C*(((1.5*SIN(2*XI))**2)-3)))-(1.5*C*SIN(2*XI))
      Z=(D2*B)/(D2-DI)
      A=ATAN((D2-DI)/B)
      D4=(DI+D2)/2
      CT=(2/SIN(XI))*(SQRT(M/(S*T)))
      CC=(2/SIN(XI-A))*SQRT(M/(S*T)))
      SS3=CT*SIN(XI)+CC*SIN(XI-A)+D2*COS(XI)-B*SIN(XI)
      SIS2=D2*COS(XI)-B*SIN(XI)
      VCR = C*T*D4
      FS=(T*S*SS3)
      PI=((Z-B+CT)*SIN(XI))-(SS3/2.0)
      QI=2.0*M*(((Z-B)/CT)+(D2/(CC*SIN(A))))
      Q2=(Z-B)*SIN(XI)*SS3
      Q3=((D2/SIN(A))-CC)*SIN(XI-A)*SIS2
      WLI=((FS*PI)/EI)+VCR
      WUI=((QI+(S*T*(Q2+Q3)*0.5))*(1.0/EI))+VCR
      WRITE(6,801)XI,CT,CC,WLI,WUI
  801 FORMAT(1H,6X,F5.2,15X,F8.2,15X,F8.2,15X,F15.3,15X,F15.3)
  400 CONTINUE
      WRITE(6,895)
  895 FORMAT(1HI,30X,'**************************************')
      WRITE(6,898)M,B,EI
  898 FORMAT(1H,30X,'M=',F15.2,1X,'B=',F6.2,2X,'EI=',F6.2)
      WRITE(6,899)Z,A
  899 FORMAT(1H,30X,'Z=',F7.1,5X,'A=',F4.2)
      WRITE(6,900)
  900 FORMAT(1H,30X,'**************************************')
      GO TO 100
      END
```

A2.2 Computer Program for the Collapse Loads with Reduced Plastic Moment Capacity of Flanges

```
      MASTER VULOI
      REAL M
  100 READ(5,200)M,SI,T,DI,D2,EI,XI,C,ATF,SYF,B,CI,C2
  200 FORMAT(13F0.0)
      IF(M.EQ.99.9) CALL EXIT
      ACF=ATF
      S=(SQRT(((SI)**2)+C*(((1.5*SIN(2*XI))**2)-3)))-(1.5*C*SIN(2*XI))
      Z=(D2*B)/(D2-DI)
      A=ATAN((D2-DI)/B)
      D4=(DI+D2)/2
      CT=(2/SIN(XI))*(SQRT(M/(S*T)))
      CC=(2/SIN(XI-A))*(SQRT(M/(S*T)))
      SS3=CT*SIN(XI)+CC*SIN(XI-A)+D2*COS(XI)-B*SIN(XI)
      VCR=C*T*D4
      FS=(T*S*SS3)
      PI=((Z-B+CT)*SIN(XI))-(SS3/2.0)
      AI=S*SIN(XI-A)*COS(XI-A)+2*C*SIN(A)*COS(A)
      A2=S*SIN(XI)*COS(XI)+C
      WLI=((FS*PI)/EI)
      A9=0.00
      GO TO 250
  777 CONTINUE
      WLI=(WLI+ACC)/2.00
      IF(A9.LE.9.0) GO TO 250
      WLI=(WLI+ACC)/2.00
      WLI=(WLI+ACC)/2.00
      WLI=(WLI+ACC)/2.00
      WLI=(WLI+ACC)/2.00
      IF(EI.GT.200.0) GO TO 250
      WLI=(WLI+ACC)/2.00
      WLI=(WLI+ACC)/2.00
  250 FCI=(WLI+(FS*SIN(XI)))/SIN(A)
      IF(A9.GT.250) GO TO 999
      IF (FCI.LT.0.00)FCI=0.00
      FTI=FCI*COS(A)-FS*COS(XI)
      IF(FTI.LT.0.00)FTI=0.00
      SCF=(FCI-((AI*CC*T)/2.0))/ACF
      STF=(FTI+((A2*T*CT)/2))/ATF
      X2=SCF/SYF
      IF(X2.LT.0.00)X2=0.00
      IF(X2.GT.1.00)X2=1.00
      RMPC=M*(1.0-((CI*((X2)**2))+C2*X2))
  500 X3=STF/SYF
      IF(X3.LT.0.00)X3=0.00
      IF(X3.GT.1.00)X3=1.00
      RMPT=M*(1.0-((CI*((X3)**2))+C2*X3))
  600 CT=(2/SIN(XI))*(SQRT(RMPT/(S*T)))
      CC=(2/SIN(XI-A))*SQRT(RMPC/(S*T)))
      SS3=CT*SIN(XI)+CC*SIN(XI-A)+D2*COS(XI)-B*SIN(XI)
      ACC=WLI
      FS=(T*S*SS3)
      PI=((Z-B+CT)*SIN(XI))-(SS3/2.0)
      WLI=(((FS*PI)+(RMPC-RMPT))/EI)
```

```
      PDIF = ABS((ACC-WLI)*100.00/ACC)
      A9=A9+1.00
      WRITE(6,800)S,SS3,VCR
  800 FORMAT(1H1,10X,'S=',F10.3,10X,'SS3=',F10.3,'VCR=',F10.3)
      WRITE(6,810)FS,FCI,FTI
  810 FORMAT(1H, 10X,'FS=',F10.3,10X,'FCI=',F10.3,'FTI=',F10.3)
      WRITE(6,820)X2,SCF,RMPC
  820 FORMAT(1H,10X, 'X2=',F5.3,10X,'SCF=',F8.3,10X,'RMPC=',F15.3)
      WRITE(6,830)X3,STF,RMPT
  830 FORMAT(1H,10X,'X3=',F5.3,10X,'STF=',F8.3,10X,'RMPT=',F15.3)
      WRITE(6,840)CT,C,EI
  840 FORMAT(1H,10X,'CT=',F10.3,10X,'CC=',F10.3,10X,'EI=',F5.1)
      WRITE(6,850)WLI,ACC,PDIF
  850 FORMAT(1H,10X,'WLI=',F15.3,10X,'ACC=',F15.3,10X,'PDIF=',F7.2)
      WRITE(6,860)A9
  860 FORMAT(1H,10X,'A9=',F5.0)
      IF(PDIF-1.0)778,777,777
  778 WLT=WLI+VCR
      WRITE(6,350)
  350 FORMAT(1H1,30X,'*********************************************')
      WRITE(6,880)
  880 FORMAT(1H,1X,'XI',14X,'WLT',10X,'FCI',13X,'SCF',12X,'RMPC',12X,'F
     ITI',12X,'STF',10X,'RMPT')
      WRITE(6,890)XI,WLT,FCI,SCF,RMPC,FTI,STF,RMPT
  890 FORMAT(1H,F4.2,7(3X,512.2))
      WRITE(6,895)
  895 FORMAT(1H1,30X,'************************************')
      WRITE(6,898)M,EI,B
  898 FORMAT(1H,30X,'M=',F15.2,1X,'EI=',F6.2,2X,'8=',F6.2)
      WRITE(6.900)
  900 FORMAT(1H,30X),'************************************'
  999 GO TO 100
      END
```

APPENDIX 3

A3. Membrane Stresses in the Web Plate of Tapered Beams Loaded at the Tip

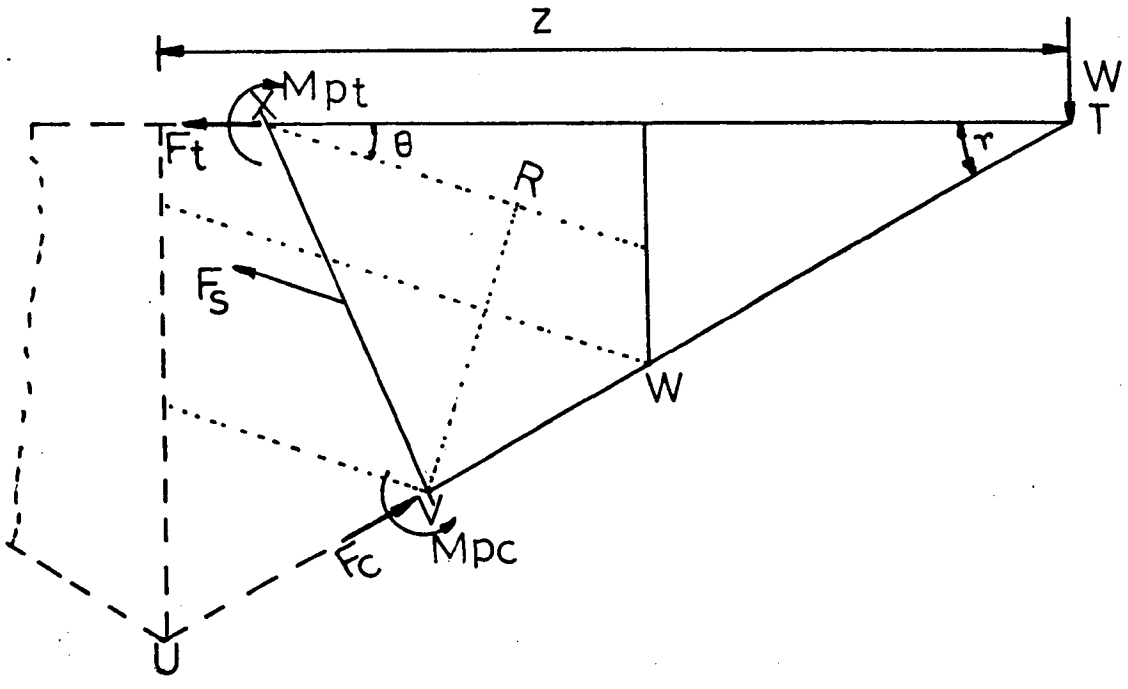

Figure A3.1

A3.1 General

In order to show that the tensile membrane stresses do not form in the web panel of a tapered beam loaded at the tip, it will be demonstrated here that even if it is assumed that the membrane stresses form in the web panel, their magnitude can be shown equal to zero.

A3.2 Proof

Consider a section, X-V, passing through the plastic hinge positions at X and V. The forces acting on the section are shown in Figure A3.1. Considering the vertical equilibrium of forces and taking moments about the position X, the following equations can be obtained:

$$\Sigma V = 0$$

$$W - F_s.\sin\theta - F_c.\sin\gamma = 0$$

$$\therefore F_c.\sin\gamma = [W - F_2.\sin\theta] \qquad (A3.1)$$

$$\Sigma M_x = 0$$

$$W.z + F_s.\left[\frac{VR}{2}\right] - F_c.z.\sin\gamma = 0$$

By substituting the value of $F_c.\sin\gamma$ from equation (A3.1),

$$W.z + F_s.\frac{(VR)}{2} - z.[W - F_s.\sin\theta] = 0$$

i.e. $$F_s\left[\frac{VR}{2} + z.\sin\theta\right] = 0$$

$$F_s = 0$$

Clearly for any positive value of (VR), the magnitude of 'F_s' will be zero.

APPENDIX 4

A4. Listing of Computer Program for the Analyses of Strain Gauges and Rosettes Readings

```
      MASTER ROS22
      REAL M
      DIMENSION  ISG(36)
      DIMENSION STRAINI(95),STRESS(50)
      DIMENSION ISI(95),II(99),NN(95)
      DIMENSION AVG(58)
      DIMENSION IC(95),ICC(95),STRAIN(95),STRAIN2(95),ALOAD(3)
      DIMENSION EI(18),E2(18),FI(18,F2(18),THETA(18)
      PY=3.14159
      ICN=26
      ICK=1
      YE=200000
C     YE=YOUNG MODULUS OF ELASTICITY IN N/MM2
      E=YE/1000000
      M=3
      DO 300 J=1,93,5
  300 READ(5,400)(IC(I),STRAINI(I), I=J,J+4)
  400 FORMAT(5(I3,F6.0.4X))
      DO 410 JI=1,54
      AVG(JI)=(STRAINI(JI)+STRAINI(JI+27))/2
  410 CONTINUE
  425 NT=0.00
  450 NT=NT+1
      DO 500 K=1,93,5
  500 READ(5,600)(ICC(I),STRAIN2(I),I=K,K+4)
  600 FORMAT(5(I3,F6.0,4X))
      NROS=0
      DO 750 KROS=1,27,3
      NROS=NROS+1
      NN(NROS)=9+NROS
      STX=(STRAIN2(KROS)+STRAIN2(KROS+27))/2-AVG(KROS)
      ST45=(STRAIN2(KROS+1)+STRAIN2(KROS+28))/2-AVG(KROS+1)
      STY=(STRAIN2(KROS+2)+STRAIN2(KROS+29))/2-AVG(KROS+2)
      PI= (STX+STY)/2
      P2=(SQRT((STX-ST45)**2+(ST45-STY)**2))*0.707
      EI(NROS)=PI+P2
      E2(NROS)=PI-P2
      F(NROS)=(STX+STY-(2.0*ST45))
      FI(NROS)=(E*M*(M*EI(NROS)+E2(NROS)))/((M**2)-1
      F2(NROS)=(E*M*(EI(NROS)+M*E2(NROS)))/((M**2)-1)
      IF(STX.EQ.STY)GO TO 650
      THETA(NROS)=(ATAN(F(NROS)/(STX-STY))/2)*57.30
      GO TO 750
  650 THETA(NROS)=PY/2
  750 CONTINUE
      DO 800 KST=55,59
      L=KST-54
      ISG(L)=ICC(KST)
      ISI(L)=ICC(KST+5)
      STRAIN(L)=(STRAIN2(KST)+STRAIN2(KST+5)-STRAINI(KST)-STRAINI(KST+5
     1))/2
```

```
      STRESS(L)=STRAIN(L)*E
  800 CONTINUE
      DO 801 I=65,71
      LZ=I-64+5
      ISG(LZ)=ICC(I)
      ISI(LZ)=ICC(I+7)
      STRAIN(LZ)=(STRAIN2(I)-STRAINI(I)+STRAIN2(I+7)-STRAINI(I+7))/2
      STRESS(LZ)=STRAIN(LZ)*E
  801 CONTINUE
      DO 850 KLD=91,93
      LM=KLD-90
      STR=STRAIN2(KLD)-STRAINI(KLD)
      ALOAD(LM)=STR/48.00
  850 CONTINUE
      WRITE(6,930)(ALOAD(I),I=1,3)
  930 FORMAT(1H1,10X,'LOAD 1=',F10.3,/1H,10X,'LOAD 2=',F10,3,/1H,10X,
     1'LOAD3=',F10.3)
      WRITE(6,935)
  935 FORMAT(1H,10X,'ALL LOADS ARE IN KN')
      WRITE(6,936)
  936 FORMAT(1H,10X,'E1 AND E2 ARE THE PRINCIPAL STRAINS IN MCSTRAIN')
      WRITE(6,937)
  937 FORMAT(1H,10X,'F1 AND F2 ARE THE PRINCIPAL STRESSES IN N/MM2')
      WRITE (6,938)
  938 FORMAT(1H,10X,'THETA IS THE INCLINATION OF PR.PLA.TOTHE XAXIS')
      WRITE(6,939)
  939 FORMAT(1H,10X,'FAI IS THE SHEAR STRAIN IN MICRO STRAIN')
      WRITE(6,950)
  950 FORMAT(1H,10X,'ROSETTE NO',15X,'E1',10X,'E2',10X,'F1',10X,'F2',
     110X,'THETA',10X,'FAI')
      WRITE(6,955)(I,NN(I),E1(I),E2(I),F1(I),F2(I),THETA(I),F(I),I=1,NR
     1OS)
  955 FORMAT(1H,10X,14,1H,,12,10X,6F10,2)
      WRITE(6,959)
  959 FORMAT(1H,10X,'CHANEL 104 TO 113 INDICATES STRAIN GAUGE IN COMP.F
     1LANGE',/1H,10X,'CH 114 TO 127 ARE THE STRAIN GAUGE IN TENSION FLAN
     2GE')
      WRITE(6,960)
  960 FORMAT(1H,10X,'NO OF STRAIN GAUGE',25X,'MICRO STRAIN',20X,
     1STRESSES IN N/MM2')
      WRITE(6,961)(ISG(I),ISI(I),STRAIN(I),STRESS(I),I=1,12)
  961 FORMAT(1H,15X,15,1H,,15,25X,F15.5,15X,F15.5)
      ICK=ICK+1
      IF(ICK-ICN)425,425,701
  701 CALL EXIT
      END
```

APPENDIX 5

STRESS/STRAIN CURVES FOR THE WEB AND FLANGE MATERIAL

A5.1 Stress/strain curve from Instron tension tests:-

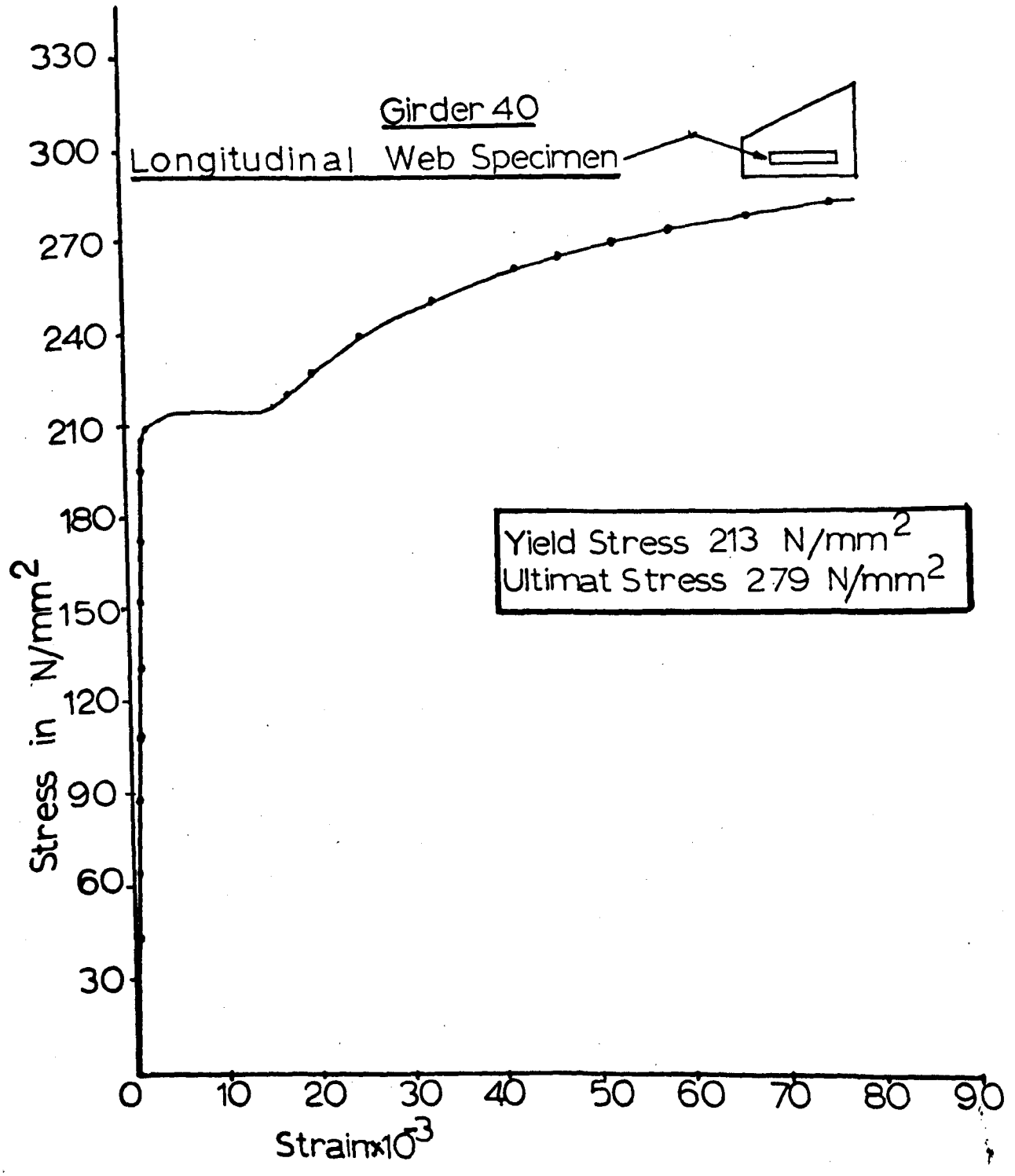

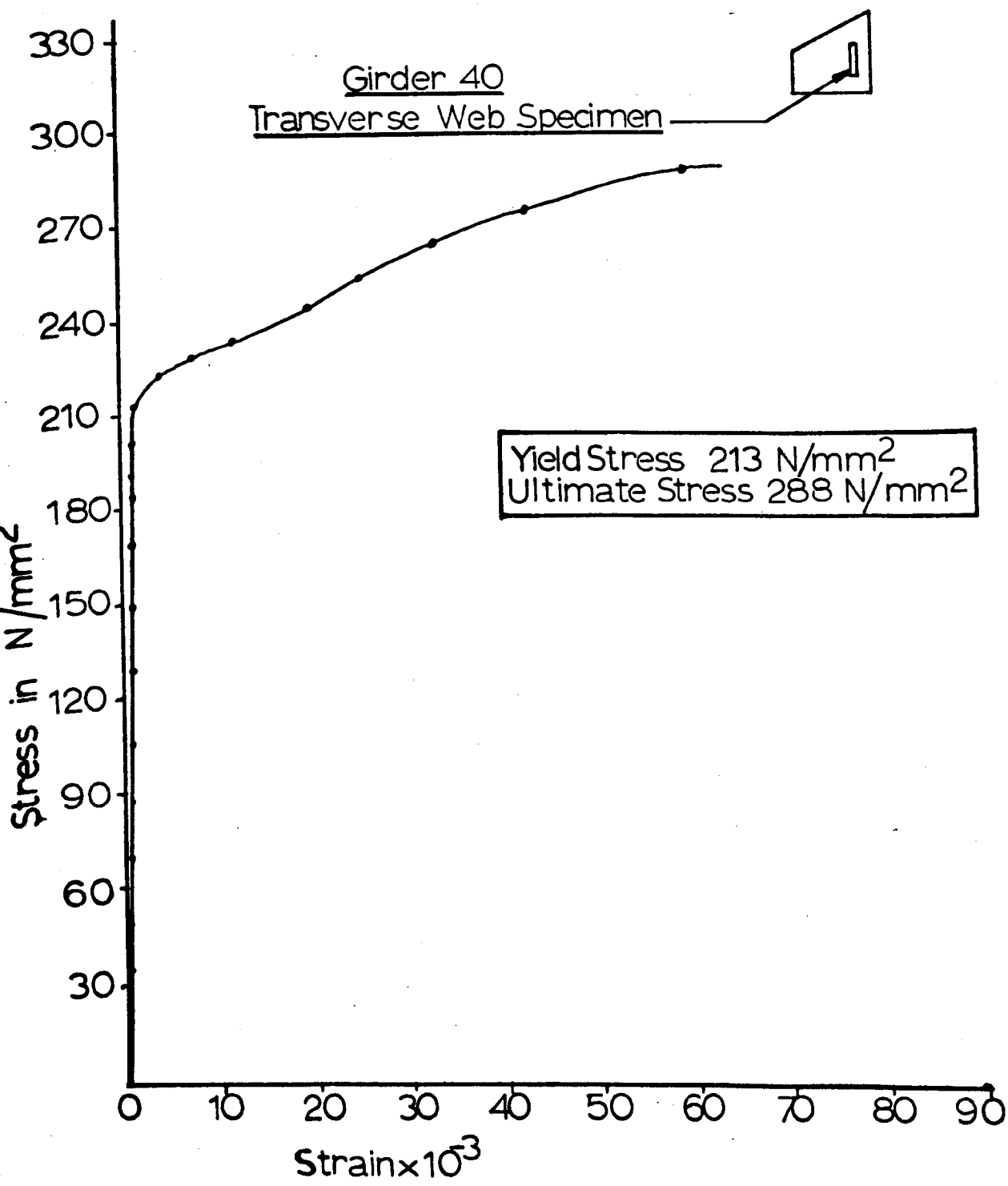
Girder 40
Transverse Web Specimen
Yield Stress 213 N/mm2
Ultimate Stress 288 N/mm2
Stress in N/mm2
330
300
270
240
210
180
150
120
90
60
30
0
10
20
30
40
50
60
70
80
90
Strain×10^3

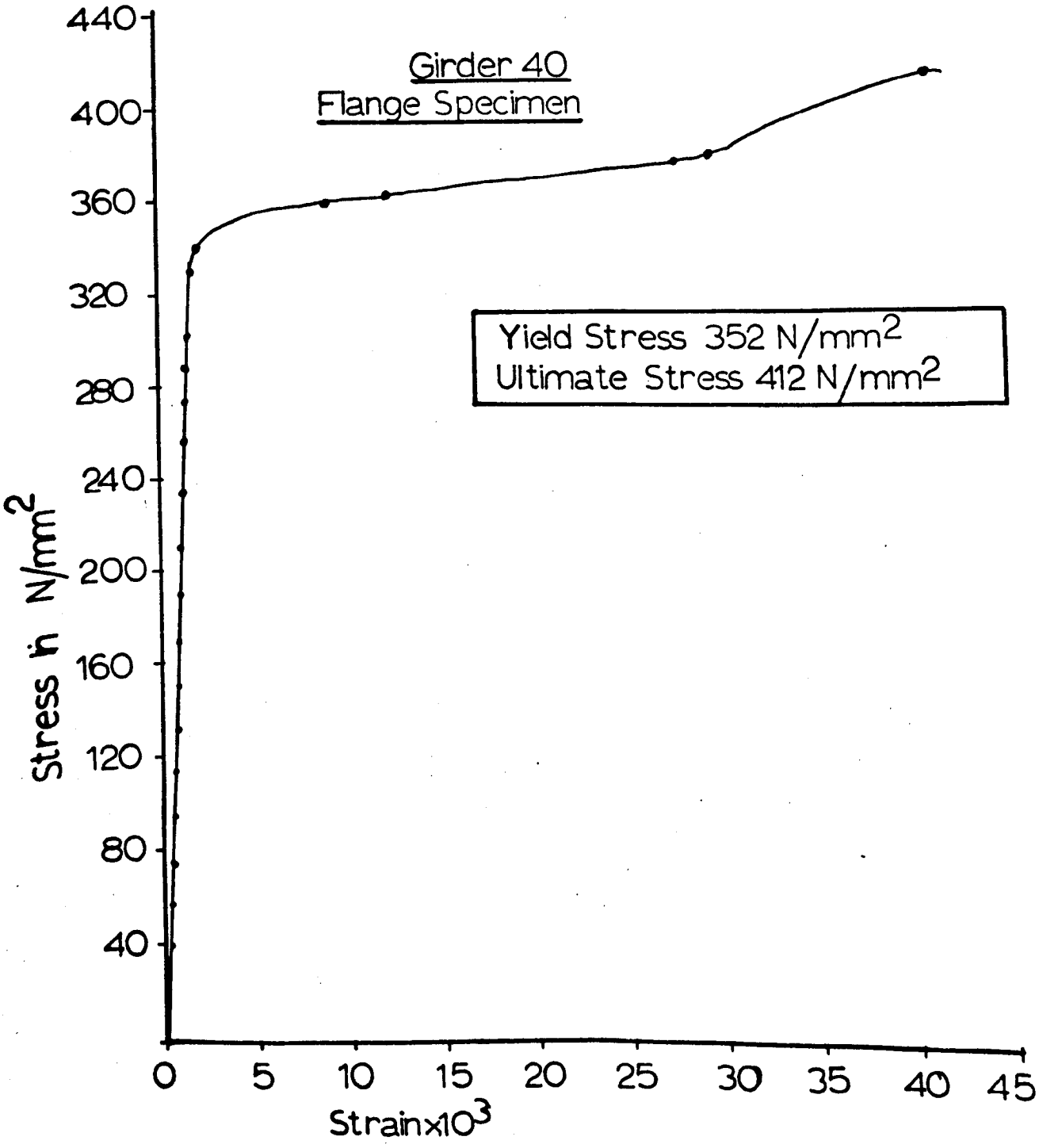
Girder 40
Flange Specimen
Yield Stress 352 N/mm2
Ultimate Stress 412 N/mm2
Stress in N/mm2
440
400
360
320
280
240
200
160
120
80
40
0
5
10
15
20
25
30
35
40
45
Strain x10^3

A5.2 Typical curve for yield stresses obtained from Tensometer tests

GIRDER - 10 WEB SPECIMEN

Yield Stress - 255 N/mm^2

Ultimate Stress - 373 N/mm^2

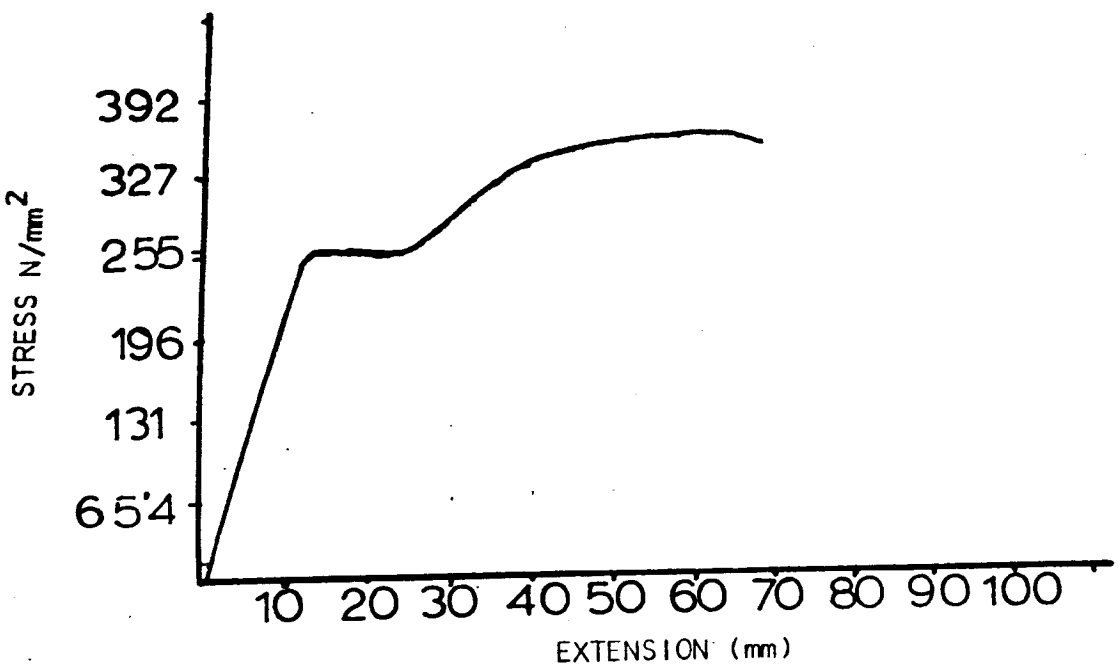

GIRDER - 10 FLANGE SPECIMEN

Yield Stress - 336 N/mm^2

Ultimate Stress - 480 N/mm^2

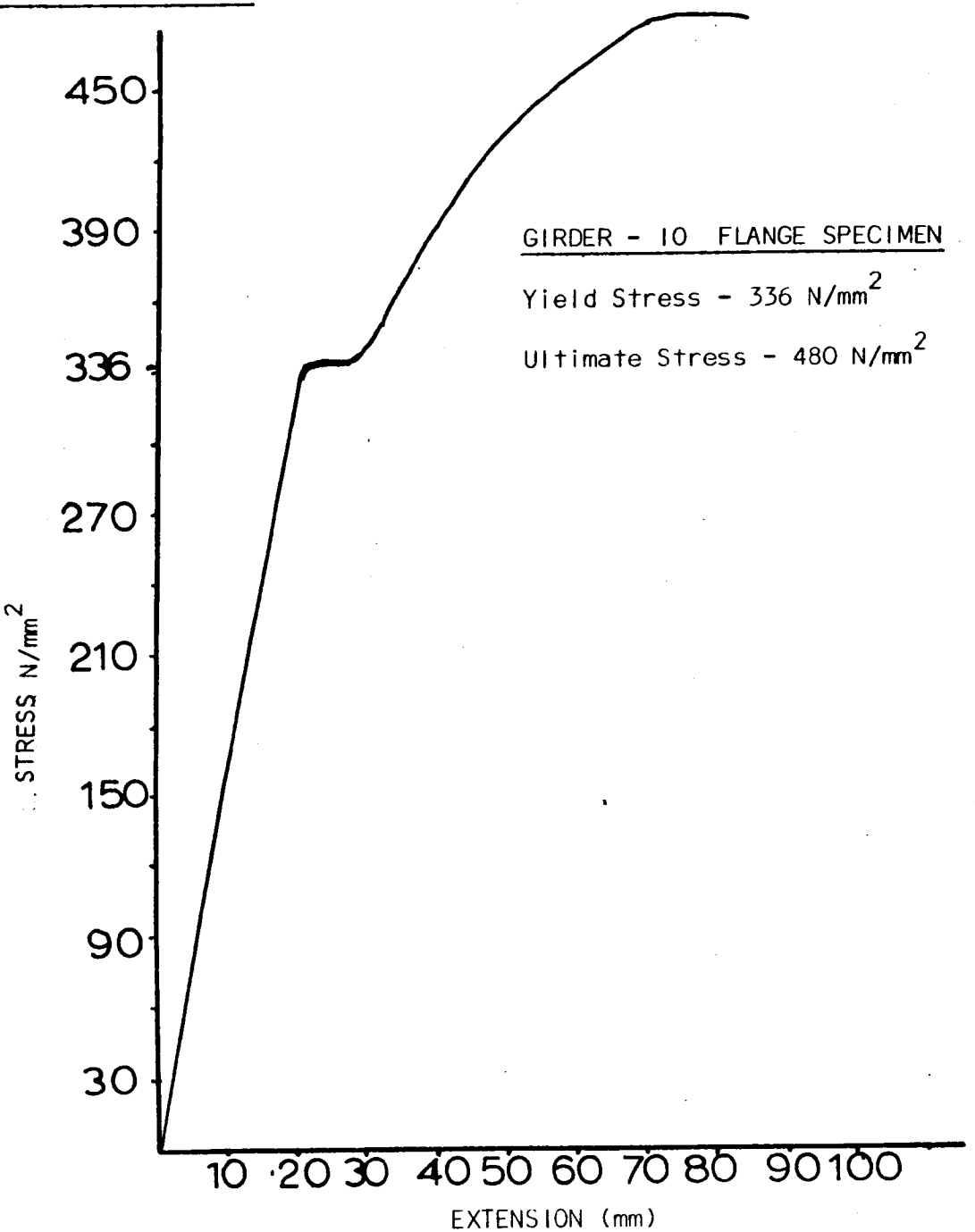

A5.2.1

GIRDER - 20 WEB SPECIMEN

Yield Stress - 276 N/mm^2

Ultimate Stress - 330 N/mm^2

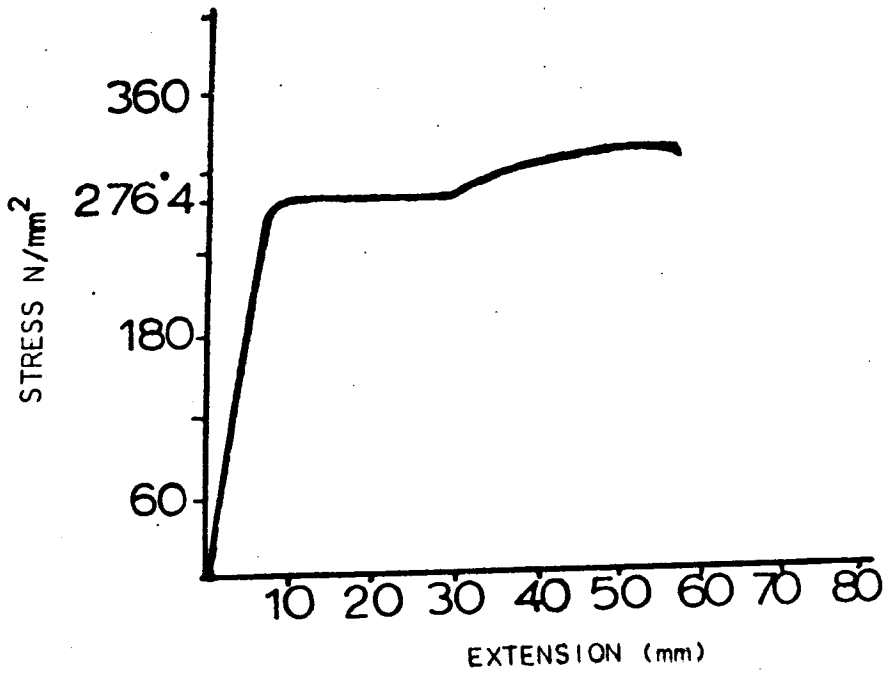

GIRDER - 20 FLANGE SPECIMEN

Yield Stress - 300 N/mm^2

Ultimate Stress - 480 N/mm^2

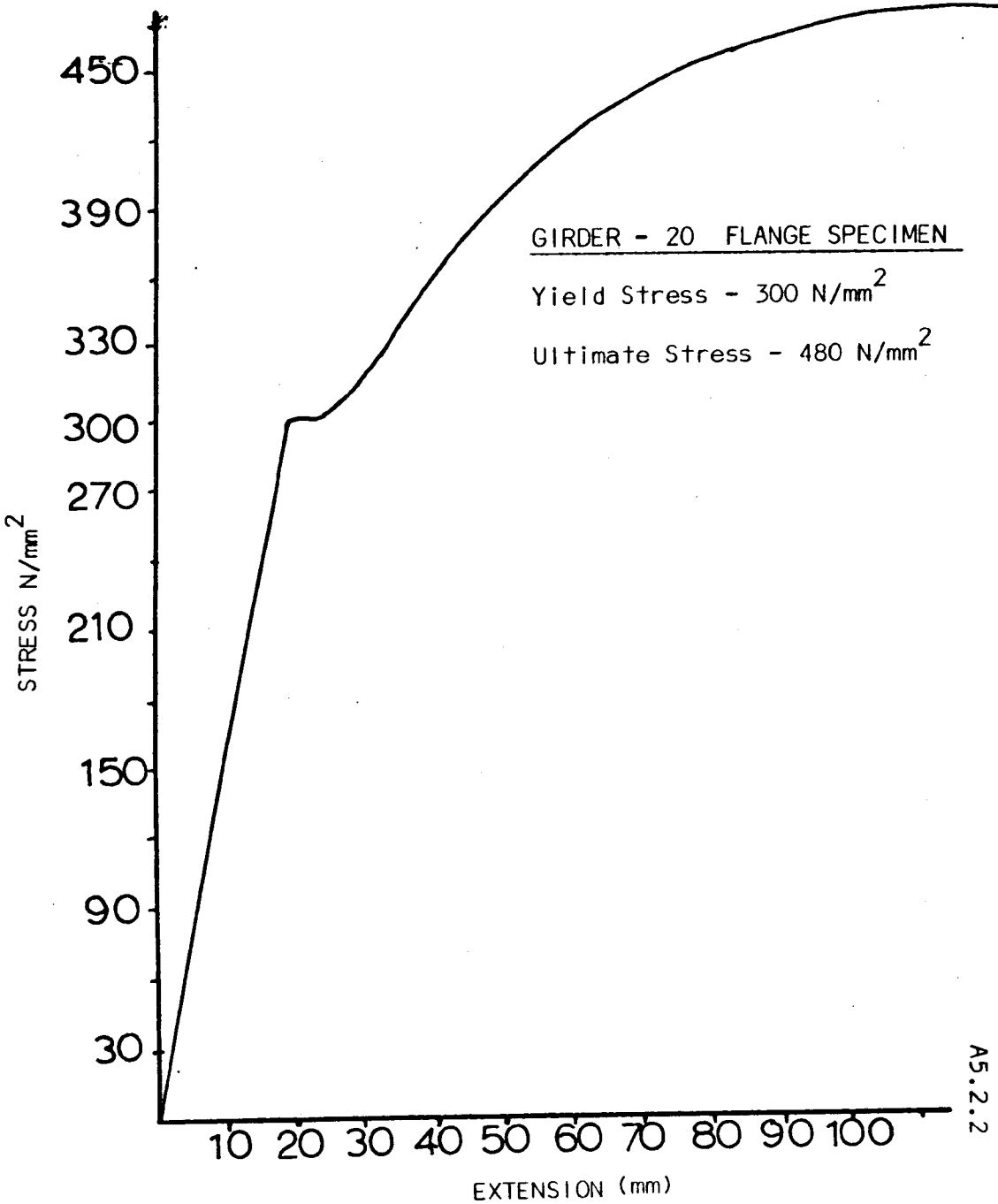

A5.2.2

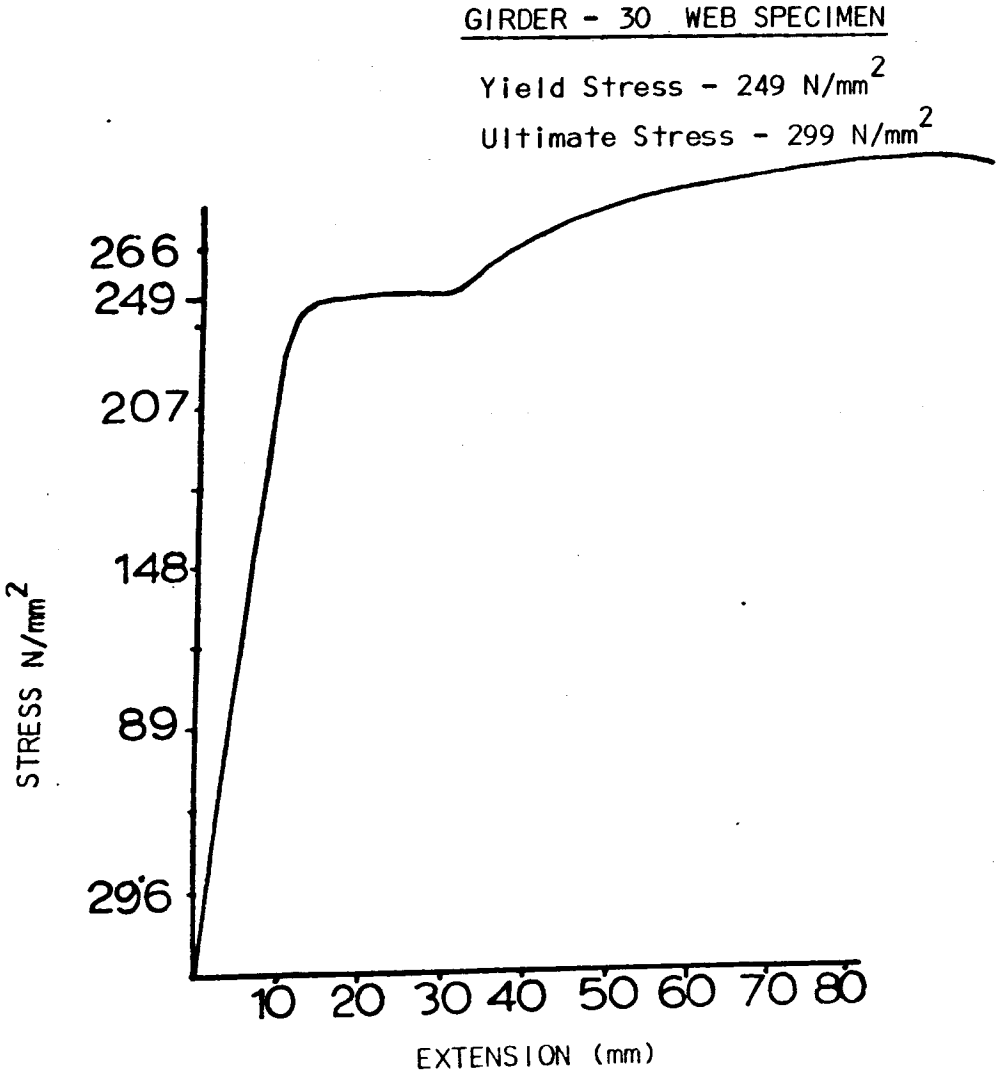
GIRDER - 30 WEB SPECIMEN
Yield Stress - 249 N/mm2
Ultimate Stress - 299 N/mm2
STRESS N/mm2
266
249
207
148
89
296
10 20 30 40 50 60 70 80
EXTENSION (mm)

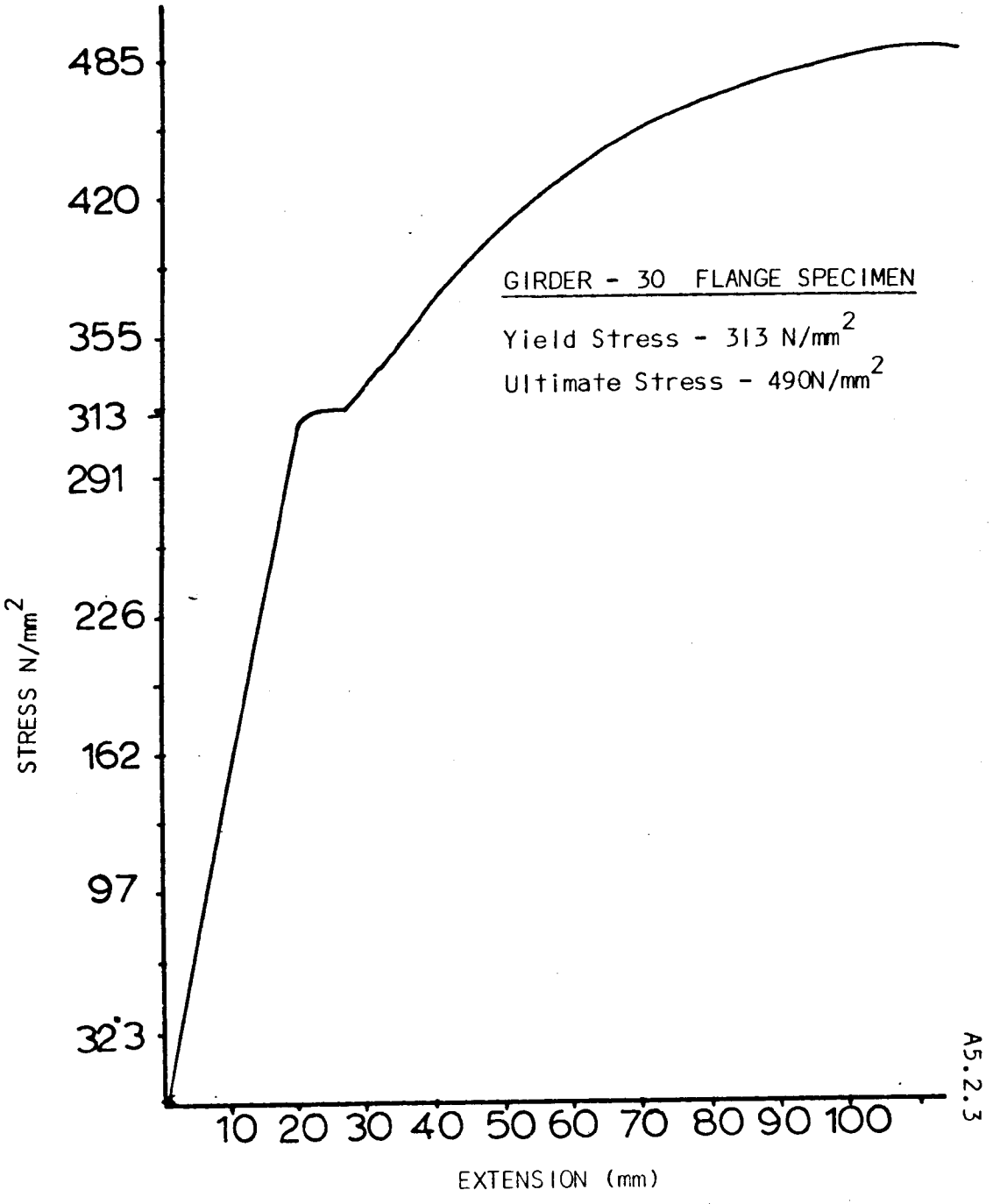
GIRDER - 30 FLANGE SPECIMEN
Yield Stress - 313 N/mm2
Ultimate Stress - 490N/mm2
STRESS N/mm2
485
420
355
313
291
226
162
97
323
10 20 30 40 50 60 70 80 90 100
EXTENSION (mm)

A5.2.3

GIRDER - 40 WEB SPECIMEN

Yield Stress - 239 N/mm^2

Ultimate Stress - 304 N/mm^2

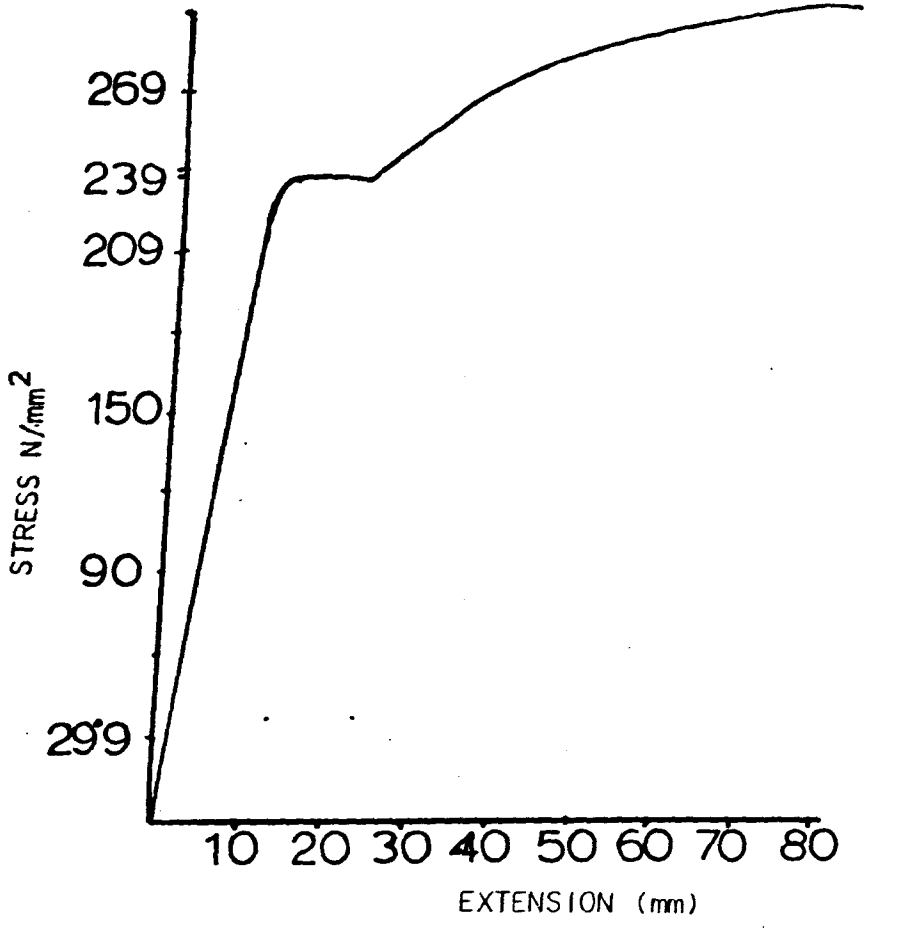

GIRDER - 40 FLANGE SPECIMEN

Yield Stress - 324 N/mm^2

Ultimate Stress - 469 N/mm^2

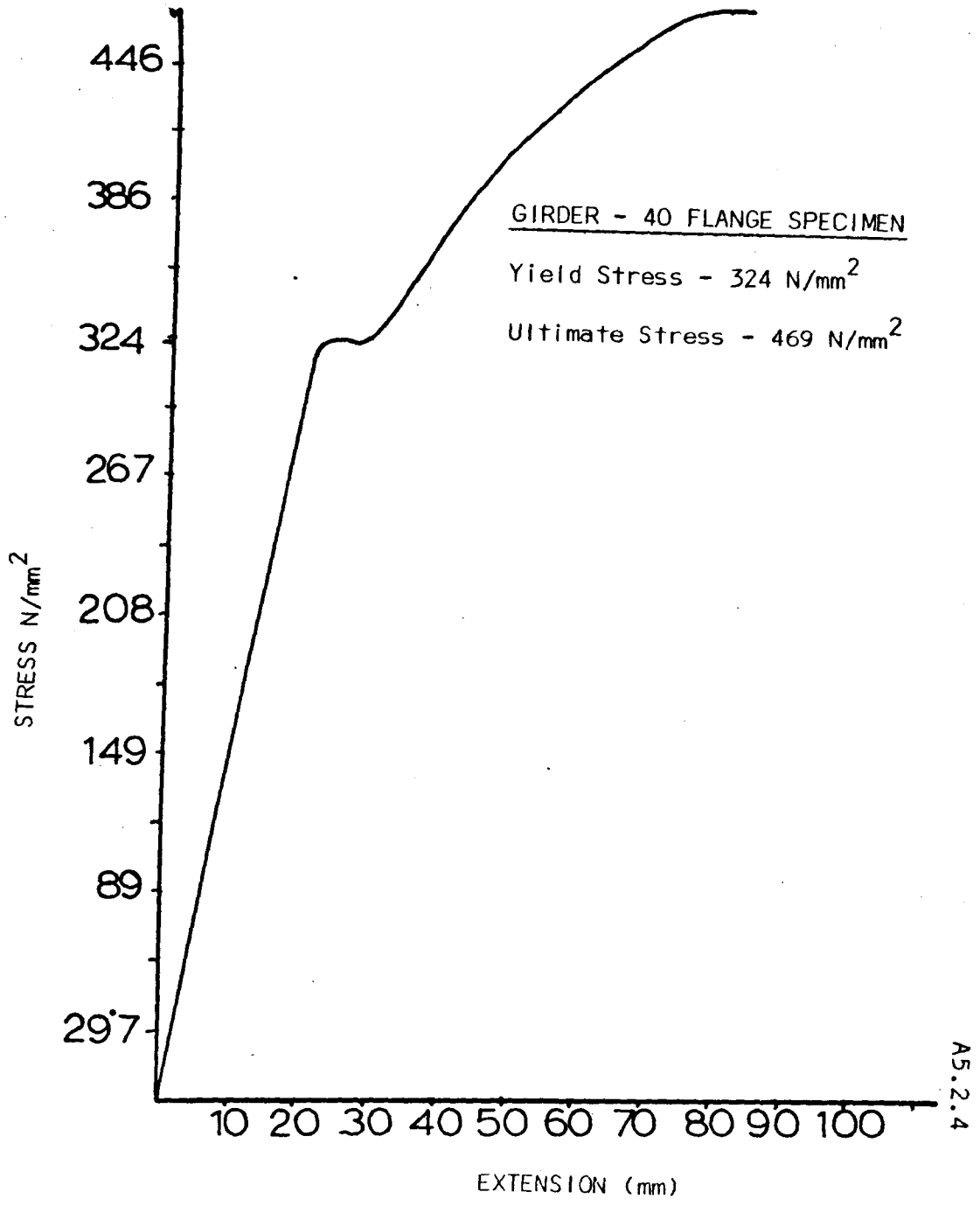

A5.2.4

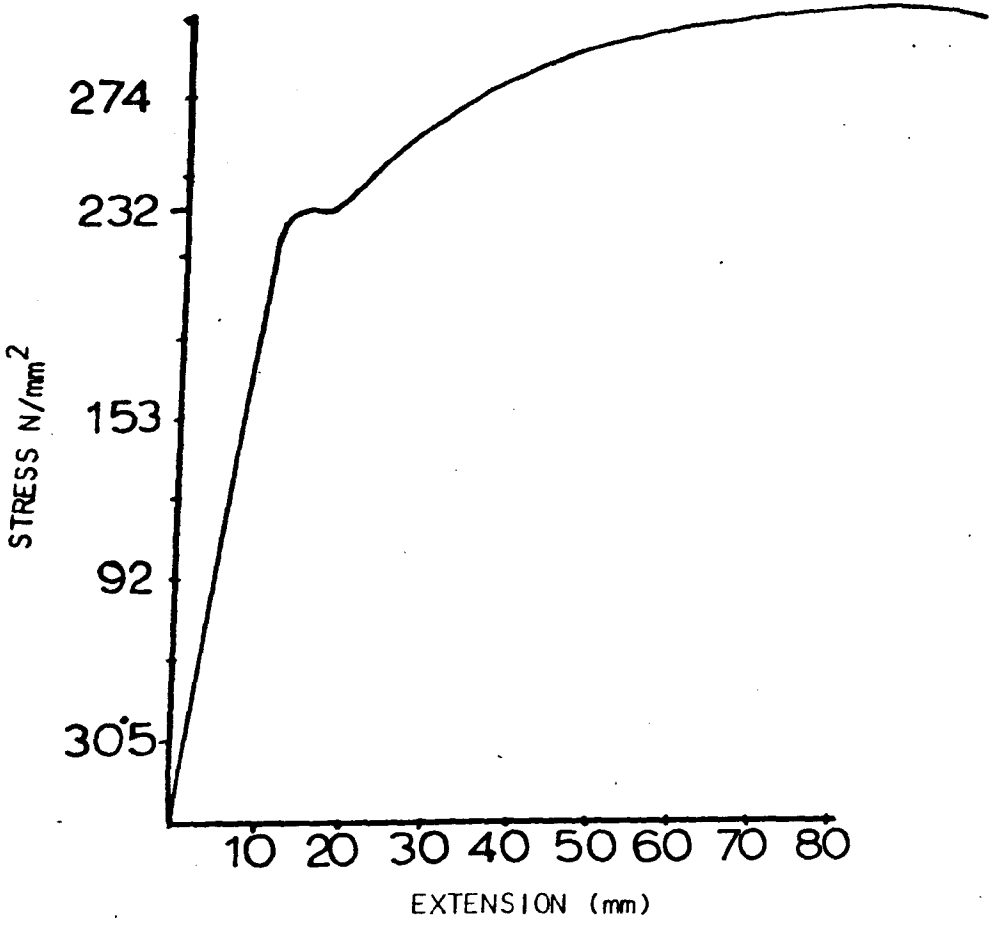
GIRDER - 50 WEB SPECIMEN
Yield Stress - 232 N/mm2
Ultimate Stress - 311 N/mm2
274
232
153
92
30·5
STRESS N/mm2
10 20 30 40 50 60 70 80
EXTENSION (mm)

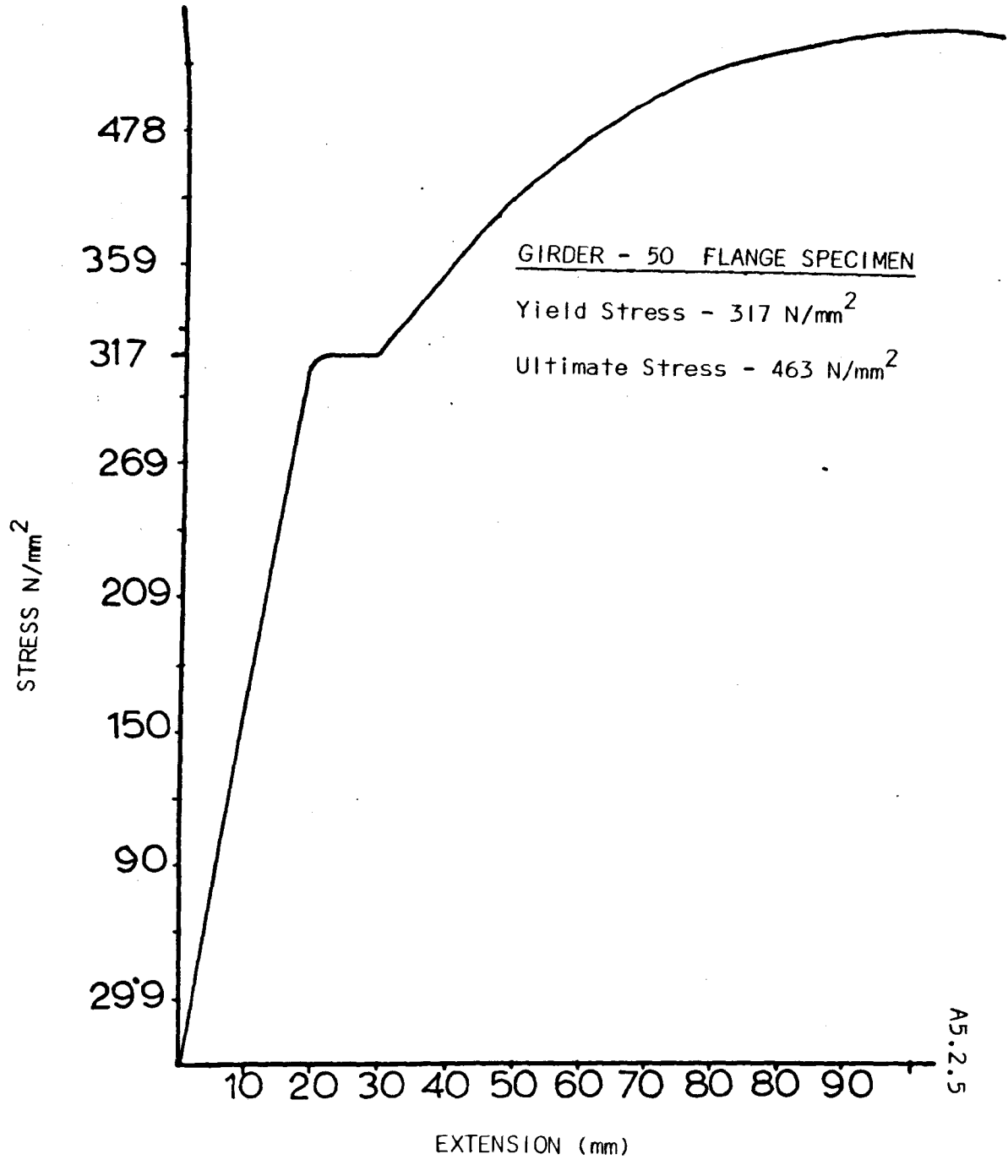
GIRDER - 50 FLANGE SPECIMEN
Yield Stress - 317 N/mm2
Ultimate Stress - 463 N/mm2
478
359
317
269
209
150
90
29·9
STRESS N/mm2
10 20 30 40 50 60 70 80 80 90
EXTENSION (mm)
A5.2.5

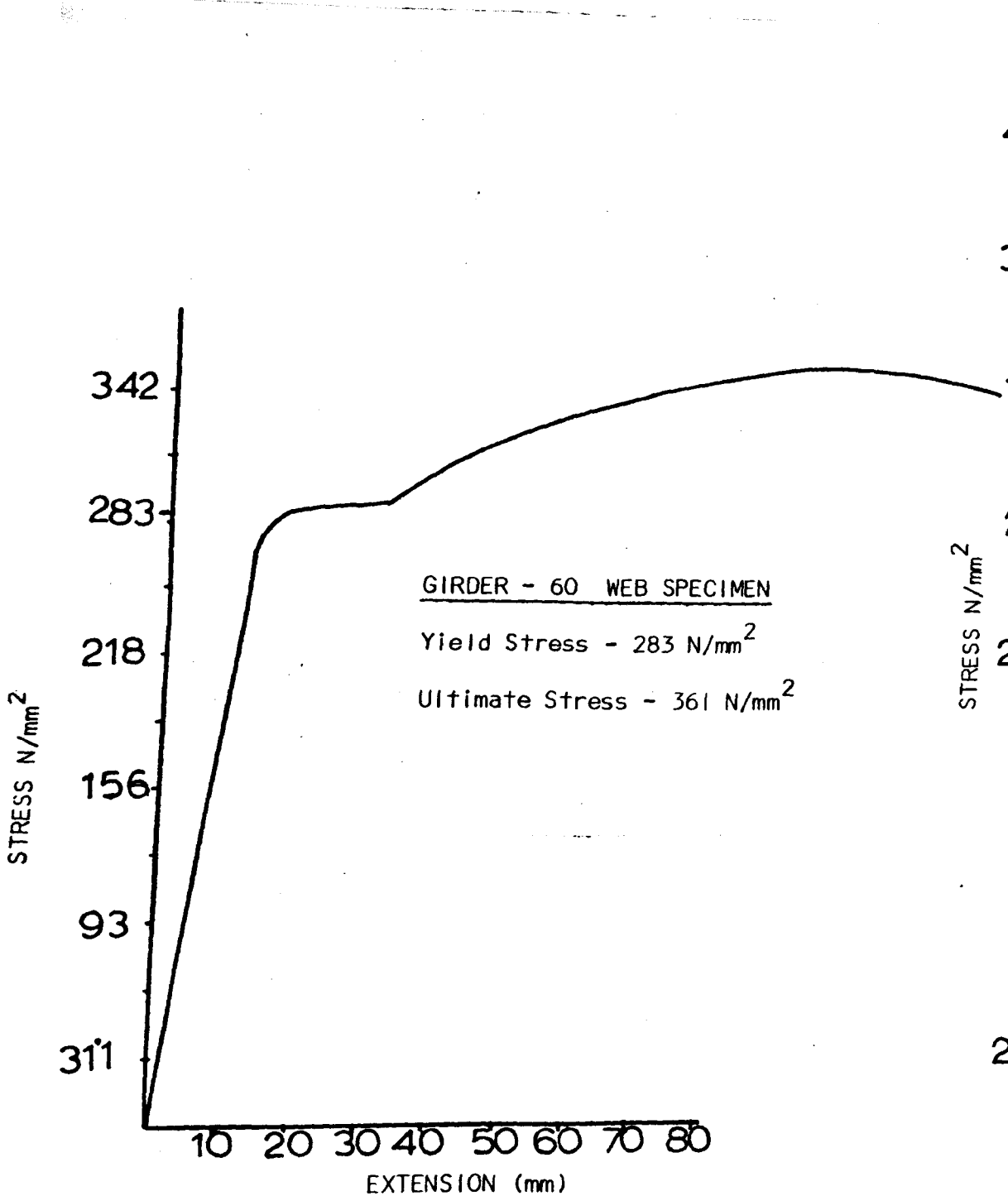
342
283
218
156
93
31·1
STRESS N/mm²
10 20 30 40 50 60 70 80
EXTENSION (mm)
GIRDER - 60 WEB SPECIMEN
Yield Stress - 283 N/mm²
Ultimate Stress - 361 N/mm²

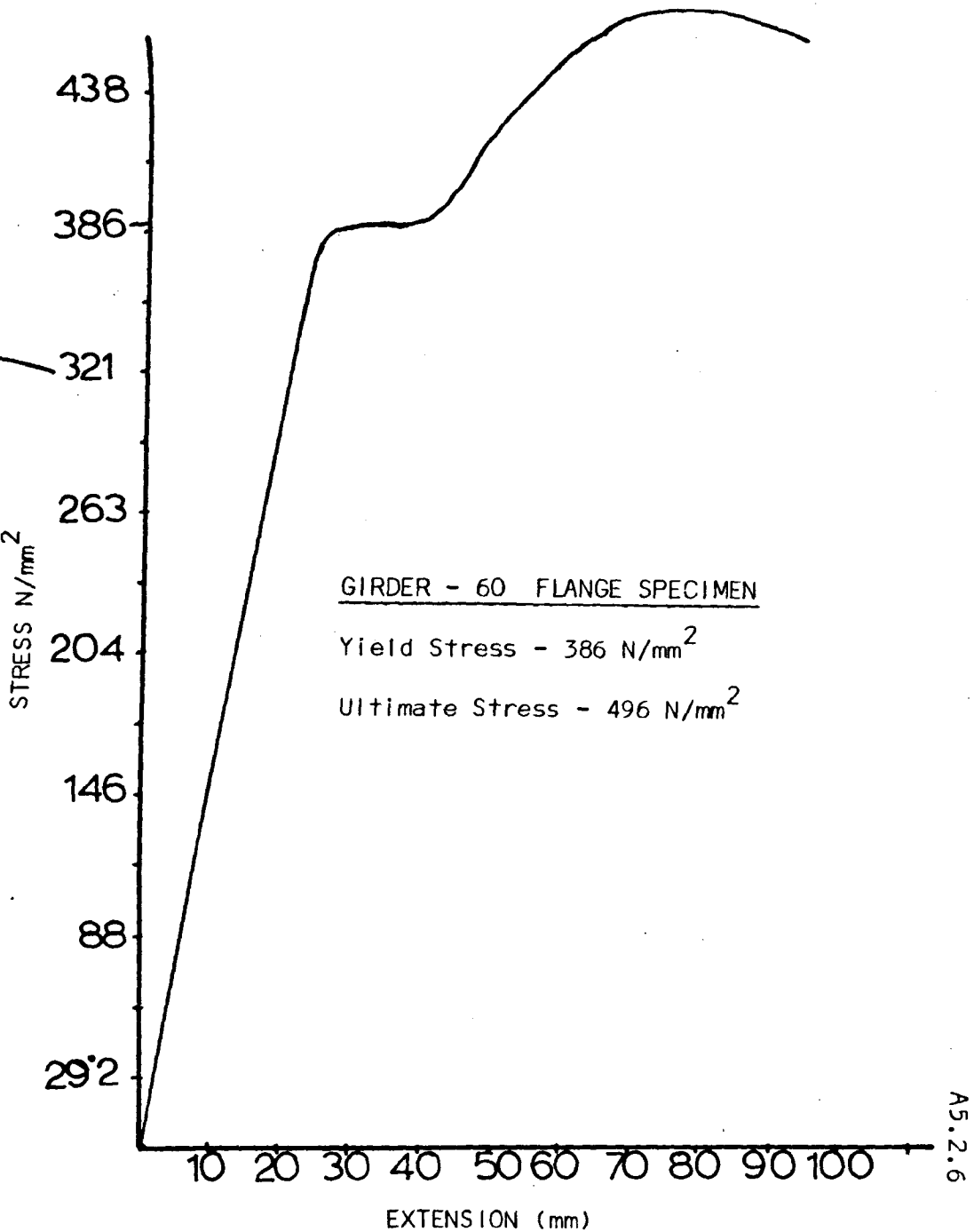
438
386
321
263
204
146
88
29·2
STRESS N/mm²
10 20 30 40 50 60 70 80 90 100
EXTENSION (mm)
GIRDER - 60 FLANGE SPECIMEN
Yield Stress - 386 N/mm²
Ultimate Stress - 496 N/mm²

A5.2.6

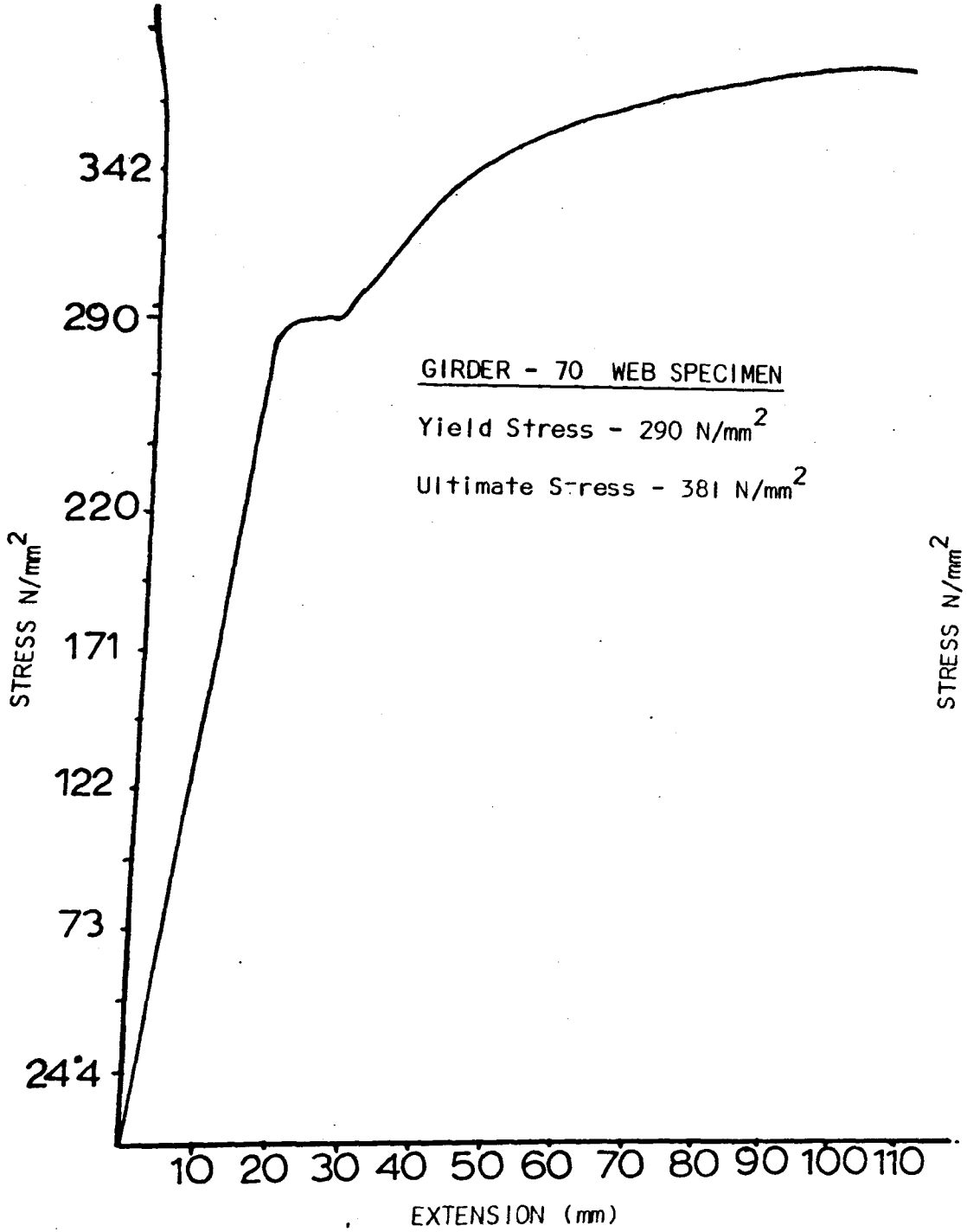
342
290
220
171
122
73
24·4
STRESS N/mm²
10 20 30 40 50 60 70 80 90 100 110
EXTENSION (mm)
GIRDER - 70 WEB SPECIMEN
Yield Stress - 290 N/mm²
Ultimate Stress - 381 N/mm²

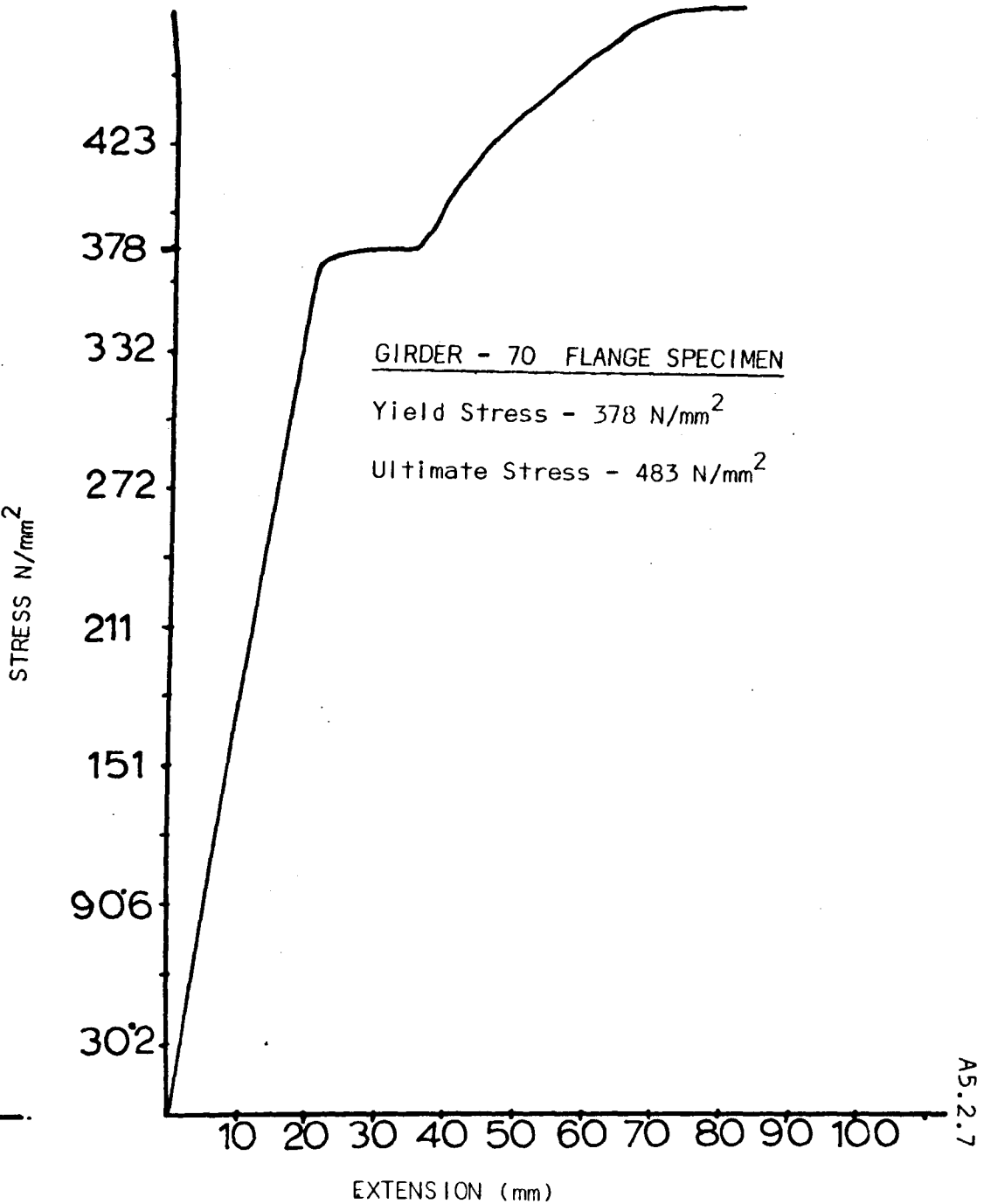
423
378
332
272
211
151
90·6
30·2
STRESS N/mm²
10 20 30 40 50 60 70 80 90 100
EXTENSION (mm)
GIRDER - 70 FLANGE SPECIMEN
Yield Stress - 378 N/mm²
Ultimate Stress - 483 N/mm²

A5.2.7

APPENDIX - 6

A6 PLOTTED PROFILE OF WEB PANELS FOR THE BEAMS LOADED INSIDE THE TIP

Girder - 10A

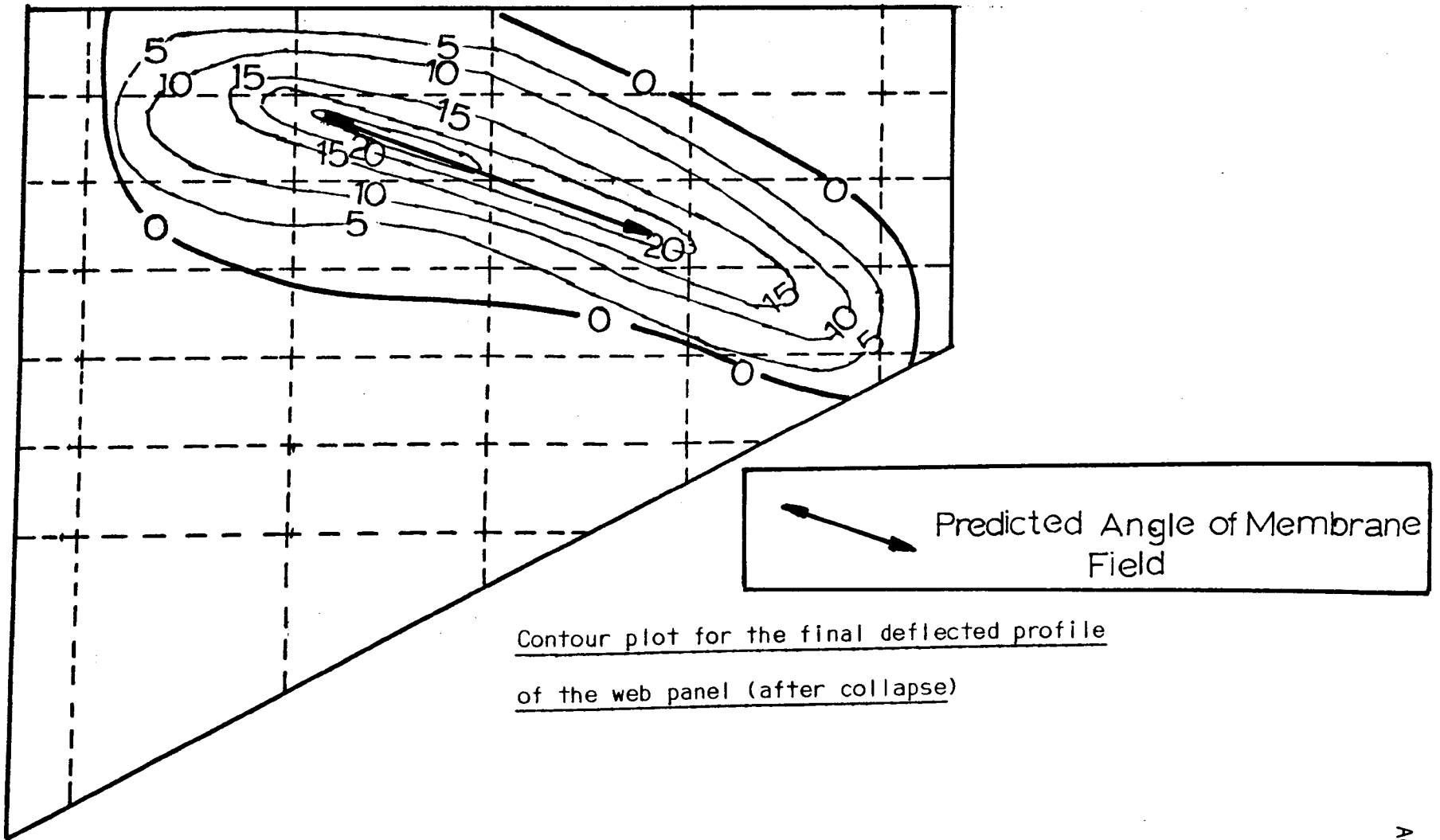

Contour plot for the final deflected profile

of the web panel (after collapse)

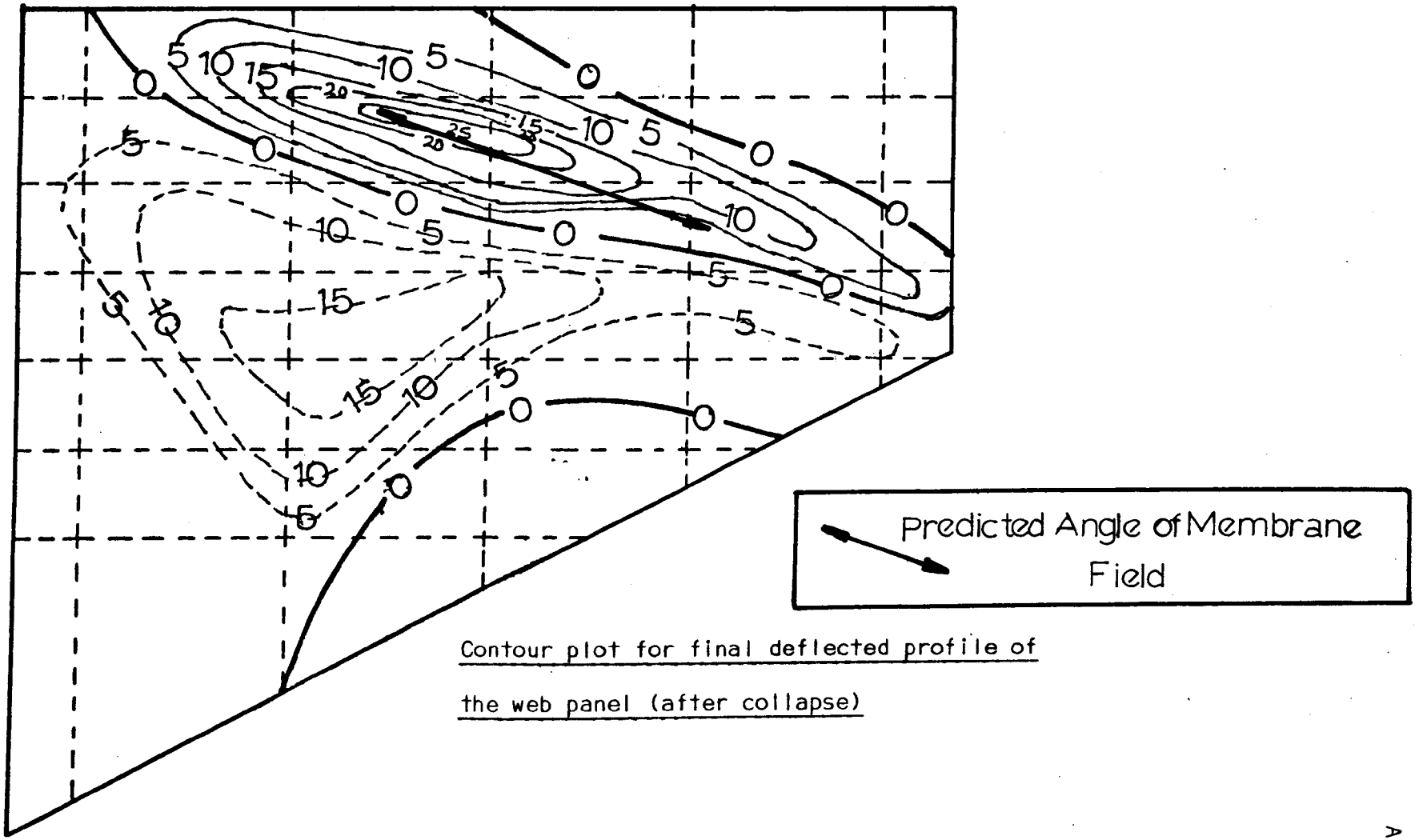

Contour plot for final deflected profile of the web panel (after collapse)

A6.3 Girder 20A

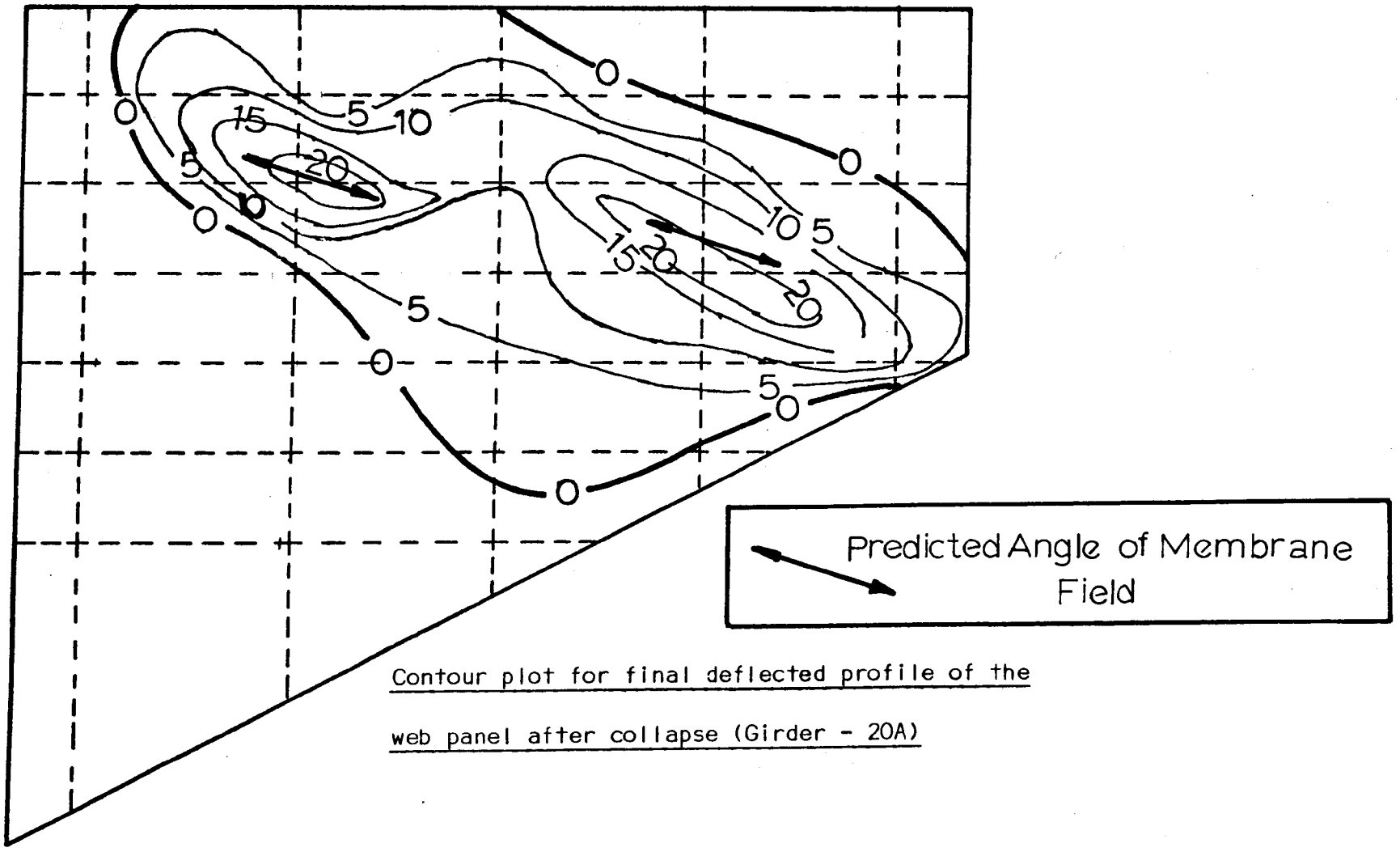

Contour plot for final deflected profile of the web panel after collapse (Girder - 20A)

A6.4 Girder 70A)

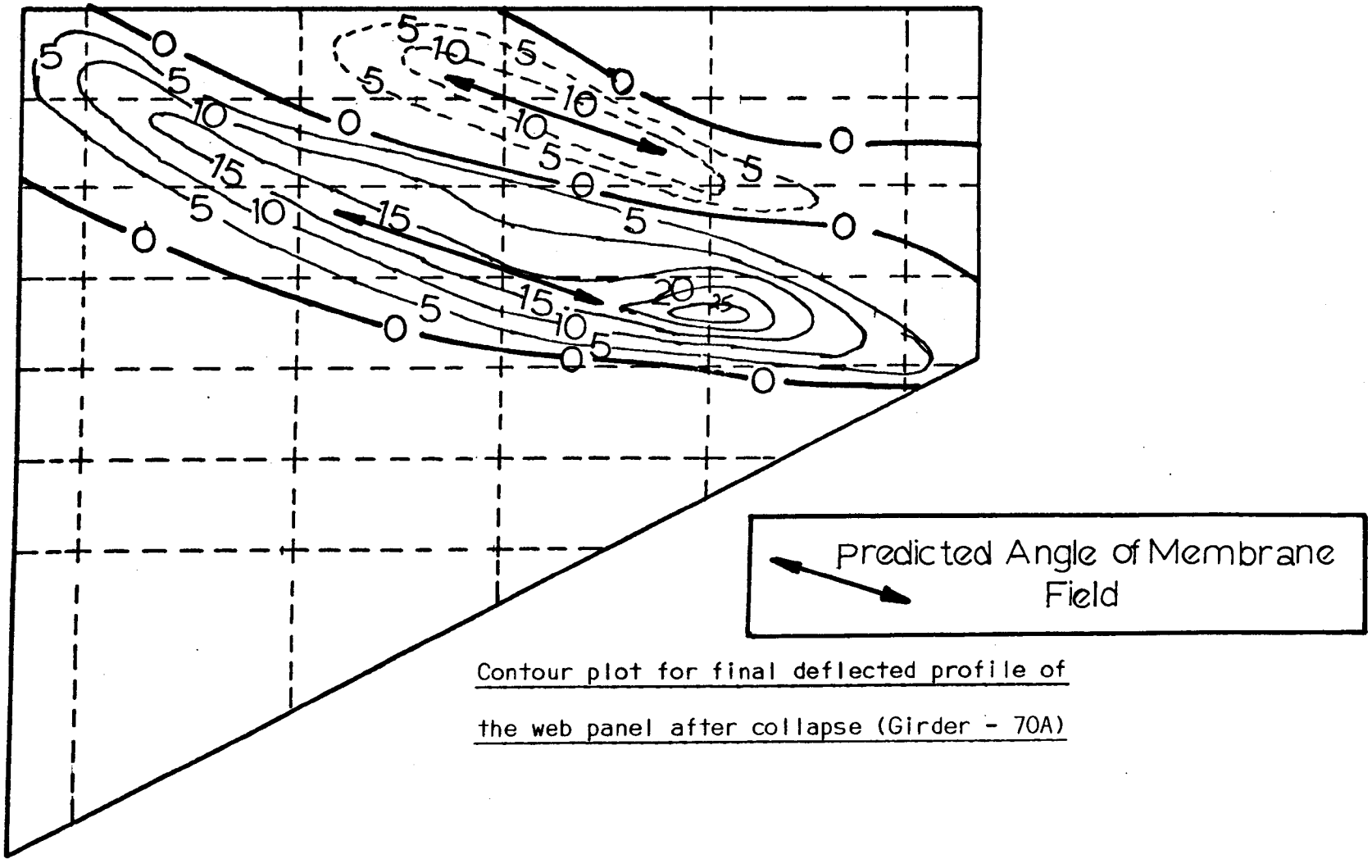

Contour plot for final deflected profile of the web panel after collapse (Girder - 70A)

A6.5 Girder 70B

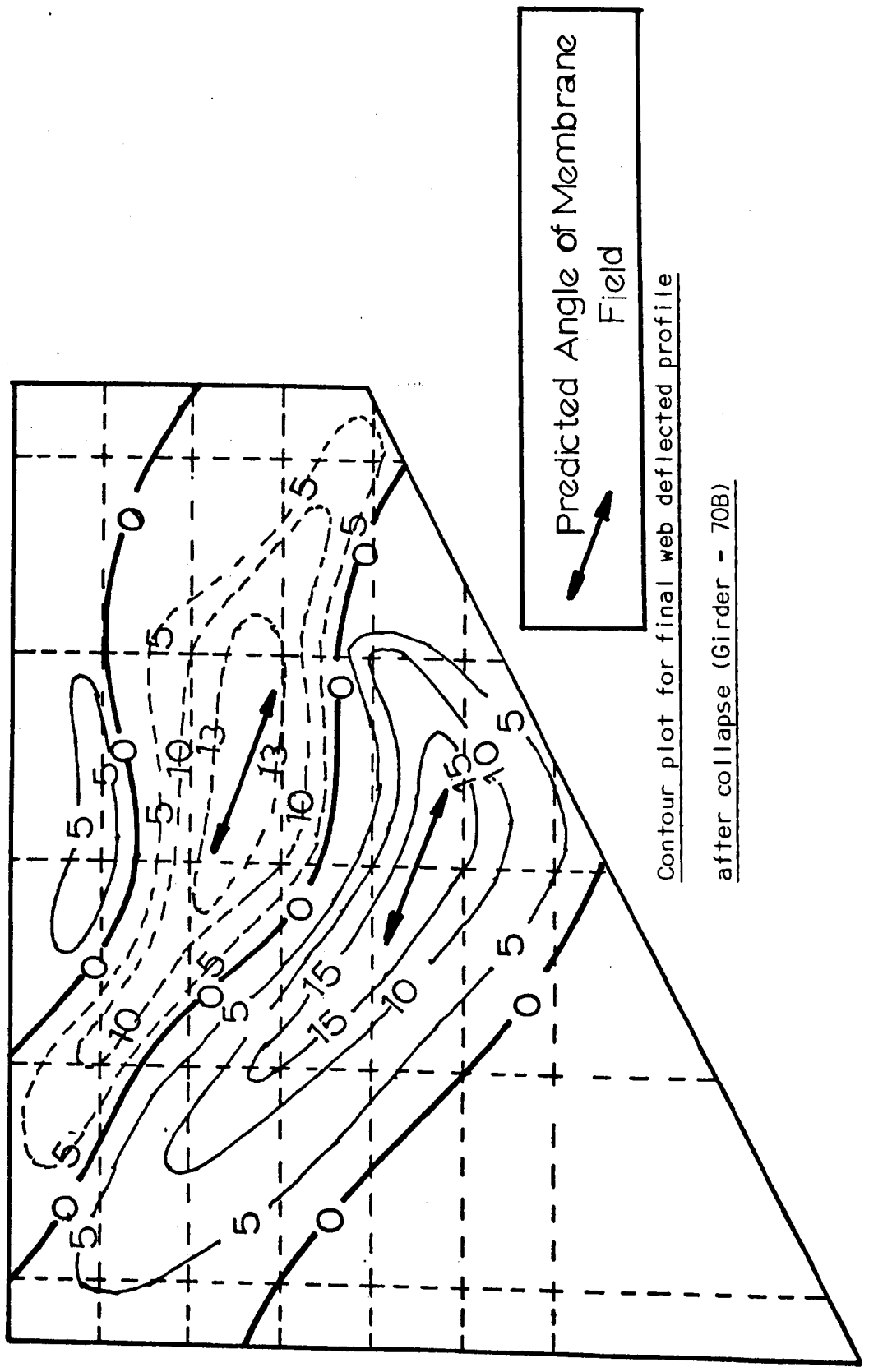

Contour plot for final web deflected profile after collapse (Girder - 70B)

APPENDIX - 7

A7 PLOTTED PROFILES OF WEB PANELS FOR THE BEAMS LOADED OUTSIDE THE TIP

A7.1 - Girder 30A

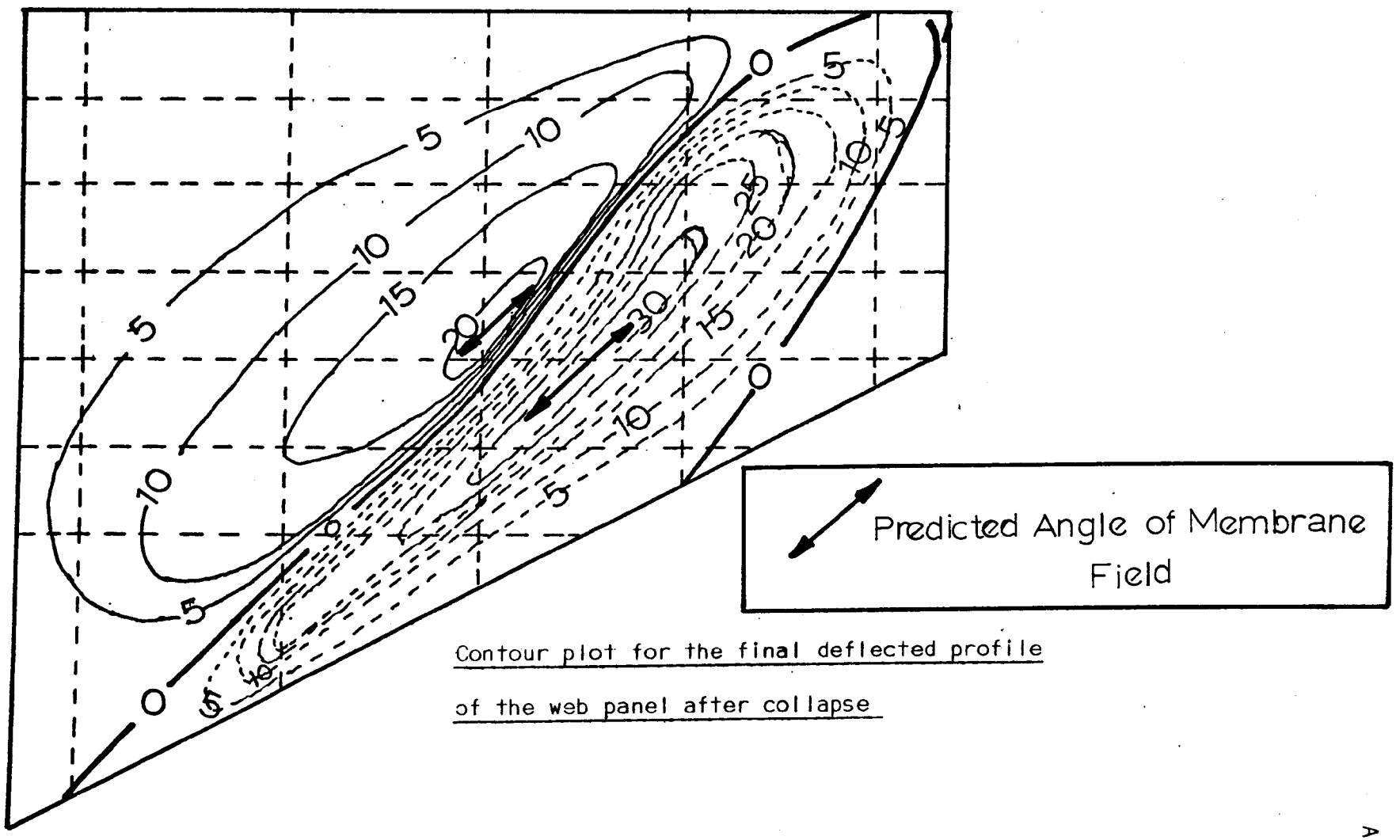

Contour plot for the final deflected profile of the web panel after collapse

A7.2 Girder 30B

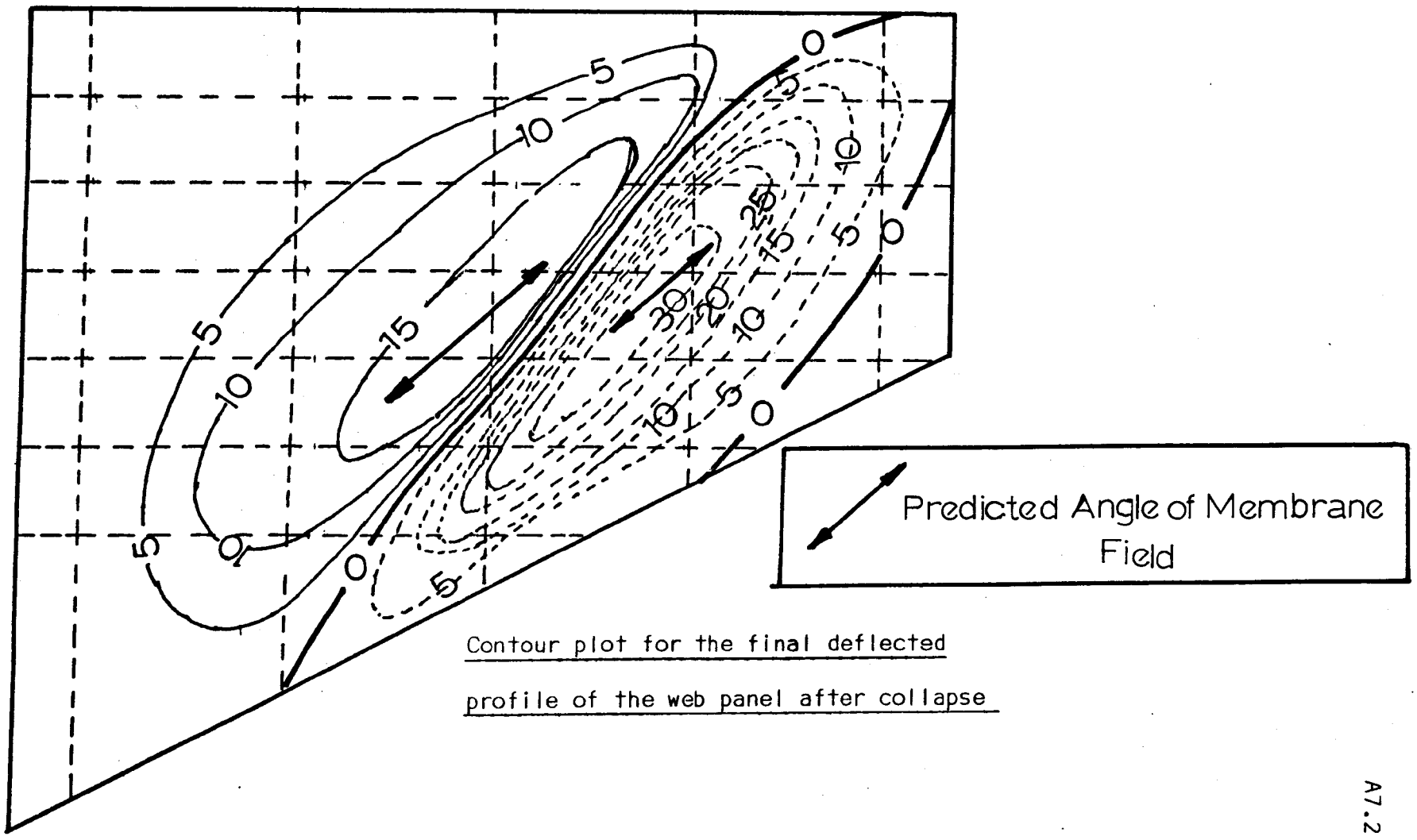

Contour plot for the final deflected profile of the web panel after collapse

A7.3 Girder 40A

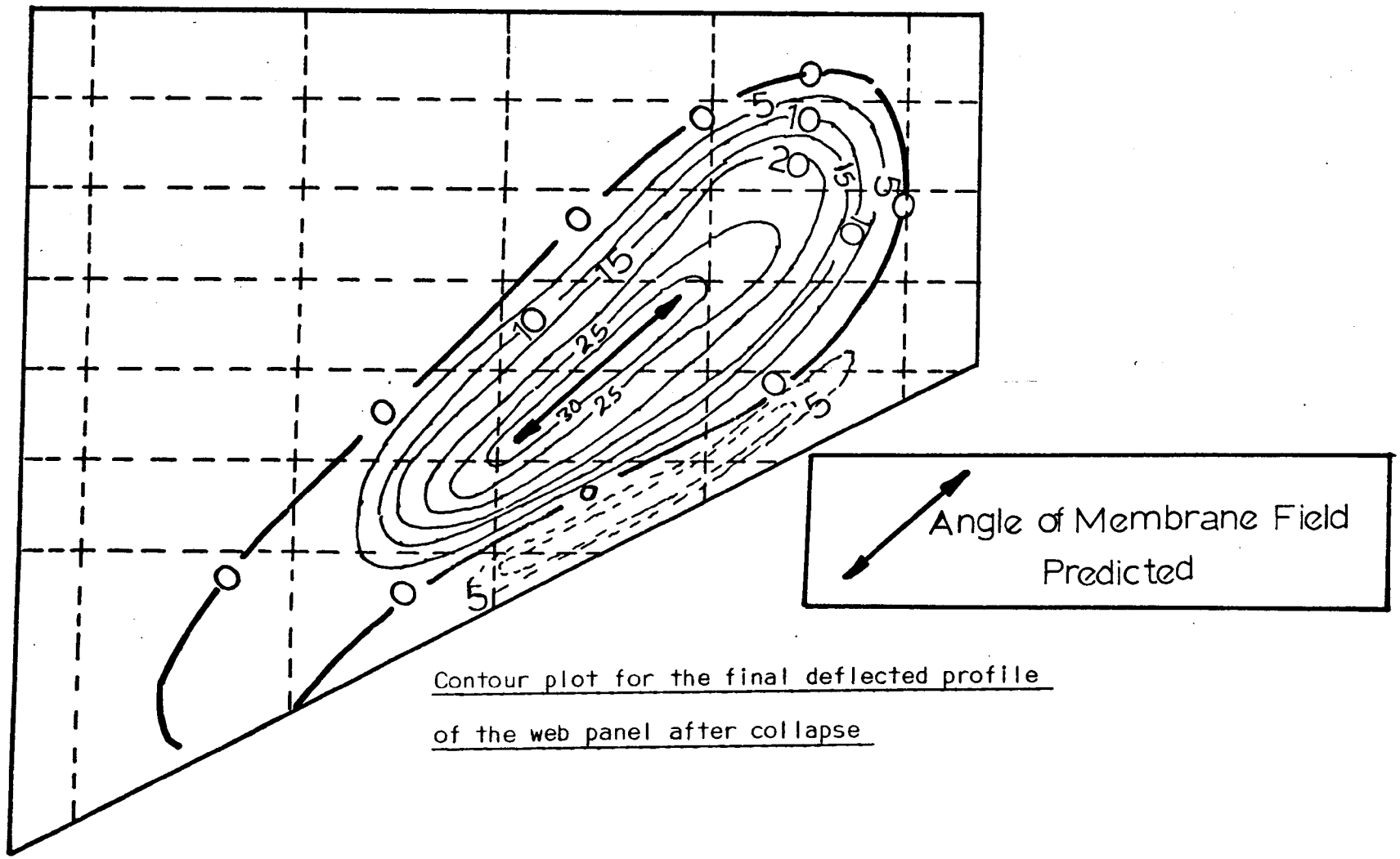

Contour plot for the final deflected profile of the web panel after collapse

APPENDIX-8

A8 PLOTTED PROFILE OF THE WEB PANEL FOR THE BEAMS LOADED AT THE TIP

A8.1 Girder - 50B

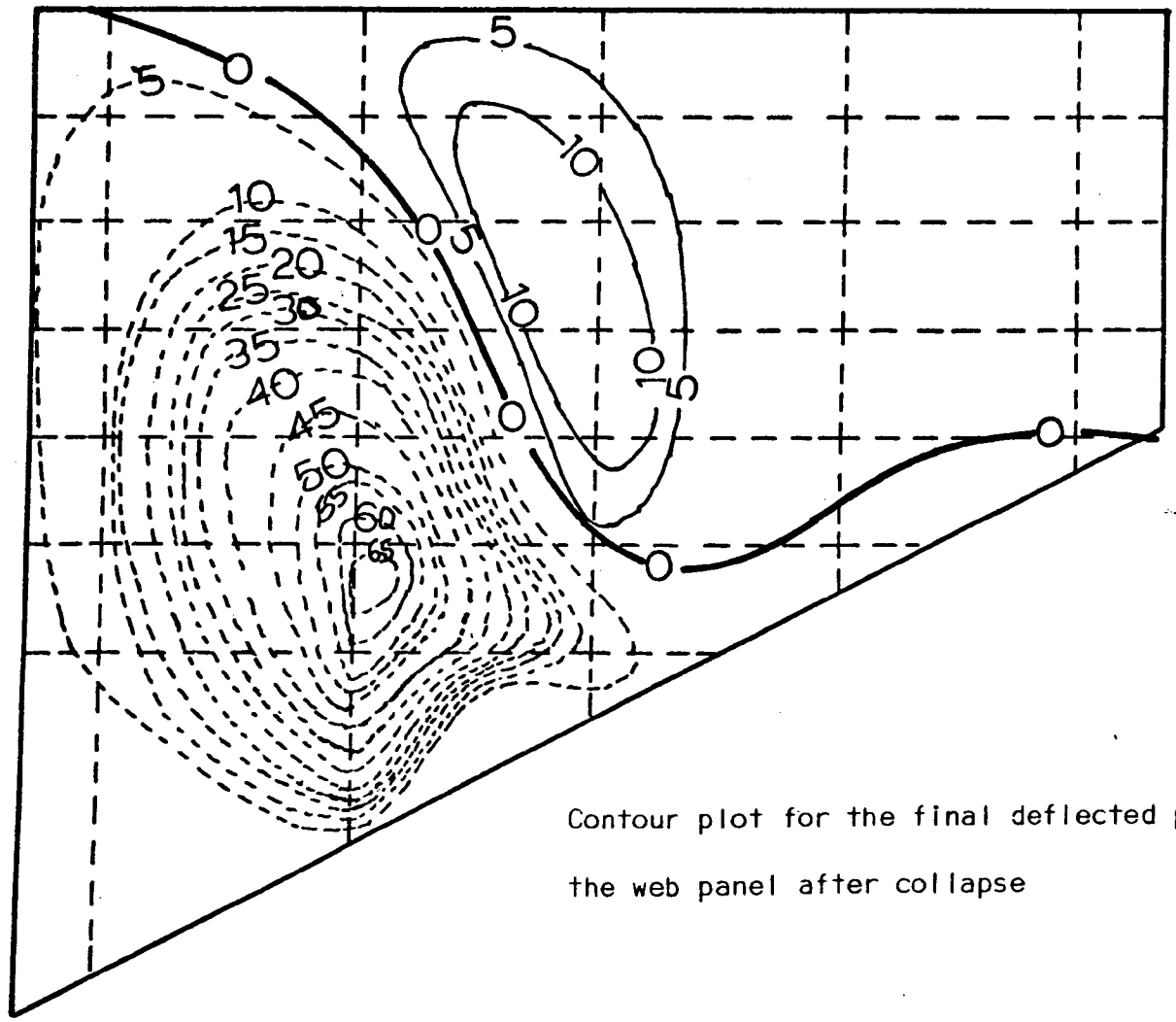

Contour plot for the final deflected profile of the web panel after collapse